



HAL
open science

Applications of cellulose nanocrystals: thermal, rheological and mechanical properties of new materials

Marcos Mariano

► **To cite this version:**

Marcos Mariano. Applications of cellulose nanocrystals: thermal, rheological and mechanical properties of new materials. Material chemistry. Université Grenoble Alpes, 2016. English. NNT: 2016GREAI046 . tel-01560014

HAL Id: tel-01560014

<https://theses.hal.science/tel-01560014>

Submitted on 11 Jul 2017

HAL is a multi-disciplinary open access archive for the deposit and dissemination of scientific research documents, whether they are published or not. The documents may come from teaching and research institutions in France or abroad, or from public or private research centers.

L'archive ouverte pluridisciplinaire **HAL**, est destinée au dépôt et à la diffusion de documents scientifiques de niveau recherche, publiés ou non, émanant des établissements d'enseignement et de recherche français ou étrangers, des laboratoires publics ou privés.

THÈSE

Pour obtenir le grade de

DOCTEUR DE LA COMMUNAUTÉ UNIVERSITÉ GRENOBLE ALPES

Spécialité: **Matériaux, mécanique, génie civil, électrochimie**

Arrêté ministériel : 7 août 2006

Présentée par

Marcos MARIANO

Thèse dirigée par **Alain DUFRESNE**

et codirigée par **Nadia EL KISSI**

préparée au sein du **Laboratoire Génie des Procédés Papetiers et Laboratoire Rhéologie et Procédés** dans le cadre de l'École Doctorale **Ingénierie - Matériaux, Mécanique, Environnement, Energétique, Procédés, Production (I-MEP2)**.

Applications of Cellulose Nanocrystals:

Thermal, rheological and mechanical properties of new materials

Thèse soutenue publiquement le **22 septembre 2016**,

devant le jury composé de :

M. Christian CARROT

Professeur à l'Université Jean Monnet, Saint Etienne (Rapporteur)

Mme Jannick DUCHET-RUMEAU

Professeur à l'Institut National des Sciences Appliquées, Lyon (Rapporteur)

M. Yves GROHENS

Professeur à l'Université de Bretagne Sud, Lorient (Président)

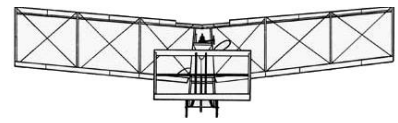
M. Alain DUFRESNE

Professeur à Grenoble INP (Directeur de Thèse)

Mme Nadia EL KISSI

Directrice de Recherches, CNRS – Université de Grenoble (Co-directrice de Thèse)





“Os contratempos e desastres são qualidades negativas.”
(The setbacks and disasters are negative qualities)

Santos Dumont, father of aviation.

*Dedicado à minha família, pelo encorajamento e
tranqüilidade sobre os quais apoio minhas decisões.*

Acknowledgements

During the last years I have dedicated myself to the realization of this work. Since no man is an island, I believe that is fair to register here a small part of my gratitude to the people that helped me in any sense.

Firstly, I am grateful to Prof. Alain Dufresne for the opportunity to develop this thesis here in France. In the same way, I thank Dr. Nadia El Kissi for offering me her time and acquisitions in this obscure domain called rheology. There are no doubts that your knowledge, lightness and helpfulness during the last three years made everything easier on these turbulent times. Also, I would like to thank Prof. Valdir Soldi for the incentives and motivations that brought me here. Yet, thanks to the members and collaborators of LGP2 and Laboratoire Rhéologie et Procédés for the technical support and skills, specially Cecile B. Sillard, Mohamed Karrouch and Hélène Galliard.

Maybe the difficult part is to thank my dear friends. I believe that in many moments I made myself clear about how I felt about those closest people, your importance and my gratitude. I am sure that they can recognise themselves in these words. Along the last years I had the pleasure to meet different people that are truly generous and helpful. In many moments they help me through words or actions, being motivated by friendship or just kindness. Thus, I do not have enough words to devote to you. Those who lived with me, shared some drinks, were neighborhoods or in some point had felt this same foreign-loneliness, thank you.

Finally, I also would like to say thanks to the members of the committee for your contribution in this work. You can be sure that it will help me to better evaluate and develop this manuscript. Also, I gratefully acknowledge the Brazilian National Council for Scientific and Technological Development (CNPq) and "Ciência Sem Fronteiras" (CsF) program for the financial support and opportunity to develop this document and its related publications.

PREFACE AND LIST OF PUBLICATIONS

This document reports the basic literature review and experimental work performed from 2013 to 2016. The data here presented were obtained by the author using the structure of two research units based in Grenoble (France): The Laboratoire Rhéologie et Procédés (LRP) and the Laboratoire de Génie des Procédés Papetiers (LGP2). Both are part of the LabEx Tec 21 (Investissements d’Avenir - grant agreement n°ANR-11-LABX-0030) and of the PolyNat Carnot Institut (Investissements d’Avenir - grant agreement n°ANR-11-CARN-030-01). The author was financed by the Brazilian government through the “Science without borders” program.

Some parts of this work (and additional research developed between 2013 and 2016) are available as scientific publications in the following formats:

Publication in scientific Journals:

- [1] M. Mariano, N. El Kissi, A. Dufresne, Cellulose nanocrystals and related nanocomposites: Review of some properties and challenges, **J. Polym. Sci. Part B Polym. Phys.** 52 (2014) 791–806.
doi:10.1002/polb.23490
- [2] M. Mariano, N. El Kissi, A. Dufresne, Melt processing of cellulose nanocrystal reinforced polycarbonate from a masterbatch process, **Eur. Polym. J.** 69 (2015) 208–223.
doi:10.1016/j.eurpolymj.2015.06.007
- [3] M. Mariano, N. El Kissi, A. Dufresne, Cellulose nanocrystal reinforced oxidized natural rubber nanocomposites, **Carbohydr. Polym.** 137 (2016) 174–183.
doi:10.1016/j.carbpol.2015.10.027
- [4] M. Mariano, N. El Kissi, A. Dufresne, Impact of cellulose nanocrystal aspect ratio on crystallization and reinforcement of poly(butylene adipate-co- terephthalate), **J. Polym. Sci. Part B Polym. Phys.** 54 (2016), 2284–2297.
doi: 10.1002/polb.24139
- [5] M. Mariano, N. El Kissi, A. Dufresne, Structural reorganization of CNC in injection-moulded CNC/PBAT materials under thermal annealing, **Langmuir.** (2016).
doi: 10.1021/acs.langmuir.6b03220
- [6] M. Mariano, N. El Kissi, A. Dufresne, Cellulose Nanomaterials: Size and Surface influence on the thermal and rheological behavior, **Revista Polímeros**, *Accepted*.
- [7] Wilson Pires Flauzino Neto, Marcos Mariano, Ingrid Souza Vieira da Silva, Jean-Luc Putaux, Harumi Otaguro, Daniel Pasquini, Alain Dufresne, Mechanical properties of natural rubber nanocomposites reinforced with high aspect ratio cellulose nanocrystals isolated from soy hulls, **Carbohydrate Polymers.** 153 (2016), 143 – 152.
doi: 10.1016/j.carbpol.2016.07.073

- [8] Wilson Pires Flauzino Neto, Jean-Luc Putaux, Marcos Mariano, Yu Ogawa, Harumi Otaguro, Daniel Pasquini and Alain Dufresne, Comprehensive morphological and structural investigation of cellulose I and II nanocrystals prepared by sulfuric acid hydrolysis, **RSC Advances**. (2016), 76017 – 76027.
doi: 10.1039/c6ra16295a

Published in Conferences proceedings:

Communications

- [1] M. Mariano, N. El Kissi, A. Dufresne, Influence of coated cellulose nanocrystals in thermal and mechanical properties of extruded thermoplastic materials. **1st International EPNOE Junior Scientists Meeting** - ISBN 978-961-248-473-6, 2015.
- [2] A.A. Lucas, L.A. Pessan, W.A.R. Neto, G.F. Siqueira, A. Dufresne, M. Mariano, A. J. de Menezes, Nanocomposite triphasic mono-component obtainment from cellulose fibers modified by oxypropylation reaction. **13° Congresso Brasileiro de Polímeros**, 2015.
- [3] M. Mariano, W.A.R. Neto, A.J. de Menezes, G.F. Siqueira, L.A. Pessan, A.P. Barbosa, A. Dufresne, A.A. Lucas, Obtenção de Nanofibrilas de Celulose a partir de espécies pioneira e nobre da Floresta Amazônica: Caroba e Pau Rosa. **13° Congresso Brasileiro de Polímeros**, 2015.
- [4] M. Mariano, N. El Kissi, A. Dufresne, Coated cellulose nanocrystals / polycarbonate nanocomposites obtained by extrusion. **2015 nanoTAPPI international conference**, 2015.

Oral communications

- [1] Conference: **1st International EPNOE Junior Scientists Meeting**
Local: Wageningen (Netherlands) – January, 2015.
- [2] Conference: **Journée « Polysaccharides » du Groupe Français des Polymères**
Local: Grenoble (France) – March, 2015.
- [3] Conference: **2015 nanoTAPPI international conference**
Local: Atlanta (USA) – June, 2015.
- [4] Conference: **2016 nanoTAPPI international conference**
Local: Grenoble (France) – June, 2016.

Book chapters

- [1] M. Mariano, C. Zornio, F. M. Fakhouri and S. Martelli, Handbook of composite from renewable materials, eds. V. K. Thakur, M. K. Thakur and M. R. Kessler, Wiley, 2016, p. 500.

CONTENTS

RESUMÉ	11
GENERAL INTRODUCTION	25
CHAPTER I:	
Literature Review.....	27
CHAPTER II:	
Cellulose Nanocrystal Reinforced Oxidized Natural Rubber Nanocomposites	109
CHAPTER III:	
Melt processing of cellulose nanocrystal reinforced polycarbonate from a Masterbatch process	139
CHAPTER IV:	
I) Impact of cellulose nanocrystal aspect ratio on crystallization and reinforcement of PBAT	169
II) Structural reorganization of CNC in injection-moulded CNC/PBAT nanocomposites under thermal annealing	201
GENERAL CONCLUSIONS.....	231
APPENDIX	233

RESUME

Introduction

Omniprésents dans notre vie depuis le début des années 1900, les polymères sont aujourd'hui présents dans de nombreux procédés industriels. Avec une large gamme de propriétés, ces macromolécules peuvent provenir de sources renouvelables comme les végétaux ou de sources non renouvelables comme le pétrole. Dans le premier cas, les polymères sont normalement classifiés comme des biopolymères. Les avantages de cette classe de matériaux sont, bien sûr, l'abondance de la source mais également leur biodégradabilité.

Parmi ces polymères, on trouve le polymère le plus abondant sur Terre, la cellulose. Avec une production annuelle estimée entre 1.3×10^{10} [1] et 1.5×10^{11} tonnes [2], la cellulose est utilisée pour la production de matériaux composites en jouant le rôle d'agent de renfort ou pour la production de combustibles par hydrolyse pour obtenir de l'éthanol et autres dérivés. Ces applications multiples sont possibles grâce à la structure particulière que présente la cellulose. L'unité monomère est formée de deux unités glucose qui sont reliées par une liaison glycosidique 1,4 (C-O-C) et qui forme l'unité de base, la cellobiose. Une représentation de cette unité monomère est reportée sur la Figure 1.

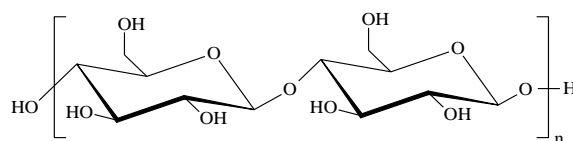


Figure 1. Structure chimique de la cellulose.

Les chaînes de cellulose sont organisées de manière à permettre la formation de multiples liaisons hydrogène (H...H) intramoléculaires et intermoléculaires. Ces liaisons donnent des caractéristiques particulières de flexibilité et de résistance aux fibres de cellulose. En plus des applications traditionnelles comme fibres et source de polysaccharides de faible poids moléculaire, les matériaux dérivés de la cellulose peuvent également présenter d'autres propriétés liées à sa structure interne. Avec l'évolution de la science et des techniques de caractérisation comme les microscopies et la diffraction des rayons X, il a été constaté que cette structure est organisée en micro et nanofibres ce qui permet l'extraction de fibrilles et domaines cristallins individualisés de taille nanométrique.

Les nanofibrilles de cellulose (CNF) et les nanocristaux de cellulose (CNC) sont généralement regroupés dans un ensemble plus grand appelé nanocellulose. Les CNC, aussi appelés cellulose nanocristalline (ou même whiskers de cellulose) ont suscité depuis les années 90 un intérêt scientifique, notamment pour leur potentiel de

renfort mécanique dans les composites. Les nanocristaux de cellulose sont une structure rigide sous forme de bâtonnets ayant un diamètre compris entre 5 et 20 nm et quelques centaines de nanomètres de longueur. Ces domaines cristallins sont présents dans la structure primaire des fibres végétales et sont intercalés avec des zones amorphes, comme représenté sur la Figure 2.

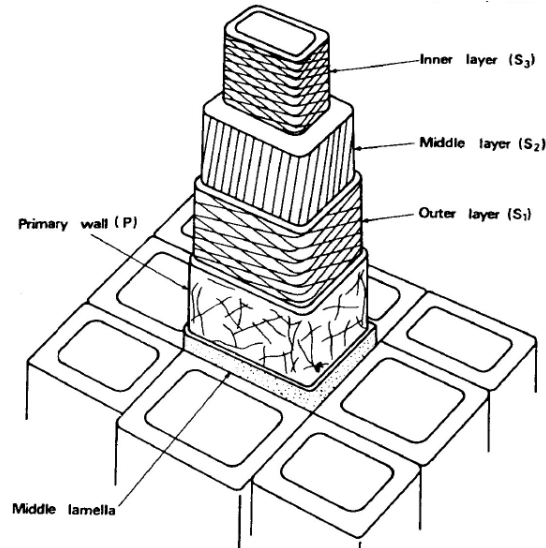


Figure 2. Structure schématique de la fibre de cellulose élémentaire.

Depuis les premières applications des nanocristaux de cellulose comme élément de renfort dans une matrice polymère sous forme de suspension (latex)[3,4], les méthodologies d'extraction et les domaines d'applications ont énormément évolués, comme montre le nombre de publications scientifiques liées à ce matériau.

Pendant longtemps l'extraction des CNC a été réalisée à l'échelle du laboratoire avec l'utilisation d'acides forts comme HCl, H₂SO₄, HNO₃, etc. Cette méthodologie avait comme objectif d'utiliser les acides pour provoquer l'hydrolyse des liaisons glucosides des parties amorphes de la structure cellulosique et isoler ainsi les nanodomains cristallins. De plus, l'utilisation de H₂SO₄ est devenue populaire en raison de l'insertion de charges négatives à la surface de la particule. Cette nouvelle surface chargée est responsable de la stabilité électrostatique des particules en suspension et permet ainsi d'éviter les agglomérations irréversibles inhérentes aux nanomatériaux [5,6].

Le traitement appliqué à la fibre pour l'obtention des CNC est plus rapide et agressif que le traitement utilisé pour la production de CNF. Pour ces dernières, l'objectif étant l'individualisation des fibrilles, il n'est pas nécessaire de dissoudre les zones amorphes et le matériau est normalement obtenu après un prétraitement enzymatique ou oxydatif, suivi par un procédé mécanique [7,8]. Ces particules sont beaucoup plus longues que les CNC et ont, individuellement, des propriétés mécaniques plus faibles.

Il s'agit là en fait de la principale caractéristique des CNC. Leurs propriétés mécaniques sont comparables à des matériaux comme le Kevlar ou l'acier en raison de leur faible densité (1.56 g.cm^{-3}). Différentes techniques ont été utilisées pour mesurer les propriétés mécaniques des CNC et les valeurs rapportées pour le module du cristal de cellulose I (cellulose native) peuvent être supérieures à 136 GPa. En comparaison, cette valeur est de 2 à 3 fois plus élevée que celle des fibres de verre (50-80 GPa) [9]. Ces valeurs sont une conséquence de l'arrangement moléculaire des chaînes de cellulose dans le cristal. Le niveau élevé de cristallinité des CNC se traduit par une faible mobilité des chaînes dans un large intervalle de température et procure à ces matériaux une stabilité mécanique unique jusqu'à la température de dégradation.

Malgré ces propriétés intéressantes et l'abondance du matériau brut dont on peut les extraire, les applications des CNC pour des produits commerciaux restent limitées en raison des limitations liées à l'utilisation de procédés industriels. En effet, les matériaux produits à base de CNC sont généralement préparés par la technique de coulée/évaporation. Ce procédé permet de bien contrôler les propriétés comme l'humidité, la dispersion des particules et aussi d'assurer la formation d'un réseau tridimensionnel des particules qui peut améliorer énormément les propriétés mécaniques et barrière des composites [10–12]. Cependant, ce procédé n'est pas facilement transposable à l'industrie en raison de la durée de l'étape d'évaporation de l'eau (ou autre solvant) présente dans le système.

Une alternative à la technique de coulée/évaporation serait l'application du procédé d'extrusion et/ou de moulage par injection pour la production des composites. Ces procédés sont beaucoup plus rapides que l'évaporation et permettent une production de matériaux en plus grande série. Par ailleurs, ils n'utilisent pas de solvants et peuvent donc être considérés comme des procédés plus verts que la coulée/évaporation. Il y a cependant des points négatifs. Ils sont essentiellement associés à des problèmes de dispersion, de dégradation thermique et de propriétés mécaniques plus faibles. Avec cette méthode, l'échantillon est soumis à des contraintes mécaniques importantes imposées par l'équipement, qui empêche la formation du réseau 3D de particules. Par ailleurs, la qualité de la dispersion est fortement dépendante de la compatibilité entre la matrice et la nanoparticule. Une fois qu'il n'y plus de processus de dissolution et de mélange avec une suspension de CNC, l'enchevêtrement entre chaînes polymères et particules doit être réalisé mécaniquement et on est donc confronté à des viscosités élevées.

Actuellement, la recherche sur les matériaux à base de CNC est en train d'évoluer. La Figure 3 montre le nombre de publications liées à des mots-clés comme

«CNC» et «cellulose nanocrystals» ajouté à des termes plus spécifiques comme «composites», «casting» et «extrusion» depuis 2005.

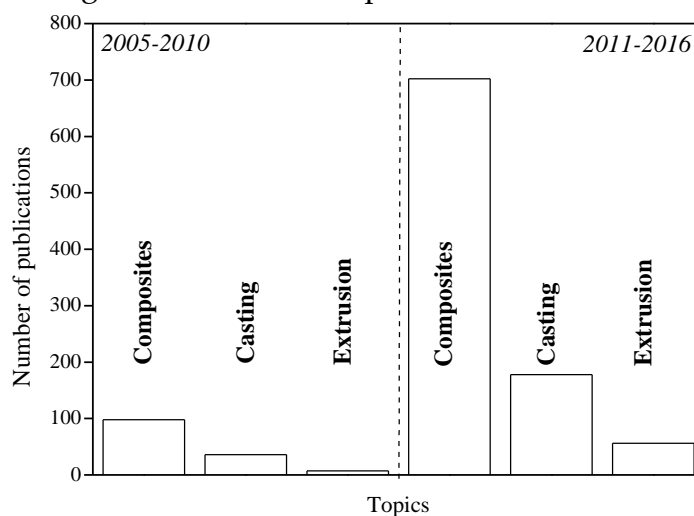


Figure 3. Nombre de publications liées aux termes cités depuis 2005 – Web of Science.

Globalement, le nombre de publications liées aux composites a augmenté de 700% pour la période 2011-2016 par rapport à 2005-2010. Il est intéressant de remarquer que la recherche basée sur les matériaux produits par coulée/évaporation est toujours plus importante que pour l'extrusion. Cependant, le nombre de publications liées à la coulée/évaporation a augmenté de 180% contre 800% pour l'extrusion. Cet intérêt accru pour le domaine de la mise en œuvre des composites à base de CNC à l'état fondu provient de la motivation créée par la possible application industrielle de ces matériaux et par l'avancée lente, mais significative, dans les techniques d'optimisation de leur production.

Au cours de cette période, quelques publications ont introduit par exemple des méthodologies de modification chimique[13,14], d'enrobage des nanoparticules [15,16] et plus récemment l'utilisation de mélanges maîtres (masterbatches)[17] comme techniques permettant d'améliorer la dispersion des nanoparticules. Par ailleurs, le problème de la dégradation thermique des CNC peut être contourné par l'utilisation de réactions de neutralisation, capables d'éliminer les acides résiduels de la surface des nanocristaux et améliorer ainsi leur résistance thermique[18].

Cependant, la dispersion des particules au niveau nanométrique est encore un défi. Les méthodologies appliquées ont besoin d'études plus approfondies. Ce paramètre est particulièrement important, car une fois les matériaux élaborés par extrusion, il n'y a pas formation d'un réseau percolant de nanoparticules et l'addition d'une quantité plus importante de nanoparticules est requis pour atteindre les propriétés désirées[19].

Pour l'instant, les informations relatives à la qualité de la dispersion des CNC et son influence sur les microstructures formées après traitement par extrusion ou

injection sont limitées. Plus récemment, quelques publications scientifiques ont commencé à rapporter des données sur l'influence des conditions de mise en forme et de la cristallinité pour les systèmes à base de CNC et d'un polymère dans le domaine des hautes températures. Les mêmes lacunes peuvent être observées pour les données rhéologiques, pour lesquelles les informations trouvées sont normalement basées sur des résultats obtenus pour des systèmes asymétriques, par exemple quelques argiles et les nanotubes de carbone.

Dans ce contexte, la thèse développée ici présente quelques études qui cherchent à combler quelque unes des lacunes décrites ci-dessus. Le travail a été mené dans l'intention d'étudier différentes possibilités de préparer et de caractériser ces systèmes composites. La plus grande attention est portée aux interactions entre polymère et nanocristaux, pour des matériaux préparés premièrement par coulée/évaporation puis en se concentrant sur des matériaux préparés par extrusion et injection. Les chapitres qui composent ce document sont décrits à la suite.

Chapitres et conclusions générales

Le **Chapitre 1** présente une revue de la littérature et des concepts de base utilisés pendant la thèse. Le **Chapitre 2** est intitulé «Nanocomposites de caoutchouc naturel renforcés par des nanocristaux de cellulose». Dans ce chapitre, les particules de caoutchouc présentes dans la suspension de latex ont été oxydées en surface par addition de KMnO_4 en conditions contrôlées. L'objectif était d'induire l'oxydation des doubles liaisons présentes dans la structure du caoutchouc naturel (NR), composé de monomère polyisoprène, comme représenté sur la Figure 4.

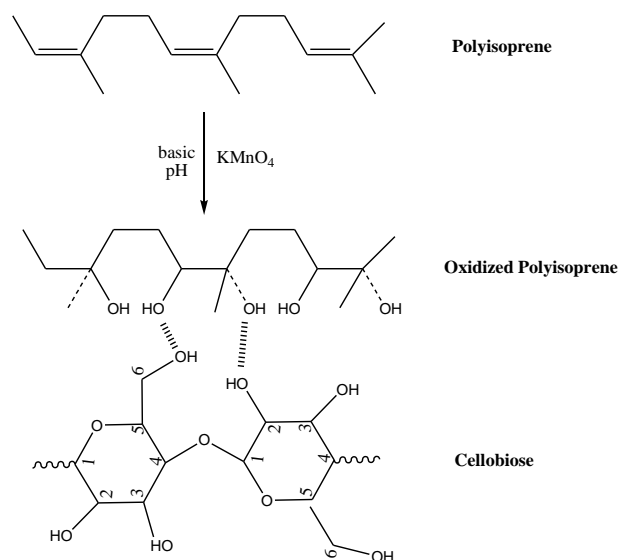


Figure 4. Représentation de la structure du polyisoprène et de sa forme oxydée.

Cette oxydation a été réalisée à différents niveaux, calculés en fonction de la surface des nanocristaux de cellulose présents dans le composite. Cette oxydation a été réalisée afin de promouvoir de nouvelles interactions entre la matrice polymère et la nanocharge de type liaisons hydrogènes entre les groupes hydroxyles présents dans les deux phases. La technique de coulée/évaporation a été utilisée pour produire des films avec et sans nanoparticules, qui ont ensuite été caractérisés par rhéologie, analyses mécaniques (Figure 5), gonflement et propriétés thermiques.

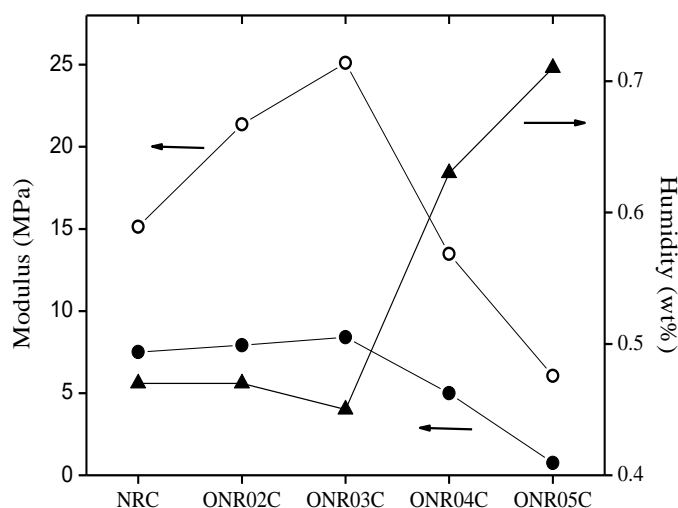


Figure 5. Corrélation entre le module déterminé à partir des essais de traction (●) et DMA (○) et la quantité d'eau (▲) pour les nanocomposites non oxydés et oxydés et renforcés avec 5 % en poids de CNC.

Pour les composites avec un taux de 5% de CNC (en masse), l'analyse FTIR a mis en évidence l'oxydation des liaisons C=C présentes sur le monomère du NR. L'analyse rhéologique de la suspension a montré que les interactions entre le NR et les nanoparticules sont plus significatives après oxydation avec une augmentation de la viscosité du système, proportionnelle au taux d'insertion de groupes -OH.

Pour les échantillons avec un faible taux d'oxydation, nous avons pu observer une résistance accrue au gonflement lorsque ceux-ci sont immergés dans le toluène et dans le même temps, une augmentation des propriétés mécaniques. Les essais de traction cycliques ont montré que pour ces échantillons, les interactions interfaciales entre les nanoparticules et le polymère sont plus fortes. Cependant, quand le taux d'oxydation augmente, l'hydrophilie des chaînes de caoutchouc est observable. Ces échantillons présentent une forte diminution des propriétés mécaniques et sont complètement dissous lorsqu'ils sont immergés dans le toluène. Ces observations nous ont permis de suspecter que pour des niveaux trop élevés, le matériau devient plus hydrophile et les chaînes sont probablement dégradées en raison des conditions drastiques d'oxydation.

Le **chapitre 3** est intitulé «Mise en œuvre à l'état fondu de polycarbonate renforcé par des nanocristaux de cellulose par un procédé masterbatch». Dans ce chapitre, des composites à base de polycarbonate (PC) et de CNC ont été obtenus par la technique d'extrusion. Ce procédé implique de hautes températures (200°C) et la dégradation thermique devient alors un problème pendant la préparation des matériaux. Pour limiter cette dégradation, un mélange maître (masterbatch) contenant environ 30% de CNC a été produit et utilisé comme base pour la préparation des films.

Le chapitre donne une description de la méthodologie de la préparation des masterbatches, qui implique une étape d'échange de solvant (de l'eau à la pyridine) et la précipitation dans un non solvant. Pour vérifier l'influence de cette étape, des composites ont été préparés avec du polycarbonate commercial mais également avec du polycarbonate dissous/précipité, comme pour le matériau du masterbatch.

Cette technique de préparation montre que la préparation du masterbatch peut améliorer la stabilité thermique des nanocristaux et permettre l'extrusion sans dégradation. La dispersion des CNC entre les chaînes de PC permet probablement d'éviter la dégradation en raison de la protection physique des nanoparticules qui complique la conduction de chaleur mais également de O₂. Malheureusement, la présence des CNC semble réduire la stabilité thermique du polymère et accélérer sa dépolymérisation, Figure 6. Nous avons observé que le polymère présente des masses molaires plus faibles après extrusion.

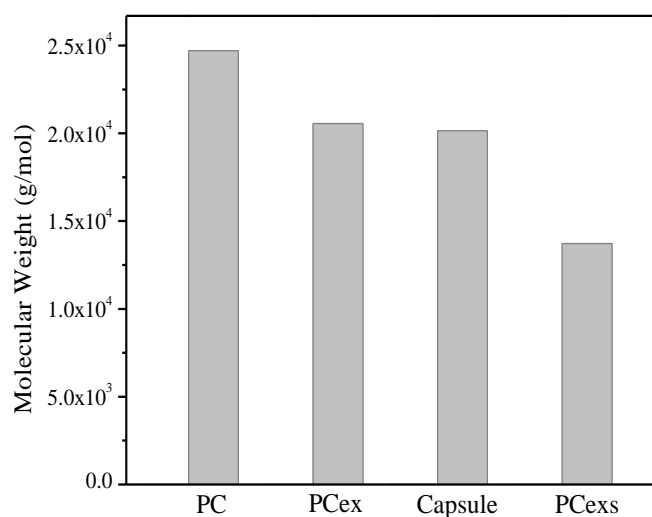


Figure 6. Masse molaire viscosimétrique obtenue pour les granulés de PC, le PC (PCex) broyé et extrudé, dissous-précipité (Capsule) et dissous-extrudé PC (PCexs).

Cet effet est encore plus remarquable pour les échantillons qui sont passés par le processus de dilution/précipitation (PCexs). Pour ces échantillons, la réduction de masse molaire a été amplifiée en comparaison avec les échantillons pour lesquels le polymère a été directement extrudé avec le masterbatch (PCex). La conséquence de cette dégradation est visible sur les propriétés mécaniques des matériaux. Les films avec une masse molaire plus faible sont plus fragiles et les analyses aux rayons-X ont montré une cristallisation plus élevée pour ces échantillons. Cette augmentation de la cristallinité se traduit par une diminution de la transmittance à la lumière mais également par une augmentation des propriétés mécaniques comme le module. Tableau I.

Tableau I. Données expérimentales (E_e) et valeurs calculées avec le modèle de Halpin-Kardos (E_p) pour le module de conservation des nanocomposites CNC/PC à 175°C.

Matériau	PCex		PCexs	
	E_e (MPa)	E_p (MPa)	E_e (MPa)	E_p (MPa)
PC	1.90	2.02	7.08	7.53
PC + 1% CNC	2.29	2.09	58.9	7.64
PC + 3% CNC	4.07	2.26	72.4	7.90

Le **chapitre 4** est dédié aux systèmes à base de polybutylène-adipate-téréphtalate (PBAT) et de nanocristaux de cellulose. Le chapitre est divisé en deux parties. La première partie est focalisée sur l'influence de la cristallisation que les nanocristaux peuvent induire sur la matrice polymère après le processus d'extrusion. Trois sources différentes de CNC ont été choisies pour permettre l'obtention de nanoparticules avec différents facteurs de forme L/d.

Des nanocristaux de l'Université du Maine (L/d 22), de fibres de sisal (L/d 39) et de fibres de capim dourado (L/d 50) ont montré différentes aptitudes à induire la cristallisation de la matrice PBAT, aussi bien pour les temps courts que pour les temps longs. Des nanocomposites ont été préparés par extrusion en utilisant un taux de particules correspondant au seuil de percolation. Cela a créé une sorte de compétition entre la taille de la particule et sa fraction volumique dans le composite pour les différents nanocristaux. Dans cette étude, les nanocristaux de capim dourado présentent le plus grand rapport longueur/diamètre et sont, également, responsables de la cristallisation la plus significative de la matrice, Figure 7.

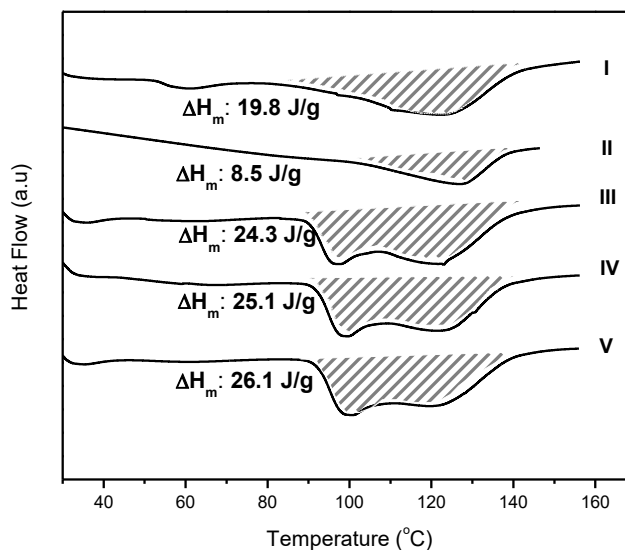


Figure 7. Thermogrammes DSC pour le PBATC₅₀. De haut en bas: (I) matériau extrudé, (II) 2nd cycle de chauffage pour le matériau extrudé et pour le matériau conditionné (III) 2, (IV) 6 et (V) 18 heures à 85°C.

Ensuite, l'influence des nanoparticules et de la cristallisation sur les propriétés mécaniques des nanocomposites a été étudiée. Les résultats les plus importants sont reportés dans le Tableau II. Comme on pouvait s'y attendre, tous les CNC induisent un effet de renfort mécanique au polymère. L'amplitude de cet effet de renfort est également fortement dépendante de la cristallinité.

Tableau II. Module d'Young déterminé par essai dynamique DTST (E_{DTST}) et test de traction (E_T) pour le PBAT et les nanocomposites renforcés par des CNC après extrusion et après conditionnement à 85°C pendant 18h. L'augmentation relative (R.I.) de module après conditionnement est également notée.

Sample	Extruded		18h annealing		R. I.	
	E_{DTST} (MPa)	E_T (MPa)	E_{DTST} (MPa)	E_T (MPa)	DTST (%)	Tensile (%)
PBAT	56	40.5 ± 1.1	67	46.6 ± 1.9	19.6	15.0
PBATC ₂₂	67	44.3 ± 1.3	70	49.7 ± 1.4	25.0	22.7
PBATC ₃₉	61	44.7 ± 1.1	64	45.5 ± 1.0	14.3	12.4
PBATC ₅₀	69	47.2 ± 3.1	76	51.6 ± 2.1	35.7	27.4

Dans la deuxième partie, des nanocomposites ont également été préparés par extrusion/injection puis caractérisés en termes d'organisation structurale. Le titre de

cette partie est «Réorganisation structurale des CNC dans les nanocomposites CNC/PBAT moulés par injection par recuit thermique».

Comme dans la partie précédente, les nanocristaux ont été obtenus à partir de la fibre de capim dourado et utilisés pour la préparation de nanocomposites avec le PBAT. Dans cette partie, notre étude s'est focalisée sur les caractérisations rhéologiques des matériaux aux températures élevées. Des nanocomposites avec 0.5, 1 et 2 fois la fraction massique de nanocristaux nécessaire pour atteindre le seuil de percolation théorique ont été préparés. Les analyses rhéologiques ont montré l'effet de renfort des CNC sur la matrice, Figure 8. Evidemment, la valeur de G' augmente de manière progressive avec l'addition des nanocristaux sans modification visible des valeurs de viscosité et de G'' .

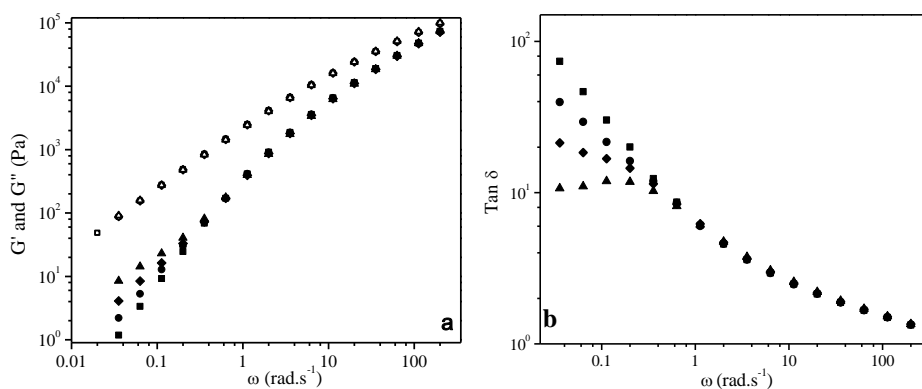


Figure 8. Courbes SAOS (small amplitude oscillary shear) (a) et variation de $\text{Tan } \delta$ pour le PBAT (■), PBATC_{0.9} (●), PBATC_{1.8} (◆), PBATC_{3.6} (▲). Dans (a) G' est représenté par des symboles noirs et G'' par des symboles blancs.

Puisque le réseau percolant de CNC ne s'est pas formé avec la technique d'extrusion, l'état de dispersion des particules a été étudié. Après l'organisation des particules, imposée pendant l'extrusion, il y a toujours des forces de désorganisation présentes dans le système qui ont pour origine l'entropie et les mouvements Browniens des nanoparticules.

Ces forces sont plus importantes lorsque la matrice polymère est à une température plus élevée que T_g . Cependant, même l'influence des mouvements Browniens sur le polymère à l'état fondu est très limitée en raison de la viscosité élevée du système. Selon l'équation de Stokes-Einstein adaptée pour les nanocristaux, ces nanoparticules présentent une mobilité de 165 nm.h^{-1} . Une valeur très basse si on la compare à la mobilité de 2 mm.h^{-1} de ces particules en milieu aqueux. Malheureusement, le conditionnement des échantillons à 170°C , donc au-

dela de la fusion du PBAT, est limité à 30 min. Cette courte période est une limitation imposée par la dégradation de la cellulose. Les propriétés de l'échantillon ont été évaluées par rhéologie traditionnelle (c'est-à-dire SAOS) et par la technique de rhéologie 2D.

Les résultats de SAOS ont montré un changement de viscosité et de la valeur de G' , ainsi que dans la pente de la courbe $G' \times \omega$, suggérant une modification de la structure des particules après conditionnement. Cette possible réorganisation a été étudiée par l'utilisation de la rhéologie 2D (2D-SAOS). Cette expérience a montré un caractère anisotrope très clair des échantillons contenant les particules nanométriques, Figure 9. Par ailleurs, on peut également observer une petite modification des propriétés viscoélastiques des composites après conditionnement. Toutefois, cette modification est trop subtile pour affirmer qu'il est possible de réorganiser la structure des particules au sein du composite.

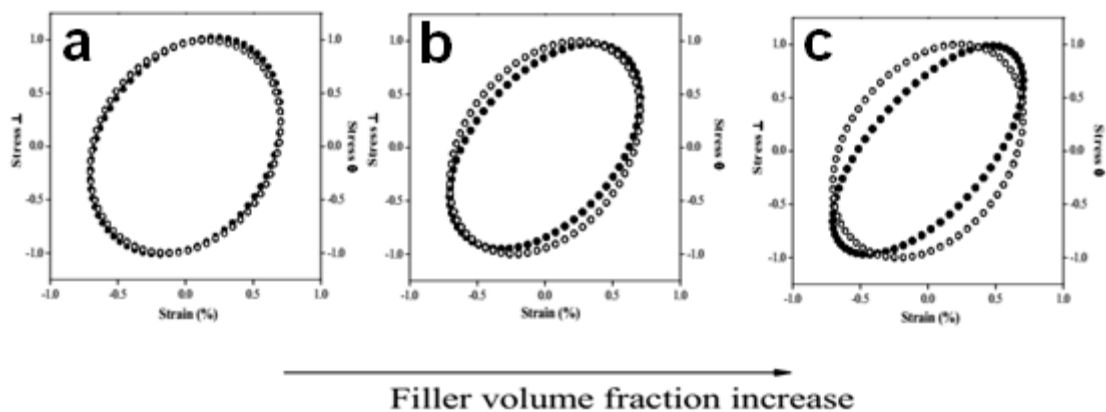


Figure 9. Projection de la contrainte normale (o) et de la contrainte angulaire (●) en fonction de la déformation imposée obtenue par 2D-SAOS. Les échantillons PBAT (a), PBATC_{1.8} (b) et PBATC_{3.6} (d) sont représentés. Les données ont été obtenues à 1 rad.s⁻¹.

Les essais de fluage ont montré des résultats similaires. Grâce à ces tests il a été possible d'observer une modification de la structure des particules qui suggère une plus grande dispersion. Cependant, il est clair que les particules ne sont pas complètement réorganisées sous forme de réseau 3D.

Références

- [1] W. Sandermann, Die "wahren" dimensionen im makromolekularen bereich. Holz Roh- Werkst 31 (1973) 11.
- [2] D. Klemm, B. Heublein, H.-P. Fink, A. Bohn, Cellulose: fascinating biopolymer and sustainable raw material, *Angew. Chem. Int. Ed.* 36(2005)3358-3393.
- [3] V. Favier, G.R. Canova, J.Y. Cavaille, H. Chanzy, A. Dufresne, C. Gauthier, Nanocomposite Materials from Latex and Cellulose Whiskers, *Polym. Adv. Technol.* 6 (1995) 351–355.
- [4] V. Favier, H. Chanzy, J.Y. Cavaille, Polymer Nanocomposites reinforced by Cellulose Whiskers, *Macromolecules.* 28 (1996) 6365–6367.
- [5] P. Rämänen, P. a. Penttilä, K. Svedström, S.L. Maunu, R. Serimaa, The effect of drying method on the properties and nanoscale structure of cellulose whiskers, *Cellulose.* 19 (2012) 901–912. doi:10.1007/s10570-012-9695-3.
- [6] Y. Peng, D.J. Gardner, Y. Han, A. Kiziltas, Z. Cai, M. a. Tshabalala, Influence of drying method on the material properties of nanocellulose I: thermostability and crystallinity, *Cellulose.* 20 (2013) 2379–2392. doi:10.1007/s10570-013-0019-z.
- [7] O. Nechyporchuk, M.N. Belgacem, F. Pignon, Rheological properties of micro-/nanofibrillated cellulose suspensions: wall-slip and shear banding phenomena., *Carbohydr. Polym.* 112 (2014) 432–9. doi:10.1016/j.carbpol.2014.05.092.
- [8] P. a Penttilä, A. Várnai, K. Leppänen, M. Peura, A. Kallonen, P. Jääskeläinen, et al., Changes in submicrometer structure of enzymatically hydrolyzed microcrystalline cellulose., *Biomacromolecules.* 11 (2010) 1111–7. doi:10.1021/bm1001119.
- [9] M. Mariano, N. El Kissi, A. Dufresne, Cellulose nanocrystals and related nanocomposites: Review of some properties and challenges, *J. Polym. Sci. Part B Polym. Phys.* 52 (2014) 791–806. doi:10.1002/polb.23490.
- [10] L. Tang, C. Weder, Cellulose whisker/epoxy resin nanocomposites., *ACS Appl. Mater. Interfaces.* 2 (2010) 1073–80. doi:10.1021/am900830h.
- [11] G. Siqueira, J. Bras, A. Dufresne, Cellulose whiskers versus microfibrils: influence of the nature of the nanoparticle and its surface functionalization on the thermal and mechanical properties of nanocomposites., *Biomacromolecules.* 10 (2009) 425–32. doi:10.1021/bm801193d.
- [12] X. Xu, F. Liu, L. Jiang, J.Y. Zhu, D. Haagenson, D.P. Wiesenborn, Cellulose Nanocrystals vs. Cellulose Nanofibrils: A Comparative Study on Their Microstructures and Effects as Polymer Reinforcing Agents, *Appl. Mater. Interfaces.* 5 (2013) 2999 – 3009.
- [13] R.J. Moon, A. Martini, J. Nairn, J. Simonsen, J. Youngblood, Cellulose nanomaterials review: structure, properties and nanocomposites., *Chem. Soc. Rev.* 40 (2011) 3941–94. doi:10.1039/c0cs00108b.

- [14] D. Roy, M. Semsarilar, J.T. Guthrie, S. Perrier, Cellulose modification by polymer grafting: a review., *Chem. Soc. Rev.* 38 (2009) 2046–64. doi:10.1039/b808639g.
- [15] L. Lemahieu, J. Bras, P. Tiquet, S. Augier, A. Dufresne, Extrusion of Nanocellulose-Reinforced Nanocomposites Using the Dispersed Nano-Objects Protective Encapsulation (DOPE) Process, *Macromol. Mater. Eng.* 296 (2011) 984–991. doi:10.1002/mame.201100015.
- [16] K. Ben Azouz, E.C. Ramires, W. Van den Fonteyne, N. El Kissi, A. Dufresne, Simple Method for the Melt Extrusion of a Cellulose Nanocrystal Reinforced Hydrophobic Polymer, *ACS Macro Lett.* 1 (2012) 236–240. doi:10.1021/mz2001737.
- [17] A. Nicharat, J. Sapkota, E.J. Foster, Pre-mixing and masterbatch approaches for reinforcing poly(vinyl acetate) with cellulose based fillers, *Ind. Crops Prod.* (2016). doi:10.1016/j.indcrop.2016.02.061.
- [18] M. Roman, W.T. Winter, Effect of sulfate groups from sulfuric acid hydrolysis on the thermal degradation behavior of bacterial cellulose, *Biomacromolecules.* 5 (2004) 1671–1677.
- [19] F. Alloin, A. D'Aprèa, A. Dufresne, N. El Kissi, F. Bossard, Poly(oxyethylene) and ramie whiskers based nanocomposites: influence of processing: extrusion and casting/evaporation, *Cellulose.* 18 (2011) 957–973. doi:10.1007/s10570-011-9543-x.

GENERAL INTRODUCTION

Since the first investigations on cellulose based nanocomposites and reinforcing effect of cellulose nanocrystals, more than 20 years ago, a long way was covered. Today, supported by technological advances, an increasing volume of scientific research is available. It drives these nanomaterials towards the expected properties that they need to present in order to occupy markets and factories along the next years...

From the first controlled hydrolysis until today, many drawbacks were overcome in nanocellulose production. In the last years, surface modification and extrusion process became an effective way to obtain dispersed filler, prepared without solvent or long preparation period. Here, we have focused on the preparation of materials without cellulose nanocrystal surface modification. Instead, matrix modification or use of a masterbatch were investigated due to their simplicity. Several characterization techniques are used to provide a broad view about thermal, mechanical, rheological and chemical properties of the obtained materials.

This thesis is divided into four chapters that investigate the influence of the use of cellulose nanocrystals as filler in composites based on different polymers.

Chapter I covers the literature review about composites and cellulose nanocrystals. It includes relevant themes such as viscoelastic behavior, rheology and impressive results found in the literature for the discussed topics.

Chapter II proposes polymer matrix modification as a way to increase the compatibility between the nanofiller and a hydrophobic polymer. Produced by casting/evaporation method, natural rubber was chosen as matrix due to its large range of applications, flexibility and well-known properties. Different techniques were used to understand the effect of the introduction of -OH group on the polymer particle surface. The influence of the degree of oxidation, particle/matrix interactions and humidity were explored to explain the visible structural and rheological behavior of the samples.

The next two chapters describe the use of melt processing techniques such as extrusion, hot-pressing and injection-molding used to produce the nanocomposites. The use of a masterbatch to avoid early thermal degradation of the nanocrystals is reported in Chapter III. In this section, by using polycarbonate as matrix, the CNC particles were coated by the polymer and the materials prepared by extrusion at high temperatures. The effect of masterbatch production and processing on the mechanical properties are then discussed.

Chapter IV describes the effect of coating the polymer by a layer of CNC from water suspension. This chapter is divided into two parts. In the first one,

nanocomposites based on Poly(butylene adipate-co-terephthalate) are prepared by extrusion. The effect of CNC, from different sources, on the composite crystallinity is discussed. The second part investigated the influence of nanorods on the rheological properties of the material using 2D rheology to perform studies about the material anisotropy.

Complementary relevant data can be found in the Appendix at the end of this manuscript. This section presents some primary investigations about different properties of different nanomaterials obtained from pristine cellulose with focus on thermal and some rheological properties. Also, usefull nomenclatures, experimental data and additional references can be found.

CHAPTER I

Literature Review

Some parts of this chapter are based on **Cellulose nanocrystals and related nanocomposites: Review of some properties and challenges**, published in **Journal of polymer science, Part B: Polymer physics**, 2014, 52, 791–806 and **Influence of natural fillers size and shape into mechanical and barrier** to be published in "**Handbook of Composite from Renewable Materials: Volume 3 Physico-chemical and Mechanical Characterization**", Chapter 17. *In press*.

CONTENTS

1 INTRODUCTION.....	31
2 THERMAL PROPERTIES OF POLYMERS	33
2.1 Polymers.....	33
2.2 Thermal properties and molecular transitions	35
2.3 Thermoplastics and elastomers	36
2.4 Crystallization behavior	40
3 MULTIPHASIC SYSTEMS	45
3.1 Composites and colloids	43
3.2 Viscoelasticity	45
3.3 Mechanical properties of composites.....	48
3.4 Rheological properties of colloids and polymer melts.....	49
4 CELLULOSE NANOCRYSTALS: PREPARATION AND PROPERTIES	56
4.1 Cellulose biosynthesis and crystallinity	56
4.2 Cellulose hydrolysis	63
4.3 A background about surface energy and nanomaterials.....	67
4.5 Cellulose nanocrystals: Mechanical properties and reinforcement potential.....	70
4.6 Colloidal behavior and rheology	72
4.7 Thermal stability	77
4.8 Toxicity and biodegradability	79
5 CNC NANO-REINFORCEMENT.....	80
5.1 Percolation theory	81
5.2 Processing technique	83
5.3 Nanocomposite properties	87
6 REFERENCES	90

1 INTRODUCTION

This chapter has as major objective to provide the needed background and offer an actual scenario of the related research. As mentioned in the general introduction, the advances in the cellulose technology field, especially in the extraction and utilization of nanomaterials, are quite exciting nowadays.

Here, we try to revise all the stages of this step-by-step development using relevant publications to illustrate it. At the end, the developed thesis is a consequence of the accumulated knowledge that is used to elucidate and propose new questions about the topic.

Concerning the literature references, Figure I reflects a time-line distribution of scientific papers on the topic. From the total number of publications cited in this introductory chapter, part of them are classic publications related to the beginning of the structural characterization and properties of cellulose, dating from the 60's and 70's. This number of publications grows in the 80's and 90's due to the development of some basic concepts about materials and their characterization.

However, the most significant number of publications here dates from the last 10 to 15 years. This is due to the significant and exponentially growing number of publications in the area since 2000, attributed to new research interests and a resurgence of interest for renewable materials.

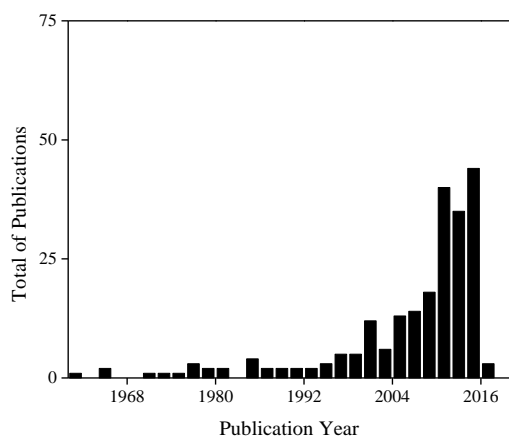


Figure I. The number of publications cited in this chapter and classified by year.

It is quite interesting to note that in the first decade of this century major part of the publications were devoted to the expansion of extraction methodologies and use of new sources, as well as preparation of nanocomposites based on casting/evaporation. This scenario started to change in the last 5 to 6 years when chemical modification, melt processing and more diverse characterization techniques started to be explored.

This chapter is divided into four parts. The first one contains a broad overview about polymers and their molecular properties, being focused on thermal behavior and crystallization properties. This is expanded during the second part for some properties of these materials - in solution or filled with diverse fillers - in multiphase systems.

The last two parts are more specific on cellulose properties. The importance of its structure and how to isolate its crystalline domains are covered along with a description of the characteristics of these particles. Their role in polymer nanocomposites, especially mechanical and rheological properties, is the topic of the last part.

2 THERMAL PROPERTIES OF POLYMERS

2.1 Polymers

A scientific milestone was reached in the beginning of the 20th century. In its early first years, most precisely in 1907, the humanity entered in the Polymer Age (or Plastic Age)[1]. Today, there is no question that it has become a humanity landmark. Now, living in this age means that plastics are an essential material; being the foundation of countless technological innovations and a new improved way of life.

Featuring a remarkable range of properties, these materials have different origins. Natural, oil-based or synthetic polymers are present in almost all industrial processes that we know due to their excellent all-round properties, easy molding and manufacturing. At the same time, their presence also causes an increasing concern about the environment since they are stable and most of them are not readily degraded in the ambient conditions [2] . In developed countries, the presence of non-biodegradable plastics in the municipal solid waste reaches 20-25% of the total mass discarded every year [3].

As a way out of this problem, nowadays the polymer research focus is on production of biodegradable plastics or recycling processes. This is possible because during the last 100 years we tried to better understand the chemistry and constitution of polymers. Even though since the 19th century the scientific community has been working with polymer properties and natural polymers modification, some advances are still necessary.

For example, the control of the chemical composition of macromolecules and their degree of polymerization can generate tailored materials. Properties such as good thermal isolation, electronic conductance, flexibility, toughness, high elasticity, chemical resistance, transparency, etc, can be certainly found in some classes of polymers. In general ways, independently of the source or chemical constitution, different classes of polymers can present common properties. These final characteristics will define their end applications. At least three big classes of polymers can be defined based on this concept:

Thermoplastics: with properties of hard or tough elasticity, can be melted due to the presence of crystalline domains.

Elastomers: a class well represented by rubbers, are soft, elastic and usually cannot be melted.

Thermosets: that have as characteristics the hard elasticity, normally presenting crosslinks and cannot be melted [4].

Some examples of popular polymers and their properties are collected in Table I.

Concerning their application in composites, the chemical and physical properties will define the most suitable methodology. The chemical composition is important to predict the possible interactions between the polymer and the filler. Melt processing is dependent on physical properties and casting preparation depends of a suitable solvent to solubilize the material. Many of these properties will be discussed in sequence.

Table I. Examples of common polymers

Polymer	Polymer Classification	Synthetic	Biobased	Readily Biodegradable
Cellulose	-	no	yes	yes
Lignin	-	no	yes	yes
“Green” Polyethylene	thermoplastic	yes	yes	no
Natural Rubber	elastomer/thermoset*	no	yes	yes
Nylon	thermoplastic/elastomer	yes	no	no
Poly(butylene adipate-co-terephthalate)	thermoplastic	yes	no	yes
Polycarbonate	thermoplastic	yes	no	no
Polyethylene	thermoplastic	yes	no	no
Polyimide	thermoset	yes	no	no
Poly(lactic acid)	thermoplastic	yes	yes	yes
Polyurethane	thermoplastic/thermoset*	yes	no	no
Polystyrene	thermoplastic	yes	no	no
Polyvinyl Chloride	thermoplastic	yes	no	no
Starch	thermoplastic*	no	yes	yes

*under certain conditions

2.2 Thermal properties and molecular transitions

As defined in sequence, the behavior of polymers can be between elastic and rubbery, which is strongly dependent on temperature. This is directly associated with the molecular structure of the macromolecule. They can present phase-transitions at given temperatures according to, for example, the mobility of the chains, their ramifications, molecular weight, etc. [4]

Looking closer, these characteristic transitions are normally associated with relaxation processes and free volume. In relaxation processes, the effect of thermal motion on the orientation of polymer molecules is considered. When a deformation is imposed to the chains due to some applied stress, the free energy increases (due to the entropy reduction). If this force keeps the polymer in the deformed state, the stress relaxation will cause a reduction on the chain motions and dissipate energy as heat. This relaxation depends on how the segments react to the thermal motion in terms of group movement and cooperativity of the chains. Those effects are used to

predict and explain the different behaviors of the material depending on the temperature range [5].

The free volume concept considers the existence of free space into the polymer structure. Polymeric chains can use this free space (or volume) to move and perform internal movements. As a consequence, the increase of the free volume can provide more freedom to side chains and groups [6]. These effects are related to the polymer mobility and, at some level, reflects its macroscopic properties, increasing the flexibility of the chains and causing the called α , β and γ relaxations (Figure 1).

The α relaxation (as the glass transition, T_g) is normally the main relaxation in polymeric materials and involves most of the molecules. It's an amorphous characteristic transition, since an ideal crystalline material would not have a T_g . The amorphous regions in partially crystalline polymers also assume to display a glassy state, being independent of the degree of crystallinity in a first approximation [5].

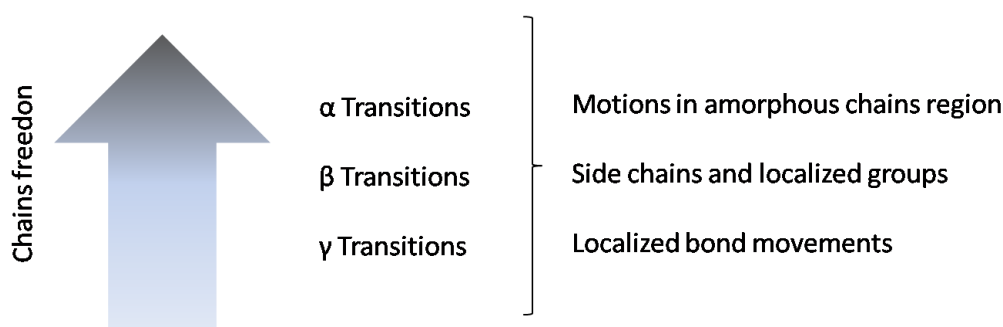


Figure 1. Relation between chain movements and polymeric relaxations.

Crystalline domains present chains movement at higher temperatures. The melting point (T_m) is related to the motion of the chains, causing material flow. However, some materials suffer from thermal degradation before T_m , which is normally the case for cellulose, as an example.

Thermal degradation. Besides the molecular transitions caused by the temperature modification, polymers can also present thermal degradation. As for other degradation mechanisms (e.g. photochemical and high energy radiation), the conditions in which the material starts to decompose are strongly dependend on its molecular characteristics.

It is expected for a polymer that contains in its backbone chain a peroxide group $-O-O-$ (138 kJ.mol^{-1}) to start to degrade before a polymer based on $-C=C-$ (612 kJ.mol^{-1}) bonds. This is because, from a structural point of view, polymers are less stable than metals or silicates. Due to the organic characteristic of the chains and covalent bonds between the atoms the degradation of polymers is completed before

600°C, presenting a practical utilization range until maximum 200°C against 2000 or 3000°C for inorganic materials[7].

The degradation of the polymer is also dependent on the surrounding atmosphere and other factors like the heating rate and its own physical arrangement (i.e. films, grains, powder, etc). When in air, polymers are easily degraded by oxidation reactions that decrease its thermal stability in comparison to degradation mechanism in nitrogen atmosphere [8].

Many characterization techniques use the heating rate as a tool to estimate parameters such as activation energy. Mathematical methods such as Ozawa [9] and Red-Fern [10] models and their adaptations, use different heating rates and the ensuing displacement of the curve to higher temperatures to estimate parameters that can be used to understand the degradation mechanism of polymers. This degradation temperature is usually quite higher than transitions temperature. For example, some thermoplastic polymers could present thermal degradation at temperatures 200 to 300°C higher than their melting point.

However, some polymers can present their degradation at lower temperatures than their thermal transitions. In this case, temperatures such as T_g and T_m are just theoretical values and cannot be observed by common thermal based techniques like differential scanning calorimetry (DSC). It happens due to the relation between entangled chains and molecular movement restriction. Polymers that present lower crystallinity have higher entanglement levels (especially in for high molecular weight chains), which leads to chains with restricted motion capacity. This limitation of freedom motions induces difficulty for the chains to dissipate thermal energy, causing an earlier degradation [7]. It also strongly depends on intermolecular interactions.

2.3 Thermoplastics and elastomers

Contrarily to other classes of polymers, thermoplastic materials can be deformed and molded without significant degradation by solubilization in a suitable solvent or by thermal processing. Among thermoplastic polymers, it is possible to found materials with very different properties. For example, they can vary from optically transparent to opaque, depending on the way the light is internally scattered by the molecules [4].

Their capacity of processing and optical properties make these polymers very interesting for high temperature processing. Table II shows some thermal properties for polycarbonate (PC) and poly(butylene adipate-co- terephthalate) (PBAT), both thermoplastic polymers.

These data show how the properties of the same polymer can vary. It happens because most semicrystalline polymers have final properties which are governed by their supermolecular morphology. It means that the final properties of the polymer are controlled by its composition and physicochemical environment during processing. Crystallization is a good example of a phenomenon that can rule many polymeric properties [11,12].

Polycarbonate. It was firstly synthesized by Einho in the late 1890s and it is an amorphous thermoplastic polymer with characteristics of toughness and transparency. Today, bisphenol-A PC is one of the most used materials to manufacture products like CDs, DVDs, Blu-Rays, glasses and other products. Some remarkable PC's characteristics are its low heat conductivity, high impact resistance, dimensional stability, ability to be molded, electrical properties, transparency and optical properties. Some of the disadvantages of PC can include poor resistance to marring, scratching, abrasion, and solvents. However, it can be overcome by using additives, stabilizers, and fillers.

Some PC's physical and mechanical properties can be severely reduced by recycling. For example, after ten recycling cycles its tensile strength can present a reduction of 30% [13,14].

All its macroscopic properties are a consequence of its structural arrangement. PC contains aromatic rings that make it less flexible, noncrystalline, hard, and thermally stable. It also results in high T_g and T_m (Table II) that make it hard to process. Especially the high molecular weight fractions that are quite viscous. For practical issues, it is not recommended to adopt extrusion as processing technique [15].

PBAT. It is a semicrystalline polymer whose main characteristics are its softness and biodegradability. As a thermoplastic polymer, it presents a T_g and T_m , but the presence of two monomer units: butylene terephthalate (BT) and butylenes adipate (BA) unit, imparts specific thermal transitions. In the last years several works have reported the use of this polymer in blends with polylactic acid (PLA) to try to get the best of its combined properties [16–18]. Applications in biomedical field is also suggested due to its chemical structure (aliphatic polyester) and easy production, as an oil-based polymer, unlike most aliphatic polyesters that comes from microorganisms or high production polymerizations [19].

A clear distinction between these polymers can be done due to their different morphology. PC is known as a virtually amorphous polymer and PBAT as a semicrystalline material. For some processing conditions such as high pressure

during injection molding, PC can develop a small extent of crystallinity (8%), while PBAT can present a crystallinity around 20% due to the crystallization of PBT units. [20,21]

Elastomers. This class of materials is formed by netlike crosslinked molecules that normally cannot be melted without total structure degradation. Such as thermoplastic polymers, elastomers are soft elastic above and hard elastic (or brittle) below T_g [4]. Due to their particular properties, especially their high elasticity, they are used in many fields and have a particular importance in automotive industry.

This elasticity is a reversible process directly dependent of the chemical constitution of polymeric chains. During stretching, the random coils of the polymer chains are uncoiled and start to align and tend to form crystals, decreasing the material entropy and liberating heat [22]. Some examples of elastomers are butadiene resin (BR), styrene butadiene resin (SBR), polyurethane resin (PUR) and natural rubber (NR). The last one comes from a natural source, which represents an advantage over synthetic non-renewable rubbers derived from petroleum.

NR is a natural polymer obtained as water suspension by extraction from the *Havea Brasiliensis* tree. Composed of cis-1,4-isoprene units, it presents, in comparison to synthetic rubbers (as isoprene rubber, which is the synthetic NR analogous), much higher strength properties. According to Karino (2007), these properties are not much dependent on the presence of proteins, but from other components such as phospholipids present in the naturally obtained suspension and its higher stereoregularity [23]. Technologically, NR is important due to its great presence in industry and commodities. After a process of vulcanization, the formation of a cross-linked structure can bring to the rubber a higher resistance to deformation and it can become an important commodity polymer to be used in the tire industries, for example.

Apparently an amorphous solid at room temperatures, NR also becomes a polycrystalline material after cooling or during stretching. In the first case, the higher rate of crystallization seems to be around -25°C and strongly dependent on the presence of non-rubber components in the material (e.g. fatty acids) [24]. In the last case, microcrystalline domains become oriented in the tension direction and the material displays a fiber-like pattern in X-Ray diffraction [25]. It happens due to a phenomenon called stress-induced crystallization.

Table II. Thermal properties of PBAT and PC.

	Process	Temp. (°C)	Ref.	
Bisphenol-A-Polycarbonate	Synthesis/polymerization	230	[26]	
		290	[27]	
	Crystallization	300	[28]	
		190	[29,30]	
	Molecular Transitions	α	147	[31,32]
		β	-28	
		γ	-88	
	Melting point	210 - 240	[30]	
		220 - 260	[26]	
		242	[33]	
Thermal Degradation onset	450	[34]		
	388	[35]		
Poly(butylene adipate-co- terephthalate)	Synthesis/polymerization	230 - 270	[36]	
		210 - 270	[37]	
	Crystallization	60 - 90	[38]	
		48	[39]	
		63	[40]	
	α -Molecular Transitions	-28	[41]	
		-34	[40]	
	Melting point	110	[41]	
		121	[38]	
		120	[39]	
	Thermal Degradation onset	384	[40]	
		410	[42]	

2.4 Crystallization behavior

General Aspects. The development of crystallinity in a polymer is thermodynamically driven by the material's thermal history. For a polymer with very high molecular weight, the crystalline arrangement is a state with lower free energy than the liquid state for temperatures below the melting point [43].

Once this lower energy state is available, the chains start to be reorganized and the crystalline regions are formed under the influence of secondary bonds (i.e. no covalent bonds are involved). These cohesive forces, like dispersion bonding, dipole bonding or hydrogen bridge bonds can deeply influence the polymer properties such as density, swelling behavior, chemical and electrical properties, besides the mechanical properties [4]. Crystallization can be induced in quiescence conditions. If the material was melted-cooled in the adequate conditions, i.e. passing by its crystallization temperature (T_c), the chains will organize themselves. Isothermal or non-isothermal processes can generate different crystallization levels, depending on the matrix specific properties (such as volume of the groups in the backbone).

Normally the crystal growth generates a spherulitic organization that arises from a central point. The organization of the chains can be represented by the fringed micelle and lamella models, being the last one the most popular (with many theory variations about how the chains can be rearranged to form the crystalline domains) [43]. The emergence of crystallinity causes many physical modifications for the material. Properties like light transparency and mechanical properties are affected by the crystallization level. In fact, one of the principal signs of amorphous - crystalline transitions is the appearance modifications in the material, transparent colorless material to opaque and white. [44]

Some studies about polycarbonate crystallinity used a combination of solvents to improve the material organization and determine crystalline parameters. The orthorhombic arrangement with dimensions of $a=1.19\text{nm}$, $b=1.01\text{nm}$ and $c=2.15\text{nm}$ were founded and an increase of density from 1.20 to 1.30 g/cm^3 could be achieved [44].

Compared to other polymers, the kinetic of crystallization for PC is very slow. In his work about PC crystallization, Sohn (2000) used induction periods of 40 – 50 hours at 185°C to cause a significant crystallinity on the polymer [20]. Münstedt (2011) could observe small signs of crystallization after 6 hours annealing [45]. Also, it seems that the use of plasticizers or nucleating agents can induce a molecular weight reduction in the polymer. In some cases, this reduction can lead the molecular weight to reach 50% of the initial value [46]. However, it is also possible to increase the crystallization kinetic by the use of solvents or proper conditions of temperature

and time. In this case, the material is no longer amorphous and starts to exhibit multiple melting peaks around 230°C [47,48].

Also as thermoplastic, PBAT is a semi-crystalline polyester that commonly presents rubbery characteristics, which confers it a low modulus value. This rubbery properties are a consequence of its lower crystallization rate and crystallinity [49]. Besides the similarities of being thermoplastic and low-crystallinity polymers, the mechanical properties of PBAT are very different from polycarbonate, which is very rigid at ambient conditions. The influence of the chains structure in their thermal properties becomes clear by analyzing the α -relaxation of both materials, a separation of more than 100°C can be founded.

Formed by two different units, DT (dimethyl terephthalate) and BA (butylene adipate), PBAT shows relatively flexible chains. The DT is normally assumed as responsible for the crystallinity present in the material and BA composes the amorphous part. However, this concept seems to be uncertain. Shi (2005) suggests that DT units can be responsible at maximum for 20% of PBAT crystallization, which necessarily makes BA units a component of crystalline arrangement in higher crystallized structures [38].

Since biodegradation processes are significantly affected by the material morphology, the control of this property is important to explain certain effects concerning biodegradability of polyesters [41]. Many studies try to control the crystallization capacity of PBAT by the addition of nanofillers such as clays [42], graphite [11] and nanocellulose [50]. As for PC, with the increase of crystallization the PBAT also can exhibit multiple melt crystalline peaks in DSC. The most plausible explanation for this fact is the formation of different populations of crystalline domains. These domains can present different levels of thermal stability and reorganization of the chains during heating of the material [48].

Stress-induced crystallization (SIC). The SIC takes place because the stretching of long chains can distort the macromolecules from their most probable conformation (an entangled conformation). In this case, a decrease in the conformational entropy can be achieved and less conformational entropy needs to be sacrificed during crystallization, making easier the process. It can happen for example during extrusion process (where a fixed stress pulls the sample), when the sample is cut or during mechanical characterization in a stress/strain test.

As mentioned above, the SIC is observed, for example, for some elastomers. The macroscopic behavior of these materials can be explained by a series of phenomena that arise during their deformation process. Among them, the stress-induced crystallization is probably the most important one. SAXS measurements for

NR compound during mechanical stress-strain tests show that polymeric chains with low molecular weight facilitate the SIC if compared to higher molecular weight chains due their higher capacity to crystallize. Also, the amount of oriented chains in the sample amorphous phase seems to not change during the test (being kept around 5% in the referenced study) because it tends to create a crystalline phase quite easily [51]. Some authors already found that the strain crystallization starts around an elongation of 400% and the maximum crystallization was defined around 20-30%. The ensuing mechanical behavior seems to not change dramatically for low filled nanocomposites. [52]

The role of nucleating agents. When some external particles are present during polymer cooling from the melt state, it can influence how the chains will be organized. A heterogeneous nucleation can occur when a filler with sufficient density (a foreign surface) is added to the polymer melt, producing a “transcrystalline” region in contact with the outside particle surface. In that case, the crystallization kinetics will be higher than for the neat or bulk polymer. However, this behavior is dependent on the matrix and filler properties.

Gray (1974) defines some principal conditions that can lead to the creation of a crystalline region in the presence of external particles as: (i) morphology rather than the surface chemistry will govern the nucleation process; (ii) presence of a temperature gradient; (iii) shear forces may induce nucleation and (iv) the presence of strain at surfaces in the viscous medium [53]. Its incorporation could lead to different crystallization paths and increase or even decrease the degree of crystallization [53,54]. Many experimental works show examples of crystallization in composites. Table III shows the variation of the degree of crystallinity ($\Delta\chi$) for some semi-crystalline polymers used as matrix. No clear relationship is found between the nucleating particle content and crystallinity. This becomes particularly true for nanoparticles, were the nucleation role of the filler is strongly dependent on the preparation of the material.

Table III. Examples of crystalline index variation after fillers addition.

Matrix	Filler	Filler amount (%)	$\Delta\chi$	Ref
HDPE	Curauafiber	30	- 6%	[55]
HDPE	CNC	3	+ 4%	[56]
PBAT	Redmud	10	- 3%	[57]
PBAT	CNF	1	+ 5 %	[50]
PVA	Carbon nanotubes	1	- 6%	[58]

However, many explanations could be found to explain a reduction in crystallinity after the filler addition. Probst (2004) justifies that lower enthalpies and

melting temperatures for filled PVA matrix can be attributed to matrix degradation. Also, the author remarks that materials crystallized from solutions present different mechanisms from those which are crystallized from the melt, the last one can present more physical obstacles [58]. The role of nanofillers as nucleating agents in composites induced during polymer melt processing will be discussed further.

Regardless the driving forces for crystallization, its extent can be confirmed by the use of different methodologies, that can be chosen according to the material properties. The most popular and simple characterization technique is based on thermal analysis (i.e. DSC). However, as discussed before, some materials have no thermal transitions that can be used to estimate this value. In this case, alternative techniques such as XRD and RMN can be used as a way to obtain these values.

3 MULTIPHASIC SYSTEMS

3.1 Composites and colloids

Composites. Owing to their viscoelastic properties, many polymers are not suitable for applications that demand high mechanical stress. In that case, the use of polymers as matrix for the production of composites can broaden polymer applications by increasing their toughness. In a general way, composite productions are based on the addition of particulate fillers into the polymeric matrix, forming a two-phases material that shows very different properties from the neat material. These fillers can originate from metallic, vegetal, glass or carbon sources. It can provide particles with

Table IV. Density and Young Modulus of common fillers.

Filler	Density (g/cm ³)	E' (GPa)
Cotton fiber	1.5 – 1.6	5.5 - 12
Carbon fiber	1.7	230 - 240
Glass fiber	2.5	70
Kevlar 29	1.44	60 - 125
Stainless Steel	7.7 – 8.1	210

very specific properties, as shown in Table IV. As a consequence, by choosing the right particle it is possible to tailor the system features.

Density, physical or chemical resistance are easily adjustable parameters directly linked to the nature of the filler.

They govern the mechanical properties and permeability of the final material [59]. However, after their life cycle these materials are normally mixed with other residues (such as food waste) hindering the recycling process and leading to land filling or incineration, causing environmental problems [60]. To avoid this undesirable side effect, more ecofriendly composites (or biocomposites) can be produced to replace these materials.

In biocomposites, vegetal fibers are generally combined with sustainable polymers to produce green materials that can readily biodegrade. Besides the easy decomposition, natural fibers can present other advantages. For example,

compared to glass or carbon fiber composites, natural fibers have higher acoustic damping, making these fibers suitable for noise attenuation [61]. They also display lower density than glass fibers that can generate beneficial applications for transportation industry.

The same kind of multiphasic material definition can be given for nanocomposite. However, in that case the dispersed phase presents at least one dimension in the nanometric scale (normally smaller than 100 nm). For these systems, the most popular fillers are cellulose, starch and chitin nanocrystals, cellulose nanofibers, carbon nanotubes, and nanoclays [52,62–67]. A deep discussion about it will be done further, with focus on cellulose nanocrystal nanocomposites.

Colloids. According to Shaw (1980), the colloid science concerns systems which contain components in the range of 1 nm to 1 μ m. Despite it was described properly by the term “microheterogeneous” it is difficult to distinguish between colloidal and non-colloidal systems. The author also states that factors that contribute to the colloidal nature are particle size and shape, surface properties, particle-particle and particle-solvent interactions.

In these systems it is important to understand the influence of aggregation on the final properties of the colloidal suspension. The aggregation can form particles with diverse forms that not necessarily correspond to the original form of the individual or primary particles [68]. This is the currently problem for nanoparticles. In this scale, the agglomeration becomes a critical parameter once it is very difficult to reverse it and separate the particles. Colloidal systems are founded in nature (natural rubber), industry (paints) and pharmaceutical areas.

A key issue with all colloidal dispersions (suspensions) is their ability to remain for long periods as systems containing single independent unaggregated particles. In general, particles with colloidal dimensions can be dispersed in a liquid medium and remain stable as a consequence of the Brownian motion. On the other hand, dispersions can often be subjected to quite adverse conditions such as high shear, addition of electrolyte, high temperatures, freezing cycles, etc. Those systems that could retain the single particle state are called colloidally stable. Whereas when particles associate to form aggregates or clumps, they are classified as unstable. The boundary between stability and instability is of major importance in the consideration of colloidal dispersions and normally can be easily achieved by parameters such as zeta potential [69].

3.2 Viscoelasticity

It can be easily observed that polymers under stress behave differently from other materials such as steel or water. These differences are based upon the molecular properties of each material, that are reflected in its mechanical and rheological properties. Unlike water or metal plates, that are formed by small molecules, polymers are formed by long chains (macromolecules) that provide to these materials very particular properties.

In materials science, maybe the most important characteristic of materials are how they behave under an applied force over a certain temperature range. When a force is applied to a body (with a well-defined area), a deformation results. The relationship between the applied force (F) and the sample cross-sectional area (A) corresponds to the stress (σ), Equation III.

$$\sigma = \frac{F}{A} \quad \text{Eq. I}$$

In traditional stress/strain tests, the deformation caused by the stress in the material, is called strain (γ) and under low strain level it is related to the original dimension of the material (y) and its variation (Δy) after the stress imposition, Equation IV.

$$\gamma = \frac{\Delta y}{y} \quad \text{Eq. II}$$

The experimental conditions under which the stress is applied can strongly affect the deformation of the material: direction, time, frequency of stress and temperature are important parameters to consider during mechanical tests. If the test is realized at constant temperature and applying a constant strain rate a stress/strain curve can be obtained. This type of test can show a linear region that obeys the so called Hook's law (Equation V). This law states that the deformation of the material is linearly related to the stress applied through a spring constant and is a characteristic of pure *elastic* materials.

$$\sigma = E \cdot \gamma \quad \text{Eq. III}$$

In this linear region we can obtain one of the most important parameters for the material characterization, the tensile modulus (also known as Young's modulus). This parameter is frequently used as a quantitative way to characterize the material stiffness. Very stiff materials are assumed as *elastic*. An ideal *elastic* material stores the energy and can restore its initial condition when the stress is no longer applied due

to the entropy (Equation VII) [5]. For materials which are completely elastic, the deformation is proportional to the applied tension, following the Hook's law. This kind of material has a tendency to have higher viscosity and longer relaxation time [70].

$$f = -T \left(\frac{\partial S}{\partial l} \right)_{Tp} \quad \text{Eq. IV}$$

where: f is the force that restores the initial condition of the elastic material (being opposed to the work), S the polymer entropy, l is the deformation, T the temperature and p the pressure (that should be constant). For polymeric materials this becomes true for temperatures below the T_g . In this temperature range the chains don't have enough energy to deform in the measurement time scale, so that $\frac{\partial S}{\partial l} = 0$.

Materials with an opposite behavior are called *viscous*. In these viscous materials there are no effects such as past memory, which means that after the load removal the material remains in the deformed state. In other words, the response of these materials to deformation is dependent only on the instantaneous values of time and deformation rate. Besides, a perfectly viscous material obeys the Newton's law. So, it means that the stress and the shear strain have a direct relationship that is called *viscosity*. The viscosity is a measure of the resistance to flow and capacity to dissipate energy that the material possesses.

The characteristics of the material, like the elastic and viscous properties, have a direct influence on the final process conditions and properties of resultant product. The mechanical properties of the material are usually evaluated by oscillatory tests. If the sample is submitted to some oscillatory solicitation (as a sinusoidal stress), its response also will be sinusoidal. However, the time-dependence for the resulting stress will depend of its viscoelastic behavior [71]. Cassu (2005) shows that the sinusoidal stress can be expressed by equation VII [70].

$$\sigma(t) = \sigma_0 \cdot \sin(\omega t) \quad \text{Eq. V}$$

In this case, the response of the material will depend on the loss angle (δ) in equation VIII and can be rewritten as (Equation IX):

$$\gamma(t) = \gamma_0 \cdot \sin(\omega t + \delta) \quad \text{Eq. VI}$$

$$\gamma(t) = \gamma_0 \cdot \sin(\omega t) \cdot \cos(\delta) + \gamma_0 \cdot \cos(\omega t) \cdot \sin(\delta) \quad \text{Eq. VII}$$

According to these equations, if the response of the material is in phase with the stress oscillation the loss angle will be ZERO and the material will present an ideal *elastic* behavior. If the response of the material is completely out of phase with the oscillatory stress the loss angle will be 90° and the material will show a viscous behavior. Clearly, polymers and polymeric composites have an intermediary behavior between the elastic-viscous extremes ($0 < \delta < 90$). This behavior is a particular

Table V. Behavior of purely elastic and purely viscous materials

δ (degrees)	0	90
$\sin(\delta)$	0	1
$\cos(\delta)$	1	0
$\gamma(t)$	$\gamma_o \cdot \sin(\omega t)$	$\gamma_o \cdot \cos(\omega t)$
Ideal behavior	Elastic	Viscous

property called *viscoelasticity*. This is summarized in Table V.

As discussed in the last section, this particular behavior is directly related to the molecular movements of the chains and their relative motion. The total chains mobility and properties define the properties to this class of materials that are dependent of external conditions such as temperature, time and even molecular weight.

Indeed, polymeric materials tend to show unusual behavior in comparison to low molecular weight molecules. Some classical examples are the capacity to some polymeric liquids to climb the agitating rod upon agitation, even against the centrifuge force, and the swelling upon extrusion through a die (Barrus effect) [72]. These phenomena are unique because they involve properties markedly different from low molecular weight solids, liquids or gases. These materials can show behaviors like rapid stretch under tension, tensile strength and high modulus (stiffness) when fully stretched, rapidly retracting and recovering their original dimensions [5].

The relationship between this elastic and viscous components of the polymer can be related to the modulus functions (E or G, were E is the tensile modulus and G the shear modulus). This modulus can be decomposed in two parts:

(i) the dynamic storage modulus E' (or G') which is a measurement of the mechanical energy that can be stored by the material upon loading and restored when releasing the stress and is related to the elastic component of the system (Equation X).

$$E' = (\sigma_o / \gamma_o) \cdot \cos(\delta) \quad \text{Eq. VIII}$$

(ii) The viscous component is given by the dynamic loss modulus E'' (or G''), that is proportional to the energy dissipated by the material (Equation XI).

$$E'' = (\sigma_o / \gamma_o) \cdot \sin(\delta) \quad \text{Eq. IX}$$

The relationship between these two components is called $\tan\delta$ (or damping factor) and can offer some important information about the chain flexibility, being

associated to the T_g . In fact, the damping expresses the capacity of the material in converting mechanical energy to heat (Equation XIII).

$$\frac{E''}{E'} = \frac{E \cdot \sin \delta}{E \cdot \cos \delta} = \tan \delta \quad \text{Eq. X}$$

A typical curve of the evolution of the storage modulus (E') with temperature is given in Figure 2. In this figure it is possible to note that E' values are dependent on temperature due to the thermal relaxations present in most polymers, as described before.

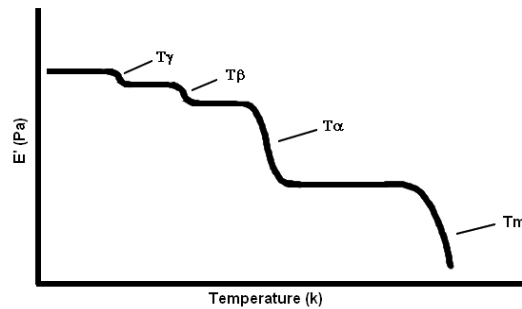


Figure 2. Evolution of the storage modulus for a polymeric material in a broad temperature range

3.3 Mechanical properties of composites

Independently of the filler chosen, the reinforcement effect caused by the filler to the polymer is based on the stress transfer mechanism from the entangled chains of the matrix to the filler. After compounding, the composite is formed by three phases: *the filler*, as the discontinuous or dispersed phase; *the polymeric matrix*, the continuous phase and the *interphase* between these phases. This last one can present distinct properties from those of the bulk matrix due to its direct interactions with the filler surface; which can be of different types: mechanical immobilization of the chains, electrostatic forces, chemical bonds, or related to the presence of internal stresses, voids or microcracks in the interlayer. Therefore, it is expected that the filler/matrix interface may have a strong influence on the viscoelastic properties of polymer composites. [73]

It is well documented that in short fiber composites the aspect ratio of the filler can influence the composite properties and control the stress transfer phenomenon. [74] The key point to understand the influence of this parameter on the composite mechanical properties is related to the difference between high aspect ratio and continuous-fiber systems. Even for very high aspect ratio composites, the material strength rarely reaches more than 70% of continuous system values for the same volume fraction. [75] An example is illustrated in Figure 3 where continuous (length/diameter - L/d - tendency to infinity - ∞), unidirectional and random systems

are compared using the same volume fraction and, in Figures 3.b and 3.c, the same aspect ratio for fiber composites.

The mechanical properties of the composite seem to decrease when the organization level of the filler in the matrix goes down, i.e. $E_{,\sigma_a} > E_{,\sigma_b} > E_{,\sigma_c}$ (where E and σ are the modulus and stress, respectively). Unfortunately, the most used processes for composites production, like casting/evaporation, injection-molding or extrusion normally generate materials with random organized filler.

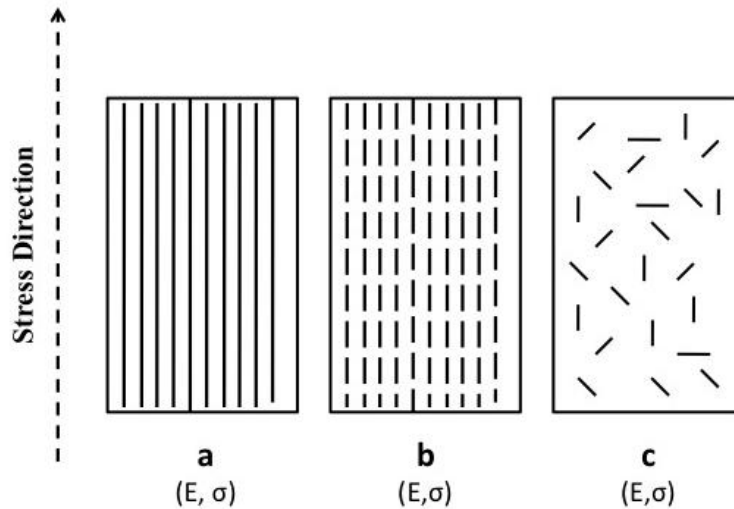


Figure 3. Aspect ratio and orientation effect on composites with a) continuous fibers, b) unidirectionally aligned short fibers and c) random short fibers system.

In systems with good matrix - filler adhesion, the stress transferred to the interfacial phase can reach a limit value that is equivalent to the yield shear strength of the matrix. As described in Figure 4, while the elongation of the composite continues, an increase in the load transferred to the filler occurs. For a perfect matrix-filler adhesion, in some point the ultimate strength of the fiber is reached and fracture occurs in the central region of the filler ($L/2$), region of concentrated stress. After the break, the cylinder generates two new shorter cylinders (and two new ends). The normal stress at the new broken end becomes zero and contains (i) stress concentration at the void created by the broken fiber, (ii) high shear stress concentration in the matrix near the fiber ends and (iii) an increase in the average normal stress in adjacent fibers. [61]

This stress increase in the surrounding fibers can cause domino effect in the composite rupture governed by: partial debonding of the adjacent fibers from the matrix, the formation of microcracks, plastic deformation of the matrix and fiber break due to high average normal stresses. These mechanisms explain why fillers with high aspect ratio are more efficient to provide mechanical reinforcement. Comparing short to long fibers, the last ones can produce a more efficient entrapment effect in the polymer, causing a kind of confinement of the polymer chains and lead to higher levels of stress transfer. [76]

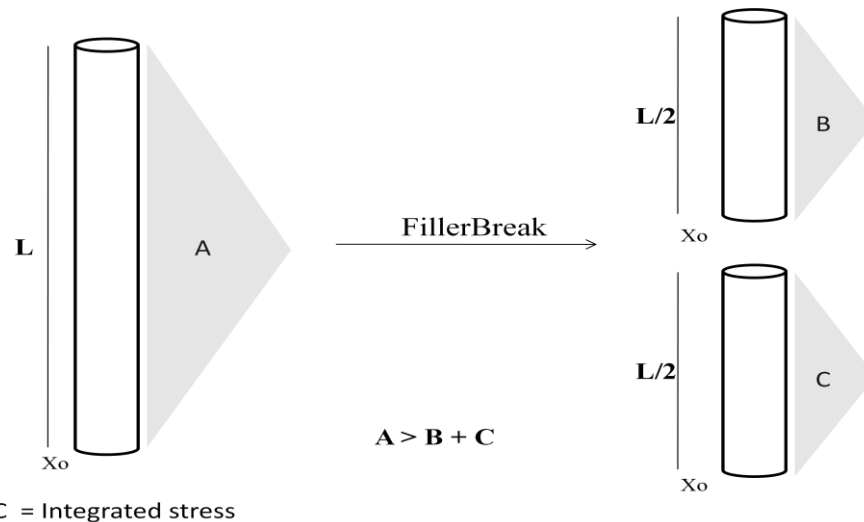


Figure 4. Representation of the stress distribution around the fiber after fracture.

Besides, in composites where a high volume fraction of filler is present, the shape of the particles is also relevant because some mechanical properties are dependent on the density and porosity of the material. Also, the shape seems to have influence on its adhesion with the polymer. That makes sense because particles with different shapes will present different surface areas for the same volume fraction. Furthermore, the mechanism of stress transfer can be modified. For example, for spherical fillers (that are symmetrical particles) we have a stress concentration at the poles of the particles (if the modulus of the filler is higher than that of the matrix) and ultimately this can cause debonding, which differs from the previous described fiber behavior under stress. [61]

3.4 Rheological properties of colloids and polymer melts

A different approach to investigate the viscoelastic properties of materials is to perform rheological experiments. In this kind of test, the stress is not applied in a one-dimensional axis in relation to the material, such in traditional tensile tests, but with an angular variation between two plates (or cones).

The rheometric tests can provide parameters related to the mechanical properties of a system and its rheological behavior. In the case of suspensions and polymer melts, the obtained data provide information about how the material flow and deform through the interpretation of parameters such as viscosity, shear stress and shear rate.

The basic concepts of rheological measurements came from the end of the XVth century. At the time, Newton defined the viscosity of a fluid as “the resistance of its molecules to flow due to internal friction”. In its mathematical definition, Newton used a system based on two plates to describe the system (Figure 5).

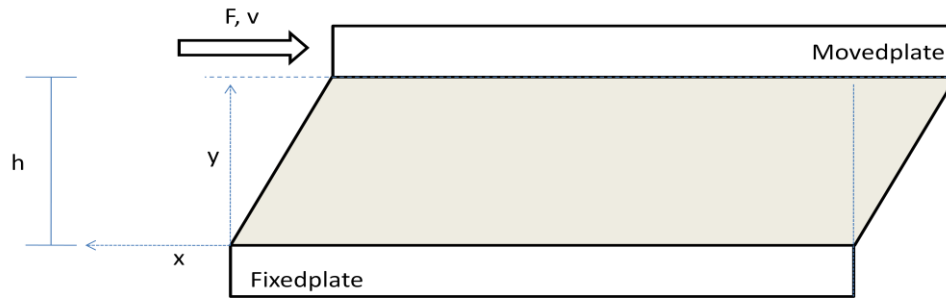


FIGURE 5. Parallel plate model.

In this model, a top plate with an area A (m^2) is moved with a velocity V (m/s) by a force F (N), while the bottom plate remains in a fixed position. In that situation the velocity profile is linear in y direction and the velocity gradient dv/dh is constant. The force per area (F/A) required to keep the relative velocity between the plates is directly proportional to the velocity gradient. This proportionality is provided by a coefficient, the viscosity (η), Equation XIII.

$$\frac{F}{A} = \eta \frac{dv}{dh} \quad \text{Eq XI}$$

where F/A is known as shear stress (τ, σ) and dv/dh as shear rate ($\dot{\gamma}$) from which it is possible to obtain the Newtonian equation for viscosity (Equation XIV).

$$\eta = \frac{\tau}{\dot{\gamma}} \quad \text{Eq XII}$$

As extention of these equations, the discussion about elastic (such as metals) or viscous (such as liquids) materials could become quantitative. Some basic ideas are in Equations XIII and XIV.

$$\sigma = \eta \cdot \dot{\gamma} \quad \text{Eq. XIII}$$

$$\sigma = G \cdot \gamma \quad \text{Eq. XIV}$$

where: σ is the stress, η is a constant called viscosity, $\dot{\gamma}$ is the shear rate, G is the shear modulus and γ is the shear deformation.

Rheological behavior. The fluids which behavior can be described by Equation XIV are called Newtonian fluids. In this kind of flow, the viscosity value is constant over the whole shear rate range. This behavior is quite similar to the one presented by elastic materials that obey to the Hook's Law. Fluids that present a nonlinear behavior are called non-Newtonian.

As described before, the fluids are one limit case in materials properties (being opposed to elastic materials) and present a *viscous* behavior. These systems are

represented by materials that tend to flow (under a certain force and temperature), being classified as:

- (I) Plastic fluids (Bingham fluids), having a yield point with pseudoplastic behavior;
- (II) Newtonian, that show a linear behavior;
- (III) Pseudoplastic, fluids get thinner as shear increases;
- (IV) Dilatant fluids, increase their viscosity as shear rate increases.

These characteristics can be represented by the curves in Figure 6.

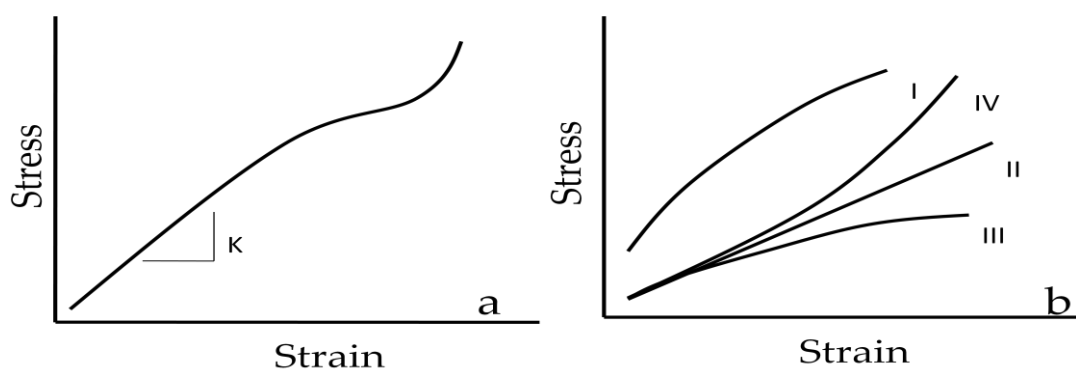


Figure 6. a) Hook's Law for elastic materials and b) Newtonians and non-Newtonians behaviors.

For many real fluids a critical level of stress is needed before the flow initiation. This critical point is called *yield point* and once this point is reached the fluid begins to flow. A pure *Newtonian* behavior is, in general, a property of pure liquids where η is a well-defined quantity for a given temperature and pressure, which is dependent of τ and $\dot{\gamma}$.

The linear *Newtonian* behavior is not a normal characteristic for structured fluids. These complex systems have a tendency to not obey a simple linear relationship between the applied stress and the flow. *Pseudoplastic* materials do not have a yield stress and behave in a non-linear way, flowing instantaneously with the stress application and showing a decrease in the viscosity with shear rate increase (shear thinning behavior). An opposite phenomenon is characteristic on *dilatant* fluids, where an increase in the viscosity occurs with shearing increase (shear thickening). [77] Despite temperature and shear rate effects, the viscosity of some materials also changes with time. The shear rate can break the internal structure of these fluids and a defined time is needed to rebuild this network and stabilize the viscosity values. When a steady plateau is reached in the viscosity value it means that equilibrium of structures construction and breakdown was established. This phenomenon is called *thixotropy* (Figure 7.a).

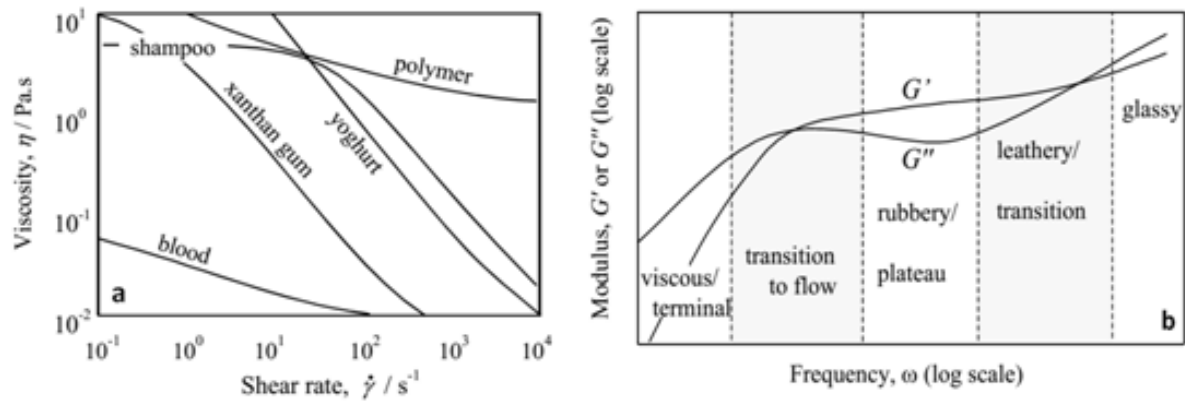


Figure 7. Common flow and oscillatory tests response. [78]

In complex systems, the presence of fibers and other solid particles can change the rheological behavior of liquids. Bulk rheological properties of dispersions are dependent of the net potential energy and have their flow behavior controlled by thermodynamic (i.e. electrostatic and steric repulsion) and hydrodynamic interactions, besides the Brownian motion. Hydrodynamic disturbance of the flow is caused directly by the presence of particles and, as particles interactions, it can increase the viscosity of the suspension. [79]

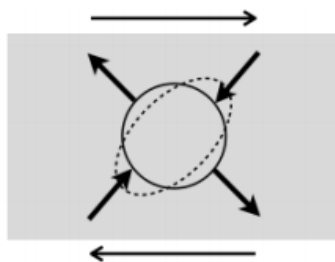


Figure 8. Stress relation of particles in fluids. [80]

The effect of particles addition to viscosity was resolved by Einstein that described it, for diluted solutions, by Equation XV. During shear, a determined spherical volume of liquid becomes an ellipsoid due to the imposed stress that causes disturbance to the quiescence conditions of the system, corresponding to the dotted line in Figure 8. If the volume is replaced by a solid sphere, the particle will not deform and will apply a stress on the liquid (arrows). The total sum of stress produced by the single particles causes a viscosity increase. [80]

$$\eta = \eta_s \left(1 + \frac{5}{2} \phi\right) \quad \text{Eq. XV}$$

This equation is independent of particle shape for diluted suspensions, i.e. there is no interaction among the particles. However, for more concentrated systems the concentration does matter and the viscosity variation is defined by different equations where a form factor is defined. [78]

These suspensions can present two time dependent-phenomena: shear thinning or shear thickening. In the first one, a decrease of the apparent viscosity occurs within the time evolution. This effect is particularly common in systems with asymmetric particles that can perturb the flow for low shear rates and have a

tendency to become ordered when the shear rate increases, causing a viscosity decrease. The second one is the opposite effect, normally associated to dilatation of the material where surface tension makes difficult the movement of the particles due to the high level of packing.

Small amplitude oscillatory shear (SAOS). Besides viscosity tests, oscillatory tests are also important because some fluids, such as polymers, can present a viscoelastic response when submitted to the imposition of a sinusoidal stress.

As a result, the fluid can present a liquid or gel-like behavior, depending on its microstructure. An example of response obtained for this kind of tests is given in Figure 7.b. During the measurement the values of the storage (G') and loss (G'') modulus can be observed as a function of a defined angular frequency range. These experiments are designed to measure the strength of a suspension, molten composite or polymer. In a suspension or molten composite, for example, the level of the storage modulus is related to the gel strength of the system and its behavior can be classified as; liquid: $G'' < G'$ (low volume fraction) or gel, where $G' \gg G''$ (high volume fraction).

The formation of a three-dimensional network structure can occur due to the association of particles within the liquid phase. Solid fillers dispersed into a liquid phase provide the largest component effect in fluids that show deviation from a Newtonian behavior and become non-Newtonian. [81]

Besides viscosity that is dependent of the shear rate, the shear history can impact the rheological properties of non-Newtonian fluids. These systems can be affected by previous stress to which it was exposed. Unlike the viscosity tests, oscillatory measurements do not destroy the fluid structure. It is not a continuous rotational test and the experiments are performed in the linear viscoelastic range of the fluid. [82]

For polymers and composites at higher temperatures (i.e. after the material fusion), the oscillatory tests can present well defined coefficients. In the case of polymers, the characteristic slope of the first part of the G' vs ω curves is equal to 2 (and the slope for G'' vs ω is equal to 1) and a deviation from these values can be a sign of micro-heterogeneities. [83,84]

These specific values result from the reptation theory. Proposed in the 80's [85], it is based on the assumption that the polymer chains are confined in a tube, whose edges are defined by the forces imposed by neighboring chains. This theory was based on the inflexibility of the chains, caused by long term entanglements that prevent the chains to present nodes or even to fold and cross imaginary plane twice [86].

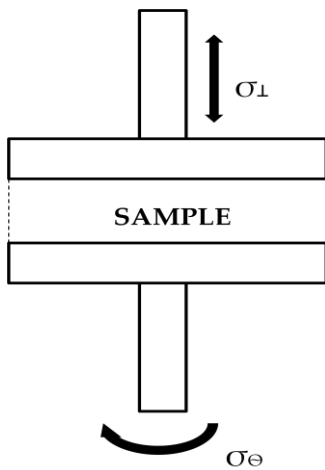


Figure 9.2D-SAOS
simplified representation
of device.

On the other hand, it is common to observe deviations from these values at lower shear rates for nanocomposites. Hassanabadi (2014) had found a well-defined value of $G' \sim \omega^{0.5}$ for materials that reach rheological percolation, independently of the nature and form factor of the particle. [87]

Also, for distinct mechanical tests it's important to note the use of different definitions of the strain. In tensile tests the strain is defined as the length increase fraction, while for shear (rheometric) tests the strain is the distance moved by the plate divided by the sample thickness. In both type of tests, the stress is defined as the force divided by the area and the modulus is the stress divided by the strain. The relationship between

the tensile and shear modulus is expressed in Equation XVI.

$$E = 2(1 + \mu) \cdot G \quad \text{Eq. XVI}$$

Where μ is the Poisson's ratio. Experimentally, this number is very close to 0.5 for rubbery materials and slightly less for thermoplastic polymers. So, the equation becomes $E = 3G$ [88].

2D-SAOS. As an extension of the traditional oscillatory tests, some authors proposed the SAOS experiments in two dimensions (2D-SAOS) [89,90]. As described by Mobuchon et al. (1997), the bidirectional flow is the result of coupled axial (γ_{\perp}) and conventional (γ_{θ}) oscillatory deformations, that are described by the follow equations [91].

$$\gamma_{\theta} = \gamma_{\theta}^0 \sin(\omega t) \quad \text{Eq. XVII}$$

$$\gamma_{\perp} = \gamma_{\perp}^0 \sin(\omega t + \delta_{\gamma}) \quad \text{Eq. XVIII}$$

This experiment is based on the imposition of a oscillatory stress by superposing the oscillatory flow in the vorticity direction, being different from parallel superposition, where the flow and superimposed shear are coupled [92]. Figure 9 represents the experimental set-up of the adapted equipment.

Since the orthogonal oscillation is mechanically performed by an adaptation of the traditional rheometer, Kim et al (2013) have shown a limitation on the orthogonal oscillations measurements to approximately 10 rad/s. This Z axis oscillation seems to show some influence of inertial effects over this frequency. [92]

4 CELLULOSE NANOCRYSTALS: PREPARATION AND PROPERTIES

4.1 Cellulose biosynthesis and crystallinity

Cellulose extraction. Being a component of natural fibers, cellulose is the most abundant polymer on Earth. It is composed of D-glucopyranose ($C_6H_{11}O_5$) units linked through $\beta(1,4)$ links, forming cellobiose, the repeating unit of cellulose. Even if it is difficult to determine experimentally the degree of polymerization of native cellulose, it is supposed to be close to 10.000, corresponding to a molecular weight around 3.2×10^6 g.mol⁻¹. [93] The formed rings of cellulose are in the chair conformation and its hydroxyl groups in equatorial positions, Figure 10, while the hydrogen groups are in axial position.

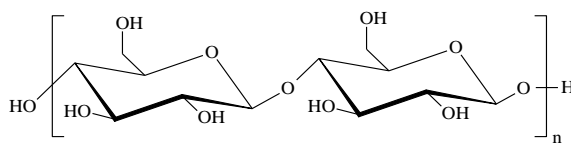


Figure 10.Representation of cellulose monomer (cellobiose) structure.

Normally embedded in an amorphous matrix of hemicelluloses, resins and lignin, many authors suggest methodologies to isolate cellulose from their natural matrix environment before its use. It generally involves basic and/or oxidative treatments [94,95] that can affect the morphology of cellulose, or acidic treatment with peracids. [96,97] This step is very important because it can change the crystalline organization and polymorphism of cellulose, as well as chemical and thermal stability of the material. Classically, the matrix material can be removed to extract cellulose from plant fibers using chemical treatments consisting of alkali extraction and bleaching. The alkali extraction treatment (usually with 2% NaOH at 80°C) allows the removal of soluble polysaccharides. The subsequent bleaching treatment removes most of the residual phenolic molecules like lignin or polyphenols.

Cellulose biosynthesis. Inside the plant, cellulose chain organization forms a complex structure of layers that have different functions and physical-chemical properties. Figure 11 represents the organization of the cellulose inside the cell wall in a coniferous. The second wall S2 of cellulose tends to be more packed while S1 and S3 layers are thinner and had a “cross helical” organization. Some studies indicate a prevalence of lignin in the intermediary layer S2 and in the primary wall, especially in leaf fibers and hardwoods.

The degree of polymerization (DP) of cellulose in nature varies according to the plant species and where it is located. For example, the primary wall DP is lower and

more heterogeneous compared to the secondary cell wall. In the first one, shorter cellulose chains can occur and their DP values are in a range of 2 000 to 6 000, while in the second one (that can be responsible for until 94% of the cellulose composition of the plant) there is an increase in the homogeneity and the DP can reach up to 14000. [98,99]

The level of DP present in each layer of the plant structure is a consequence of different agents acting during biosynthesis of cellulose. By the way, cellulose biosynthesis is a complex process that involves, at least 10 complexes (groups of particles) present in the plasma membrane with functional specialization roles in gene expression, regulation and, probably a catalytic function. [100]

These complexes are visualized as rosette-like structures with 20–30 nm in diameter. Some evidence suggests that cellulose is formed in the plasma membrane or outside it and the terminal complexes seem to be associated with the microfibril ends, being related to its elongation. This task is a very complex process once the microfibrils have between 30 and 200 chains that should be elongated at the same rate. [99,101]

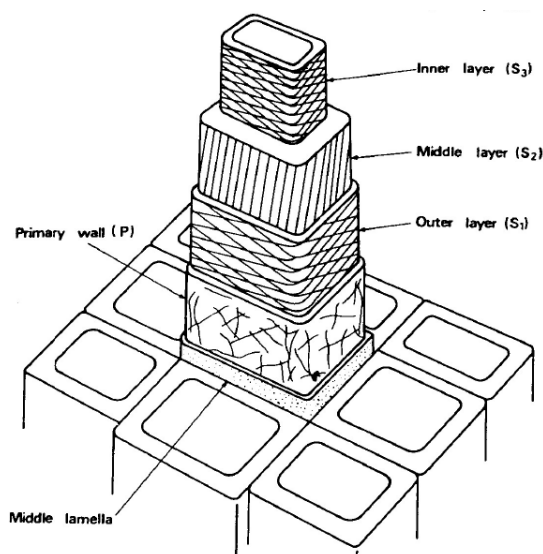


Figure 11. Illustration of the cell wall structure.

The natural synthesis of cellulose is responsible to give many particular characteristics to this material. In some species there is a variation when the secondary cell wall is deposited. This stage can occur during or after the plant growing and with or without the presence of lignin. This is why among the same species, even the cellulose formation is strongly dependent on parameters like soil, age of the plant, climate conditions, etc.

Crystal formation. Another important event happens during the cellulose biosynthesis. In addition to the chain prolongation, the carbohydrate molecules have a tendency to organize themselves as crystals. This happens because along the cellulose chain organization a hydrogen bond complex based on the –OH groups, available on the rings, is formed resulting in the formation of a network of intra- and intermolecular bonds. It causes the crystallization that follows the addition of glucose units to the chains by the terminal complexes, where the present proteins govern the microfibril crystalline form. [99]

In fact, the cellulose structure is a classic example of supramolecular system. Interactions such as hydrogen bonding, van der Waals, or dispersive forces (i.e. non covalent interactions) are intrinsically related to the cohesion between cellobiose monomers that result in fiber-like structure of cellulose and its nanometric crystalline domains. [102]

Thermodynamically, the crystal formation can be explained by the competition between entropy and enthalpy effects during the packing of cellulose chains. According to Qian (2005), the hydrogen bonds are stronger in the cellulose crystal in comparison to the single chains or sheets [103]. This indicates that during the packing of the chains, the –OH groups are closer. In that situation there is a loss in the conformational degree of freedom of the molecules, causing the formation of hydrogen bonds as compensation. The formation of bonds is an exothermic process ($\Delta H < 0$) that causes a decrease in enthalpy and this can compensate the rigidity and decrease of the entropy. It can keep the system stable with a negative overall energy ($\Delta G < 0$). As expected by the Gibbs equation (Equation XIX).

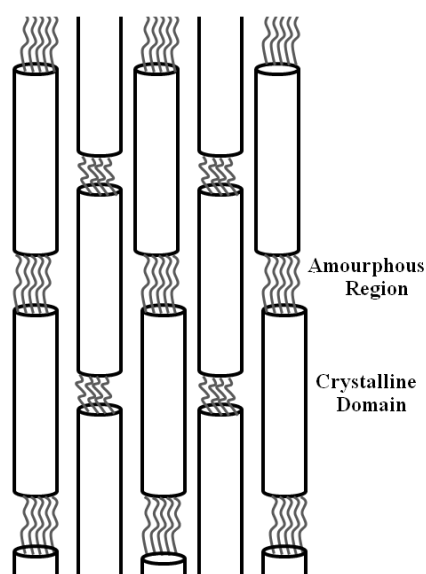


FIGURE 12. Schematic organization of crystalline and amorphous domains in cellulose fiber

$$\Delta G = \Delta H - T\Delta S \quad \text{Eq. XIX}$$

The ordered crystalline structures are around 2-20 nm in width and up to few microns for the length. These crystalline domains are alternated with amorphous regions in the fibril structure. For some plant species these amorphous regions can represent up to 50% of the structure, while in bacterial cellulose and cellulose extracted from some algae the crystalline domains corresponds to almost 100% of the fibril [104].

These crystalline domains are almost defects-free. The interspersation happens because the crystal size is able to increase by the deposition of new monomers, but after some point the

hydrogen bonds can no longer compensate these effects. At this time, the system will be dominated by the entropy effects, causing disorder. This can explain the regular amorphous regions in the cellulose structure that can be observed in Figure 12.

Hydrogen bonds and mechanical properties. More than being responsible of the formation of crystalline domains in cellulose, hydrogen bonds are responsible for the life as we know. The energy values of these bonds can vary between 2 and 45 kcal.mol⁻¹ depending on the physical state of the sample and charge of the donor/acceptor atoms, which can be classified as weak, low barrier and very strong. This last one can be present for oxygen atoms, at a distance smaller than 2.5 angstroms.[102] Despite its lower energy values - much lower than for covalent bonds - its role is remarkable in the properties of water, as cohesive force that keep wood, concrete and our body together. In some processes, especially biological processes, the small value of these bonds become an advantage since it allows the quick changes of bonds in the structure, making easy the activation/deactivation of some processes.

In polar covalent bonds such as O-H, N-H and F-H, the gap in the density of charge between these two atoms is unusually large. Once the H atom is particularly small, it allows to other atoms to get close to this polar group (e.g. O-H). This results in secondary bonds that can be strongly attractive or moderately directional, orienting the neighboring molecules in solid, liquid or gas states [105].

In cellulose, hydrogen bonds are responsible for particular characteristics such as insolubility and mechanical properties. It is known that uncharged cellulose molecules tend to present poor solubility in aqueous solutions at moderate pH (4 – 10) and ionic strength (0.1 - 10 mM). However, the introduction of negative charges can increase its solubility, depending on the solution conditions [106]. It happens due to the separation of the chains by a swelling effect decreasing the influence of the hydrogen bonds in the microstructure.

Concerning the mechanical properties, many authors tried to estimate the mechanical constants of cellulose microfibers between the decades of 60's and 90's. Despite obtaining some discrepant values, ranging between 70 and 296 GPa, they were able to figure out the importance of the hydrogen bonds in these properties. Without the consideration of hydrogen bonds, some theoretical calculations showed a decrease of almost 40% in the young's modulus of the fibers. [107]

To explain such a great influence in the final properties of the material a synergism should occur between the hydrogen bonds and the covalent bonds present in the molecule. Altaner (2014) states that, under strain, the elongation of the cellulose chains can stretch the zig-zag conformation. After that, the glycosidic chains

start to be elongated and the hydrogen bond between O(3)H – O(5) becomes longer, but the O(6)H – O(2)H bond keeps its dimensions. Figure 13 suggests that if the molecule pivot was the glycosidic oxygen (O1) a stretch that elongates the O(3)H – O(5) link should shorten the O(6)H – O(2)H link. The maintenance of the dimensions in the O(6)H – O(2)H bonds suggests that the glycosidic bond can slightly stretch itself and cancel the compression of that bond. Alternatively, a rotation of the bond C5-C6 can also provide the needed mobility to keep the O(6)H – O(2)H distance. The structure of the cellulose chains seems to be defined by the glycosidic bond, but the cooperation of the O(3)H – O(5) is important to keep the tension stiffness of the molecules and that hydrogen bond will not break until the glycosidic bond itself breaks. [108]

Theoretical calculations performed by Bergensträhle (2008) have shown that the different hydroxyl groups present on cellulose chain act by forming H-bonds at different levels. By these calculations, O2H2 group can perform an average number of 1.6 bonds with the surrounding medium, against 1.8 for O6H6. Due to its intramolecular character, the average interaction number of O3H3 is only 0.6 [109].

Cellulose polymorphism. The crystalline domains of cellulose can be found in six different polymorphic conformations (I, II, III₁, III₁₁, IV₁, IV₁₁), i.e. it can be organized in different ways according the chains arrangements. The most common cellulose polymorph in nature is cellulose type I, explaining why it is the focus of major studies in the area. Nowadays, it is known that type I cellulose is also divided in I α and I β and normally plants and bacteria presents a mixture of them in its composition. Simon (88) postulated that the form I α is present at the surface of the crystalline regions while the I β form can be founded in the center of the structure.

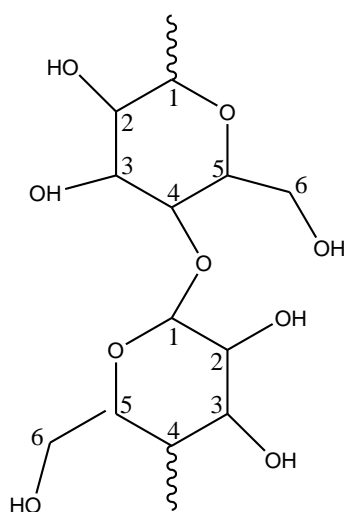


Figure 13. Cellobiose PlanarRepresentation.

The first one is more common in primitive organisms and the second one in higher plants [110].

Despite cellulose I abundance, the most stable polymorph is the type II. This polymorph is more thermodynamically favorable and normally in vitro crystallization of cellulose gives rise to it instead of cellulose I. [99]

The second most studied cellulose form (cellulose type II) can be obtained from cellulose I by regeneration of mercerization. The most popular technique to interconvert cellulose is the mercerization process. Developed by John Mercer, this method consists in transforming cellulose I to cellulose II using

concentrated NaOH solutions. Since the 80's Sarko, Nishimura and Okano have studied the mechanism involved in the mercerization process. [111–114] According to these studies, the interconversion of crystalline phase from cellulose I (with parallel chains) to cellulose II (antiparallel chains) passes through a kind of intermediary state called Na-Cellulose (antiparallel chains), that is an organized state of swollen cellulose.

There are different theories about the exact mechanism of cellulose conversion. In general terms, some authors suggest that during the mercerization process the hydrogen bonds network is disrupted and long chains can undergo a conformational change through folding. [110]

Other authors suggest that the crystalline conversion is, in fact, dependent on the amorphous phase present at the surface of cellulose crystalline domains. In this phase it is possible to find chains in parallel and antiparallel conformations (*up* and *down* directions). These randomly positioned chains are fundamental to the progressive deposition of the antiparallel crystalline domains.

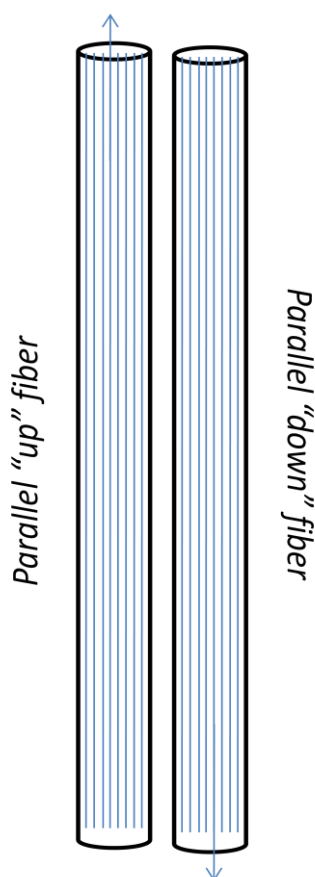


Figura 14. Parallel fibers on *up* and *down* direction.

Also, besides the parallelism between the chains in the cellulose nanofibers, these fibers themselves can be in opposed directions (Figure 14). When the fiber swells, during the mercerization process, the cellulose I chains are put away one from each other and slowly the antiparallel Na-Cellulose begins to be formed in a crystal-to-crystal phase transformation, with cellulose I crystalline domains beginning to diminish in size [115]. Independently of the theory, the new II antiparallel structure seems to have lowest energy, being stable in the presence of NaOH and when dried.

The Na-Cellulose becomes cellulose II with the NaOH removal. The conversion $I \rightarrow II$ is irreversible and depends on the amorphous content of the fiber, type II cellulose being less crystalline than type I. Experimentally this conversion is dependent on the NaOH concentration, temperature, time and cellulose mechanical disposition, once the conversion seems

to be faster for non-stressed samples due to the higher chain mobility.

During the regeneration process the cellulose fiber is dissolved in suitable conditions to be regenerated (recrystallized) by adding a non-solvent. This process is normally used in studies of cellulose recrystallization as a way to obtain information about morphology, texture and many properties of the new regenerated material. Regenerated cellulose presents a XRD pattern characteristic of cellulose II polymorph. However, in these fibers the cellulose chains seem to be perpendicular to the main axis of the fiber and not parallel as for other polymorphs (Figure 15) [116].

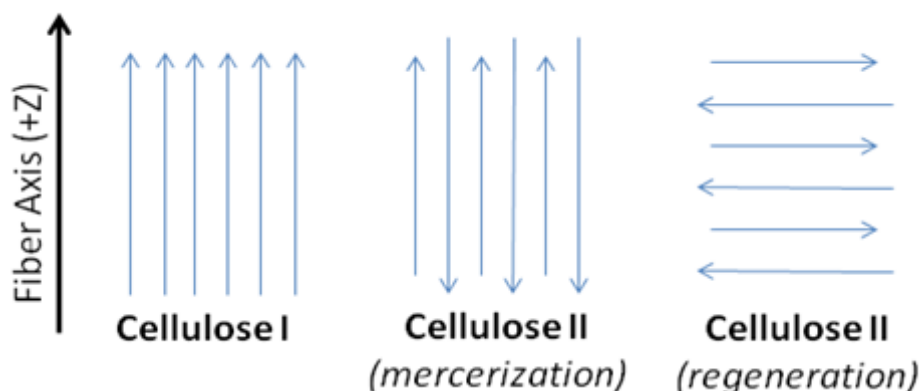


Figure 15. Schematic representation of parallel and anti-parallel cellulose chains

Nanomaterials derived from this cellulose can present interesting characteristics of dispersion. Contrarily to pristine cellulose, that is difficult to disperse/redisperse in water (which causes a limitation in production of composites) the regenerated cellulose seems to be easily dispersed in the solvent [117].

Recently, some researchers were able to produce and isolate different polymorphs of cellulose nanomaterials starting from the same source [118]. Also, unpublished data from our group show that it is possible to produce nanocrystals with polymorphism type II by previous fiber mercerization or regeneration during hydrolysis. These materials present very different aspect ratio, thermal stability and molecular arrangement. The application of cellulosic nanomaterials with different properties will be discussed along the chapter.

Despite the technique used to obtain cellulose II polymorph, it is possible to see that the crystalline domains can show different form factors from the rodlike structure founded in cellulose I. Some different cellulose nanocrystals images are shown in Figure 16. It is possible to observe the influence of the source and polymorphism on the final shape and size of the nanoparticles.

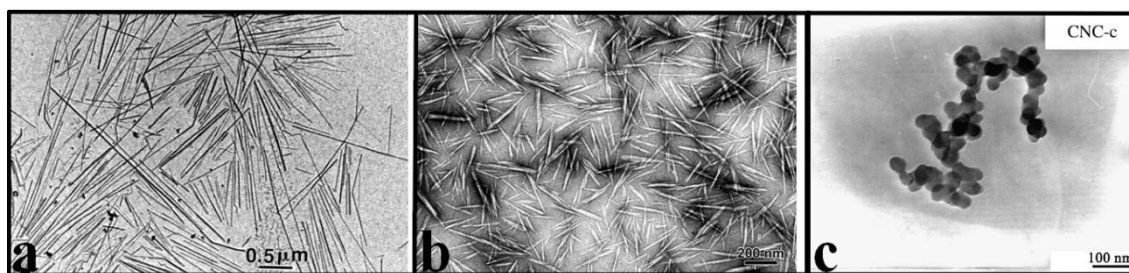


Figure 16. TEM images of cellulose nanocrystals type I for (a) tunicate[119] and (b) ramie [120]; and type II (c) Cotton [121].

Different polymorphs can present distinct reactivity and composite applications. Some crystalline dimensions can be founded in Table VI and the preparation techniques will be discussed in sequence.

Table VI. Dimensions and form of some cellulose II nanomaterials.

Source	Shape	Dimensions (nm)	Reference
Wood pulp	Rodlike	2 - 6 (D); 25 - 50 (L)	[122]
Microcrystalline cellulose	Quasi-spherical	200 (D)	[117]
Microcrystalline cellulose	Spherical	60 (D)	[121]
Wood cellulose	Rodlike	4 - 7 (D); 100 - 200 (L)	[123]
Cotton	Rodlike	14 (D) - 76 (L)	[124]
Lyocellfibers	Spherical	45 (D)	[125]

4.2 Cellulose hydrolysis

The preparation of cellulose nanomaterials can be performed by different techniques. The use of temperature and pressure[126], acid [127], mechanical and enzymatic treatments [128,129] can generate cellulose nanocrystals or nanofibers. For cellulose nanocrystals, the amorphous regions of the fiber are removed and the crystalline domains are isolated as a rigid nanorod particle. The preparation of cellulose nanofibers is based on the defibrillation of pristine cellulose and can preserve the amorphous part in order to show a higher length and flexibility.

In any case, the preparation of different classes of particles is possible due to the reactivity of some groups from cellulose. A good example is the utilization of acids or Tempo-mediated oxidation to perform or facilitate the hydrolysis/defibrillation of the chains at different levels.

Cellulose reactivity. In the beginning of the 70's, a series of works about cellulose were published by Rowland. These publications explored the role of the hydroxyl groups in the reactivity and crystallinity of the cellulose fiber.

In a paper published in 1972 the different reactivity of the hydroxyl groups (linked to C2, C3 and C6) present in crystalline and amorphous regions was studied for cellulose derived from cotton. [130]

In highly ordered domains the hydroxyl group in the C3 position is almost completely unavailable to react due its contribution to intramolecular hydrogen-bonds. Experimental results also showed an intermediate reaction rate for OH(6) and a high reaction rate for OH(2) group. The last one was generally assumed as completely substituted and used as reference value to estimate the rate reaction of the other hydroxyl groups. The amorphous domains were proposed as regions with very different surfaces compared to crystalline domains. These regions have just a few hydrogen bonds OH(3) – O(5) and O(6) – O(1) and even that bonds are weaker than in crystalline regions, being more accessible. In these regions, experimental results showed similar reaction rates for C2,C3 and C6 hydroxyl groups.

Other studies applied the same methodology to cellulose coming from different sources and very different availabilities were found for the same hydroxyl groups. The rayon fiber and *Valonia ventricosa*, showed a completely different relation between O(3)H/O(2)H and O(6)H/O(2)H due the difference in the hydrogen bonds disposition for cotton family. Different sources, like sisal, showed low availability for O(3)H and O(6)H due their higher order of crystallinity, the opposite occurring in wood Kraft pulps. [131]

The meaning of Rowland results seems to be that the characteristic of hydroxyl groups available to react are ruled by the order level in the domain and the cellulose source. The first one is related to the intermolecular distance that influences the packing of the chains, and the hydrogen-bonds force in the intramolecular bonds. The second one its related to the type of interaction O(x)H – O(y)H present in the microfiber. The hydrolysis of cellulose which aims in isolating the nanocrystals is strongly influenced by these availability changes in cellulose hydroxyl groups. Even if the amorphous regions seem to have lower intramolecular hydrogen bond interaction (having similar availability for all hydroxyl groups) the surface of the crystalline domains can react in different ways to different experimental conditions. Thus, the degradation of the crystalline domain and the production of sugars should be avoided by choosing the best parameters according to each cellulose source.

Acid Hydrolysis. The extraction of cellulose nanocrystals from cellulosic fibers usually consists in an acid-induced destructuring process, involving diffusion of acid molecules into cellulose fibers and following cleavage of glycosidic bonds. This acid hydrolysis step is followed by centrifugation, dialysis and ultrasonication. Different strong acids have been shown to successfully degrade non-crystalline (amorphous)

regions of cellulose fibers to release crystalline cellulosic nanoparticles, such as sulfuric, hydrochloric, phosphoric, hydrobromic, nitric acids, and a mixture composed of hydrochloric and organic acids [98].

Due to the different cohesion forces and accessibility of the acid into the fibers, different natural fibers demand different experimental conditions to obtain the longest and most crystalline as possible nanoparticle. Some kinetic and theoretical studies have been used to adapt the best hydrolysis conditions and establish some parameters. [132] Nevertheless, the hydrolysis treatment to prepare cellulose nanocrystals with sulfuric acid has been extensively investigated and appears to be the most effective method. An extended list of sources used for production of cellulose nanocrystals can be found in Appendix B. Some examples of experimental conditions are reported in Table VII.

One of the main reasons for using sulfuric acid as a hydrolyzing agent is that if nanocrystals are prepared using hydrochloric acid, their ability to disperse in polar solvents is limited and the suspension is unstable tending to flocculate. Indeed, during hydrolysis, sulfuric acid reacts with the surface hydroxyl groups via an esterification process allowing the grafting of anionic sulfate ester groups ($-OSO_3^-$). These sulfate groups are randomly distributed on the surface of the cellulosic nanoparticle. The presence of these negatively charged sulfate ester groups induces the formation of a negative electrostatic layer covering the nanocrystals and promoting their dispersion in water. The high stability of sulfuric acid-hydrolyzed cellulose nanocrystal suspensions results therefore from an electrostatic repulsion between individual nanoparticles. However, it compromises the thermal stability of the nanoparticles.[133] Nevertheless, the stability can be achieved by performing a neutralization of the nanoparticles suspension by sodium hydroxide (NaOH) [120].

Table VII. Common experimental conditions to perform fibers Hydrolysis

Source	Acid	[Acid]	Time	Temp. (°C)	Ref.
Bacterial cellulose	HCl	37 wt%	48 h	60	[64]
Bamboo	H ₂ SO ₄	64 wt%	130 min	45	[134]
Capimdourado	H ₂ SO ₄	65 wt%	45 min	75	[135]
Cassava	H ₂ SO ₄	6.5 M	20-40 min	60	[136]
Chili leftover	H ₂ SO ₄	64 wt%	45 min	45	[137]
Cotton	HCl	4 M	3 h	80	[138]
Kenaf	H ₂ SO ₄	65 wt%	variable	45	[139]
MCC	<i>Pressure: 20.3 MPa</i>		60 min	120	[126]
Paper	H ₃ PO ₄	6.2 – 10.7 M	variable	variable	[140]
Sisal	H ₂ SO ₄	60 wt%	45 min	30	[141]
Soyhulls	H ₂ SO ₄	64 wt%	30-40 min	40	[127]
Sugarcane	H ₂ SO ₄	6 M	30-75 min	30	[142]
Sugarcane	C ₂ H ₄ O ₂ / HNO ₃	80 /70 wt%	20 min	110	[143]
Tunicates	H ₂ SO ₄	48 wt%	13 h	55	[144]

Other acids also can promote modifications in the crystalline content of the nanocrystal. For example, it seems that Cl^- and CH_3COO^- can show higher inclination to promote the breakage of the hydrogen bonds (compared to SO_4^{2-} and PO_4^{3-}). When this happens in the crystalline regions of cellulose, it facilitates the swelling of the crystal and, as a result, the isolated cellulose nanocrystal demonstrates a lower crystallinity index [145].

Regenerated cellulose seems to present (as cellulose III) a crystalline structure with primary hydroxyl groups relatively more accessible and therefore could be more available for reactions in comparison to cellulose I. Also, it is not uncommon to found a mixture of cellulose I and II nanocrystals after hydrolysis [127]. This probably happens due the reactional conditions that can cause some solubilization of the cellulose chains leading to the formation of regenerated cellulose by the process described in the previous section.

The nomenclature used to designate these acid-hydrolyzed crystalline cellulose nanoparticles has been unclear for a long time and different descriptors including cellulose whiskers or nanowhiskers, nanocrystalline cellulose or even cellulose microcrystals have been used in literature. However, recently TAPPI (Technical Association of the Pulp and Paper Industry) has proposed to standardize the terminology (Standard Terms and Their Definition for Cellulose Nanomaterial - WI 3021). Nomenclature, abbreviation and dimensions applicable to each sub-group are reported in Figure 17. Today, the rodlike crystalline domains are suggested to be called cellulose nanocrystals.

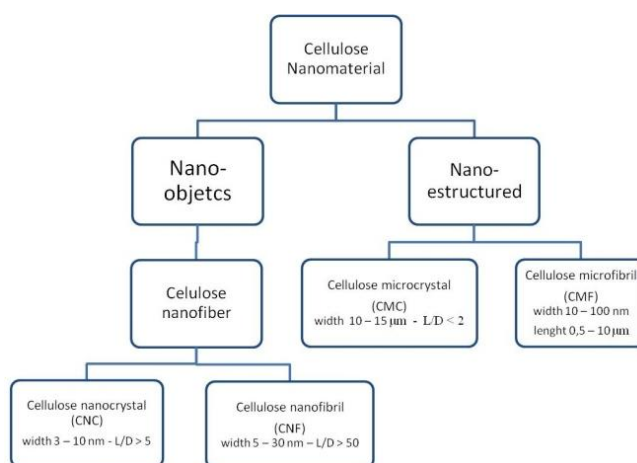


FIGURE 17.Standard terms for cellulose nanomaterials (TAPPI WI3021).

The outstanding properties of cellulose nanocrystals are already well known. Renewable, strong, lightweight and low-cost nanomaterials, they are good candidates to be used into renewable polymer matrices as filler to produce sustainable, and environmentally friendly nanocomposites.

Besides the packing level of chains organization, CNC particles present another particular property which distinguishes them from the amorphous phase of cellulose. In the amorphous domains of cellulose, the mechanical properties are isotropic, i.e. the same elastic modulus is found in any direction. CNC have three different values of elastic modulus, creating new properties in dependence of its orientation. However, the mechanical properties of the amorphous phase can vary with the humidity content due its capacity to swelling, an effect that is minimized for CNC. [132]

On the other hand, the swelling of the crystalline domains can just occur in specific conditions (such as during the mercerization process). Recently, Lazko (2014) used ionic liquids to swell the cellulose and proceeded the acid hydrolysis in mild conditions, using from 1 to 4% sulfuric acid [146]. The amorphous part of cellulose consists probably of chains present at the surface of the microfibrils. For small microfibers the surface area is approximately equal to the amorphous content. However, even this surface area (amorphous) possesses some degree of organization. The amorphous cellulose cannot be considered as an amorphous material by definition. [99]

4.3 A background about surface energy and nanomaterials

In 1960, Feynman described, in a seminal work, the hole of the Van der Waals attractions in nanomaterials as “..It would be like those old movies of a man with his hands full of molasses, trying to get rid of a glass of water” [147]. The importance of long range interactions (LRI) was recognized since the nanoscience very beginning and now different forces (not only van der Waals) appear as an important parameter in many research areas. [148]

Table VII. Primary and secondary interactions

Primary	Secondary
Van der Waals(Electrodynamic)	Hydrogenbonding Hydrophobic
London Induction, Orientation Coulombic(Electrostatic)	Hydration Osmotic Steric
Acid-base (Polar)	Enthalpy-driven Entropy-driven Steric

Fundamentally, all the atomistic interactions are electromagnetic by nature. However, many *phenomena* have enough specificity to be studied and used in different ways. French (2010) decided to suggest a division of LRI in primary and secondary interactions where the second ones are subsets of primary interactions specific to a class of materials, or a macroscopic phenomenon that does not

persist down to the atomic interaction level, Table VII. [148]

The interactive forces between two rodlike particles and the magnitude of these interactions depend of the particles orientation. The interaction energy between two parallel (or cross) cylinders is comparable to inter-molecular energy such as hydrogen bond energy. The number of hydroxyl groups in cellulose nanocrystals is around 7.2 OH/nm^2 . This value is calculated based on CNC unit cell. The hydrogen bonds between two parallel CNC in contact have an estimated value of $7.5 \times 10^{-16} \text{ J}$, almost two orders of magnitude higher than van der Waals energy in colloids. [149]

For short distance, hydrogen bond is dominant in the particle interactions. Long particle interactions are predominantly dominated by van der Waals. The magnitude of hydrogen bonding causes the irreversible agglomeration of CNC after drying. As option, chemical modifications can be used to overcome this hydrogen bonding and facilitate the material re-dispersion.

Nanoscale. The properties of a given material are very different according to the size of its particles. Even if formed from the same kind of molecules, the behavior of a material can be completely changed with the reduction of the size. This is the great attractive of the actual nanoscience. When we go down to the nanoscale, coming close to dimensions above 10^{-9} m , we strongly increase the superficial area of the particles.

As the size of a particle is decreasing down to the nanometer scale gradual and important changes occur. A spherical particle with 30 nm in diameter has about 5% of its atoms on its surface; with 10 nm this number changes to almost 15% and a very small particle 3 nm in diameter can have about 50% of its atoms on the surface. As a consequence, both the specific surface area (A_{sp}) and total surface energy increase. It brings the nanomaterial a strong tendency for agglomeration. With more superficial molecules, the behavior starts to change from the macro solid state to molecular state behavior. In fact, the nanomaterials present a state of matter between these two forms, the bulk and the molecular.

The chemical environment of an atom in a bulk state is very different from a surface atom. For this last one, there is a higher electronic density due the lack of neighbors to disperse charges, these atoms are highly unsaturated. Since for these materials the surface effects are not negligible anymore, there is a change in the material properties due the new characteristics in the electronic transport and catalytic properties. [150]

Rittigstein (2007), discussed the changes in materials properties, like T_g , according to the size (thickness) of the particles. The T_g has different values for the molecules at free surface compared to bulk materials, being a predominant effect in

nanoscale. [151] Nanocomposites can present deviations in this transition depending on the interactions between nanoparticles and polymer. If this interaction is attractive the T_g value can increase, and the opposite can occur if the nanoparticles – polymer interaction generates free surfaces. In systems with moderate or strong attractions, the T_g values could increase with the reduction of the particles size.

Agglomeration. When a group of particles reaches the thermodynamical equilibrium all the components should have the same chemical potential, even in different aggregates. This relation can be expressed by Equation XX.

$$\mu_n = \mu^{\circ}_n + \frac{kT}{n} \text{Log} \left(\frac{X_n}{n} \right) \quad \text{Eq. XX}$$

where μ_n is the chemical potential of a molecule (or particle) in an aggregate of n components, μ°_n is the standard part of the chemical potential (the mean interaction free energy per molecule) in aggregates of n components and X_n is the concentration of molecules in aggregates of number n . When we take $n=1$, μ°_1 and X_1 correspond to the isolated components in solution.

Aggregation occurs only when there is a favorable difference in the cohesive energies between the molecules in the aggregated and the dispersed states. If all the molecules in different-sized aggregates (including monomers) experience the same interaction with their surroundings, as shown from equation XX, the value of μ°_n will remain constant for different aggregates. In that case the potential can be assumed as $\mu^{\circ}_1 = \mu^{\circ}_2 = \mu^{\circ}_3 = \mu^{\circ}_n$. In the case of differences in cohesive energies between the aggregate and dispersed states, we can have two situations: (i) If μ°_n increases as n increases. In this case, Eq XX shows that the occurrence of large aggregates becomes even less probable. (ii) When μ°_n progressively decreases as n increases and we have $\mu^{\circ}_n < \mu^{\circ}_1$ and the formation of large aggregates is favorable. These conditions also can determine the size and polydispersity of the aggregates. In the specific case of particles with a rod-like structure, Israelachvilli (2011) do some approximations to show that μ°_n decreases when one-dimensional aggregates are formed. [105]

Cellulose nanocrystal surface. Particles agglomeration is an important drawback for nanocellulose science, mainly because it is a relevant issue concerning the material behavior during dry processing. Normally these nanomaterials are obtained in aqueous medium after the mechanical, acid or enzymatic treatment and drying is normally avoided due the effect known as hornification. This term is a general designation for the irreversible agglomeration, reorganization and co-crystallization of the nanometric particles or even cellulose fibers [152].

When the cellulose is dried, the fibers are packaged together. In some cases, it happens with sufficient orientation that allows the fibers to form some kind of additional crystallite zones, restricting the swelling and making difficult the material redispersion.[153] In micro-scale, it causes a material porosity reduction due the closure of medium and large pores and cracks. In nano-scale, it causes a surface area reduction and undermines the principal actor of these particles unique properties.

Even the dry methodology seems to interfere in some CNC properties. While samples dried by freeze-drying equipment seem soft and look like snowflakes, the air dried samples take a compact film shape, as direct consequence of different water output mechanisms. Ramanen (2012) studied these effects and concluded that the individual CNC structure or crystallinity are not modified with the drying process. However, the different nanoscale packing can change the thermal stability of the material. For example, in air dried nanocrystals it is possible to observe a higher weight residue due its more compact structure. [154]

4.5 Cellulose nanocrystals: Mechanical properties and reinforcement potential

Intrinsic Modulus. As a reinforcement phase into a composite, the principal role of the CNC is to provide a mechanical barrier against stress. This is possible due to its higher moduli values in comparison to the polymer phase.

For cellulose I in native cellulose, which is a mixture of two polymorphs (cellulose I α and I β), the average experimental value of modulus is around 137 GPa [173]. As described before, this value can decrease to 92 GPa if no intramolecular hydrogen bonding are considered. In cellulose II, the same average experimental value is around 113 GPa. This lower value is ascribed to the different intramolecular hydrogen bonds network positions between I and II cellulose polymorphs. Again, it evidences how important is the role of intramolecular bonding on the determination of the crystallite modulus and chain deformation mechanism.

Besides the polymorph variations, these values are indicative of impressive mechanical properties. It confirms that cellulose crystal is an ideal candidate for the processing of reinforced polymer composites. Its Young's modulus with a density for crystalline cellulose around 1.5-1.6 g.cm⁻³, is much higher than the one of glass fibers, around 70 GPa with a density around 2.6 g.cm⁻³, which are classically used in composite applications. It is similar to Kevlar (60-125 GPa, density around 1.45 g.cm⁻³) and potentially stronger than steel (200-220 GPa, density around 8 g.cm⁻³). Indeed, the specific Young's modulus, which is the ratio between the Young's modulus and the density, of cellulose crystal is around 85 J.g⁻¹ whereas it is around 25 J.g⁻¹ for steel

[155]. A complete table of mechanical properties of individual cellulose nanocrystals can be achieved in Appendix B.

Aspect ratio. At this point, it is clear that the source of CNC can influence its applications. Besides the modulus of the crystalline domains, its size is also a key parameter for the final properties.

Rheological and mechanical performances are strongly dependent of the particle capacity to form an organized structure. The relationship between length and diameter (L/d) of the particle becomes the basis of these properties. A short list of cellulose nanocrystals extracted from different sources with the typical dimensions of the nanorods are given in Table VIII.

It is clear that cellulose from different sources can produce nanoparticles with different dimensions and mechanical properties. In this case, the values of the modulus (E') reported in the Table are derived from the study of Bras (2011), Figure 18. This work intended to elucidate the impact of the aspect ratio on the particle-particle interaction, one of the most important parameters for cellulose nanocomposites. In this experiment, casting films were produced using cellulose nanocrystals from different sources and their modulus was determined. In general, it seems that longer nanocrystals can present better mechanical properties [156].

Table VIII. Modulus value for CNC films from different sources

Source	L/d	E' (GPa)	ν_{RC}	Ref
Cotton	11.3	2.13	6.2	[157]
Hardwood	20.0	0.4	3.5	[158]
Palm Tree	42.6	7.7	1.6	[159]
Sisal	43.0	8.5	1.6	[160]
Tunicin	66.7	15.0	1.0	[161]
CapimDourado	67.0	10.9	1.0	[74]

Although the film properties don't exactly reflect the mechanical properties of the individual nanoparticles (for which the modulus values are more than 10 times higher) a strong correlation was founded between the nanoparticle aspect ratio and the film modulus. Rodlike particles with higher L/d showed the tendency of produce stronger films, probably due to the formation of stronger H-bonds between these particles. The role of CNC aspect ratio in composites will be discussed in the next section as part of the percolation theory.

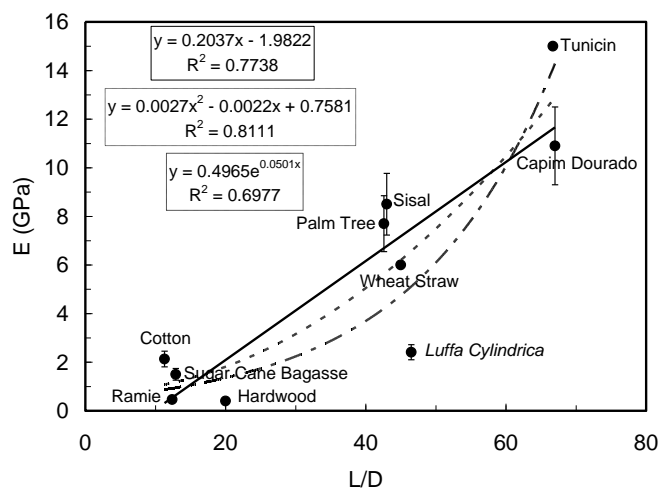


Figure 18. Evolution of the Young's modulus of cellulose nanocrystal films determined from tensile tests as a function of the aspect ratio of constituting nanocrystals.

4.6 Colloidal behavior and rheology

The rheological properties of a suspension are influenced by the particle microscopic interactions. In his book, Coussot (1997) reported five effects that impact the macroscopic properties of the suspensions: Brownian movement, hydrodynamic, colloidal forces, molecular packing and inertia [162].

Some of these effects are also discussed by Mewis and Vermant (2000). The viscosity seems to be affected by several parameters and particle characteristics. For example, there is a strong correlation between shear rate and Brownian movements. At sufficiently low shear rates the Brownian movement dominates the particle flow due to the convective motion, which preserves the original particle interactions and equilibrium structure. However, for higher shear rates this movement is overcome by the mechanical flow and the viscosity values decrease (despite a certain hydrodynamic consistency) and a shear thinning region is developed. [163]

The thixotropic effect is directly related to the particle shape. Even spherical particles can generate this effect due to the size distribution in the sample, because in a sample with a large size distribution the particles can be packed more densely (with small particles among large ones), changing the viscosity. For non-spherical particles, such as CNC, another characteristic, like the aspect ratio, should be considered [164].

Not only the filler size can impact the suspension properties (such as viscosity) but also the filler loading and geometry can modify considerably the particle viscosity. Particles as CNCs are studied as non-spherical particles. In these suspensions, the viscosity values are strongly dependent on the particle orientation, and its alignment with the flow. In this case, the flow tends to organize the particles

due to hydrodynamic forces while the Brownian motion tends to cause random organization of the particles. Particles with higher L/d present higher zero-shear viscosity due to the increase inaccessible volume for other particles. When randomly oriented, these anisotropic particles lead to a higher barrier against the flow. Under shear, these elongated particles can be oriented and the viscosity decreases, resulting in lower values if compared to spherical particles. It seems that the maximum packing fraction decreases as the aspect ratio of the filler in the suspension increases[165]. The rheological properties of a suspension are therefore directly dependent on the particle size. Figure 19 shows the influence of the particle shape on the properties of the suspension.

Considering this influence, cellulose source and isolation method become crucial, since nanoparticles with different L/d can be obtained. The impact of the particle source in the suspensions behavior is also justified by the surface area of the particles. For example, Dimic-Misic (2014) draws attention to the fact that microfibrils having 6 nm in diameter and $1\mu\text{m}$ in length result in 2.3×10^{16} particles. g^{-1} with a specific surface area of $431 \text{ m}^2.\text{g}^{-1}$. This area corresponds to 106 cellulose fibers with specific surface area of $1 \text{ m}^2.\text{g}^{-1}$ that was reported by Klemm (2011). [81,166]

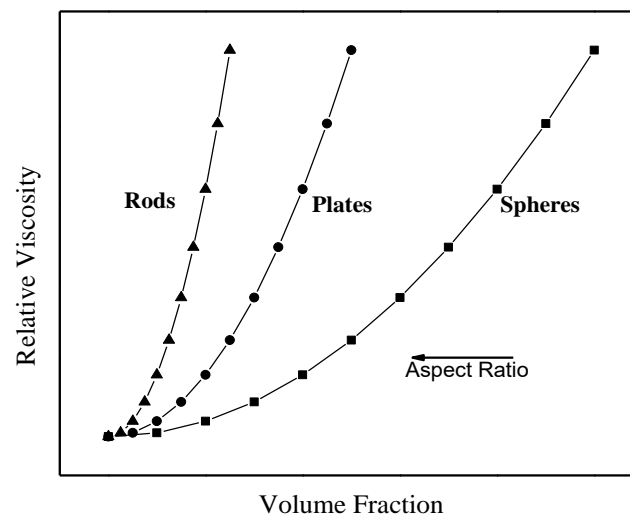


Figure 19. Influence of particle shape on rheological properties of a suspension. Adapted from [148] .

If the particles present in the suspension have a tendency to agglomeration, they can generate loose aggregates that can immobilize water, increasing the particle volume fraction. This effect can increase the suspension's viscosity. As for non-symmetric particles, when increasing the shear rate these aggregates have a tendency to break-up or align themselves. The second case only occurs at very high shear rates, but both effects lead to a viscosity decrease. Above a critical volume, it is possible to

observe the formation of aggregate-connected-networks, that can result in a gel-like behavior. Different mechanisms of flocculation can occur, differentiating weak and strong flocculated gels [82].

In diluted suspensions of charged particles, the imposed shear can distort the double layer and introduce additional energy dissipation that will have as consequence a viscosity increase. Rheologically, due to a strong networking tendency and large water retention capacity, NFC suspensions are highly viscous if compared to CNC. Table IX shows some values of viscosity for CNF and CNC suspensions at different concentrations.

Both particle systems present thixotropic behavior and are semi-transparent to visible light. However, nanofibers present a more complex suspension microstructure due to the long-flexible shape of the fibers, that cause complex entanglements and consequently stronger fibrous network [79].

Table IX. Viscosity of different Nano-cellulose particles in suspension.

	η (Pa.s)	ϕ (wt%)	L/d	Ref.
	750	2	-	[128]
CNF	100	1	> 500	[253]
	90	1	> 80	[254]
CNC	8	3	12	[255]
	5	1	55	[256]
	0.1	1	16	[257]

A good macroscopic example about the importance of the nanofiber form factor to understand its self-entanglement effect was described by Raymer and Smith (2006). In these systems, headphone cables with L/d ratio between 150 and 1800 present very different entanglement probabilities. The researchers have observed that cables with intermediary lengths (i.e. L/d around 900)

have a probability of almost 60% to present at least one knot when exposed to a turbulent environment [167].

Also, wall-slip phenomena have been reported for nanocellulose aqueous systems. Nechyporchuk (2014) reported wall-slip phenomena for NFC suspensions when smooth geometries are used in the experiment. In this publication, the flow instabilities were detected by flow observation and it was noticed that the wall-slip took place over a wide range of shear rates [128]. For cellulose nanocrystal suspensions, the rheological behavior is characterized by distinct behaviors according to the particle micro organization. In viscosimetric measurements, three regions are very easy to visualize due to a pronounced shear thinning behavior. It happens because with the shear rate increase, the rodlike particles start to align themselves with the flow, reaching a low-viscosity *plateau* when the particles are predominantly aligned [168].

Many particles become charged when in contact with water, resulting in electrical double layer formation attracting secondary charge. Cellulosic substrate is an example of negatively charged particle. This negative charge is normally

attributed to the presence of sulfate or carboxylic groups at the surface. Sabet *et al* (2012) show that CNC with different surface charge densities can present different rheological behavior by influencing the needed concentrations to a liquid crystal – gel transition [169].

As a rodlike particle, CNC suspensions can present different properties according to the organization level of its nanostructure. For example, the suspension can show a *Liquid crystal (LCs) behavior*. Lyotropic LCs is a class of liquid crystals formed by the mix of rodlike structures (as, for example, cellulose nanocrystals) with a liquid. The particles that can form LCs possess normally some specific features, which will be determinant for the type of mesomorphism [71]. For example, liquid-crystalline polymers (LCPs) have their properties intrinsically linked to the chemical composition of the polymer chains. In polymers, normally, the chemical composition can determine the dimensions and flexibility of the particles. The particle flexibility can drive the dynamic of the polymer particles in suspension and as a consequence the LCPs properties. Rigid rodlike structures have more possibility to form an ordered system than flexible ones. Three examples of particle arrangements are given in Figure 20.

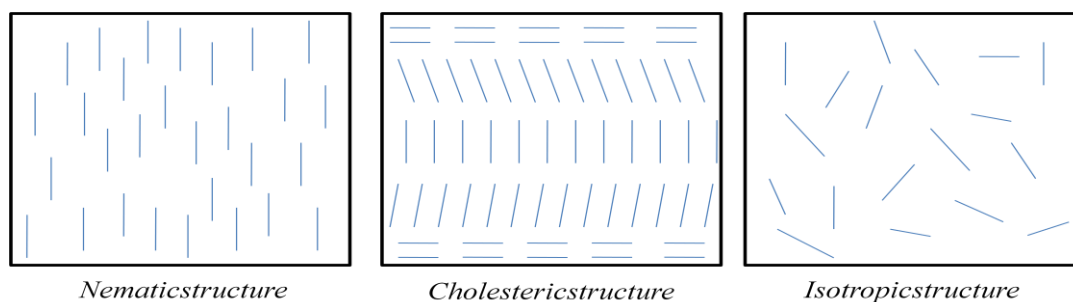


Figure 20. Representation of different organizations of rodlike particles in suspension.

Anisotropy – anisotropy is a property of the matter. Systems with this organization have different properties depending on the considered direction, being the opposite of the isotropy.

Nematic structure – Nematic phases are formed when the particles are not necessarily organized by their position, but they became aligned at long range with their axes being parallel.

Cholesteric Phase – This structure organization is nominated due to its discovery in cholesterol derivatives. Due to some asymmetric packing, the system presents some angle between adjacent particles that creates a longer-order arrangement with a helical structure.

The behavior of rod particles in suspension is controlled by thermodynamic. Above a certain particle density, the entropy of organization is lower for parallel structures and a nematic phase begins to be favored, generating a spontaneous

nematic phase. For cellulose nanocrystals the nematic phase seems to present a particular preference for a *left-hand* rather than *right-handed* chirality [170].

Optical properties. The optical properties of cellulose nanocrystals are directly linked to their organization in suspension and rheology. These particles are organized in the suspension depending on their concentration. For concentrated suspensions (above a critical concentration) it is possible to find a LCs behavior, where a chiral nematic phase is formed. In these conditions, the nematic phase can be enhanced by placing the suspension under a magnetic field where the ordered phase becomes more oriented with its cholesteric axis parallel to the applied field, a consequence of the negative diamagnetism property of the particle [171]. This field creates a bigger chain of particles that can be modified with time, magnitude and frequency of the applied field [172].

The regime transitions can be calculated with Equations XXI (diluted-semi diluted regime) and XXII (semi-diluted to concentrated regime).

$$\phi^* = d^2L / L^3 \text{ Eq. XXI}$$

$$\phi^{**} = d^2L / L^2d \text{ Eq. XXII}$$

Under certain conditions, these suspensions can be concentrated to produce solid semi-translucent films. These films have optical properties (a characteristic of chiral nematic liquid crystals) that can be controlled. The nematic pitch, i.e. the distance over which the organized particles experience a 360° twist, and the refractive index of the film, can determine a narrow wavelength in which the film will show iridescence due to the helicoidal arrangement of the birefringent layers [173].

Different finger prints behavior and circular dichroism (CD) results can be obtained for cellulose nanocrystal suspensions and films due their observation under polarized light. In CD experiments the wavelength of maximum reflection (λ) can be used to obtain information about the nematic pitch (P) by Equation XXIII [174].

$$\lambda = n.P \quad \text{Eq. XXIII}$$

where n is the average refractive index. The optical properties of cellulose nanocrystal films can be controlled by parameters like ionic strength, temperature and concentration

4.7 Thermal stability

Many properties of cellulose are intrinsically bonded to its molecular characteristics, i.e. its chemical bonds. A good example is described by McComb and Williams (1981). His work describes some properties of recycled paper and shows how the mechanical properties of cellulose fibers strongly depend on their pre-treatment. It was clear that acid-recycled papers have poor mechanical properties in comparison to basic-recycled papers since the last ones can present mechanical properties more similar to the virgin fibers [175]. This effect is caused by the presence of acid and oxygen. These two elements can cause the breakage of glycosidic bonds, which are the major force of cellulose cohesion. The ensuing depolymerization has as consequence the decrease of mechanical properties. The effect is more pronounced in the amorphous part of the fiber, but it can be observed also for the surface chains of the crystalline domains.

The argument that cellulose degradation is catalyzed by the presence of acid is a logical approach to the problem considering the nature of the reactions involved in the initiation of the degradation. However, this simple relation seems to be limited. Julien (1993) has published a study where cellulose samples were impregnated with acid solutions at different pH and their thermal properties were tested. This study showed how the nature of the acid can strongly influence cellulose degradation. For example, varying the pH from 0.5 to 7 in an HCl solution resulted for the impregnated cellulose in a degradation gap of 40°C. At the same time, the same variation of pH for H₂SO₄ solutions could modify the degradation temperature by almost 130°C. Nitric acid shifted the degradation curve by less than 15°C [176].

It is important to note that the effect of a specific acid towards cellulose depends also on the acid thermal properties. The acid cannot strongly influence the degradation of cellulose if its degradation or evaporation temperature is lower than the cellulose degradation temperature range.

It is remarkable that sulfuric acid was able to cause a much higher decrease to the fiber thermal stability when compared to other acids. Julien (93) also proposed a reaction mechanism between the sulfuric acid and cellulose that is dependent of the nucleophilic character of the acid and could lead to dehydration, accelerating the thermal degradation [176]. It is given in Figure 21. This is well known for CNC studies since many publications have shown a dependency between CNC thermal stability and hydrolysis conditions. Besides the drawback of thermal stability reduction for CNC, sulfuric acid is popular because it can insert charged groups at the surface of the nanoparticles. These negatively charged particles become more stable in suspension due electrostatic repulsion. Other acids, such as hydrochloric

acid, seem to produce nanoparticles more thermally resistant but cannot provide this electrostatic repulsion, leading to material coalescence.

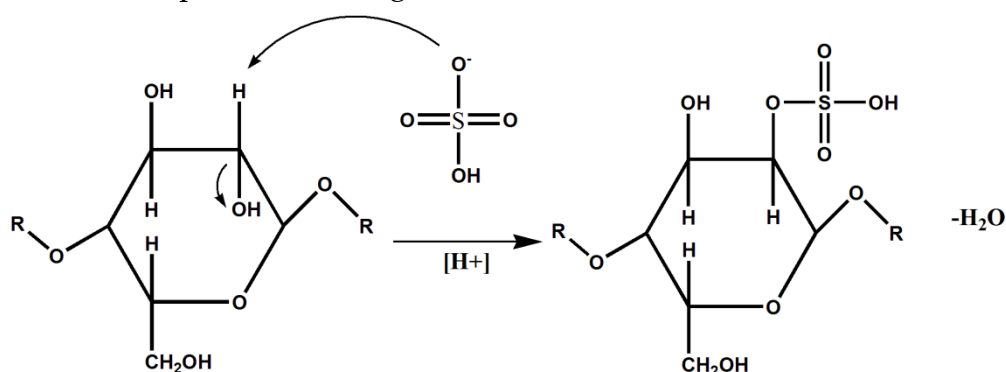


Figure 21. Scheme of cellulose sulfation during acid hydrolysis.

Since sulfuric acid is the most popular acid in this procedure, the presence of sulfate groups (or even the sulfur content) and charge density is associated to an earlier thermal degradation. However, no quantitative relation seems to be found until now. Some literature data about CNC degradation and surface charge are plotted in Figure 22. The complete data are in Appendix B.

These data, obtained from different publications, show that it seems to exist a relationship between the surface charge (here, represented by the zeta potential) and the degradation of the material. This relationship suggests that the charge density at the surface of the nanocrystal is a significant parameter for the degradation of cellulose.

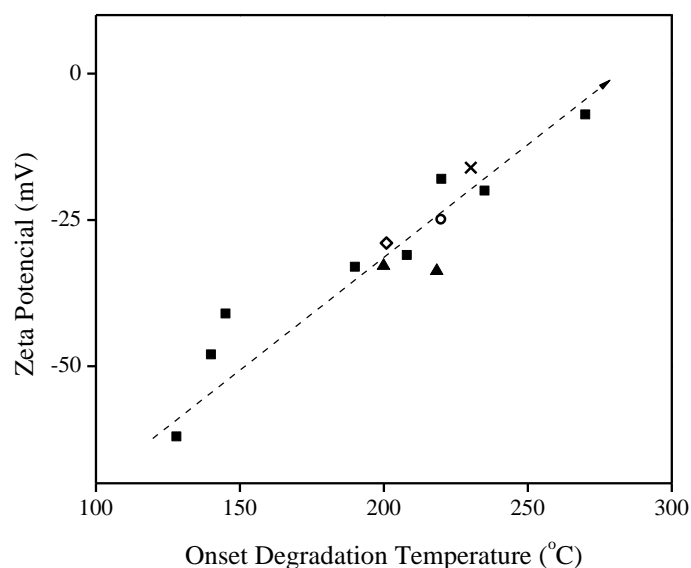


Figure 22. Relationship between degradation temperature and zeta potential for CNC produced by (x) microbial hydrolysis, (o) ammonium persulfate, (▲) TEMPO, (◇) phosphoric and (■) sulfuric acid.

For H₂SO₄-hydrolyzed samples, the presence of residual acid can be avoided by using a neutralization step that increase the thermal degradation onset temperature [121,133]. Figure 23 illustrates two mechanisms of cellulose desulfation by diluted NaOH solution and heat.

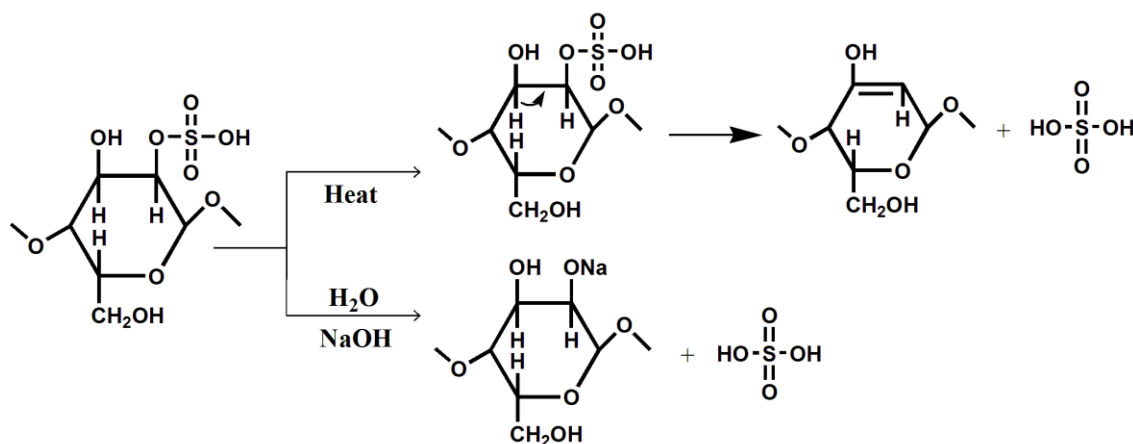


Figure 23. Scheme of cellulose desulfation by heat and basic NaOH solution.

However, it is possible to observe that when alternative agents are responsible to provide negative charges on the surface of the nanoparticle, such as TEMPO reaction, phosphoric acid or ammonium persulfate, a similar relation is founded. In fact, it is difficult to find a direct relation between degradation and surface charge or S content because other factors such as molecular weight of the cellulose, or polymorph arrangement are also very important for this degradation mechanism. However, it seems that it exists a tendency for more negatively charged samples to present earlier degradation.

The use of acids during cellulose hydrolysis also causes an increase in the residual mass after the material pyrolysis. It is known that sulfate and phosphate groups can serve as flame retardants. In general, the presence of anions seems to increase the final amount of char in the sample. Also, this is directly related to the level of surface functionalization [140,176].

4.8 Toxicity and biodegradability

As actual as the nanotechnology research is the concern about the risks that these particles can cause to environment and human health. Some materials as silver nanoparticles are known for their bactericidal action and since they can permeate the skin, some questions were raised about their safety. These safety issues are also asked about nanocellulose materials.

The first remark about these materials is the fact that at the body physiological pH (4.7) CNC shows a degree of ionization equal to 1 (i.e. the particles are negatively charged), which avoids aggregation [177]. However, Ca^+ and Na^+ ions present in the body fluids can induce particles aggregation. Then, it becomes necessary to develop cytotoxicity assessment.

Some tests performed to evaluate the toxicity of the CNC seem to show results that point towards the same direction. At the first moment, some toxicity was observed in cytological tests (using for example pulmonary cells). However, in these tests it seems to be hard to exclude the effects of the presence of acid at the particle surface and the size variation of the sample, which also seem to cause modifications of the results [178,179]. Hua (2015) affirms that cell viability was compromised when cultivated in nanocellulose based film, despite the fact that no cytotoxicity was founded and that it was also highlighted that surface contaminants could influence the results [180].

For in vivo tests (oral and dermal evaluations), no signs of toxicity were found up to now in nematodes or albino rats [178,181]. In biodegradability, some concern is related to the surface variations of the particles at nanoscale, especially after drying of the material. In this case, the hydroxyl groups can form strong hydrogen bonds that make difficult the material degradation. However, the biodegradability of the material seems to be dependent on the particle size just about how fast the material degrades, since all samples tested until now were biodegradable and no ecotoxicity was found among the formed residues [181].

Here, it is important to note that nanocellulose is also cited as a promising material in biomedical applications such as drug delivery and cellular growth systems besides its application for antimicrobial materials [179,182,183].

5 CNC NANO-REINFORCEMENT

Since the introduction of nano objects for nanocomposites preparation, a progressive increasing interest on the subject was observed. Today, a constant and significant growth in nanomaterial research is based on its scientific potential and popularization of the necessary technology. Contrarily to traditional composites, the use of nanomaterials allows a significant reduction of the filler content to reach significantly improved properties. Since these particles can present a much higher surface area, the same reinforcement potential can be reached with a considerable lower volume fraction. This is interesting because lighter and stronger materials can be produced. Figure 24 shows how the surface area drastically increases when the particle diameter is reduced for a rod-like particle with a density of 1.5 g.cm^{-3} .

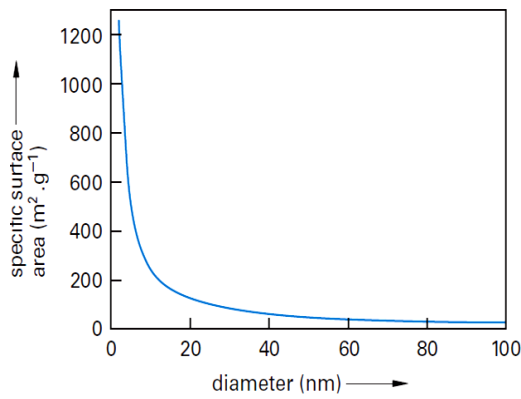


Figure 24. Evolution of the specific surface area of rod-like nanoparticles as a function of their diameter.

compared to strongly bonded ones[184–186]. Also, the chains mobility is affected in nanocomposite materials. For these systems, with well-dispersed nanofiller, T_g can exhibit substantial deviations in comparison to the bulk polymer. It decreases when polymer–nanofiller interfaces are on free surfaces and increases for wetted interfaces with attractive interactions. The first effect can be propagated into the film reducing the T_g of thin materials [187]. Cellulose nanomaterials, in addition to the higher modulus presented by the crystalline domains, can overcome some natural limitations of the natural fibers. Pristine natural fibers are sensitive to the environment conditions and can fail with time. For example, variations of pH and humidity can strongly influence their properties.

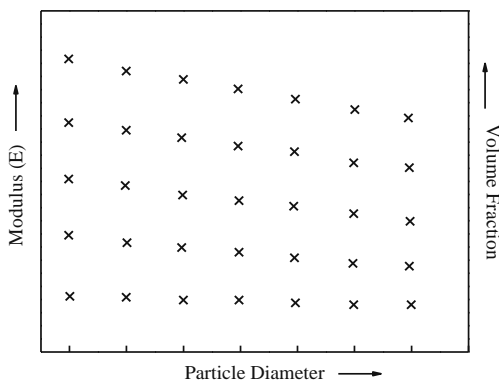


FIGURE 25. Variation of the modulus as a function of particle diameter

Some studies showed how a particle size variation can modify the modulus value of the polymeric matrix. The magnitude of this change depends on the volume fraction of the filler. Figure 25 tries to illustrate this effect. For composites with the same volume fraction, a decrease on the modulus seems to occur when the particle diameter increases. This effect seems to be more pronounced for higher volume fractions and weakly bonded particles as

This intrinsic advantage of nanocrystalline domains started to be explored almost 20 years ago by a series of publications that show their potential to reinforce elastomers [188–190]. At that time, also, it was observed that the mechanical reinforcement provided by the nanorods could not be easily predicted by the traditional mathematical models. The introduction of a percolation theory was used to explain the outstanding reinforcement that these particles can provide.

5.1 Percolation theory

Such as for traditional composites, the reinforcement caused by the nanofiller is, in a first stage, dependent on the polymer-chains interactions. According to Kutvonen *et al* (2012), the reinforcement effect caused by the nanoparticles can be

explained by dynamic arguments, assuming that nanoparticles are more mobile than the polymeric chains, which can provide better resistance against deformation due to improvement of local tension release. Also, the nanoparticles have ability to create temporary bonds between the chains, thus creating a filler-polymer network [191].

For nanorods, like cellulose nanocrystals, the reinforcing capability is classically attributed to a percolation phenomenon. This term is referred to the lowest volume fraction of rigid particles (v_{rc}) that can provide the necessary number of individual rods, arranged randomly, to build a continuous 3D rigid network. This volume fraction is of great interest because it is the onset point for many mechanical, rheological and electrical (if applicable) properties [192]. Indeed, the percolation network is one of the cornerstones of polysaccharide nanofiller theory of reinforcement capacity.

At sufficiently high temperature (when the polymer stiffness could be assumed to be much lower than the one of the reinforcing phase), the material stiffness will depend only on the percolating rigid phase volume fraction and stiffness of the percolating network (Equation XXIV).

$$E_C = \Psi \cdot E_R \quad \text{Eq. XXIV}$$

were, E_C and E_R are the tensile moduli of the composite and rigid phase, respectively, and Ψ is a parameter corresponding to the volume fraction of the percolating rigid phase adapted by Ouali (1991), which is calculated from Equation XXII [193].

$$\Psi = v_r \cdot \left(\frac{v_r - v_{rc}}{1 - v_{rc}} \right)^b \quad \text{Eq. XXV}$$

With $b = 0.4$ for a 3D network, v_r is the volume of the rigid phase and v_{rc} is the percolation threshold defined by Equation XXVI.

$$v_{rc} = \frac{0.7}{L/d} \quad \text{Eq. XXVI}$$

The aspect ratio (L/d) is normally determined by microscopic methods, like AFM or TEM [194,195], although it can also be obtained by more complex techniques, like SAXS, DLS and XRD [117,144,195,196].

These systems are much more sensitive to the effects caused by the nanofiller. Parameters such as aspect ratio, filler orientation and dispersion, besides matrix morphology alteration due to the filler addition are responsible for nanocomposite properties.

Concerning the mechanical reinforcement, it is well documented that in short fibers composites the aspect ratio of the filler can influence the composite properties

and control the stress transfer phenomenon [74]. Also, rods with higher L/d requires less particles to reach the percolation threshold, resulting in a lower number of rod ends under stress, and lower number of cracks. In general terms, the percolation mechanism states an optimal volume fraction of filler. As a consequence, this assumption also brings a limit in the maximum composite properties improvement. Below this volume fraction, the reinforcement is only partial and over it the reinforcement cannot increase, or can even decrease. A clear consequence of voids created by agglomerated particles. It is also clear that particles with higher aspect ratios will need a lower volume fraction to reach the percolation limit.

For CNC nanocomposites, the definition of percolation is always related to mechanical reinforcement. However, alternative definitions of percolation can be found in literature. Although widely used in the composites field, there is no exclusive definition of percolation events for CNC particles. Other rodlike systems, such as carbon nanotubes, use definitions of percolation for defined electrical properties of the composite. Also, rheological measurements can provide a rheological percolation, as discussed before. Figure 26 illustrates common representations of the rodlike particle organization at the percolation point.

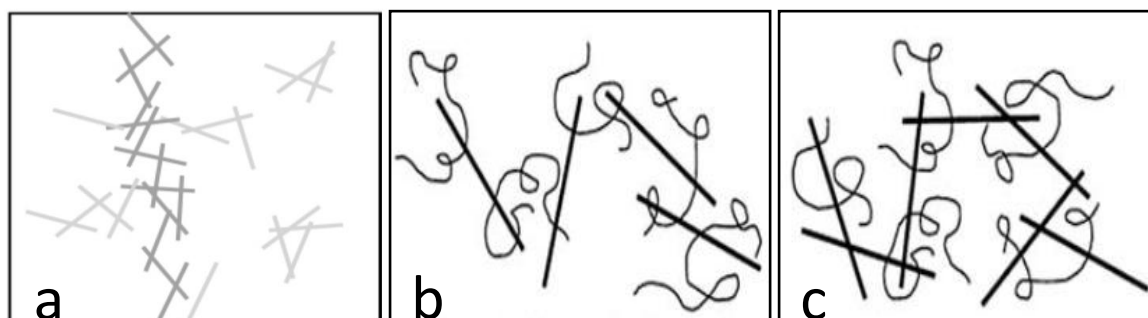


Figure 26. Representation of mechanical (a), rheological (b) and electrical (c) percolation. Figures from refs [197,198].

5.2 Processing technique

Besides its potential to act as reinforcing filler in polymeric matrix, some aspects related to processing of cellulose nanocrystal nanocomposites are not completely explored due to some intrinsic limitations. In general, the nanomaterials containing cellulose nanocrystals are prepared by casting-evaporation, melt-compounding, electrospinning and layer-by-layer (LBL) techniques. Table X resumes some publications where these different processing methods were applied.

Casting-evaporation is probably the most popular applied technique to obtain cellulose nanocomposites. A large volume of scientific publications has focus in this

type of material due to the particularities of each system. Suitable polymer solvents and filler – polymer interactions are the major challenges in that approach.

Table X. Literature examples of CNC-based materials.

	Processing	Polymer	CNC source	Filler content (wt%)	Ref.
Others	Casting-Evaporation	Epoxy Resin	Cotton	0 – 24 *	[199]
		Methylcellulose	Soy hulls	0 – 10	[200]
		Natural Rubber	Cassava	0 – 10	[136]
		PA-6	MCC	5	[201]
		PVA	MCC/Flax	0 - 5	[202]
	Extrusion	PA-6	cotton	0 – 1	[203]
		PLA	Ramie	0 – 3	[204]
		PE	Ramie	0 – 15	[205]
		PE	Curauá	0 – 9	[56]
		PEO	Cotton	0 – 9	[135]
		PS	Cotton	0 – 20	[206]
		PVAc	Paper	0 – 12	[207]
	Electrospinning	Polycaprolactone	Ramie	0 – 7.5	[208]
		Epoxy Acrylate	MCC	0 – 8	[209]
		PVA	Ramie	0 -15	[210]
LBL		PAH	-	1	[211]
	Resins	Cotton	1	[212]	

Volume fraction *

The basic principle of this technique is to provide a good dispersion of the CNC within the polymer chains by dissolution of the matrix with a suitable solvent. During the drying process (that can take few days in some cases) the nanoparticles can keep their mobility in the suspension due to Brownian movement and the rearrangement is possible, creating the possibility of interaction between the nanocrystals and structuring the percolation network. The final particles structure is represented in Figure 27a.

Casting preparation demands previous steps and adaptation of the system in some cases. The composite homogenization is simple in the case of water soluble polymers, which are quite convenient matrices to prepare cellulose nanocrystal nanocomposites. Since the nanoparticles are normally obtained in a water suspension, the polymer solubilization and good nanocrystal dispersion are easy steps to perform for these systems. If there is no need to dry the cellulose nanocrystal (that makes difficult its dispersion) a good dispersion of the suspension can be ensured by short-time ultrasound treatment. Polymers with a hydrophilic character

normally can interact with the hydroxyl groups, present at the nanocrystal surface, creating new hydrogen bonds and a synergic effect that can improve the final material properties. However, hydrophobic polymers matrices bring one drawback for polysaccharide based nanocomposite preparation. These natural particles have a strongly polar character and this makes difficult their dispersion in nonpolar solvents. Recently, some techniques have been reported as a way to avoid this problem. The use of solvent exchange [199], chemical modification [205], surfactant adsorption [137] and their combinations arise as ways to prepare cellulose nanocomposites by increasing the filler/matrix interactions.

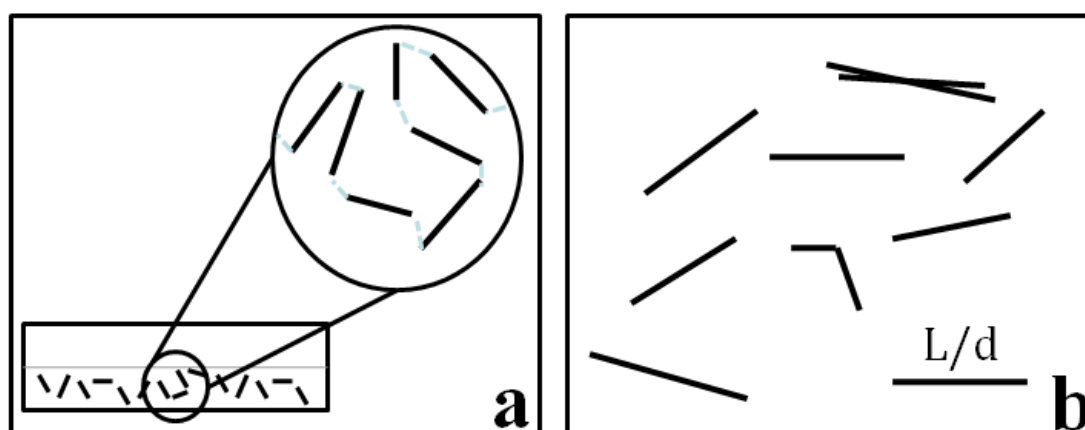


Figure 27. Casting evaporation (a) and extruded material (b).

SAXS experiments show that the long CNC deposition time normally causes gradient of distribution for the CNCs inside the matrix, one the faces of the composite being more filled with nanoparticles than the other. This can generate materials with different surfaces properties.

Melt-compounding processes (extrusion, injection-molding, hot-pressing) are attractive ways to prepare materials due their high capacity of production, economic viability and no use of solvents [206,213,214]. For thermoplastic composites the traditional hot processing step involves increase of the temperature above the material T_m (or T_g) to enhance the mobility of the chains without melting or softening of the dispersed phase. This is not the case for CNC since this material does not present T_g and T_m before its degradation temperature. For these systems, the polymer matrix can even exert some extra functions such as to protect the nanomaterial from external degradation (coating), to keep the filler organization and even to avoid aggregation. On the other hand, the filler acts like an inflexible material that can support great part of the imposed stress and receive energy from the matrix [215].

Different from casting process, melt preparation normally involves the imposition of strong shear to the material. Such as in rheological experiments, this

shear stress coming from the equipment screws or pressure caused by the injection-molding process tends to organize the nanorods and does not allow the formation of percolating network. Pignon (1997) performed rheological experiments in which the structure of a laponite based nanocomposite was followed by light scattering. After a critical shear rate, the destruction of the structure was observed (by a Butterfly-like scattering pattern) [216].

Using this processing technique, the poor interactions between the filler and the matrix also can be a drawback. The simple mixture between the polymer and nanocellulose in dry state (such as powder) does not provide a very homogeneously dispersed composite. Again, the strong aggregation of cellulose nanoparticles cannot be reversed by extrusion and the use of dried cellulose becomes a problem since it is difficult to avoid agglomerations without previous sample preparation [205,213].

The hydrophilic character of the matrix is also important here, if the filler-filler interactions are stronger than filler-polymer interactions, the nanoparticles will tend to agglomerate. Some alternatives to improve the dispersion of dried cellulose have been proposed. The use of a masterbatch preparation is reported as a good way to improve the dispersion of the filler. Zammarano (2011) shows using fluorescence analysis that the interface between the nanoparticles and the polymer tends to increase by using this kind of sample preparation [217]. Also, a physical protection of the sample created by the coating of the particles can avoid early thermal degradation [203]. More complex, but also effective, the use of surface modification of the nanoparticles also allows good dispersion, even in very hydrophobic matrix [205].

Nevertheless, not all polymers are suitable for extrusion. Some polymers are not easy to be processed due to high level of entanglement of the chains or viscosity. In addition to that, the extrusion process is much more “aggressive” to the material. In this processing technique the screw rotation speed is a very important parameter concerning the final mechanical properties of the material. An increase in the rotation speed causes an increase in the stress and modifies the final properties of the composite [218,219]. Also, it can cause physical damage to the cellulose nanocrystals, breaking the particles and causing degradation [220], what is quite surprising considering the dimensions of the filler. Inceoglu et al. (2011) showed the effect of screw speed and processing time on the filler breakage. However, these effects seem to be less effective for particles smaller than 500 μm . [221]

Besides, some polymers require high temperature processing, which can cause early thermal degradation of the polysaccharide. As a consequence, the final organization of the material differs from the cast/evaporated materials, as illustrated in Figure 27.

Other techniques. Electrospinning and layer-by-layer assembly are techniques which can also be used with the objective of reinforcement or construction of microstructured layered materials. Considering the two most popular preparation methodologies, casting and extrusion, we can see that both present limitations. The polymer characteristics will be determinant in the process due to the need of optimization of parameters like temperature, surface adhesion, time, etc. Due to the polar surface of the nanocrystals, the most important characteristic of the polymeric matrix is its hydrophilic/ hydrophobic behavior. Some publications show that cast-evaporated materials can present higher mechanical improvement if compared to the same system produced by extrusion [220].

5.3 Nanocomposite properties

Independently of the preparation technique, CNC can provide good improvement to the mechanical and barrier properties of the matrix. Several studies already reported that this filler can significantly rise the modulus value and decrease the permeability, even below the percolation threshold [222]. In general, shorter CNCs are used for barrier properties control while long nanoparticles are more efficient to improve mechanical properties. Concerning the utilization of longer rodlike particles, it was already described in a previous section why these particles can provide a stronger reinforcement to the matrix. Table 8 shows results obtained by the inclusion of cellulose nanorods to a rubber matrix. The increase of the modulus is visible after the addition of the filler. Also, regardless the preparation methodology, it is possible to observe the tendency of increasing reinforcement effect for samples where higher L/d particles were used.

Table 8. Effect of different fillers in different natural rubber nanocomposites

L/d	Filler content(wt%)	Matrix modulus	Composite modulus	Ec/Em*	Reference
76	5	2.2 MPa	33.5 MPa	15.2	[136]
67	5	0.6 MPa	20.9 MPa	34.8	[74]
43	5	0.5 MPa	6.4 MPa	12.8	[159]
21	5	1.3 MPa	7.5 MPa	5.8	[223]
16	5	1.7	17.8 MPa	10.5	[224]
13	10	-	-	6.3	[225]

*Ec - composites modulus and Em - matrix modulus

For low cellulose nanocrystal contents ($\varphi <$ percolation threshold) other phenomena are assumed to explain the observable results. In general, different interfacial effects are responsible for the mechanical improvements. *Filler – matrix*

interaction seems to be the primary motivation of mechanical improvements in most cases. The creation of new hydrogen bonds reduces the mobility of the polymeric chains, even above T_g , and increase the modulus value.

Many publications reported a modification in T_g value when the nanoparticle fraction increases suggesting a modification in the chain mobility without increase in the material crystallinity.

Matrix crystallization. The crystallinity of the material seems to be influenced by the presence of cellulose nanocrystals. These nanoparticles can increase the crystallization rate of the polymer, leading to a faster formation of spherulites, but not necessarily increase of the final crystalline fraction [226]. It can induce the crystallization for semicrystalline [227] or amorphous polymers [228]. A comparison of the mechanical properties between amorphous and semicrystalline composites of poly(hydroxyoctoate) showed that cellulose nanocrystals can cause a transcristallization phenomenon and lead to higher mechanical properties in the semicrystalline polymer [229]

Three-phase materials (interfacial layer) As described above, the presence of cellulose nanocrystals can modify the behavior of polymer chains in the vicinity of the interfacial zone through interactions. The presence of the nanoparticle induces the creation of an interphase with properties different from those of the bulk matrix. Due to the surface properties of nanomaterials it is expected that a well dispersed filler creates a significant interphase volume fraction in the nanocomposite. This material can be regarded as a three-phase material. It was suggested that the interface properties can gradually change from the filler surface to the bulk matrix. This interfacial layer was estimated by Dufresne (2000) to 2.7 nm, a reasonable value for a particle with 15 nm of width [230].

Creation of new bonds. The reinforcement can result from covalent bonds between the filler and the matrix resulting from an in situ polymerization, for example. Some works show improvement in the composite properties due to the creation of covalent bonds between the nanocrystals and polycaprolactone [208] or polyurethane [231]. Also, for elastomeric matrices the presence of the filler in rubber compounds can create additional *cross-links* due to the new *polymer – fillers* interactions [232]. These new interactions can lead to the formation of a dense network that is harder to deform and is one of the main driving force for crystallization, having a strong influence on the SIC [51,233].

In some studies, a degradation of the mechanical properties is observed. Normally, this is attributed to problems such as poor filler dispersion [213], influence of plasticizers that causes a plasticizer – filler competition [56] or CNC degradation [206].

Melt composites. Composites in the molten state can be studied by rheological measurements. It can provide information about filler-matrix interactions, particle dispersion, polymer molecular weight, etc. An important feature of these techniques for the study of nanocomposites is the possibility of investigating the mechanical behavior of the material according to the nanoparticle volume fraction without influence of the crystallinity that has a major influence on its properties in the solid state. On the other hand, the response of the system depends on the composite preparation.

Described by Song and Zheng (2014) as “quite charming but controversial” the rheology of nanofilled polymers is at some point an extension of the previous topic. However, it is necessary to have the polymer matrix to evaluate the filler structure and matrix chain dynamics in a jointly way, something that is completely dependent on the interactions between nanorods and polymer chains [234,235].

The presence of the filler can cause radical modifications in polymer behavior. For example, when increasing the filler content a liquid-solid transition can be observed and many authors have reported viscosity variation after nanofiller inclusion. In different systems it can lead to increase or decrease of the viscosity, what goes against Einstein’s equation (Equation XV). The reasons about why it is possible to observe such a decrease are still not well solved [236]. It seems especially curious for CNC systems since, such as for aqueous suspensions, for non-spherical fillers an extra energy dissipation is needed and tends to increase the viscosity value [165].

Concerning the modulus value, the addition of a filler usually causes the increase of the elastic modulus. Khoshkava (2014) attributed it to the possible formation of a particle network [237]. This solid-like behavior, especially at lower frequencies, is described in many studies about rodlike nanocomposites. For many different systems, a rodlike network (or partial network) can be formed and restrains the long-range motion of polymer chains. Then, an independency of G' and ω can be observed. For nanocomposites, the low- ω region starts to become a plateau when the filler amount increases. This plateau also can be attributed to strong interfacial interactions that dominates G' values over the Brownian movement, that tends to make the suspension behaves as a liquid. [234]

For high- ω , the presence of the nanofiller seems to not influence the polymeric chains movement. It suggests that the nanorods do not influence the short-range dynamics of polymeric chains. In other words, nanorods can have a strong influence on polymer chain relaxations (long-range motion), but have little effect on polymer motion (short-range motion) at the distances scales of an entanglement length [235].

Other particular rheological properties, such as short linear viscoelastic region, high resistance to flow, δ lower than 1 and G' higher than G'' over a broad range of frequencies could be attributed to this network.

6 REFERENCES

- [1] R.C. Thompson, S.H. Swan, C.J. Moore, F.S. vom Saal, Our plastic age., *Philos. Trans. R. Soc. Lond. B. Biol. Sci.* 364 (2009) 1973–1976. doi:10.1098/rstb.2009.0054.
- [2] Y. Zheng, E.K. Yanful, A.S. Bassi, A review of plastic waste biodegradation., *Crit. Rev. Biotechnol.* 25 (2015) 243–50. doi:10.1080/07388550500346359.
- [3] K. Leja, G. Lewandowicz, Polymer Biodegradation and Biodegradable Polymers – a Review, *Polish J. Environ. Stud.* 19 (2010) 255–266.
- [4] R. Klein, *Laser Welding of Plastics*, Wiley, 2011.
- [5] F.W. Billmeyer, J. Wiley, *Textbook of polymer science*, Third Edit, Willey, 1984.
- [6] K.P. Menard, *Dynamical Mechanical Analysis A practical Introduction*, 2nd ed., CRC Press, 2008.
- [7] M. De Paoli, *Degradação e estabilização de polímeros*, ChemKeys, 2008.
- [8] F.E.. Lucas, B.C. Soares, E.E.. Monteiro, *Caracterização de polímeros*, E-papers, 2001.
- [9] T. Ozawa, A New Method of Analyzing Thermogravimetric, *Bull. Chem. Soc. Jpn.* 38 (1965) 1881–1886.
- [10] R.E.. Kahrizangi, M.H. Abbasi, Evaluation of reliability of Coats-Redfern method for kinetic analysis of non-isothermal TGA, *Trans. Nonferrous Met. Soc. China.* 18 (2008) 217 – 221.
- [11] S. Feng, D. Wu, H. Liu, C. Chen, J. Liu, Z. Yao, et al., Crystallization and creep of the graphite nanosheets based poly(butylene adipate-co-terephthalate) biocomposites, *Thermochim. Acta.* 587 (2014) 72–80. doi:10.1016/j.tca.2014.04.020.
- [12] G. Siqueira, C. Fraschini, J. Bras, A. Dufresne, R. Prud'homme, M.-P. Laborie, Impact of the nature and shape of cellulosic nanoparticles on the isothermal crystallization kinetics of poly(ϵ -caprolactone), *Eur. Polym. J.* 47 (2011) 2216–2227. doi:10.1016/j.eurpolymj.2011.09.014.
- [13] F. Ronkay, Effect of Recycling on the Rheological , Mechanical and Optical Properties of Polycarbonate, 10 (2013) 209–220.
- [14] A.C. Finkle, *Cellulose – Polycarbonate Nanocomposites : A novel automotive window alternative by*, (2011).
- [15] Y.-C. Ahn, H.-J. Kim, A study on the rheological properties and processability of polycarbonate, *J. Appl. Polym. Sci.* 86 (2002) 2921–2929. doi:10.1002/app.11752.

- [16] F. Signori, M.-B. Coltelli, S. Bronco, Thermal degradation of poly(lactic acid) (PLA) and poly(butylene adipate-co-terephthalate) (PBAT) and their blends upon melt processing, *Polym. Degrad. Stab.* 94 (2009) 74–82. doi:10.1016/j.polymdegradstab.2008.10.004.
- [17] M. Nofar, a. Maani, H. Sojoudi, M.C. Heuzey, P.J. Carreau, Interfacial and rheological properties of PLA/PBAT and PLA/PBSA blends and their morphological stability under shear flow, *J. Rheol. (N. Y. N. Y.)*. 59 (2015) 317–333. doi:10.1122/1.4905714.
- [18] R. Al-Itry, K. Lamnawar, A. Maazouz, Improvement of thermal stability, rheological and mechanical properties of PLA, PBAT and their blends by reactive extrusion with functionalized epoxy, *Polym. Degrad. Stab.* 97 (2012) 1898–1914. doi:10.1016/j.polymdegradstab.2012.06.028.
- [19] K. Fukushima, M.-H. Wu, S. Bocchini, A. Rasyida, M.-C. Yang, PBAT based nanocomposites for medical and industrial applications., *Mater. Sci. Eng. C. Mater. Biol. Appl.* 32 (2012) 1331–51. doi:10.1016/j.msec.2012.04.005.
- [20] S. Sohn, Crystallization behavior of bisphenol-a polycarbonate : effects of crystallization time , temperature , and molar mass crystallization behavior of bisphenol-a polycarbonate : effects of crystallization time , temperature , and molar mass, Virginia Polytechnic Institute and State University, 2000.
- [21] L. Xia, F. Li, B. Shentu, Z. Weng, Thermal Degradation Behavior and Flame Retardancy of Polycarbonate Containing Poly[(phenylsilsesquioxane)-co-(dimethylsiloxane)] and Potassium Diphenyl Sulfonate, *J. Macromol. Sci. Part B.* 52 (2013) 310–318. doi:10.1080/00222348.2012.700239.
- [22] G.B.. Kauffman, R.B. Seymour, I. Natural Rubber, *J. Chem. Educ.* 67 (1990) 422–425.
- [23] T. Karino, Y. Ikeda, Y. Yasuda, S. Kohjiya, M. Shibayama, Nonuniformity in natural rubber as revealed by small-angle neutron scattering, small-angle X-ray scattering, and atomic force microscopy., *Biomacromolecules.* 8 (2007) 693–9. doi:10.1021/bm060983d.
- [24] A.K. Bhowmick, H. Stephens, *Handbook of Elastomers*, 2nd ed., CRC Press, 2000.
- [25] G. Rajkumar, J.M. Squire, S. Arnott, A New Structure for Crystalline Natural Rubber, 58 (2006) 7004–7014.
- [26] S. Radhakrishnan, V. S, S. Sivaramt, Structure and morphology of polycarbonate synthesized by solid state polycondensation, 35 (1994) 3789–3791.
- [27] M.S. Rama, S. Swaminathan, Polycarbonate/Clay Nanocomposites via in Situ Melt Polycondensation, *Ind. Eng. Chem. Res.* 49 (2010) 2217–2227. doi:10.1021/ie9015649.
- [28] J. Lu, D. Xi, R. Huang, L. Li, Crystal Morphology of High-Pressure Crystallized Bisphenol-A Polycarbonate, *J. Macromol. Sci. Part B.* 50 (2011) 1018–1030. doi:10.1080/00222348.2010.497435.
- [29] F. Gallez, R. Legras, J.P. Mercier, Some new aspects of the crystallization of bisphenol-A polycarbonate, *Polym. Eng. Sci.* 16 (1976) 266 – 283.
- [30] G.E. Wissler, B. Crist, Glass transition in semicrystalline polycarbonate, *J. Polym. Sci. Polym. Phys. Ed.* 18 (1980) 1257–1270. doi:10.1002/pol.1980.180180608.

- [31] J.M. Pochan, H.W. Gibson, M.F. Froix, D.F. Hinman, Dielectric Relaxation Studies of Bisphenol A-Diphenyl Carbonate/Lexan Polycarbonate Solid Solutions, *Macromolecules*. 11 (1978) 165–171. doi:10.1021/ma60061a029.
- [32] Y. He, B. Zhu, Y. Inoue, Hydrogen bonds in polymer blends, *Prog. Polym. Sci.* 29 (2004) 1021–1051. doi:10.1016/j.progpolymsci.2004.07.002.
- [33] G. Ji, F. Li, W. Zhu, Q. Dai, G. Xue, X. Gu, Rapid Crystallization of Polycarbonate by Shock-Cooling and Freeze-Drying Method, *J. Macromol. Sci. Part A*. 34 (1997) 369–376. doi:10.1080/10601329708014962.
- [34] B.N. Jang, C. a. Wilkie, The thermal degradation of bisphenol A polycarbonate in air, *Thermochim. Acta*. 426 (2005) 73–84. doi:10.1016/j.tca.2004.07.023.
- [35] G. Gedler, M. Antunes, V. Realinho, J.I. Velasco, Thermal stability of polycarbonate-graphene nanocomposite foams, *Polym. Degrad. Stab.* 97 (2012) 1297–1304. doi:10.1016/j.polymdegradstab.2012.05.027.
- [36] N. Jacquél, R. Saint-Loup, J.-P. Pascault, A. Rousseau, F. Fenouillot, Bio-based alternatives in the synthesis of aliphatic–aromatic polyesters dedicated to biodegradable film applications, *Polymer (Guildf)*. 59 (2015) 234–242. doi:10.1016/j.polymer.2014.12.021.
- [37] K. ZHU, W-P. ZHU, Y-B. GU, Z-Q. SHEN, W. CHEN, G-X. ZHU, Synthesis and Characterization of Poly(butylene adipate-co- terephthalate) Catalyzed by Rare Earth Stearates, *Chinese J. Chem.* 25 (2007) 1581–1583. doi:10.1002/cjoc.200790292.
- [38] X.Q. Shi, H. Ito, T. Kikutani, Characterization on mixed-crystal structure and properties of poly(butylene adipate-co-terephthalate) biodegradable fibers, *Polymer (Guildf)*. 46 (2005) 11442–11450. doi:10.1016/j.polymer.2005.10.065.
- [39] Y. Iwakura, Y. Li, K. Nakayama, H. Shimizu, Strengthening of Poly (butylene adipate- co - terephthalate) by Melt Blending with a Liquid Crystalline Polymer, 109 (2008) 333–339. doi:10.1002/app.
- [40] L.C. Lins, S. Livi, J. Duchet-Rumeau, J.-F. Gérard, Phosphonium ionic liquids as new compatibilizing agents of biopolymer blends composed of poly(butylene-adipate-co-terephthalate)/poly(lactic acid) (PBAT/PLA), *RSC Adv.* 5 (2015) 59082–59092. doi:10.1039/C5RA10241C.
- [41] K. Kuwabara, Z. Gan, T. Nakamura, H. Abe, Y. Doi, Crystalline/Amorphous Phase Structure and Molecular Mobility of Biodegradable Poly(butylene adipate-co-butylene terephthalate) and Related Polyesters, *Biomacromolecules*. 3 (2002) 390–396. doi:10.1021/bm0156476.
- [42] J.-H. Chen, M.-C. Yang, Preparation and characterization of nanocomposite of maleated poly(butylene adipate-co-terephthalate) with organoclay., *Mater. Sci. Eng. C. Mater. Biol. Appl.* 46 (2015) 301–8. doi:10.1016/j.msec.2014.10.045.
- [43] V. Ratta, Crystallization, Morphology, Thermal Stability and Adhesive Properties of Novel High Performance Semicrystalline Polyimides, Faculty of Virginia Polytechnic Institute and State University, 1999.
- [44] J.T. Blender, Handbook of Polycarbonate Science and Technology, Marcel Dekker INC, 2000.

- [45] H. Münstedt, Influence of crystallinity on rheological properties of unfilled and particle-filled polycarbonates, *Polymer (Guildf)*. 52 (2011) 3677–3680. doi:10.1016/j.polymer.2011.06.040.
- [46] B. Falkai, W. Rellensmann, Kristallisation von Polycarbonaten, *Die Makromol. Chemie*. 75 (1964) 112–121.
- [47] a. Siegmann, P.H. Geil, Crystallization of polycarbonate from the glassy state. part II. Thin films melted and quenched, *J. Macromol. Sci. Part B*. 4 (1970) 273–291. doi:10.1080/00222347008212503.
- [48] S. Sohn, a Alizadeh, H. Marand, On the multiple melting behavior of bisphenol-A polycarbonate, *Polymer (Guildf)*. 41 (2000) 8879–8886. doi:10.1016/S0032-3861(00)00110-5.
- [49] F. Chen, J. Zhang, Effects of plasticization and shear stress on phase structure development and properties of soy protein blends., *ACS Appl. Mater. Interfaces*. 2 (2010) 3324–32. doi:10.1021/am100751c.
- [50] T. Mukherjee, M. Czaka, N. Kao, R.K. Gupta, H.J. Choi, S. Bhattacharya, Dispersion study of nanofibrillated cellulose based poly(butylene adipate-co-terephthalate) composites., *Carbohydr. Polym*. 102 (2014) 537–42. doi:10.1016/j.carbpol.2013.11.047.
- [51] S. Toki, I. Sics, S. Ran, L. Liu, B.S. Hsiao, S. Murakami, et al., New Insights into Structural Development in Natural Rubber during Uniaxial Deformation by In Situ Synchrotron X-ray Diffraction, *Macromolecules*. 35 (2002) 6578–6584. doi:10.1021/ma0205921.
- [52] H. Angellier, S. Molina-Boisseau, A. Dufresne, Mechanical Properties of Waxy Maize Starch Nanocrystal Reinforced Natural Rubber, *Macromolecules*. 38 (2005) 9161–9170. doi:10.1021/ma0512399.
- [53] D.G. GRAY, “Transcrystallization” induced by mechanical stress on a polypropylene melt, *Polym. Lett. Ed*. 12 (1974) 645–650.
- [54] R.I.C. Chivrac, E. Pollet, L.U.C. Ave, Nonisothermal Crystallization Behavior of Poly (butylene adipate- co -terephthalate)/ Clay Nano-biocomposites, *J. Polym. Sci. Part B Polym. Phys*. 45 (2007) 1503–1510. doi:10.1002/polb.
- [55] D. O. Castro, E. Frollini, J. Marini, A. Ruvolo-Filho, Preparação e Caracterização de Biocompósitos Baseados em Fibra de Curauá, Biopolietileno de Alta Densidade (BPEAD) e Polibutadieno Líquido Hidroxilado (PBHL), *Polímeros*. 23 (2013) 65–73.
- [56] D. Oliveira de Castro, E. Frollini, A. Ruvolo-Filho, A. Dufresne, “Green polyethylene” and curauá cellulose nanocrystal based nanocomposites: Effect of vegetable oils as coupling agent and processing technique, *J. Polym. Sci. Part B Polym. Phys*. 53 (2015) 1010–1019. doi:10.1002/polb.23729.
- [57] L. Liu, Y. Zhang, F. Lv, B. Yang, X. Meng, Effects of red mud on rheological, crystalline, and mechanical properties of red mud/PBAT composites, *Polym. Compos.* (2015) n/a–n/a. doi:10.1002/pc.23378.
- [58] O. Probst, E.M. Moore, D.E. Resasco, B.P. Grady, Nucleation of polyvinyl alcohol crystallization by single-walled carbon nanotubes, *Polymer (Guildf)*. 45 (2004) 4437–4443. doi:10.1016/j.polymer.2004.04.031.

- [59] J.M. Lagaron, R. Catalá, R. Gavara, Structural characteristics defining high barrier properties in polymeric materials, *Mater. Sci. Technol.* 20 (2004) 1–7. doi:10.1179/026708304225010442.
- [60] M. Ho, H. Wang, J.-H. Lee, C. Ho, K. Lau, J. Leng, et al., Critical factors on manufacturing processes of natural fibre composites, *Compos. Part B Eng.* 43 (2012) 3549–3562. doi:10.1016/j.compositesb.2011.10.001.
- [61] P.K. Mallick, *Fiber-Reinforced Composites*, Third Edit, Taylor and Francis Group, 2007.
- [62] A.K. Bledzki, J. Gassan, *Composites reinforced with cellulose based fibres*, 24 (1999) 221–274.
- [63] M. V Tzoumaki, T. Moschakis, C.G. Biliaderis, Effect of soluble polysaccharides addition on rheological properties and microstructure of chitin nanocrystal aqueous dispersions., *Carbohydr. Polym.* 95 (2013) 324–31. doi:10.1016/j.carbpol.2013.02.066.
- [64] I.A. Sacui, R.C. Nieuwendaal, D.J. Burnett, S.J. Stranick, M. Jor, C. Weder, et al., Comparison of the Properties of Cellulose Nanocrystals and Cellulose Nano fi brils Isolated from Bacteria, Tunicate, and Wood Processed Using Acid, Enzymatic, Mechanical, and Oxidative Methods, *Appl. Mater. Interfaces*. (2014) 6127 – 6138.
- [65] K. Gopalan Nair, A. Dufresne, Crab shell chitin whisker reinforced natural rubber nanocomposites. 1. Processing and swelling behavior., *Biomacromolecules.* 4 (2003) 657–65. doi:10.1021/bm020127b.
- [66] P. Jindal, M. Goyal, N. Kumar, Mechanical characterization of multiwalled carbon nanotubes-polycarbonate composites, *Mater. Des.* 54 (2014) 864–868. doi:10.1016/j.matdes.2013.08.100.
- [67] M. Chan, K. Lau, T. Wong, M. Ho, D. Hui, Mechanism of reinforcement in a nanoclay/polymer composite, *Compos. Part B Eng.* 42 (2011) 1708–1712. doi:10.1016/j.compositesb.2011.03.011.
- [68] D.J. Shaw, *Introduction to Colloid and Surface Chemistry*, 3rd ed., Butterworths, 1980.
- [69] F.. Candau, R.. Ottewill, eds., *COLLOIDAL PROPERTIES OF LATEX PARTICLES*, 1990.
- [70] S.N.. Cassu, M.I. Felisberti, Comportamento dinâmico-mecânico e relaxações em polímeros e blendas poliméricas, *Quim. Nova.* 28 (2005) 255–263.
- [71] C.D. Han, *Rheology and Processing of Polymeric Materials*, Oxford university Press, 2007.
- [72] C.D. Han, *Rheology in Polymer Processing*, Academic Press, 1976.
- [73] N.M. Alves, C. De Azurcm, Molecular Motions in a Polycarbonate Composite as Studied by Thermally Stimulated Recovery and Dynamic Mechanical, *Macromol. Symp.* 148 (1999) 437 – 454.
- [74] G. Siqueira, H. Abdillahi, J. Bras, A. Dufresne, High reinforcing capability cellulose nanocrystals extracted from syngonanthus nitens (Capim Dourado), *Cellulose.* 17 (2010) 289 – 298.
- [75] S.M. Lee, *Handbook of Composite Reinforcements*, Willey, 1992.

- [76] R.L. Oréface, Effect of Particle Morphology on the Mechanical and Thermo Mechanical Behavior of Polymer Composites, *J. Brazilian Soc. Mech. Sci.* 23 (2001) 1–10.
- [77] PerkinElmer, *Dynamic Mechanical Analysis (DMA): A Beginners Guide*, PerkinElmer, 2013.
- [78] H.A. Barnes, *A Handbook of Elementary Rheology*, University of Wales, 2000.
- [79] F. Martoia, C. Perge, P.J.J. Dumont, L. Orgéas, M. a Fardin, S. Manneville, et al., Heterogeneous flow kinematics of cellulose nanofibril suspensions under shear., *Soft Matter*. 11 (2015) 4742–55. doi:10.1039/c5sm00530b.
- [80] W.C.K. Poon, *Colloidal Suspensions*, Claredon Press, 2012.
- [81] K.D. Mistic, *Micro and nanofibrillated cellulose (MNFC) as additive in complex suspensions : influence on rheology and dewatering*, Aalto University, 2014.
- [82] N. Willenbacher, K. Georgieva, *Rheology of Disperse Systems*, in: U.. Brockel, W.. Meier, G. Wagner (Eds.), *Prod. Des. Eng. Formul. Gels Pastes*, 1st ed., Wiley, 2013: pp. 7 – 49.
- [83] K.M. Lee, C.D. Han, Effect of hydrogen bonding on the rheology of polycarbonate/organoclay nanocomposites, *Polymer (Guildf)*. 44 (2003) 4573–4588. doi:10.1016/S0032-3861(03)00444-0.
- [84] M.M. Reddy, M. Misra, A.K. Mohanty, *Biodegradable Blends from Corn Gluten Meal and Poly(butylene adipate-co-terephthalate) (PBAT): Studies on the Influence of Plasticization and Destructurization on Rheology, Tensile Properties and Interfacial Interactions*, *J. Polym. Environ.* 22 (2014) 167–175. doi:10.1007/s10924-014-0640-4.
- [85] P.-G. de Gennes, Entangled polymers, *Phys. Today*. 36 (1983) 33. doi:10.1063/1.2915700.
- [86] A.M.F. Alhalawani, D.J. Curran, D. Boyd, M.R. Towler, The role of poly(acrylic acid) in conventional glass polyalkenoate cements, *J. Polym. Eng.* 36 (2016). doi:10.1515/polyeng-2015-0079.
- [87] H.M. Hassanabadi, M. Wilhelm, D. Rodrigue, A rheological criterion to determine the percolation threshold in polymer nano-composites, *Rheol. Acta*. 53 (2014) 869–882. doi:10.1007/s00397-014-0804-0.
- [88] J.V. Koleske, ed., *Paint and Coating Testing Manual*, 15th ed., American Society for Testing and Materials, 2012.
- [89] J. Vermant, P. Moldenaers, J. Mewis, M. Ellis, R. Garritano, Orthogonal superposition measurements using a rheometer equipped with a force rebalanced transducer, *Rev. Sci. Instrum.* 68 (1997) 4090. doi:10.1063/1.1148351.
- [90] M. Coletti, R. Pepi, Superposition of an orthogonal oscillation to study anisotropy in polymers, *AIP Conf. Proc.* 286 (2014) 286–289. doi:10.1063/1.4876834.
- [91] C. Mobuchon, P.J. Carreau, M.-C. Heuzey, N.K. Reddy, J. Vermant, Anisotropy of nonaqueous layered silicate suspensions subjected to shear flow, *J. Rheol. (N. Y. N. Y)*. 53 (2009) 517. doi:10.1122/1.3094911.

- [92] S. Kim, J. Mewis, C. Clasen, J. Vermant, Superposition rheometry of a wormlike micellar fluid, *Rheol. Acta.* 52 (2013) 727–740. doi:10.1007/s00397-013-0718-2.
- [93] M.J. John, S. Thomas, Biofibres and biocomposites, *Carbohydr. Polym.* 71 (2008) 343–364. doi:10.1016/j.carbpol.2007.05.040.
- [94] C. Mancera, F. Ferrando, J. Salvadó, N.E. El Mansouri, Kraft lignin behavior during reaction in an alkaline medium, *Biomass and Bioenergy.* 35 (2011) 2072–2079. doi:10.1016/j.biombioe.2011.02.001.
- [95] C. Crestini, M. Crucianelli, M. Orlandi, R. Saladino, Oxidative strategies in lignin chemistry: A new environmental friendly approach for the functionalisation of lignin and lignocellulosic fibers, *Catal. Today.* 156 (2010) 8–22. doi:10.1016/j.cattod.2010.03.057.
- [96] B.L. Brasileiro, J.L. Colodette, D.P. Veloso, A utilização de perácidos na deslignificação e no branqueamento de polpas celulósicas, *Quim. Nova.* 24 (2001) 819–829.
- [97] H.U. Suess, *Pulp Bleaching Today*, DE GRUYTER, 2010.
- [98] Y. Habibi, L. a Lucia, O.J. Rojas, Cellulose nanocrystals: chemistry, self-assembly, and applications., *Chem. Rev.* 110 (2010) 3479–500. doi:10.1021/cr900339w.
- [99] A.C.O. Sullivan, Cellulose : the structure slowly unravels, *Cellulose.* 4 (1997) 173–207.
- [100] R.A. Festucci-buselli, W.C. Otoni, C.P. Joshi, Structure , organization , and functions of cellulose synthase complexes in higher plants, 19 (2007) 1–13.
- [101] A. Endler, S. Persson, Cellulose synthases and synthesis in Arabidopsis., *Mol. Plant.* 4 (2011) 199–211. doi:10.1093/mp/ssq079.
- [102] L.J.. Prins, D.N.. Reinhoudt, P. Timmerman, The Cooperativity Concept, *Angew. Chemie Int. Ed.* (2001) 2382 – 2426. doi:1433-7851/01/4013-2383.
- [103] X. Qian, S.-Y. Ding, M.R. Nimlos, D.K. Johnson, M.E. Himmel, Atomic and Electronic Structures of Molecular Crystalline Cellulose I β : A First-Principles Investigation, *Macromolecules.* 38 (2005) 10580–10589. doi:10.1021/ma051683b.
- [104] V.I. Kovalenko, Crystalline cellulose: structure and hydrogen bonds, *Russ. Chem. Rev.* 79 (2010) 231–241. doi:10.1070/RC2010v079n03ABEH004065.
- [105] J.N. Israelachvili, *Intermolecular and Surface Forces*, 3rd ed., Academic Press, 2011.
- [106] S.M. Notley, Stretching and solvency of charged cellulose chains., *ACS Appl. Mater. Interfaces.* 1 (2009) 1218–23. doi:10.1021/am900096c.
- [107] V. Favier, *Etude de nouveaux matériaux composites obtenus à partir de latex filmogènes et de whiskers de cellulose : effets de percolation mécanique*, Grenoble INP, 1995.
- [108] C.M. Altaner, L.H. Thomas, A.N. Fernandes, M.C. Jarvis, How cellulose stretches: synergism between covalent and hydrogen bonding., *Biomacromolecules.* 15 (2014) 791–8. doi:10.1021/bm401616n.

- [109] M. Bergensträhle, K. Mazeau, L. a. Berglund, Molecular modeling of interfaces between cellulose crystals and surrounding molecules: Effects of caprolactone surface grafting, *Eur. Polym. J.* 44 (2008) 3662–3669. doi:10.1016/j.eurpolymj.2008.08.029.
- [110] I. Simon, L. Glasser, H.A. Scheraga, Structure of Cellulose. 2. Low-Energy Crystalline Arrangements, 998 (1988) 990–998.
- [111] T.. Okano, A. Sarko, Mercerization of Cellulose . I . X-Ray Diffraction Evidence for Intermediate Structures *, *J. Appl. Polym. Sci.* 29 (1984) 4175 – 4182.
- [112] T. Okano, A. Sark, Mercerization of Cellulose. II. Alkali-Cellulose Intermediates and a Possible Mercerization Mechanism, *J. Appl. Polym. Sci.* 30 (1985) 325–332.
- [113] H. Nishimura, A. Sarko, Mercerization of Cellulose. III. Changes in Crystallite Sizes, *J. Appl. Polym. Sci.* 33 (1987) 855–866.
- [114] H. Nishimura, A. Sarko, Mercerization of Cellulose. IV. Mechanism of Mercerization and Crystallite Sizes, *J. Appl. Polym. Sci.* 33 (1987) 867–874.
- [115] T. Okano, Influence of surface charge on viscosity behavior of cellulose microcrystal suspension *, (1999) 258–261.
- [116] E.D.T.. Atkins, J.. Blackwell, M.H. Litt, Texture of cellulose crystallized from hydrazine, *Polymer (Guildf)*. 20 (1979) 1978–1980.
- [117] M. Adsul, S.K. Soni, S.K. Bhargava, V. Bansal, Facile approach for the dispersion of regenerated cellulose in aqueous system in the form of nanoparticles., *Biomacromolecules*. 13 (2012) 2890–5. doi:10.1021/bm3009022.
- [118] E. Jin, J. Guo, F. Yang, Y. Zhu, J. Song, Y. Jin, et al., On the polymorphic and morphological changes of cellulose nanocrystals (CNC-I) upon mercerization and conversion to CNC-II, *Carbohydr. Polym.* In Press (2016). doi:10.1016/j.carbpol.2016.01.048.
- [119] M.N. Anglès, A. Dufresne, Plasticized Starch/Tunicin Whiskers Nanocomposites. 1. Structural Analysis, *Macromolecules*. 33 (2000) 8344–8353. doi:10.1021/ma0008701.
- [120] Y. Habibi, A. Goffin, N. Schiltz, E. Duquesne, A. Dufresne, Bionanocomposites based on poly (3 -caprolactone) -grafted cellulose nanocrystals by ring-opening polymerization, *J. Mater. Chem.* 18 (2008) 5002–5010. doi:10.1039/b809212e.
- [121] N. Wang, E. Ding, R. Cheng, Thermal degradation behaviors of spherical cellulose nanocrystals with sulfate groups, *Polymer (Guildf)*. 48 (2007) 3486–3493. doi:10.1016/j.polymer.2007.03.062.
- [122] F.J. Kolpak, J. Blackwell, M.H. Litt, Morphology of cellulose regenerated from hydrazine solution, *J. Polym. Sci. Polym. Lett. Ed.* 15 (1977) 655–658. doi:10.1002/pol.1977.130151103.
- [123] M. Hirota, N. Tamura, T. Saito, A. Isogai, Water dispersion of cellulose II nanocrystals prepared by TEMPO-mediated oxidation of mercerized cellulose at pH 4.8, *Cellulose*. 17 (2009) 279–288. doi:10.1007/s10570-009-9381-2.

- [124] Y. Yue, C. Zhou, A.D. French, G. Xia, G. Han, Q. Wang, et al., Comparative properties of cellulose nano-crystals from native and mercerized cotton fibers, *Cellulose*. 19 (2012) 1173–1187. doi:10.1007/s10570-012-9714-4.
- [125] M. Cheng, Z. Qin, Y. Liu, Y. Qin, T. Li, L. Chen, et al., Efficient extraction of carboxylated spherical cellulose nanocrystals with narrow distribution through hydrolysis of lyocell fibers by using ammonium persulfate as an oxidant, *J. Mater. Chem. A*. 2 (2014) 251–258. doi:10.1039/C3TA13653A.
- [126] L.P. Novo, J. Bras, A. Garcia, M.N. Belgacem, A. a. S. Curvelo, Subcritical water: A method for green production of cellulose nanocrystals, *ACS Sustain. Chem. Eng.* 3 (2015) 2839 – 2846. doi:10.1021/acssuschemeng.5b00762.
- [127] W.P. Flauzino Neto, H.A. Silvério, N.O. Dantas, D. Pasquini, Extraction and characterization of cellulose nanocrystals from agro-industrial residue – Soy hulls, *Ind. Crops Prod.* 42 (2013) 480–488. doi:10.1016/j.indcrop.2012.06.041.
- [128] O. Nechyporchuk, M.N. Belgacem, F. Pignon, Rheological properties of micro-/nanofibrillated cellulose suspensions: wall-slip and shear banding phenomena., *Carbohydr. Polym.* 112 (2014) 432–9. doi:10.1016/j.carbpol.2014.05.092.
- [129] W.-L. Sun, W.-F. Ye, W.-Y. Tao, Improving Enzymatic Hydrolysis of Cellulose from Rice Straw Using an Ionic Liquid [EMIM]Ac Pretreatment, *Energy Sources, Part A Recover. Util. Environ. Eff.* 35 (2013) 2042–2050. doi:10.1080/15567036.2010.532192.
- [130] S.P. Rowland, E.J. Roberts, S. Regional, The Nature of Accessible Surfaces in the Microstructure of Cotton Cellulose, 10 (1972) 2447–2461.
- [131] S.P. Rowland, P.S. Howley, Hydrogen bonding on accessible surfaces of cellulose from various sources and relationship to order within crystalline regions, *J. Polym. Sci. Part A Polym. Chem.* 26 (1988) 1769–1778. doi:10.1002/pola.1988.080260708.
- [132] K. Kulasinski, S. Keten, S. V. Churakov, D. Derome, J. Carmeliet, A comparative molecular dynamics study of crystalline, paracrystalline and amorphous states of cellulose, *Cellulose*. 21 (2014) 1103–1116. doi:10.1007/s10570-014-0213-7.
- [133] M. Roman, W.T. Winter, Effect of sulfate groups from sulfuric acid hydrolysis on the thermal degradation behavior of bacterial cellulose., *Biomacromolecules*. 5 (2004) 1671–7. doi:10.1021/bm034519+.
- [134] P.M. Visakh, S. Thomas, K. Oksman, A.P. Mathew, Crosslinked natural rubber nanocomposites reinforced with cellulose whiskers isolated from bamboo waste: Processing and mechanical/thermal properties, *Compos. Part A Appl. Sci. Manuf.* 43 (2012) 735–741. doi:10.1016/j.compositesa.2011.12.015.
- [135] M. Pereda, N. El Kissi, A. Dufresne, Extrusion of polysaccharide nanocrystal reinforced polymer nanocomposites through compatibilization with poly(ethylene oxide), *ACS Appl. Mater. Interfaces*. 6 (2014) 9365–75. doi:10.1021/am501755p.
- [136] D. Pasquini, E. De Moraes, A. Aprígio, M. Naceur, A. Dufresne, Extraction of cellulose whiskers from cassava bagasse and their applications as reinforcing agent in natural rubber, *Ind. Crop. Prod.* 32 (2010) 486–490. doi:10.1016/j.indcrop.2010.06.022.

- [137] M. Nagalakshmaiah, N. El Kissi, G. Mortha, A. Dufresne, Structural investigation of cellulose nanocrystals extracted from chili leftover and their reinforcement in cariflex-IR rubber latex, *Carbohydr. Polym.* 136 (2015) 945 – 954. doi:10.1016/j.carbpol.2015.09.096.
- [138] M. Oliveira Taipina, M.M.F. Ferrarezi, I.V.P. Yoshida, M.D.C. Gonçalves, Surface modification of cotton nanocrystals with a silane agent, *Cellulose.* 20 (2012) 217–226. doi:10.1007/s10570-012-9820-3.
- [139] H. Kargarzadeh, I. Ahmad, I. Abdullah, A. Dufresne, S.Y. Zainudin, R.M. Sheltami, Effects of hydrolysis conditions on the morphology, crystallinity, and thermal stability of cellulose nanocrystals extracted from kenaf bast fibers, *Cellulose.* 19 (2012) 855–866. doi:10.1007/s10570-012-9684-6.
- [140] S. Camarero Espinosa, T. Kuhnt, E.J. Foster, C. Weder, Isolation of thermally stable cellulose nanocrystals by phosphoric acid hydrolysis., *Biomacromolecules.* 14 (2013) 1223–30. doi:10.1021/bm400219u.
- [141] J.I. Morán, V. a. Alvarez, V.P. Cyras, A. Vázquez, Extraction of cellulose and preparation of nanocellulose from sisal fibers, *Cellulose.* 15 (2007) 149–159. doi:10.1007/s10570-007-9145-9.
- [142] E.D.M. Teixeira, T.J. Bondancia, K.B.R. Teodoro, A.C. Corrêa, J.M. Marconcini, L.H.C. Mattoso, Sugarcane bagasse whiskers: Extraction and characterizations, *Ind. Crops Prod.* 33 (2011) 63–66. doi:10.1016/j.indcrop.2010.08.009.
- [143] J. Sun, Isolation and characterization of cellulose from sugarcane bagasse, *Polym. Degrad. Stab.* 84 (2004) 331–339. doi:10.1016/j.polymdegradstab.2004.02.008.
- [144] S. Elazzouzi-Hafraoui, Y. Nishiyama, J.-L. Putaux, L. Heux, F. Dubreuil, C. Rochas, The shape and size distribution of crystalline nanoparticles prepared by acid hydrolysis of native cellulose., *Biomacromolecules.* 9 (2008) 57–65. doi:10.1021/bm700769p.
- [145] P.P. Zhang, D.S. Tong, C.X. Lin, H.M. Yang, Z.K. Zhong, W.H. Yu, et al., Effects of acid treatments on bamboo cellulose nanocrystals, (2014) 686–695. doi:10.1002/apj.
- [146] J. Lazko, T. Sénéchal, N. Landercy, L. Dangreau, J.-M. Raquez, P. Dubois, Well defined thermostable cellulose nanocrystals via two-step ionic liquid swelling-hydrolysis extraction, *Cellulose.* 21 (2014) 4195–4207. doi:10.1007/s10570-014-0417-x.
- [147] R.P. Feynman, A plenty of room at the bottom, *Eng. Sci.* (1960) 22 – 36.
- [148] R.H. French, V.A. Parsegian, R. Podgornik, R.F. Rajter, A. Jagota, J. Luo, et al., Long range interactions in nanoscale science, *Rev. Mod. Phys.* 82 (2010) 1887–1944. doi:10.1103/RevModPhys.82.1887.
- [149] V. Khoshkava, M.R. Kamal, Effect of surface energy on dispersion and mechanical properties of polymer/nanocrystalline cellulose nanocomposites., *Biomacromolecules.* 14 (2013) 3155–63. doi:10.1021/bm400784j.
- [150] S.R. Morrison, *The Chemical Physics of Surfaces*, Plenum Press, 1977.

- [151] P. Rittigstein, R.D. Priestley, L.J. Broadbelt, J.M. Torkelson, Model polymer nanocomposites provide an understanding of confinement effects in real nanocomposites., *Nat. Mater.* 6 (2007) 278–82. doi:10.1038/nmat1870.
- [152] R.S. Atalla, M.F. Crowley, M.E. Himmel, R.H. Atalla, Irreversible transformations of native celluloses, upon exposure to elevated temperatures., *Carbohydr. Polym.* 100 (2014) 2–8. doi:10.1016/j.carbpol.2013.06.007.
- [153] M.M. Nazhad, *Fundamentals of strength loss in recycled Paper*, University of British Columbia, 1994.
- [154] P. Rämänen, P. a. Penttilä, K. Svedström, S.L. Maunu, R. Serimaa, The effect of drying method on the properties and nanoscale structure of cellulose whiskers, *Cellulose*. 19 (2012) 901–912. doi:10.1007/s10570-012-9695-3.
- [155] A. Dufresne, Nanocellulose: a new ageless bionanomaterial, *Mater. Today*. 16 (2013) 220–227. doi:10.1016/j.mattod.2013.06.004.
- [156] J. Bras, D. Viet, C. Bruzzese, A. Dufresne, Correlation between stiffness of sheets prepared from cellulose whiskers and nanoparticles dimensions, *Carbohydr. Polym.* 84 (2011) 211–215. doi:10.1016/j.carbpol.2010.11.022.
- [157] M.M. de Souza Lima, R. Borsali, Rodlike Cellulose Microcrystals: Structure, Properties, and Applications, *Macromol. Rapid Commun.* 25 (2004) 771–787. doi:10.1002/marc.200300268.
- [158] S. Beck-Candanedo, M. Roman, D.G. Gray, Effect of reaction conditions on the properties and behavior of wood cellulose nanocrystal suspensions., *Biomacromolecules*. 6 (2006) 1048–1054. doi:10.1021/bm049300p.
- [159] A. Bendahou, H. Kaddami, A. Dufresne, Investigation on the effect of cellulosic nanoparticles' morphology on the properties of natural rubber based nanocomposites, *Eur. Polym. J.* 46 (2010) 609–620. doi:10.1016/j.eurpolymj.2009.12.025.
- [160] G. Siqueira, J. Bras, A. Dufresne, Cellulose whiskers versus microfibrils: influence of the nature of the nanoparticle and its surface functionalization on the thermal and mechanical properties of nanocomposites., *Biomacromolecules*. 10 (2009) 425–32. doi:10.1021/bm801193d.
- [161] V. Favier, J. Y. Cavaille, G.R. Canova, S.C. Shrivastava, Mechanical Percolation in Cellulose Whisker Nanocomposites, *Polym. Eng. Sci.* 37 (1997) 1732 – 1739.
- [162] P.. Coussot, *Mudflow Rheology and Dynamics*, CRC Press, 1997.
- [163] J.. Mewis, J. Vermant, Rheology of Sterically Stabilized Dispersions and Latices, *Prog. Org. Coatings*. 40 (2000) 111–117.
- [164] J. Mewis, N.J. Wagner, Thixotropy., *Adv. Colloid Interface Sci.* 147-148 (2009) 214–27. doi:10.1016/j.cis.2008.09.005.
- [165] D.B. Genovese, Shear rheology of hard-sphere, dispersed, and aggregated suspensions, and filler-matrix composites., *Adv. Colloid Interface Sci.* 171-172 (2012) 1–16. doi:10.1016/j.cis.2011.12.005.

- [166] D. Klemm, F. Kramer, S. Moritz, T. Lindström, M. Ankerfors, D. Gray, et al., Nanocelluloses: a new family of nature-based materials., *Angew. Chem. Int. Ed. Engl.* 50 (2011) 5438–66. doi:10.1002/anie.201001273.
- [167] D.M. Raymer, D.E. Smith, Spontaneous knotting of an agitated string., *Proc. Natl. Acad. Sci. U. S. A.* 104 (2007) 16432–7. doi:10.1073/pnas.0611320104.
- [168] B. Derakhshandeh, G. Petekidis, S. Shafiei Sabet, W.Y. Hamad, S.G. Hatzikiriakos, Ageing, yielding, and rheology of nanocrystalline cellulose suspensions, *J. Rheol. (N. Y. N. Y.)*. 57 (2013) 131. doi:10.1122/1.4764080.
- [169] S. Shafeiei-Sabet, W.Y. Hamad, S.G. Hatzikiriakos, Influence of degree of sulfation on the rheology of cellulose nanocrystal suspensions, *Rheol. Acta.* 52 (2013) 741–751. doi:10.1007/s00397-013-0722-6.
- [170] S.J. Eichhorn, Cellulose nanowhiskers: promising materials for advanced applications, *Soft Matter.* 7 (2011) 303. doi:10.1039/c0sm00142b.
- [171] M. Bercea, P. Navard, Shear Dynamics of Aqueous Suspensions of Cellulose Whiskers, *Macromolecules.* 33 (2000) 6011–6016. doi:10.1021/ma000417p.
- [172] S. Kalidindi, Z. Ounaies, H. Kaddami, Toward the preparation of nanocomposites with oriented fillers: electric field-manipulation of cellulose whiskers in silicone oil, *Smart Mater. Struct.* 19 (2010) 094002. doi:10.1088/0964-1726/19/9/094002.
- [173] M. Mariano, N. El Kissi, A. Dufresne, Cellulose nanocrystals and related nanocomposites: Review of some properties and challenges, *J. Polym. Sci. Part B Polym. Phys.* (2014) n/a–n/a. doi:10.1002/polb.23490.
- [174] J. Pan, W. Hamad, S.K. Straus, Parameters Affecting the Chiral Nematic Phase of Nanocrystalline Cellulose Films, *Macromolecules.* 43 (2010) 3851–3858. doi:10.1021/ma902383k.
- [175] R. McComb, J. Williams, The value of alkaline papers for recycling, *TAPPI J.* 64 (1981) 93–96.
- [176] S. Julien, E. Chornet, R.P. Overend, Influence of acid pretreatment (H₂SO₄, HCl , HNO₃) on reaction selectivity in the vacuum pyrolysis of cellulose that improved yields of levoglucosan are obtained by removal of inorganic, *J. Anal. Appl. Pyrolysis.* 27 (1993) 25–43.
- [177] H. Wang, C. Qian, M. Roman, Effects of pH and salt concentration on the formation and properties of chitosan-cellulose nanocrystal polyelectrolyte-macroion complexes., *Biomacromolecules.* 12 (2011) 3708–14. doi:10.1021/bm2009685.
- [178] M. Roman, Toxicity of Cellulose Nanocrystals: A Review, *Ind. Biotechnol.* 11 (2015) 25–33. doi:10.1089/ind.2014.0024.
- [179] C. Endes, S. Müller, O. Schmid, D. Vanhecke, E.J. Foster, a Petri-Fink, et al., Risk assessment of released cellulose nanocrystals – mimicking inhalatory exposure, *J. Phys. Conf. Ser.* 429 (2013) 012008. doi:10.1088/1742-6596/429/1/012008.
- [180] K. Hua, M. Strømme, A. Mihranyan, N. Ferraz, Nanocellulose from green algae modulates the in vitro inflammatory response of monocytes/macrophages, *Cellulose.* 22 (2015) 3673–3688. doi:10.1007/s10570-015-0772-2.

- [181] H. Kangas, M.H. Pitkanen, J. Vartiainen, M. Vikman, Biodegradability, composability and safety of cellulose nanofibrils (CNF) and CNF products, in: 2015 Int. Conf. Nanotechnol., TAPPI Press, Atlanta, 2015: p. 93.
- [182] N. Lin, A. Dufresne, Nanocellulose in biomedicine: Current status and future prospect, *Eur. Polym. J.* 59 (2014) 302–325. doi:10.1016/j.eurpolymj.2014.07.025.
- [183] D.O. de Castro, J. Bras, A. Gandini, N. Belgacem, Surface grafting of cellulose nanocrystals with natural antimicrobial rosin mixture using a green process., *Carbohydr. Polym.* 137 (2016) 1–8. doi:10.1016/j.carbpol.2015.09.101.
- [184] R. Kitey, H.V. Tippur, Role of particle size and filler–matrix adhesion on dynamic fracture of glass-filled epoxy. I. Macromolecular measurements, *Acta Mater.* 53 (2005) 1153–1165. doi:10.1016/j.actamat.2004.11.012.
- [185] S.-Y. Fu, X.-Q. Feng, B. Lauke, Y.-W. Mai, Effects of particle size, particle/matrix interface adhesion and particle loading on mechanical properties of particulate–polymer composites, *Compos. Part B Eng.* 39 (2008) 933–961. doi:10.1016/j.compositesb.2008.01.002.
- [186] J. Spanoudakis, R.J. Young, Crack propagation in a glass particle-filled epoxy resin Part 1 Effect of particle volume fraction and size, *J. Mater. Sci.* 19 (1984) 473–486.
- [187] P. Rittigstein, R.D. Priestley, L.J. Broadbelt, J.M. Torkelson, Model polymer nanocomposites provide an understanding of confinement effects in real nanocomposites., *Nat. Mater.* 6 (2007) 278–82. doi:10.1038/nmat1870.
- [188] V. Favier, G.R. Canova, J.Y. Cavallé, H. Chanzy, A. Dufresne, C. Gauthier, Nanocomposite Materials from Latex and Cellulose Whiskers, *Polym. Adv. Technol.* 6 (1995) 351–355.
- [189] V. Favier, H. Chanzy, J.Y. Cavaille, Polymer Nanocomposites reinforced by Cellulose Whiskers, *Macromolecules.* 28 (1996) 6365–6367.
- [190] A. Dufresne, M.R. Vignon, Improvement of Starch Film Performances Using Cellulose Microfibrils, *Macromolecules.* 31 (1998) 2693–2696.
- [191] A. Kutvonen, G. Rossi, S.R. Puisto, N.K.J. Rostedt, T. Ala-Nissila, Influence of nanoparticle size, loading, and shape on the mechanical properties of polymer nanocomposites., *J. Chem. Phys.* 137 (2012) 214901. doi:10.1063/1.4767517.
- [192] W. Chen, H. Yu, Y. Liu, P. Chen, M. Zhang, Y. Hai, Individualization of cellulose nanofibers from wood using high-intensity ultrasonication combined with chemical pretreatments, *Carbohydr. Polym.* 83 (2011) 1804–1811. doi:10.1016/j.carbpol.2010.10.040.
- [193] N. Ouali, J.Y. Cavaille, J. Perez, Elastic, Viscoelastic and Plastic Behavior of Multiphase Polymer Blends, *Plast. Rubber Compos. Process. Appl.* 16 (1991) 55–60.
- [194] R.R. Lahiji, X. Xu, R. Reifenberger, A. Raman, A. Rudie, R.J. Moon, Atomic force microscopy characterization of cellulose nanocrystals., *Langmuir.* 26 (2010) 4480–8. doi:10.1021/la903111j.
- [195] F. Azzam, L. Heux, J.-L. Putaux, B. Jean, Preparation by grafting onto, characterization, and properties of thermally responsive polymer-decorated cellulose nanocrystals., *Biomacromolecules.* 11 (2010) 3652–9. doi:10.1021/bm101106c.

- [196] Y. Jin, N. Hengl, S. Baup, F. Pignon, N. Gondrexon, M. Sztucki, et al., Ultrasonic assisted cross-flow ultrafiltration of starch and cellulose nanocrystals suspensions: characterization at multi-scales., *Carbohydr. Polym.* 124 (2015) 66–76. doi:10.1016/j.carbpol.2015.01.073.
- [197] M.A.S. Azizi Samir, F. Alloin, A. Dufresne, Review of recent research into cellulosic whiskers, their properties and their application in nanocomposite field., *Biomacromolecules.* 6 (2005) 612–26. doi:10.1021/bm0493685.
- [198] T. Chatterjee, R. Krishnamoorti, Rheology of polymer carbon nanotubes composites, *Soft Matter.* 9 (2013) 9515. doi:10.1039/c3sm51444g.
- [199] L. Tang, C. Weder, Cellulose whisker/epoxy resin nanocomposites., *ACS Appl. Mater. Interfaces.* 2 (2010) 1073–80. doi:10.1021/am900830h.
- [200] H.A. Silvério, W.P. Flauzino Neto, I.S.V. Da Silva, J.R. Rosa, D. Pasquini, R.M.N. De Assunção, et al., Mechanical, thermal, and barrier properties of methylcellulose/cellulose nanocrystals nanocomposites, *Polímeros.* 24 (2014) 683–688. doi:10.1590/0104-1428.1691.
- [201] E.H. Qua, P.R. Hornsby, Preparation and characterisation of nanocellulose reinforced polyamide-6, *Plast. Rubber Compos.* 40 (2011) 300–306. doi:10.1179/1743289810Y.0000000019.
- [202] E. Fortunati, D. Puglia, F. Luzi, C. Santulli, J.M. Kenny, L. Torre, Binary PVA bio-nanocomposites containing cellulose nanocrystals extracted from different natural sources: part I., *Carbohydr. Polym.* 97 (2013) 825–36. doi:10.1016/j.carbpol.2013.03.075.
- [203] A.C. Corrêa, E. Morais Teixeira, V.B. Carmona, K.B.R. Teodoro, C. Ribeiro, L.H.C. Mattoso, et al., Obtaining nanocomposites of polyamide 6 and cellulose whiskers via extrusion and injection molding, *Cellulose.* 21 (2013) 311–322. doi:10.1007/s10570-013-0132-z.
- [204] J.-M. Raquez, Y. Habibi, M. Murariu, P. Dubois, Polylactide (PLA)-based nanocomposites, *Prog. Polym. Sci.* 38 (2013) 1504–1542. doi:10.1016/j.progpolymsci.2013.05.014.
- [205] A. Junior de Menezes, G. Siqueira, A. a. S. Curvelo, A. Dufresne, Extrusion and characterization of functionalized cellulose whiskers reinforced polyethylene nanocomposites, *Polymer (Guildf).* 50 (2009) 4552–4563. doi:10.1016/j.polymer.2009.07.038.
- [206] N. Lin, A. Dufresne, Physical and/or Chemical Compatibilization of Extruded Cellulose Nanocrystal Reinforced Polystyrene Nanocomposites, *Macromolecules.* 46 (2013) 5570–5583. doi:10.1021/ma4010154.
- [207] J. Sapkota, S. Kumar, C. Weder, E.J. Foster, Influence of Processing Conditions on Properties of Poly (Vinyl acetate)/Cellulose Nanocrystal Nanocomposites, *Macromol. Mater. Eng.* 300 (2015) 562–571. doi:10.1002/mame.201400313.
- [208] J.O. Zoppe, M.S. Peresin, Y. Habibi, R. a Venditti, O.J. Rojas, Reinforcing poly(epsilon-caprolactone) nanofibers with cellulose nanocrystals., *ACS Appl. Mater. Interfaces.* 1 (2009) 1996–2004. doi:10.1021/am9003705.
- [209] H. Pan, L. Song, L. Ma, Y. Hu, Transparent Epoxy Acrylate Resin Nanocomposites Reinforced with Cellulose Nanocrystals, *Ind. Eng. Chem. Res.* 51 (2012) 16326–16332. doi:10.1021/ie301663q.

- [210] M.S. Peresin, Y. Habibi, J.O. Zoppe, J.J. Pawlak, O.J. Rojas, Nanofiber composites of polyvinyl alcohol and cellulose nanocrystals: manufacture and characterization., *Biomacromolecules*. 11 (2010) 674–81. doi:10.1021/bm901254n.
- [211] E.D. Cranston, D.G. Gray, Morphological and optical characterization of polyelectrolyte multilayers incorporating nanocrystalline cellulose., *Biomacromolecules*. 7 (2006) 2522–30. doi:10.1021/bm0602886.
- [212] S. Kumar, M. Hofmann, B. Steinmann, E.J. Foster, C. Weder, Reinforcement of stereolithographic resins for rapid prototyping with cellulose nanocrystals., *ACS Appl. Mater. Interfaces*. 4 (2012) 5399–407. doi:10.1021/am301321v.
- [213] L. Lemahieu, J. Bras, P. Tiquet, S. Augier, A. Dufresne, Extrusion of Nanocellulose-Reinforced Nanocomposites Using the Dispersed Nano-Objects Protective Encapsulation (DOPE) Process, *Macromol. Mater. Eng.* 296 (2011) 984–991. doi:10.1002/mame.201100015.
- [214] V. Khoshkava, M.R. Kamal, Effect of Cellulose Nanocrystals (CNC) Particle Morphology on Dispersion and Rheological and Mechanical Properties of Polypropylene/CNC Nanocomposites, *Biomacromolecules*. (2014) 3155 – 3163.
- [215] C. Xiang, H.-J. Sue, J. Chu, B. Coleman, Scratch behavior and material property relationship in polymers, *J. Polym. Sci. Part B Polym. Phys.* 39 (2001) 47–59. doi:10.1002/1099-0488(20010101)39:1<47::AID-POLB50>3.0.CO;2-2.
- [216] F. Pignon, A. Magnin, J.-M. Piau, Butterfly Light Scattering Pattern and Rheology of a Sheared Thixotropic Clay Gel, *Phys. Rev. Lett.* 79 (1997) 4689–4692. doi:10.1103/PhysRevLett.79.4689.
- [217] M. Zammarano, P.H. Maupin, L.-P. Sung, J.W. Gilman, E.D. McCarthy, Y.S. Kim, et al., Revealing the interface in polymer nanocomposites., *ACS Nano*. 5 (2011) 3391–9. doi:10.1021/nn102951n.
- [218] T. Villmow, P. Pötschke, S. Pegel, L. Häussler, B. Kretzschmar, Influence of twin-screw extrusion conditions on the dispersion of multi-walled carbon nanotubes in a poly(lactic acid) matrix, *Polymer (Guildf)*. 49 (2008) 3500–3509. doi:10.1016/j.polymer.2008.06.010.
- [219] D. Bandera, J. Sapkota, S. Josset, C. Weder, P. Tingaut, X. Gao, et al., Influence of mechanical treatments on the properties of cellulose nanofibers isolated from microcrystalline cellulose, *React. Funct. Polym.* 85 (2014) 134–141. doi:10.1016/j.reactfunctpolym.2014.09.009.
- [220] F. Alloin, A. D’Aprèa, A. Dufresne, N. El Kissi, F. Bossard, Poly(oxyethylene) and ramie whiskers based nanocomposites: influence of processing: extrusion and casting/evaporation, *Cellulose*. 18 (2011) 957–973. doi:10.1007/s10570-011-9543-x.
- [221] F. Inceoglu, J. Ville, N. Ghamri, J.L. Pradel, A. Durin, R. Valette, et al., Correlation Between Processing Conditions and Fiber Breakage During Compounding of Glass, *Polym. Compos.* (2011) 1842 – 1850. doi:10.1002/pc.
- [222] N. Follain, S. Belbekhouche, J. Bras, G. Siqueira, S. Marais, A. Dufresne, Water transport properties of bio-nanocomposites reinforced by *Luffa cylindrica* cellulose nanocrystals, *J. Memb. Sci.* 427 (2013) 218–229. doi:10.1016/j.memsci.2012.09.048.

- [223] M. Mariano, N. El Kissi, A. Dufresne, Cellulose nanocrystal reinforced oxidized natural rubber nanocomposites, *Carbohydr. Polym.* 137 (2016) 174–183. doi:10.1016/j.carbpol.2015.10.027.
- [224] K. Gopalan, A. Dufresne, Crab Shell Chitin Whisker Reinforced Natural Rubber Nanocomposites. 2. Mechanical Behavior, *Biomacromolecules*. 4 (2003) 666–674. doi:10.1021/bm0201284.
- [225] J. Bras, M.L. Hassan, C. Bruzesse, E. a. Hassan, N. a. El-Wakil, A. Dufresne, Mechanical, barrier, and biodegradability properties of bagasse cellulose whiskers reinforced natural rubber nanocomposites, *Ind. Crops Prod.* 32 (2010) 627–633. doi:10.1016/j.indcrop.2010.07.018.
- [226] M. Vestena, I.P. Gross, A.T.N. Pires, Nanocomposite of Poly(lactic acid)/Cellulose Nanocrystals: Effect of CNC Content on the Polymer Crystallization Kinetics, *J. Braz. Chem. Soc.* (2016) 1–7.
- [227] S. Camarero-Espinosa, D.J. Boday, C. Weder, E.J. Foster, Cellulose nanocrystal driven crystallization of poly(d , l -lactide) and improvement of the thermomechanical properties, *J. Appl. Polym. Sci.* 132 (2015) n/a–n/a. doi:10.1002/app.41607.
- [228] M. Mariano, N. El Kissi, A. Dufresne, Melt processing of cellulose nanocrystal reinforced polycarbonate from a masterbatch process, *Eur. Polym. J.* 69 (2015) 208–223. doi:10.1016/j.eurpolymj.2015.06.007.
- [229] D. Dubief, E. Samain, A. Dufresne, Polysaccharide Microcrystals Reinforced Amorphous Poly (-hydroxyoctanoate) Nanocomposite Materials, (1999) 5765–5771.
- [230] A. Dufresne, Dynamic mechanical analysis of the interphase in bacterial polyester/cellulose whiskers natural composites, *Compos. Interfaces*. 7 (2000) 53–67. doi:10.1163/156855400300183588.
- [231] N.E. Marcovich, M.L. Auad, N.E. Bellesi, S.R. Nutt, M.I. Aranguren, Cellulose micro/nanocrystals reinforced polyurethane, *J. Mater. Res.* 21 (2011) 870–881. doi:10.1557/jmr.2006.0105.
- [232] J. Carretero-gonza, H. Retsos, R. Verdejo, S. Toki, B.S. Hsiao, E.P. Giannelis, et al., Effect of Nanoclay on Natural Rubber Microstructure, (2008) 6763–6772.
- [233] X. Fu, G. Huang, Z. Xie, W. Xing, New insights into reinforcement mechanism of nanoclay-filled isoprene rubber during uniaxial deformation by in situ synchrotron X-ray diffraction, *RSC Adv.* 5 (2015) 25171–25182. doi:10.1039/C5RA02123E.
- [234] Y. Song, Q. Zheng, Linear rheology of nanofilled polymers, *J. Rheol. (N. Y. N. Y.)*. 59 (2015) 155–191. doi:10.1122/1.4903312.
- [235] F. Du, R.C. Scogna, W. Zhou, S. Brand, J.E. Fischer, K.I. Winey, Nanotube Networks in Polymer Nanocomposites: Rheology and Electrical Conductivity, *Macromolecules*. 37 (2004) 9048–9055. doi:10.1021/ma049164g.
- [236] R. Mangal, S. Srivastava, L. a Archer, Phase stability and dynamics of entangled polymer-nanoparticle composites., *Nat. Commun.* 6 (2015) 7198. doi:10.1038/ncomms8198.

- [237] V. Khoshkava, M.R. Kamal, Effect of drying conditions on cellulose nanocrystal (CNC) agglomerate porosity and dispersibility in polymer nanocomposites, *Powder Technol.* 261 (2014) 288–298. doi:10.1016/j.powtec.2014.04.016.
- [238] L. Tang, B. Huang, W. Ou, X. Chen, Y. Chen, Manufacture of cellulose nanocrystals by cation exchange resin-catalyzed hydrolysis of cellulose., *Bioresour. Technol.* 102 (2011) 10973–7. doi:10.1016/j.biortech.2011.09.070.
- [239] G. Siqueira, J. Bras, A. Dufresne, New process of chemical grafting of cellulose nanoparticles with a long chain isocyanate., *Langmuir.* 26 (2010) 402–11. doi:10.1021/la9028595.
- [240] J.-M. Raquez, Y. Murena, a.-L. Goffin, Y. Habibi, B. Ruelle, F. DeBuyl, et al., Surface-modification of cellulose nanowhiskers and their use as nanoreinforcers into polylactide: A sustainably-integrated approach, *Compos. Sci. Technol.* 72 (2012) 544–549. doi:10.1016/j.compscitech.2011.11.017.
- [241] P. Georgiopoulos, E. Kontou, M. Niaounakis, Thermomechanical Properties and Rheological Behavior of Biodegradable Composites, *Polym. Compos.* 35 (2014) 1140 – 1149. doi:10.1002/pc.
- [242] J.M. Raquez, Y. Nabar, R. Narayan, P. Dubois, Novel High-Performance Talc/Poly[(butylene adipate)-co-terephthalate] Hybrid Materials, *Macromol. Mater. Eng.* 293 (2008) 310–320. doi:10.1002/mame.200700352.
- [243] K.B.R. Teodoro, E.M. Teixeira, A. Campos, J.M. Marconcini, L.H.C. Mattoso, Whiskers de Fibra de Sisal Obtidos sob Diferentes Condições de Hidrólise Ácida: Efeito do Tempo e da Temperatura de Extração, *Polímeros.* 21 (2011).
- [244] N. Lin, A. Dufresne, Surface chemistry, morphological analysis and properties of cellulose nanocrystals with gradiented sulfation degrees., *Nanoscale.* 6 (2014) 5384–93. doi:10.1039/c3nr06761k.
- [245] F. Fahma, S. Iwamoto, N. Hori, T. Iwata, A. Takemura, Isolation, preparation, and characterization of nanofibers from oil palm empty-fruit-bunch (OPEFB), *Cellulose.* 17 (2010) 977–985. doi:10.1007/s10570-010-9436-4.
- [246] K. Benhamou, A. Dufresne, A. Magnin, G. Mortha, H. Kaddami, Control of size and viscoelastic properties of nanofibrillated cellulose from palm tree by varying the TEMPO-mediated oxidation time., *Carbohydr. Polym.* 99 (2014) 74–83. doi:10.1016/j.carbpol.2013.08.032.
- [247] A.E.J. Nooy, A.C. Besemer, H.V. Bekkum, Highly selective nitroxyl radical-mediated oxidation of primary alcohol groups in water-soluble glucans, *Carbohydr. Res.* 269 (1995) 89–98.
- [248] P. Russo, B. Vetrano, D. Acierno, M. Mauro, Thermal and Structural Characterization of Biodegradable Blends Filled With Halloysite Nanotubes, *Polym. Compos.* 34 (2012) 1460 – 1470. doi:10.1002/pc.
- [249] J.-H. Chen, C.-C. Chen, M.-C. Yang, Characterization of Nanocomposites of Poly(butylene adipate-co-terephthalate) blending with Organoclay, *J. Polym. Res.* 18 (2011) 2151–2159. doi:10.1007/s10965-011-9625-3.
- [250] D.G. Gray, Transcrystallization of polypropylene at cellulose nanocrystal surfaces, *Cellulose.* 15 (2007) 297–301. doi:10.1007/s10570-007-9176-2.

- [251] J. Yeh, C. Tsou, C. Huang, K. Chen, C. Wu, Compatible and Crystallization Properties of Poly (lactic acid)/ Poly (butylene adipate- co -terephthalate) Blends, *J. Appl. Polym. Sci.* 116 (2010) 680 – 687. doi:10.1002/app.
- [252] M.R. Kamal, V. Khoshkava, Effect of cellulose nanocrystals (CNC) on rheological and mechanical properties and crystallization behavior of PLA/CNC nanocomposites, *Carbohydr. Polym.* 123 (2015) 105–114. doi:10.1016/j.carbpol.2015.01.012.
- [253] G. Agoda-Tandjawa, S. Durand, S. Berot, C. Blassel, C. Gaillard, C. Garnier, et al., Rheological characterization of microfibrillated cellulose suspensions after freezing, *Carbohydr. Polym.* 80 (2010) 677–686. doi:10.1016/j.carbpol.2009.11.045.
- [254] M.-C. Li, Q. Wu, K. Song, S. Lee, Y. Qing, Y. Wu, Cellulose Nanoparticles: Structure–Morphology–Rheology Relationships, *ACS Sustain. Chem. Eng.* 3 (2015) 821–832. doi:10.1021/acssuschemeng.5b00144.
- [255] E.E.U. Benavides, G. Ao, V.A.. Davis, C.L. Kitchens, Rheology and Phase Behavior of Lyotropic Cellulose Nanocrystal Suspensions, *Macromolecules.* 44 (2011) 8990–8998.
- [256] M.-C. Li, Q. Wu, K. Song, Y. Qing, Y. Wu, Cellulose Nanoparticles as Modifiers for Rheology and Fluid Loss in Bentonite Water-based Fluids., *ACS Appl. Mater. Interfaces.* 7 (2015) 5006–16. doi:10.1021/acсами.5b00498.
- [257] S. Shafiei-Sabet, W.Y. Hamad, S.G. Hatzikiriakos, Rheology of Nanocrystalline Cellulose Aqueous Suspensions, *Langmuir.* 28 (2012) 17124–17133. doi:10.1021/la303380v.

CHAPTER II

Cellulose Nanocrystal Reinforced Oxidized Natural Rubber Nanocomposites

This chapter is based on **Cellulose Nanocrystal Reinforced Oxidized Natural Rubber Nanocomposites**. Published by **Carbohydrate Polymers**, 137 (2016), 174–183.

CONTENT

ABSTRACT.....	112
1 INTRODUCTION.....	113
2 EXPERIMENTAL	114
2.1 Materials.....	114
2.2 NR Oxidation.....	114
2.3 Preparation of Nanocomposite Films.	115
2.4 Characterizations	115
3 RESULTS AND DISCUSSION.....	116
3.1 NR Oxidation.....	116
3.2 Thermal Characterization	122
3.3 Toluene and Water Uptake.....	124
3.4 Mechanical Properties.	126
3.5 Colloidal Aqueous Behavior.	129
4 CONCLUSIONS	133
5 REFERENCES	134

ABSTRACT

Natural rubber (NR) latex particles were oxidized using KMnO_4 as oxidant to promote the insertion of hydroxyl groups in the surface polyisoprene chains. Different degrees of oxidation were investigated. Both unoxidized and oxidized NR (ONR) latex were used to prepare nanocomposite films reinforced with cellulose nanocrystals (CNCs) by casting/evaporation. The oxidation of NR was carried out to promote chemical interactions between the hydroxyl groups of ONR with those of CNCs through hydrogen bonding. The effect of the degree of oxidation of the NR latex on the rheological behavior of CNC/NR and CNC/ONR suspensions, as well as on the mechanical, swelling and thermal properties of ensuing nanocomposites was investigated. Improved properties were observed for intermediate degrees of oxidation but they were found to degrade for higher oxidation levels.

1 INTRODUCTION

According to its versatility and application volume, natural rubber (NR) is one of the most important elastomers with interesting strength, elasticity, flexibility, resilience, and abrasion resistance. Latex from rubber tree (*Hevea brasiliensis*) is virtually the source of all commercial NR and its first description appeared almost 500 years ago, during the first European expeditions to America. This biopolymer has a great economic and social importance, being practically the only rubber used until the mid-20th century. Today, NR is used in 50 thousand different products (as adhesives, tires, gloves, condoms, coatings, etc.) and its applications are still in expansion. [1,2] It is extracted as a white emulsion composed of cis-1,4-polyisoprene nanoparticles that usually exhibit a diameter of 100 nm or more. The dispersion is stabilized by phospholipids, carbohydrates, proteins and metal ions. [3,4] The drying or coalescence stage causes compaction, deformation and inter-diffusion of the individual latex particles. This phenomenon gradually improves the latex homogeneity and mechanical properties. [2]

The mechanical properties of NR can be improved and tailored by crosslinking [5] and addition of reinforcing fillers of varying chemistry and aggregate size/aspect ratio to suit the application concerned. [6-8] Moreover, due its high flexibility and low stiffness, NR is a perfect matrix to be used as a model system to study the effect of filler reinforcement. The use of filler as reinforcing agent is largely explored in materials science. Nanoparticles such as carbon nanotubes, ceramics and natural fibers, [9-12] can impart specific properties to the polymeric matrix. Not only the mechanical properties, [13-15] but also the crystallinity [16] and the permeability [17,18] of the matrix can be altered. Carbon black is the conventionally used filler in many applications of NR. It is produced from petroleum oil and is carcinogenic. Its use has therefore to be reduced through substitution with more eco-friendly components to reduce the health hazards and environmental issues. In this context, natural and renewable materials such as polysaccharide nanoparticles appear as a perfect option for the production of new light weight green composites. [19]

Among polysaccharides, cellulose is the most abundant material and cellulosic nanomaterials can be extracted from many natural resources as nanofibrils, [20,21] or nanocrystals (CNC). [22,23] The latter is generally obtained by an acid hydrolysis process of the cellulosic fiber, [24,25] which causes a depolymerization and solubilization of the amorphous regions. The extracted highly crystalline domains can be used as reinforcing agent, [26] in biomedical applications, [27] coatings, [28] and hydrogels, [29] among other applications, due to their high modulus, low density, dimensional stability and ability for surface modification. [30,31] Nanoscale fillers and concomitant high specific surface area are instrumental in imparting improved

mechanical performance to NR at low volume contents. [32] However, the efficiency of CNC on composite mechanical properties is strongly dependent on its dispersion and interactions with the matrix. These interactions can also change the rheological behavior of the latex particle/CNC suspension, which is relevant for coating applications. [33,34]

The hydrophobic NR matrix and hydrophilic CNC are inherently incompatible and insufficient molecular scale interactions can restrict the overall performance of the material. Moreover, CNC aggregates can lead to poor dispersion in the matrix and act as stress concentrator, resulting in poor properties of the composite. The conventional way to tailor and control the interfacial adhesion and interactions is the chemical grafting of specific moieties on the surface of CNC able to interact with the matrix. Another strategy, much less investigated, consists in modifying the matrix polymeric chains in contact with the filler. In the present study, oxidation of the NR latex particles (using KMnO_4 as oxidant) was performed to promote the insertion of hydroxyl groups in the surface polyisoprene chains. These groups were expected to create hydrogen bonding between the NR chains and CNC, as reported in a study aiming in improving the compatibility in blends composed of NR and starch. [35] The effect of the degree of oxidation of the NR latex on the rheological behavior of CNC/NR suspensions, and on the mechanical, swelling and thermal properties of ensuing nanocomposites was investigated.

2 EXPERIMENTAL

2.1 Materials

Potassium permanganate (KMnO_4) was purchased from Sigma Aldrich. Cellulose nanocrystals (CNCs) with 1.1% sulfur content were purchased from the University of Maine as an 11% aqueous suspension. The natural rubber (NR) latex was kindly received from Centrotrade Deutschland GmbH (Eschborn, Germany). It contained spherical particles with an average diameter around 300 nm and its solid content was about 60 wt%.

2.2 NR Oxidation

The NR latex suspension was oxidized with a KMnO_4 solution. An aqueous 0.125 mol.L^{-1} KMnO_4 solution was prepared by dissolving solid KMnO_4 in water. The NR latex suspension was diluted by adding 10 mL water to 3 g of NR (dry basis). The KMnO_4 solution was diluted to 0.0125 and $0.00125 \text{ mol.L}^{-1}$ and added dropwise to the diluted NR latex suspension under gentle stirring to oxidize the double bond

present in the isoprene (2-methyl-1,3-butadiene) monomer. The characteristic color change of the solution from pink to brown and the precipitation of solid MnO_2 indicated that the oxidation reaction was completed. NR samples with different degrees of oxidation were prepared and the oxidation level was expressed as $-\text{OH}$ groups borne by NR chains normalized to CNC particle amount. This ratio will be described in sequence.

2.3 Preparation of Nanocomposite Films

Firstly, the CNC suspension was dialyzed against water for one week to ensure neutral pH and removal of any possible salt present in the material. Then, the suspension was sonicated for 5 min to improve the dispersion of the nanoparticles. The oxidized NR latex suspension was mixed with the CNC suspension in the desired amount (we fixed the CNC content to 5 wt%) to obtain the final nanocomposite. This CNC content was lower than the percolation threshold to have direct information on the filler-matrix interactions and avoid interference of the formation of a network. The volume of the suspension was adjusted to 25 mL and it was magnetically stirred for 6 h to improve the homogenization. The mixture was casted on aluminum plates, dried in oven with air circulation at 40°C for 24 h and ensuing films were conditioned in desiccators containing silica gels for 4 days before testing. Reference CNC-free films consisting of unoxidized and oxidized NR, as well as unoxidized NR nanocomposite films were also prepared using the same protocol.

2.4 Characterizations

Atomic Force Microscopy (AFM). AFM images were obtained on a Nanoscope IIIa microscope from Veeco Instruments. A drop of a 0.01 wt% diluted CNC suspension was loaded on a mica substrate and imaged in tapping mode with a silicon cantilever. The nanocrystal dimensions were estimated from 50 measurements analyzed using ImageJ software.

UV-Visible Spectroscopy (UV-Vis). To evaluate the presence of Mn in the medium, absorbance was evaluated before and after oxidation. The tests were performed with a Shimadzu UV 2401-(PC) UV-Vis spectrophotometer within a wavelength range 300-700 nm.

Dynamic Light Scattering. NR latex suspensions with a concentration of 0.1 wt% and different degrees of oxidation were analyzed using Particle Size Analyzer VASCO

equipment. The average diameter and polydispersity index (PDI) of the particles were determined.

Fourier Transform Infrared Spectroscopy (FTIR). Infrared spectra were recorded on a FTIR Perkin-Elmer Spectrum One spectrometer. Samples were analyzed using a spectral width ranging from 600 to 4000 cm^{-1} with a 4 cm^{-1} resolution and an accumulation of 32 scans. All analyses were carried out in the ATR mode at room temperature.

Zeta Potential (ξ). NR suspensions with concentration around 0.01 wt% were analyzed on an equipment model DTS0230 from Malvern Instruments. To avoid the effects of ionic strength and pH during measurements, all the concentrated solutions were diluted in an aqueous standard solution with pH 10, ionic strength 5 mmol and 180 S/cm conductivity. This solution was prepared by the addition of diluted NaOH solution and solid NaCl into distilled water.

Rheological Experiments. The rheological behavior of the NR and CNC/NR dispersions was characterized with a DHR-3 equipment from TA Instruments. A cone (2°, 60 mm) - plate (60 mm) geometry was used to study the dilute suspensions in flow mode at 20°C. The viscosity values were always collected after stabilization. Shear rates ranging from 0.01 to 300 s^{-1} were applied for all systems. However, for some samples the measured stress was below the equipment's sensitivity limit and the determination of the viscosity was not possible until a minimum shear rate. The analyzed suspensions had the same composition as aqueous mixtures used to cast the films.

Thermal Analysis. Thermogravimetric analysis (TGA) of the samples was carried out under air atmosphere with a thermal analyzer Perkin-Elmer TGA-6 equipment from 30 to 600°C at a heating rate of 10°C.min⁻¹. Differential scanning calorimetry (DSC) analysis was performed with a TA DSC Q100 equipment. The samples (weight of 14 ± 2 mg) were sealed in aluminum pans and scanned from -80 to -20°C under a nitrogen atmosphere and heating rate of 10°C.min⁻¹.

Toluene and Water Uptake. The kinetics of toluene and water absorption was determined for all materials. The specimens were squared films with dimensions around 10 × 10 × 0.2 mm³. The films were thin enough so that the diffusion was supposed to be unidirectional. After being weighted using a four-digit balance, the samples were immersed in distilled water or toluene. They were removed at specific

intervals and weighted. The water uptake (WU) as well as toluene uptake (TU) was calculated as follows:

$$\text{WU (or TU)}(\%) = \frac{m_t - m_o}{m_o} \times 100$$

where m_o and m_t are the weights of the specimen before and after a time t of immersion, respectively.

Tensile Tests. The tensile high-strain mechanical tests were performed for cast films with two different equipments. Before mechanical analysis the samples were kept in desiccators containing silica gel for 4 days. The tensile modulus was determined using a RSA3 (TA Instruments, USA) with a load cell of 100 N. Sample dimensions were 0.7 ± 0.10 mm and 5.5 ± 0.5 mm for thickness and width, respectively, and the gap between pneumatic jaws at the start of each test was adjusted to 10 mm. The ultimate properties (strain at break and strength) were determined using an Instron 4501 machine with a load cell of 1000 N capacity. The specimen had similar dimensions as previously and the gap between pneumatic jaws at the start of each test was adjusted to 15 mm. All experiments were carried out at room temperature with a cross head speed of $0.5 \text{ mm}\cdot\text{s}^{-1}$. The results were averaged on five measurements.

Successive Tensile Tests. Successive tensile tests were performed to characterize the damage process occurring during tensile tests. They were carried out with an Instron 4501 machine with a load cell of 1000 N capacity. The specimen had similar dimensions as for tensile tests and the gap between pneumatic jaws at the start of each test was adjusted to 15 mm. At the beginning of each experiment, the sample was first stretched under a load of 1 N. Then, the experiment consisted of stretching the material at $0.5 \text{ mm}\cdot\text{s}^{-1}$ up to a certain elongation $\Delta L_1 = 15$ mm (cycle 1), then releasing the force down to 1 N, and stretching again the material up to a higher elongation $\Delta L_2 = 2\Delta L_1$ (cycle 2). This procedure was repeated with increasing elongation ΔL_i (cycle i) and seven successive tensile tests were conducted for each sample. The tensile modulus E_i for each successive cycle was determined from the initial slope of the stress-strain curve and used to calculate the relative tensile modulus, viz. the modulus of the composite measured during cycle i divided by the one measured for the same sample during the first stretching cycle, E_i/E_1 .

Dynamical Mechanical Analysis (DMA). DMA measurements were carried out with an apparatus RSA3 (TA Instruments, USA) working in the tensile mode. Rectangular strips with similar dimensions as for tensile tests were used. Tests were

performed under isochronal conditions at 1 Hz and the temperature was varied between -80 and 10°C with a heating rate of 2°C.min⁻¹.

3 RESULTS AND DISCUSSION

3.1 NR Oxidation

All the oxidation reactions were performed using CNC-free aqueous medium. The nanofiller was added to the suspension after the oxidation reaction to prevent any interference or degradation. Before casting the mixture for film preparation, the rheological behavior of the suspensions was analyzed as it can provide information about filler-polymer interaction in suspension, as will be discussed in sequence. The used CNCs were commercially available grade and extracted from hardwood, being composed of cellulose I β . The AFM image (Figure 1) shows the standard CNC rod-like particles. These particles are in the nanoscale, with dimensions around 179 \pm 40 nm for the length, and 8,3 \pm 1,8 nm for the diameter.

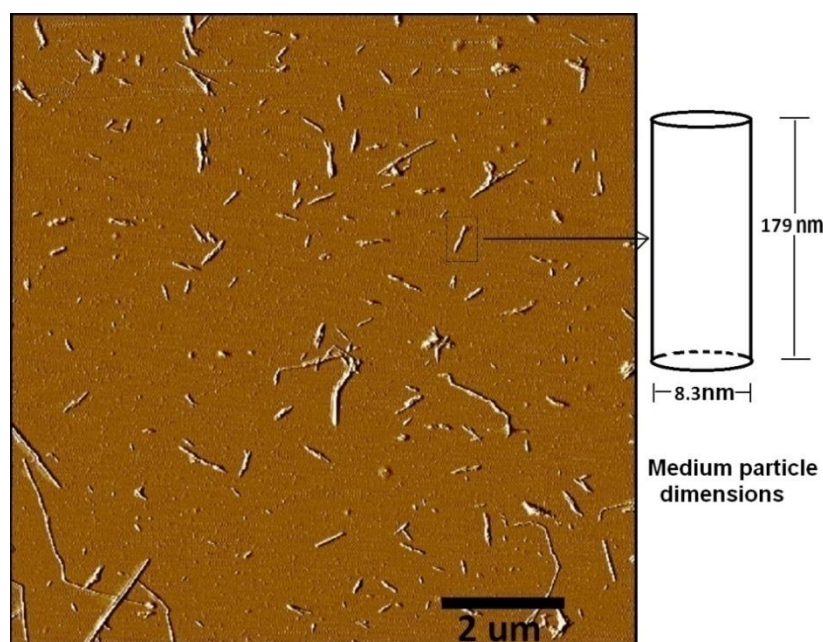


Figure 1. AFM image of CNCs after suspension drying.

These dimensions were used to estimate the area of an individual rod. Based on the CNC dry mass (5 wt% in 3 g of NR) and density of crystalline cellulose (1.6 g.cm⁻³), the total number of particles present in each sample was estimated to be around 1,7 \times 10⁻⁸ mol. This particle number was the base used to choose the different degrees of oxidation. Assuming that 1 mol of KMnO₄ can produce 2 mol of new -OH groups through the polymer oxidation reaction, the oxidant was used in such a way to obtain different ratios of hydroxyl groups and CNC as shown in Table 1.

Table 1. Codification of the samples, number of CNC particles, -OH groups borne by NR and molar ratio of NR-borne OH groups to number of CNC particles.

Sample	CNC content (wt%)	Number of CNC particles (mol)	New -OH groups (mol)	Ratio mol _{OH} :mol _{CNC}
NR	0	0	0	0
ONR2	0	0	2.5×10^{-7}	–
ONR3			2.5×10^{-6}	–
ONR4			2.5×10^{-5}	–
ONR5			2.5×10^{-4}	–
NRC			5	$1,7 \times 10^{-8}$
ONR2C	5	$1,7 \times 10^{-8}$	2.5×10^{-7}	$1,5 \times 10^1:1$
ONR3C			2.5×10^{-6}	$1,5 \times 10^2:1$
ONR4C			2.5×10^{-5}	$1,5 \times 10^3:1$
ONR5C			2.5×10^{-4}	$1,5 \times 10^4:1$

These new hydroxyl groups introduced by permanganate oxidation in the polymer chain can change the compatibility between the NR matrix and CNC due to possible hydrogen bonding interactions (Figure 2).

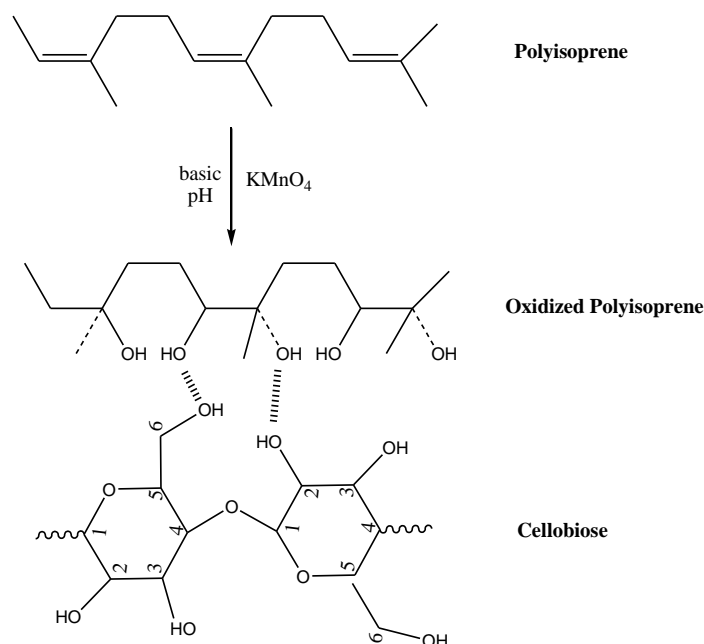


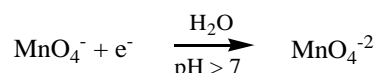
Figure 2. Scheme of NR oxidation and possible interactions between the oxidized polymer and cellulose nanocrystals.

In a basic medium, manganese (VII) ions (from MnO_4^-) are reduced to green manganese(VI) ions (in 2MnO_4^{2-}) (*Reaction I*), and then precipitated in a brown solid manganese(IV) oxide (in 2MnO_2 , manganese dioxide) (*Reaction II*).

Manganese (VII) has a characteristic absorption band in the UV region, with the maximum absorbance at 525 nm. This band can be used to confirm the oxidation reaction. During the oxidation reaction, manganese (VII) present in the suspension is

slowly converted to manganese (IV) and the characteristic purple color fades away. When an excess of MnO_4^- is present in the suspension, the purple color persists and it is indicative of the end of the reaction due the lack of double bonds available in the polymer. In this study, there was no sign of MnO_4^- in the latex suspension right after the reaction.

Reaction I



Reaction II



Figure 3 shows typical UV-Vis spectra for the diluted NR suspension after the oxidation reaction and the KMnO_4 solution used to perform the oxidation. The presence of the peak at 525 nm is obvious in the KMnO_4 solution, but no more visible in the NR suspension, indicating the complete consumption of the reagent. The peak located around 400 nm in the NR sample can be attributed to manganese (IV) due to MnO_2 formation, a consequence of the oxidant consumption.

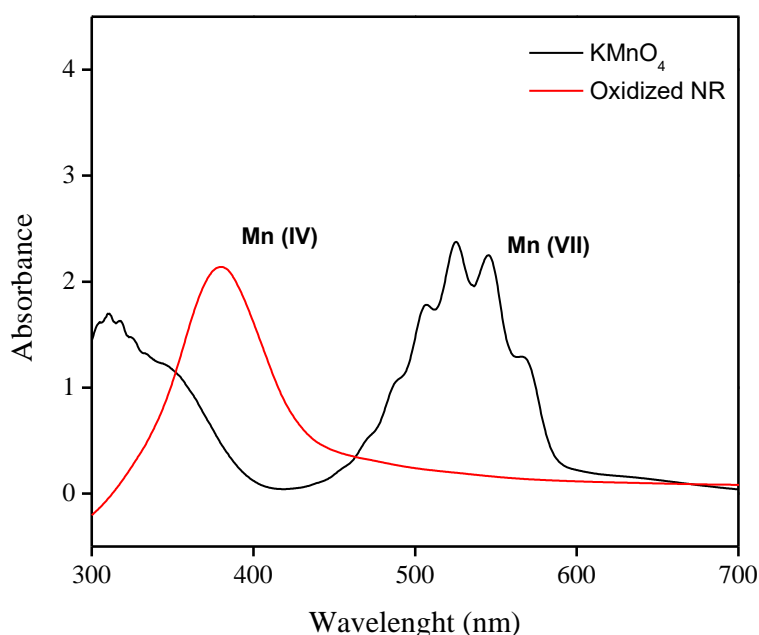


Figure 3. UV-Vis spectra for KMnO_4 solution and ONR5 suspension.

Figure 4 shows the FTIR spectra for unoxidized NR and oxidized NR (ONR) based nanocomposites. The curves don't show any sign of new signal, which suggests that secondary reactions (as aldehyde and carboxyl group formation) did not occur. Indeed, the spectra show a very characteristic curve for alkenes. Major part of the bands is related to $-\text{C}-\text{H}$ stretching and bending. Some signals dominate the spectra as $=\text{C}-\text{H}$ bending and $=\text{C}-\text{H}$ stretching at 840 cm^{-1} and 3035 cm^{-1} ,

respectively, as well as C–H bending at 1455 cm^{-1} and a series of bands between 2850 and 3000 cm^{-1} corresponding to C–H stretching. The absorbance FTIR analysis can provide information about the concentration of some species in the sample and it was used as a way to check the chemical modification of the material after the oxidation reaction. The reaction leads to the reduction of the number of unsaturated bonds -C=C- available at the surface of the latex particles, but didn't modify saturated groups, e.g. -CH_3 .

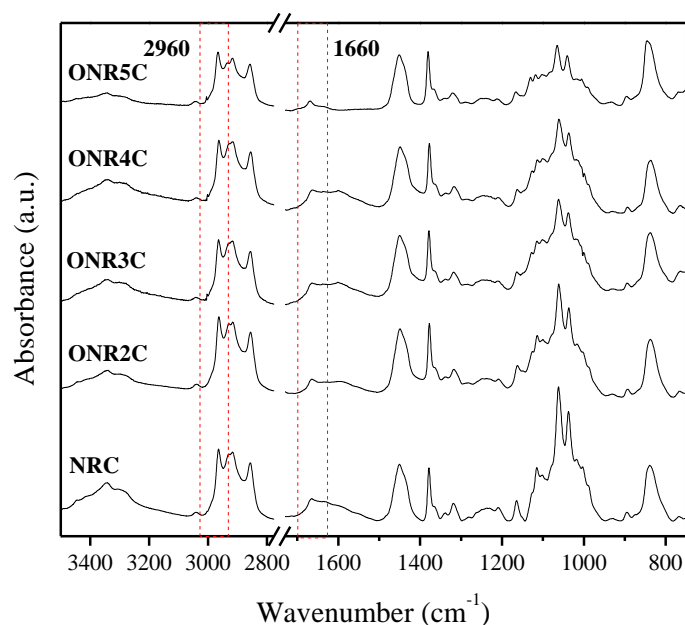


Figure 4. Absorbance FTIR spectra for NR and oxidized NR based nanocomposites.

An internal standard was used for each spectrum to investigate the decrease of the carbon double bonds in the spectrum. The magnitude of absorbance band at 2960 cm^{-1} (-CH_3) was assumed to remain constant due its inertness during the reaction and compared to the magnitude of the 1660 cm^{-1} (-C=C-) band. The values of the ratio of the magnitude of both bands, Abs_{2960}/Abs_{1660} , are shown in Figure 5 for the different NR samples.

This reduction in the unsaturated bonds leads to an increase in the $\text{-CH}_3/\text{-C=C-}$ ratio depending on the quantity of KMnO_4 used for the oxidation step. The decrease of the unsaturated bonds corroborates the manganese conversion from VII to IV and suggests the occurrence of the oxidation reaction. Still, it is worth noting that this analysis is not quantitative since the NR particles have molecules (stabilizers) on their surface that can be oxidized during the reaction. These secondary oxidations can slightly decrease the total number of -OH introduced in the polyisoprene chains.

The reaction occurrence can be also supported by the surface properties of the oxidized material. Nanocomposite films were prepared from the oxidized materials and they presented a higher hydrophilic character when

higher degrees of oxidation were performed to the NR chains. Contact angle measurements showed this relation between the degree of oxidation and hydrophilicity, with contact angle values for a water drop decreasing continuously from 98° for NRC to 55° for ONR5C. (results not shown - Table in appendix C)

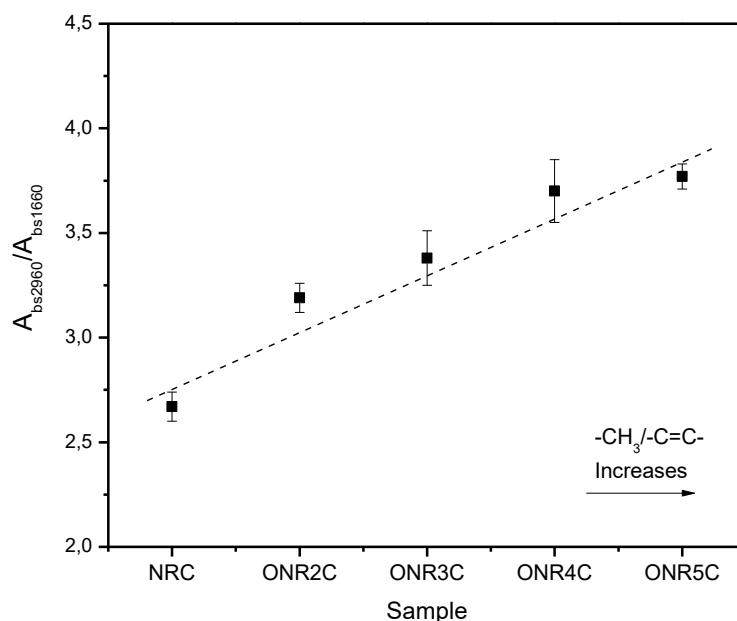


Figure 5. Absorbance ratio between $-\text{CH}_3$ and $-\text{C}=\text{C}-$ bands in the FTIR spectra for unoxidized and oxidized NR.

3.2 Thermal Characterization

The broad range of NR applications is strongly dependent of its thermal properties. An early degradation can cause worsening in the mechanical properties and gas release. Figure 6 shows the TGA thermograms obtained for CNC-free unoxidized and oxidized NR (panels a and b) and corresponding nanocomposites (panels c and d) when heated up to 650°C . Below 200°C a slight weight loss is observed for CNC-free specimens (Figure 6a) that can be attributed to the vaporization of water and NH_3 (used as NR stabilizer). This earlier mass loss is more pronounced for samples with higher oxidation levels, suggesting their higher water content ascribed to the higher hydrophilicity of these samples. The main degradation stage occurs in the temperature range $250\text{--}450^\circ\text{C}$. It is observed that the onset degradation temperature decreased as the degree of oxidation increased (Table 2). However, the dTG curves (Figure 6b) indicated that the degradation temperature remained constant regardless the oxidation level (Table 2). Around 425°C the dTG curves present a shoulder. Martins *et al* (2008) attributed this signal to crosslinked and cyclized networks, which degrade at higher temperatures. [36]

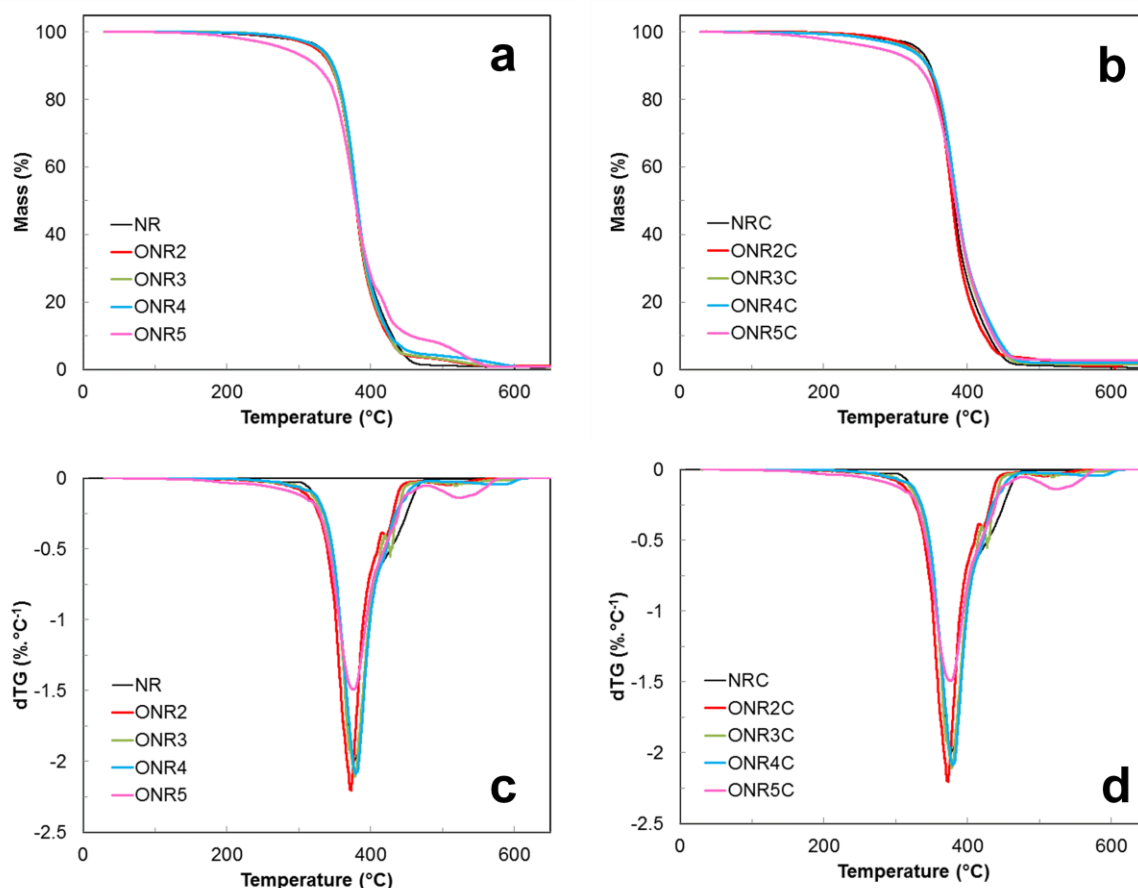


Figure 6. TGA (a,b) and dTG (c,d) curves for NR and oxidized NR (a,c), and NR and oxidized NR based nanocomposites (b,d).

Curves of TGA, obtained for nanocomposites, are reported in Figures 6c and 6d. All nanocomposites display an onset degradation temperature which is lower than the one of unoxidized neat NR and nanocomposite, but higher than their corresponding oxidized matrix (Table 2). A weak shift towards higher temperatures was observed for the dTG curves that could result from favorable interactions between the oxidized NR matrix and cellulosic filler. No clear signal associated to CNC degradation can be observed probably because of the low amount of CNC (5 wt%) and the relative broad degradation temperature range.

The residue remaining after the thermooxidative degradation of NR at 650°C is around 0.5% (Table 2) in agreement with previous studies.[36] It can be associated to the ash naturally present as a component of the latex or impurities added to the latex during the extraction and coagulation process at the plantation. It is observed that the char residue slightly increases when NR is oxidized. The metallic compound can probably increase the char residue due the formation of oxides. For nanocomposites, the char residue increases compared to their corresponding neat matrix. Sulfate groups present at the surface of CNC resulting from the sulfuric acid

hydrolysis process are known to increase the amount of charred residue, [24] indicating that these groups are flame-retardant in nature. The char residue increases as the degree of oxidation of the NR matrix increases.

Table 2. Thermal degradation data and glass transition temperature (T_g) value for NR, oxidized NR, and NR based nanocomposites reinforced with 5 wt% CNC, and zeta potential (ξ) values for NR and ONR suspensions with and without CNC.

Sample	Onset degradation temperature (°C)	dTG (°C)	Residue at 650°C (%)	T_g (°C)	ξ (mV.cm ⁻¹)
CNC	–	–	–	–	-38.4
NR	296	377	0.53	-63.6	-64.5
ONR2	265	377	0.90	-63.9	-61.5
ONR3	263	376	0.71	-64.8	-54.2
ONR4	259	378	0.82	-64.5	-52.9
ONR5	235	375	0.81	-62.6	-47.7
NRC	295	378	0.51	-64.6	-63.4
ONR2C	270	377	0.89	-64.9	-59.3
ONR3C	282	380	1.44	-64.4	-51.8
ONR4C	282	380	1.90	-64.4	-48.9
ONR5C	268	380	2.57	-62.2	-41.9

The glass transition temperature (T_g) value can provide information on how the chain mobility can be affected when adding CNC or changing the filler/matrix interactions. DSC experiments were performed for unfilled NR and nanocomposites and T_g values are collected in Table 2. The T_g value of NR remains almost unchanged when increasing its degree of oxidation or adding CNC, except for the highly oxidized sample (ONR5 and ONR5C) that shows a slight increase. It could be possibly ascribed to hydrogen bonding forces between NR chains and between NR chains and cellulosic surface that slightly hinder the molecular mobility.

3.3 Toluene and Water Uptake

The mass of sorbed liquid during immersion in either toluene or water was measured as a function of time for the unoxidized neat NR and nanocomposite, and oxidized NR based nanocomposites. Results are reported in Figure 7. All the specimens absorbed toluene during the experiment (Figure 7a). Two zones can be distinguished. The first zone, corresponding to $t < 5$ h, is characterized by fast absorption kinetics. Disruption of part of the neat NR film was observed after this time due to repetitive manipulations, preventing its weighing. In the second zone, associated with longer immersion times and observed only for nanocomposite films,

the toluene uptake stabilizes and reaches a plateau corresponding to the toluene uptake at equilibrium. Therefore, the addition of only 5 wt% CNC prevents the disruption of the NR film. A similar behavior was observed when using oxidized NR with a low degree of oxidation as matrix (ONR2C and ONR3C), even if the toluene uptake value seems to be slightly higher than for NRC at intermediate immersion times.

However, for highly oxidized NR based nanocomposites, a total dissolution of the sample occurred very quickly after only 20 min immersion in toluene. This behavior was rather unexpected since oxidation of the NR latex particles was supposed to increase the interfacial interactions between the NR chains and cellulosic surface, thus preventing the dissolution of the rubber in toluene. A possible explanation could be the degradation of NR chains during the oxidation reaction under harsh conditions that could promote the dissolution of modified rubber chains.

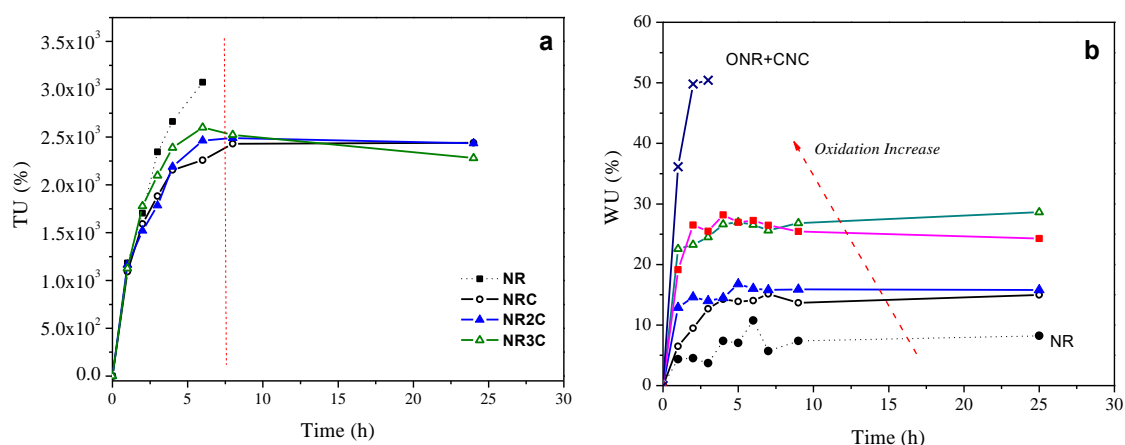


Figure 7. Evolution of (a) the toluene uptake (TU) and (b) the water uptake (WU) as a function of time at room temperature for NR (●), NRC (○), ONR2C (▲), ONR3C (Δ), ONR4 (■), and ONR5C (×). The solid lines serve to guide the eyes.

The evolution of water uptake as a function of time is reported in Figure 7b. The kinetics of absorption is fast and the WU value stabilizes after only around 2 h immersion in water. As expected, the water uptake at equilibrium was low for neat NR due to its hydrophobic character, whereas it increased significantly when adding 5 wt% CNC. Oxidation of the NR matrix was expected to bring two effects. On one hand, improved interfacial interactions should restrict the diffusion of water molecules in the vicinity of the cellulosic surface. On the other hand, the hydrophilization of NR chains would of course increase their sensitivity to water. It seems that the latter effect predominates the behavior of the composite film, since an increase of the water uptake is reported when increasing the degree of oxidation of the matrix. This effect is particularly marked for ONR5C. Moreover, the

hypothesized degradation of oxidized NR chains under harsh conditions should facilitate the swelling of the material.

3.4 Mechanical Properties

Tensile tests were performed at room temperature for NR, and nanocomposite materials reinforced with 5 wt% CNC using either unoxidized or oxidized NR as matrix. Results are reported in Table 3. As expected, an increase of both the modulus and the strength, and a decrease of the strain at break were reported when adding CNC to unoxidized NR in agreement with previous studies. [7,9,37] These previous studies showed that this alteration of the mechanical properties was observed, even below the percolation threshold of CNC. From the dimensions of CNC used in this study, the percolation threshold is around 3.6 vol%.

Table 3. Mechanical properties obtained from tensile tests for the neat natural rubber (NR), and unoxidized NR (NRC) and oxidized NR nanocomposites (ONR2-5C) reinforced with 5 wt% CNC.

Sample	Modulus(MPa)	Strain at break (%)	Strength (MPa)
NR	1.33 ± 0.39	878 ± 57	1.72 ± 0.39
NRC	7.47 ± 1.67	684 ± 69	2.08 ± 0.45
ONR2C	7.92 ± 1.02	703 ± 43	2.37 ± 0.42
ONR3C	8.36 ± 0.85	697 ± 40	2.18 ± 0.93
ONR4C	5.02 ± 1.13	570 ± 50	0.36 ± 0.05
ONR5C	0.72 ± 0.03	202 ± 58	0.11 ± 0.02

When comparing the behavior of nanocomposites prepared from unoxidized and oxidized NR, it seems that the materials with the lowest degrees of oxidation (ONR2C and ONR3C) display increased mechanical performance. However, the standard deviation is too high to conclude unambiguously. Nevertheless, a clear decrease of the mechanical properties is reported for highly oxidized nanocomposites that could originate from the decrease of the molecular weight of NR suggested from toluene swelling experiments.

Successive tensile tests were performed for these samples as described in the Experimental Section. Results are collected in Table 4. The experiment was difficult to implement with ONR5C because the sample was too soft to support the successive

mechanical solicitations. It is seen that the modulus measured during successive tensile tests for the neat unoxidized NR remains roughly constant showing the highly elastic behavior of this material. When adding 5 wt% CNC a clear decrease of the relative modulus is observed during successive cycles. It can be ascribed to the progressive damage of the filler-matrix interface. When using slightly oxidized NR (ONRC2) instead of unoxidized NR (NRC) as matrix, this decrease is less dramatic for the second cycle, probably because of stronger interface, but during the subsequent tensile cycles a similar behavior is observed. When increasing the degree of oxidation of the matrix a worsening of the mechanical behavior is reported during successive tests, possibly attributed to the lowering of the molecular weight of NR as already suggested from previous experiments.

Table 4. Relative tensile modulus E_i/E_1 obtained from successive tensile tests for the neat natural rubber (NR), and unoxidized NR (NRC) and oxidized NR nanocomposites (ONR2-4C) reinforced with 5 wt% CNC.

Sample	E_i/E_1						
	Cycle 1	Cycle 2	Cycle 3	Cycle 4	Cycle 5	Cycle 6	Cycle 7
NR	1.0	1.0	1.2	1.2	1.0	1.2	1.0
NRC	1.0	0.37	0.24	0.21	0.18	0.11	0.11
ONR2C	1.0	0.48	0.24	0.17	0.12	0.10	0.10
ONR3C	1.0	0.37	0.20	0.12	0.08	0.10	0.08
ONR4C	1.0	0.26	0.13	0.077	0.08	0.05	0.03

Figure 8 shows the isochronal evolution at 1 Hz of the storage tensile modulus as a function of temperature obtained from DMA measurements for the different sets of matrix reinforced with 5 wt% CNC. For low temperatures the NR matrix is in the glassy state and restricted molecular mobility limits the strain imposed by the applied stress resulting in a high modulus value of the material. The modulus value has been normalized to 1 GPa in this temperature range to overcome the experimental error due to sample dimensions measurements at room temperature for which it is soft. Around -65°C the modulus starts to sharply drop due to increased molecular mobility associated with the glass transition. Finally, at higher temperatures the NR matrix is in the rubbery state and the modulus tends to stabilize because of the cohesion provided by macromolecular entanglements.

When comparing the rubbery modulus of the unoxidized NR nanocomposite with its oxidized counterparts, a gradual increase is observed upon increasing the

degree of oxidation. However, for the highly oxidized sample (ONR5C) the modulus value is strongly reduced and similar to or even lower than the one for the unoxidized NR based nanocomposite.

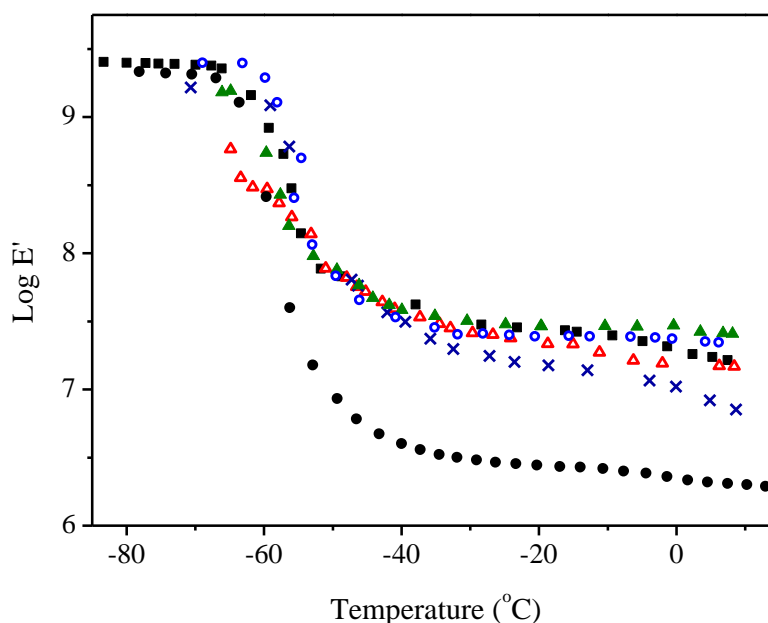


Figure 8. Evolution of the logarithm of the storage modulus as a function of temperature at 1 Hz for nanocomposites reinforced with 5 wt% CNC: NRC (●), ONR2C (○), ONR3C (▲), ONR4C (△), and ONR5C (×).

This effect can be visualized by plotting the evolution of the rubbery storage modulus estimated at 0°C as a function of the degree of oxidation (Figure 9). The tensile modulus values obtained from tensile tests are also reported in this Figure, as well as the gravimetrically determined water content of the material. The modulus determined from tensile tests is systematically lower than the one obtained by DMA.

This is obviously due, at least partially, to the temperature chosen to estimate the rubbery modulus from DMA (0°C) which is lower than room temperature adopted for tensile tests. In addition, it is worth noting that DMA involves weaker stresses than tensile tests, even in the linear region for which the modulus is determined. Therefore, the adhesion between the filler and the matrix is less involved in DMA than in tensile tests. However, the same global trend is observed with an optimal modulus value for intermediate degree of oxidation of the NR matrix. This type of behavior is usually associated to two antagonist and competitive effects. On one hand, the presence of hydroxyl groups in the NR chain can favor the interactions with the cellulosic surface, thus improving the interfacial stress transfer and stiffness of the material. This is probably the reason for the initial modulus increase. On the other hand, it promotes the possible interactions with water molecules as denoted by the increase of water content for highly oxidized samples (Figure 9). The latter effect most probably predominates over interfacial interactions explaining the final

modulus decrease. Moreover, a sharper modulus decrease vs. temperature is reported in Figure 8 indicating a possible lower molecular weight of the NR chains.

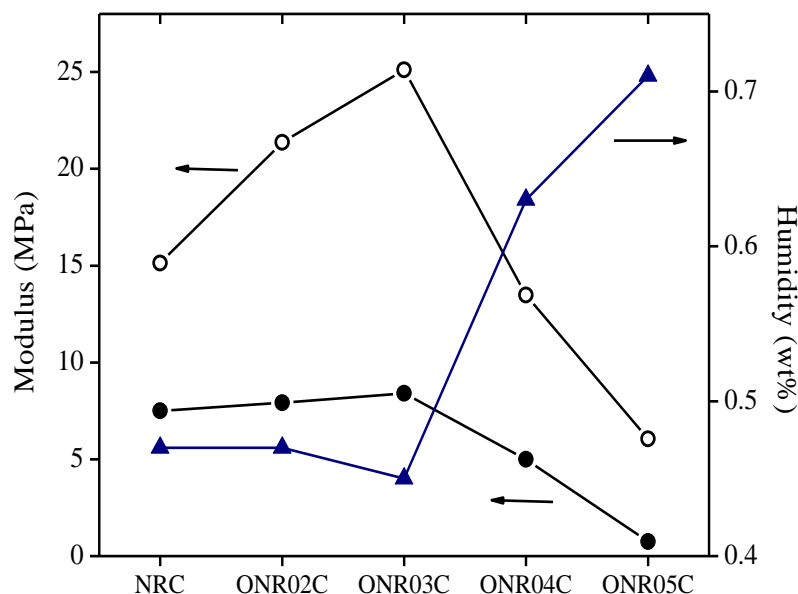


Figure 9. Correlation between the rubbery modulus determined from tensile tests (●) and DMA (○) and water content (▲) for unoxidized and oxidized NR nanocomposites reinforced with 5 wt% CNC.

3.5 Colloidal Aqueous Behavior

The mechanical tests showed that it was possible to improve the mechanical properties of the NR/CNC films by oxidizing the NR latex particles to a certain extent. This effect was hypothesized to result from favorable filler/matrix interactions ascribed to compatibilization provided by hydroxyl group insertion in the NR chains. However, as mentioned before, NR in natural form is a colloidal suspension of a hydrophobic polymer stabilized in a spherical form by natural stabilizers, such as proteins, and the oxidation of the material without previous dissolution of the matrix polymer in an organic solvent leads to only a surface oxidation, since the interior chains are not accessible to the reaction. Besides the importance of rubber materials in the solid state, their suspensions have important application as coatings. For this kind of application, the rheological properties of the system are very important.

DLS analysis was used as a way to check the possible degradation (like external chain dissolution) of the particles. Results reported in Table 3 show that regardless the oxidation level the particles present in the suspension were around 300 nm in diameter. This suggests no relation between the external chain oxidation and significant reduction in particle size, indicating no sign of particle degradation during the reaction due to external chains dissolution (although they are more

hydrophilic). The low PDI value for the different samples also suggests no short time aggregation of the particles upon oxidation.

Table 3. Diameter and polydispersity index (PDI) values obtained from DLS measurements for NR latex nanoparticles.

Sample	Diameter (nm)	PDI
NR	311	0.22
ONR2	308	0.16
ONR3	312	0.16
ONR4	295	0.24
ONR5	313	0.20

The zeta potential (ξ) has been determined for the different suspensions. Results are reported in Table 2. The ξ value increases continuously when increasing the degree of oxidation from -64 mV.cm^{-1} to -47.7 mV.cm^{-1} for NR and ONR5, respectively, which should result in a decrease in the suspension stability after oxidation. This result is rather surprising considering that the introduction of $-\text{OH}$ groups to the NR chain should provide higher electrostatic stability to the suspension in basic pH (where the hydroxyl groups could be deprotonated). According to Sansatsadeekul et al.⁴ the minimum ξ value for NR suspension occurs at pH 10 (being constant for higher pH values) attributed to ionization of carboxylic acid groups surrounding the rubber particle surface. The macromolecules at which this radical is attached can be decomposed by KMnO_4 (strong oxidant), decreasing the particle surface charge. It can be hypothesized that the oxidation step most probably destroys the stabilizers present at the particle surface, causing an increase in zeta potential. Moreover, the new $-\text{OH}$ groups at the surface can present high pKa value (the typical pKa value for alcoholic groups can be higher than 17) and keep themselves partially protonated at this pH, increasing the zeta potential.

CNC also shows a negative value for ξ . It is ascribed to the presence of surface sulfate groups resulting from the acid hydrolysis process with sulfuric acid used for their extraction. For suspensions containing both CNC and NR or ONR particles, less negative zeta potentials are reported compared to CNC-free suspensions, regardless the degree of oxidation of the latex (Table 2).

The extreme rheological conditions for the application of latex on solid surface have been estimated in terms of shear rate. [38] For the brushing step, a value higher than 5000 s^{-1} was estimated, while during the leveling of the coating, driven by the surface tension, it is lower than 1 s^{-1} . Figure 10 shows the evolution of the viscosity of different suspensions as a function of shear rate. The NR content was fixed at 12 wt%

(concentration close to what is normally used in flat paints),[39] and the CNC content was 0.6 wt% to be consistent with the composition of solid nanocomposite films. According to Bercea and Navard,[40] the critical concentration ϕ^* of the semidilute-concentrated transition for CNC suspended in water can be calculated using the rigid rod approximation:

$$\phi^{**} = \frac{d^2L}{L^2 \cdot d}$$

Where d is the diameter and L the length of the rod particles. For CNC with a length and a diameter of 179 nm and 8.3 nm, respectively, as investigated in this work, the boundary between the semidilute and concentrated regimes is $\phi^{**} = 0.46$ vol% (or 0.73 wt%). This value is higher than the volume fraction of the studied suspensions containing 0.6% wt (or 0.4vol%). It means that our rheological investigation was performed in the semidilute regime, implying that the suspensions are not completely isotropic and can show some anisotropic or nematic phases.

Figure 10a shows the rheological behavior for CNC and CNC-free NR suspensions. It is similar to results reported in literature for CNC [41] and NR. [42] For some samples a shear-thinning behavior, i.e. a viscosity decrease is observed when increasing the shear rate. This effect is more pronounced for the CNC sample, which also has higher viscosity at lower shear rates in comparison to NR. It is most probably ascribed to a random organization of the nanorods at lower shear rates, which progressively align when increasing the shear rate thus decreasing the viscosity. After complete alignment the viscosity starts to stabilize at higher shear rates. For NR suspensions, the viscosity values below 1 s^{-1} were not measurable because of the very low stresses involved, below the equipment's sensitivity limit. For NR and ONR3, an almost Newtonian flow behavior is observed between 10 and 300 s^{-1} . Moreover, when comparing both samples, no significant change is observed upon oxidation. However, a considerable increase of the viscosity is reported for the highly oxidized NR material (ONR5). It is worth noting that for this sample the number of $-\text{OH}$ groups (almost 100 times higher than for ONR3) should cause significant particle interactions resulting in higher viscosity values of the aqueous dispersion.

Figure 10b shows the influence of adding CNC to the suspensions. A clear difference is observed between unoxidized NR (NRC) and oxidized samples, mainly in the low shear rate region. In this shear rate range ($\dot{\gamma} < 1 \text{ s}^{-1}$), the viscosity should be mainly controlled by the CNC structure, since the NR latex displays a very low viscosity.

It is well-known that an increase in suspension viscosity can be attributed to either stronger particle interactions or particle size reduction. No modification in particle size was evidenced from DLS experiments. Then we can hypothesized that

the higher viscosity observed for oxidized samples compared to the unoxidized one is most probably related to improved polymer-filler and even polymer-polymer interactions in agreement with mechanical properties in the solid state and zeta potential measurements. These interactions can be broken when increasing the shear rate, resulting in a plateau value for the viscosity as observed for CNC, NRC and slightly oxidized NR samples. However, such a stabilization of the viscosity for higher shear rates is not reported for ONR5C, most probably because of stronger interactions.

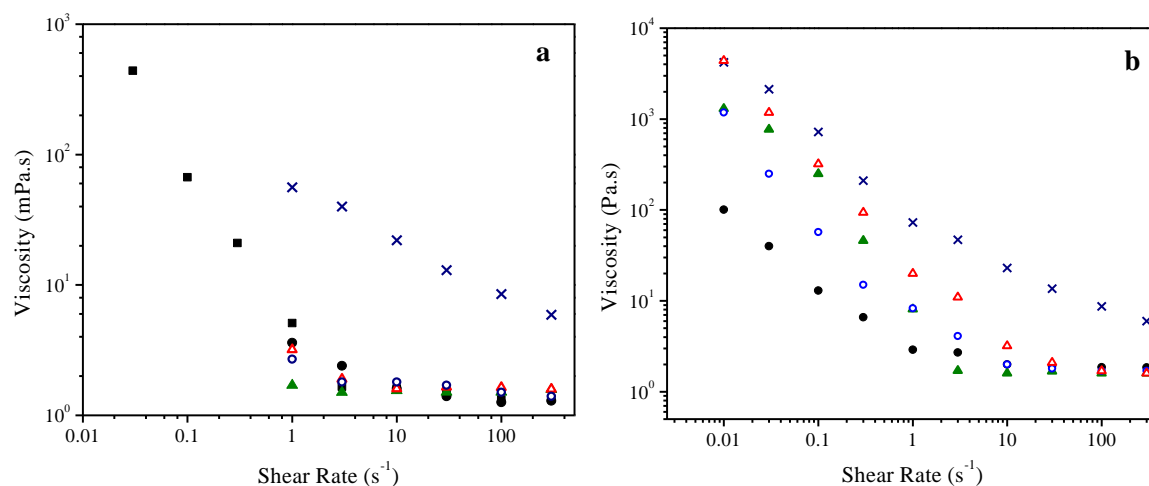


Figure 10. Evolution of the viscosity as a function of shear rate for aqueous suspensions containing (a) pristine materials: CNC (■), NR (●), ONR2 (○), ONR3 (▲), ONR4 (△), and ONR5 (×), and (b) CNC/NR mixtures: CNC + NR (●), CNC + ONR2 (○), CNC + ONR3 (▲), CNC + ONR4 (△), and CNC + ONR5 (×). The CNC content is 0.6 wt% and the NR content is 12 wt%.

4 CONCLUSIONS

Nanocomposite films have been prepared by casting and evaporating a mixture of natural rubber (NR) in latex form and cellulose nanocrystals (CNC). In order to improve the interfacial interactions between NR and CNC, oxidization of the NR latex was performed using KMnO_4 as oxidant before mixing with CNC. Different degrees of oxidation were realized with molar ratios of NR-borne OH groups to CNC nanoparticle number ranging from $5 \times 10^2:1$ to $5 \times 10^5:1$. The occurrence of induced OH groups at the surface of NR latex particles was accessed by UV-Vis and Fourier Transform Infrared spectroscopies.

The oxidization of NR latex particles decreased the onset degradation temperature, but didn't change the degradation temperature nor the glass transition temperature of the rubber. The dimensions of the particles were also preserved upon oxidization, but an increase of both the zeta potential and the viscosity of the aqueous dispersion (for the highly oxidized sample) were reported. A fixed ratio of 5 wt% CNC to NR was used to prepare the nanocomposites, i.e. below the percolation threshold of the nanoparticles. Rheological properties of the aqueous mixture evidenced improved interactions when increasing the degree of oxidation of the NR latex particles. After casting and evaporating this mixture, no significant change in the thermal behavior of the films was noticed upon oxidation.

When using NR with a low degree of oxidation, the addition of CNC prevented the disruption of the film upon immersion in toluene and improved the mechanical performance of the material. The application of successive tensile cycles highlighted stronger filler/matrix interface. However, higher water swelling was observed because of the hydrophilization of the NR chains. When using NR with higher degrees of oxidation, a fast dissolution of the specimen in toluene and a severe degradation of the mechanical properties were reported. Higher water sensitivity and probable decrease of the molecular weight of NR chains oxidized under harsh conditions were suspected to promote these effects.

REFERENCES

- [1] M.M. Rippel, F. Galembeck, Nanostructures and Adhesion in Natural Rubber: New Era for a Classic, 20 (2009) 1024–1030.
- [2] P. a. Steward, J. Hearn, M.C. Wilkinson, An overview of polymer latex film formation and properties, *Adv. Colloid Interface Sci.* 86 (2000) 195–267. doi:10.1016/S0001-8686(99)00037-8.
- [3] M. Bullaup, J. Bolze, N. Dingenouts, P. Hickl, D. Potschke, Small-angle X-ray scattering on latexes, 3066 (1996) 3043–3066.
- [4] J. Sansatsadeekul, J. Sakdapipanich, P. Rojruthai, Characterization of associated proteins and phospholipids in natural rubber latex., *J. Biosci. Bioeng.* 111 (2011) 628–34. doi:10.1016/j.jbiosc.2011.01.013.
- [5] K. Gopalan Nair, A. Dufresne, Crab shell chitin whisker reinforced natural rubber nanocomposites. 1. Processing and swelling behavior., *Biomacromolecules.* 4 (2003) 657–65. doi:10.1021/bm020127b.
- [6] J. Bras, M.L. Hassan, C. Bruzesse, E. a. Hassan, N. a. El-Wakil, A. Dufresne, Mechanical, barrier, and biodegradability properties of bagasse cellulose whiskers reinforced natural rubber nanocomposites, *Ind. Crops Prod.* 32 (2010) 627–633. doi:10.1016/j.indcrop.2010.07.018.
- [7] D. Pasquini, E. De Morais, A. Aprígio, M. Naceur, A. Dufresne, Extraction of cellulose whiskers from cassava bagasse and their applications as reinforcing agent in natural rubber, *Ind. Crop. Prod.* 32 (2010) 486–490. doi:10.1016/j.indcrop.2010.06.022.
- [8] S. Lecorre, J. Bras, A. Dufresne, Influence of the Botanic Origin of Starch Nanocrystals on the Morphological and Mechanical Properties of Natural Rubber Nanocomposites, *Macromol. Mater. Eng.* 297 (2012) 969–978. doi:10.1002/mame.201100317.
- [9] A. Bendahou, H. Kaddami, E. Espuche, F. Gouanve, A. Dufresne, Synergism Effect of Montmorillonite and Cellulose Whiskers on the Mechanical and Barrier Properties of Natural Rubber Composites, *Macromol. Mater. Eng.* 296 (2011) 760–769. doi:10.1002/mame.201000444.
- [10] J. Zhao, A.B. Morgan, J.D. Harris, Rheological characterization of polystyrene–clay nanocomposites to compare the degree of exfoliation and dispersion, *Polymer (Guildf).* 46 (2005) 8641–8660. doi:10.1016/j.polymer.2005.04.038.
- [11] P. Pötschke, A.R. Bhattacharyya, A. Janke, H. Goering, Melt mixing of polycarbonate/multi-wall carbon nanotube composites, *Compos. Interfaces.* 10 (2003) 389–404. doi:10.1163/156855403771953650.

- [12] C.M.O. Müller, J.B. Laurindo, F. Yamashita, Effect of cellulose fibers addition on the mechanical properties and water vapor barrier of starch-based films, *Food Hydrocoll.* 23 (2009) 1328–1333. doi:10.1016/j.foodhyd.2008.09.002.
- [13] P. He, Y. Gao, J. Lian, L. Wang, D. Qian, J. Zhao, et al., Surface modification and ultrasonication effect on the mechanical properties of carbon nanofiber/polycarbonate composites, *Compos. Part A Appl. Sci. Manuf.* 37 (2006) 1270–1275. doi:10.1016/j.compositesa.2005.08.008.
- [14] M.A.S. Azizi Samir, F. Alloin, A. Dufresne, Review of recent research into cellulosic whiskers, their properties and their application in nanocomposite field., *Biomacromolecules.* 6 (2005) 612–26. doi:10.1021/bm0493685.
- [15] A.L. Goffin, J.M. Raquez, E. Duquesne, G. Siqueira, Y. Habibi, A. Dufresne, et al., Poly(ϵ -caprolactone) based nanocomposites reinforced by surface-grafted cellulose nanowhiskers via extrusion processing: Morphology, rheology, and thermo-mechanical properties, *Polymer (Guildf).* 52 (2011) 1532–1538. doi:10.1016/j.polymer.2011.02.004.
- [16] S. Camarero-Espinosa, D.J. Boday, C. Weder, E.J. Foster, Cellulose nanocrystal driven crystallization of poly(*d, l*-lactide) and improvement of the thermomechanical properties, *J. Appl. Polym. Sci.* 132 (2015) n/a–n/a. doi:10.1002/app.41607.
- [17] S. Belbekhouche, J. Bras, G. Siqueira, C. Chappey, L. Lebrun, B. Khelifi, et al., Water sorption behavior and gas barrier properties of cellulose whiskers and microfibrils films, *Carbohydr. Polym.* 83 (2011) 1740–1748. doi:10.1016/j.carbpol.2010.10.036.
- [18] N. Follain, S. Belbekhouche, J. Bras, G. Siqueira, S. Marais, A. Dufresne, Water transport properties of bio-nanocomposites reinforced by *Luffa cylindrica* cellulose nanocrystals, *J. Memb. Sci.* 427 (2013) 218–229. doi:10.1016/j.memsci.2012.09.048.
- [19] N. Lin, A. Dufresne, Physical and/or Chemical Compatibilization of Extruded Cellulose Nanocrystal Reinforced Polystyrene Nanocomposites, *Macromolecules.* 46 (2013) 5570–5583. doi:10.1021/ma4010154.
- [20] N. Lavoine, I. Desloges, A. Dufresne, J. Bras, Microfibrillated cellulose - its barrier properties and applications in cellulosic materials: a review., *Carbohydr. Polym.* 90 (2012) 735–64. doi:10.1016/j.carbpol.2012.05.026.
- [21] M. Jonoobi, R. Oladi, Y. Davoudpour, K. Oksman, A. Dufresne, Y. Hamzeh, et al., Different preparation methods and properties of nanostructured cellulose from various natural resources and residues: a review, *Cellulose.* 22 (2015) 935–969. doi:10.1007/s10570-015-0551-0.
- [22] A. Dufresne, Nanocellulose: a new ageless bionanomaterial, *Mater. Today.* 16 (2013) 220–227. doi:10.1016/j.mattod.2013.06.004.

- [23] M. Mariano, N. El Kissi, A. Dufresne, Cellulose nanocrystals and related nanocomposites: Review of some properties and challenges, *J. Polym. Sci. Part B Polym. Phys.* 52 (2014) 791–806. doi:10.1002/polb.23490.
- [24] M. Roman, W.T. Winter, Effect of sulfate groups from sulfuric acid hydrolysis on the thermal degradation behavior of bacterial cellulose., *Biomacromolecules.* 5 (2004) 1671–7. doi:10.1021/bm034519+.
- [25] N. Lin, A. Dufresne, Surface chemistry, morphological analysis and properties of cellulose nanocrystals with gradiented sulfation degrees., *Nanoscale.* 6 (2014) 5384–93. doi:10.1039/c3nr06761k.
- [26] D.D. Jesus, M. Luiza, O.D. Almeida, Nanocrystals de celulose Cellulose whiskers, *O Pap.* 7 (2009) 34–52.
- [27] N. Lin, A. Dufresne, Nanocellulose in biomedicine: Current status and future prospect, *Eur. Polym. J.* 59 (2014) 302–325. doi:10.1016/j.eurpolymj.2014.07.025.
- [28] B. Poaty, V. Vardanyan, L. Wilczak, G. Chauve, B. Riedl, Modification of cellulose nanocrystals as reinforcement derivatives for wood coatings, *Prog. Org. Coatings.* 77 (2014) 813–820. doi:10.1016/j.porgcoat.2014.01.009.
- [29] N. Lin, A. Dufresne, Supramolecular Hydrogels from In Situ Host – Guest Inclusion between Chemically Modified Cellulose Nanocrystals and Cyclodextrin, (2013).
- [30] G. Siqueira, J. Bras, A. Dufresne, New process of chemical grafting of cellulose nanoparticles with a long chain isocyanate., *Langmuir.* 26 (2010) 402–11. doi:10.1021/la9028595.
- [31] Y. Habibi, L. a Lucia, O.J. Rojas, Cellulose nanocrystals: chemistry, self-assembly, and applications., *Chem. Rev.* 110 (2010) 3479–500. doi:10.1021/cr900339w.
- [32] A. Dufresne, Natural Rubber Green Nanocomposites, in: S. Thomas, R. Stephen (Eds.), *Rubber Nanocomposites*, Wiley, 2010: pp. 113 – 144.
- [37] Y. Habibi, L. a Lucia, O.J. Rojas, Cellulose nanocrystals: chemistry, self-assembly, and applications., *Chem. Rev.* 110 (2010) 3479–500. doi:10.1021/cr900339w.
- [33] F. Grüneberger, T. Künniger, T. Zimmermann, M. Arnold, Rheology of nanofibrillated cellulose/acrylate systems for coating applications, *Cellulose.* 21 (2014) 1313–1326. doi:10.1007/s10570-014-0248-9.
- [34] V. Vardanyan, B. Poaty, G. Chauve, V. Landry, T. Galstian, B. Riedl, Mechanical properties of UV-waterborne varnishes reinforced by cellulose nanocrystals, *J. Coatings Technol. Res.* 11 (2014) 841–852. doi:10.1007/s11998-014-9598-3.
- [35] E. Trovatti, J. Felix, A. Gandini, A new approach to blending starch with natural rubber, *Polym. Int.* (2014). doi:10.1002/pi.4808.

- [36] M. a. Martins, R.M.B. Moreno, C.M. McMahan, J.L. Brichta, P.D.S. Gonçalves, L.H.C. Mattoso, Thermooxidative study of raw natural rubber from Brazilian IAC 300 series clones, *Thermochim. Acta.* 474 (2008) 62–66. doi:10.1016/j.tca.2008.06.001.
- [37] G. Siqueira, H. Abdillahi, J. Bras, A. Dufresne, High reinforcing capability cellulose nanocrystals extracted from *syngonanthus nitens* (Capim Dourado), *Cellulose.* 17 (2010) 289 – 298.
- [38] T.C. Patton, *Paint Flow and Pigment Dispersion: A Rheological Approach to Coating and Ink Technology*, Wiley-Interscience, 1979.
- [39] C.F. Lu, Latex paint rheology and performance properties, *Ind. Eng. Chem. Prod. Res. Dev.* 24 (1985) 412–417. doi:10.1021/i300019a015.
- [40] M. Bercea, P. Navard, Shear Dynamics of Aqueous Suspensions of Cellulose Whiskers, *Macromolecules.* 33 (2000) 6011–6016. doi:10.1021/ma000417p.
- [41] S. Shafeiei-Sabet, W.Y. Hamad, S.G. Hatzikiriakos, Influence of degree of sulfation on the rheology of cellulose nanocrystal suspensions, *Rheol. Acta.* 52 (2013) 741–751. doi:10.1007/s00397-013-0722-6.
- [42] R. Stephen, R. Alex, T. Cherian, S. Varghese, K. Joseph, S. Thomas, Rheological behavior of nanocomposites of natural rubber and carboxylated styrene butadiene rubber latices and their blends, *J. Appl. Polym. Sci.* 101 (2006) 2355–2362. doi:10.1002/app.23852.

CHAPTER III

Melt processing of cellulose nanocrystal reinforced polycarbonate from a masterbatch process

This chapter is based on **Melt processing of cellulose nanocrystal reinforced polycarbonate from a masterbatch process**. Published by **European Polymer Journal**, 69 (2015) 208–223.

CONTENTS

ABSTRACT.....	142
1 INTRODUCTION.....	143
2 EXPERIMENTAL	144
2.1 Materials.....	144
2.2 Preparation of CNC-PC masterbatch.....	145
2.3 Preparation of nanocomposites	145
2.4 Characterizations	146
3 RESULTS AND DISCUSSION.....	149
3.1 CNC/PC masterbatch	149
3.2 CNC reinforced PC nanocomposites	155
4 CONCLUSIONS	165
5 REFERENCES	166

ABSTRACT

Cellulose nanocrystal (CNC) reinforced polycarbonate (PC) nanocomposites were obtained by melt extrusion. Highly concentrated CNC/PC masterbatch was first prepared using a dissolution/precipitation process which was then diluted by extrusion. Water from the CNC aqueous dispersion was exchanged to pyridine. PC was dissolved in this suspension and the mixture was precipitated in water. Two different methodologies were adopted for the PC matrix. In the first one, PC was submitted to the same dissolution/precipitation process than masterbatch, whereas in the second approach, the PC pellets were directly mixed with the solid masterbatch capsules. The structural, thermal and mechanical properties of ensuing nanocomposite materials were investigated.

KEYWORDS: cellulose nanocrystal, polycarbonate, nanocomposite, melt processing, extrusion

1 INTRODUCTION

An intensive interest is paid to the use of nanoparticles extracted from biomass and renewable resources. Among them, cellulose nanomaterials or nanocellulose extracted from natural fibers using mechanical or chemical procedures are most probably the most promising materials. Many potential applications are envisaged for these nanomaterials but the most obvious one is related to their reinforcing capability in nanocomposite applications [1-5]. This makes sense given the structural function of cellulose in nature.

The effective utilization of nanofiller in nanocomposite materials strongly depends on their homogeneous dispersion within the polymer matrix to avoid the loss of the nanoscale and reduction of the specific surface area. To tackle this issue most investigations reported in literature used liquid medium and casting/evaporation as the processing technique benefiting from the good dispersion level of unmodified cellulose nanomaterials in water or polar liquids, or modified nanoparticles in apolar liquid medium. In view of the emerging marketing of nanocellulose, more industrial processing techniques are highly desirable. Melt processing techniques, such as extrusion and injection molding are obviously the targeted techniques.

In composite science the classical strategy consists in matching adequately the surface properties of the dispersed particles and continuous phase to improve the interfacial adhesion. Covalent and non-covalent functionalization and the use of surfactants are common tips to disperse nanocellulose in polymers [6]. Covalent functionalization is obviously the favorite strategy that allows chemists to freely express their expertise because of the reactivity of cellulose. However, covalent functionalization of the nanofiller normally involves complicate and expensive steps which can be prohibitive for most industrial uses. Moreover, it introduces defects and deteriorates nanocellulose percolation, and the full potential of the nanofiller is lost leading to mechanical properties which are far from the expectations, even if improvement is observed compared to direct extrusion of unmodified nanoparticles [7,8].

Non-covalent functionalization is an easier way to prevent aggregation of the cellulosic nanofiller within the polymeric matrix. Poly(ethylene oxide) (PEO) has been used as a compatibilizing agent for the melt processing of cellulose nanocrystals reinforced polymer nanocomposites[9,10]. After mixing the nanoparticles and PEO in water, the freeze-dried mixture was used to prepare nanocomposite materials with a low density polyethylene (LDPE) matrix by extrusion. Greatly improved dispersion of the cellulose nanomaterial was observed but unfortunately the mechanical properties of ensuing materials were very poor because only the intrinsic mechanical properties of cellulose nanocrystals were involved[10]. A similar approach was used

to prepare CNC reinforced polylactic acid (PLA) nanocomposites [11]. A spray freeze drying technique was also shown to improve the dispersion of CNC in polypropylene (PP) over spray drying or freeze drying [12,13].

An interesting approach recently reported for the preparation of CNC reinforced LDPE consisted in preparing first an aerogel by exchanging the solvent of an aqueous CNC dispersion against acetone, impregnating the resulting organogel, in which the CNCs form a percolating network with a hot LDPE solution in toluene, and compression-molding the resulting materials[14]. Even if this template process in its present form is not directly scalable for technological exploitation, the fact that the high level of dispersion was largely maintained upon compression-molding films and also reprocessing and “diluting” such nanocomposites in an extruder bodes well for the development of alternative mixing approaches. However, it was shown that mixer design and in particular the shear rate that is applied during processing may have a significant influence on the properties of polymeric nanocomposites reinforced with CNC [15].

In the present study, coating of cellulose nanocrystals (CNCs) was performed using the same polymer as for the matrix using a dissolution/precipitation process. The ensuing highly concentrated masterbatch was then diluted by extrusion. A similar strategy was used for processing CNC reinforced polyamide 6 nanocomposites but the CNC concentration was limited to 1 wt% [16]. Polycarbonate (PC) was chosen in the present study because it is a thermoplastic polymer that is easily worked, molded, and thermoformed. It is highly transparent to visible light, with better light transmission than many kinds of glass and because of this property PC finds many applications in optical devices. This polymer is a durable material, but although it has high impact-resistance, its scratch-resistance is poor and so a hard coating is generally applied to polycarbonate eyewear lenses and polycarbonate exterior automotive components. However, the melt processing of CNC reinforced PC is a major and ongoing challenge due its high viscosities and required high temperatures.

2 EXPERIMENTAL

2.1 Materials

Polycarbonate (PC) used in this work was a commercial grade MAKROLON LQ2647, kindly provided by Bayer S.A.S. Pyridine was purchased from Sigma-Aldrich. Cellulose nanocrystals (CNCs) with 1.1% sulfur content were purchased from the

University of Maine as an 11% aqueous suspension and used without further purification.

2.2 Preparation of CNC-PC masterbatch

Solvent exchange. The main issue with nanocomposites is related to the poor dispersion of the dispersed nanomaterial in the continuous matrix. To overcome this obstacle and avoid self-aggregation of the nanoparticles, never dried CNC was used in this work. A solvent exchange procedure from water to pyridine was performed by adding a small amount of NaCl to the aqueous suspension in order to allow the precipitation of the nanocrystals. Successive cycles of centrifugation (10 min and 10,000 rpm) and substitution of the supernatant from water to pyridine were realized several times until the complete substitution of water by pyridine. The final suspension was homogenized with ultraturax.

Coating CNC with polycarbonate. The previously obtained CNC suspension in pyridine was diluted with extra pyridine and the desired amount of PC was added to obtain the weight ratios of 8/1 (pyridine/PC) and 4/1 (PC/CNC). The system was let under magnetic stirring at room temperature until the complete dissolution of PC. The suspension was syringed into water under a gentle magnetic stirring to precipitate the CNC/PC mixture. The formed solid particles were collected, washed with distilled water and dried at room temperature until no evidence of residual solvent was detected. Precipitation in water accelerates the production of CNC/PC capsules because it eliminates the necessity of solvent evaporation and facilitates the recovery of the solvent if needed.

2.3 Preparation of nanocomposites

To prepare the CNC reinforced PC nanocomposites, two different methodologies were adopted for the PC matrix. In the first one, PC was dissolved in CNC-free pyridine and precipitated in water before being mixed with the solid masterbatch capsules. In the second approach, the PC pellets were milled in a knife mill and then mixed with the solid masterbatch capsules. It means that all composites contain PC chains having undergone a dissolution/precipitation process. All polymer chains are considered when using the milling methodology to prepare the PC matrix, and only the PC chains from the capsules are considered when using the dissolution/precipitation methodology. The objective was to investigate the influence of the dissolution/precipitation step of PC chains on the final properties of the material.

In both cases the methodology for composite preparation was similar. The polycarbonate (either dissolved and precipitated, or milled) and the solid masterbatch capsules consisting of coated cellulose nanocrystals (CCNC) were dried in an oven with air circulation for 4 hours at 80°C to eliminate any residual pyridine and water. The masterbatch capsules were extruded with PC in a twin-screw micro extruder model DSM 15 Microcompounder with six heating areas and temperature gradient of 200-230°C to obtain nanocomposites with the desired CNC content. The final materials and the sample nomenclature used in this study are listed in Table 1.

Table 1. Sample nomenclature.

Nomenclature	Sample	CNC content (wt%)
CNC	Cellulose nanocrystals	100
CCNC	Coated cellulose nanocrystals	20
PC	Polycarbonate	-
PCex	Milled-extruded polycarbonate	1, 3
PCexs	Dissolved-extruded polycarbonate	1, 3

2.4 Characterizations

Microscopies. Scanning electronic microscopy (SEM) was carried on a Quanta 200 FEI device (Everhart–Thornley detector) equipment. The spherical masterbatch capsules were cut with a razor blade and gold-coated. Atomic force microscopy (AFM) images were obtained on a Nanoscope IIIa microscope from Veeco Instruments. A drop of a diluted aqueous CNC suspension with 0.01 wt% concentration that was deposited on a mica substrate and dried. It was imaged in tapping mode with a Silicon cantilever. The nanocrystal dimensions were estimated from 50 measurements analyzed using the ImageJ software.

Thermal analysis. Thermogravimetric analysis (TGA) of the samples was carried out under air atmosphere using Perkin-Elmer TGA-6 equipment by heating the samples from room temperature to 600°C with a heating rate ranging between 5 and 40°C.min⁻¹. From the thermogravimetric data it was possible to investigate the kinetics of the thermal degradation of the polymer. The Ozawa method [17] based on the kinetics equations (1-6) presented below provides information about the activation energy during thermal reactions. In this method, the data of at least three curves, with different heating rates (β), are used to obtain the activation energy (Eq. 6) associated with the desired mass loss range. The thermal equations involved in the thermal degradation calculation have been already discussed in the literature

[18,19]. They are based on the general kinetics representation of a solid-state reaction, described by (Eq. I).

$$\frac{d\alpha}{dt} = k(T) \times f(\alpha) \quad (\text{Eq. I})$$

Where $f(\alpha)$ is a function that describes how the reaction rate constant changes with the advance of the mass conversion; $\alpha = \frac{m_0 - m_t}{m_0 - m_\infty}$, with m_0 being the mass at the beginning of the reaction, m_t the mass at a determinate time t and m_∞ the mass at the end of the reaction. The parameter $k(T)$ is a temperature-dependent constant. Using the Arrhenius Equation (Eq. II), where R is the gas constant and T the temperature) the combination of these two equations can provide the introduction of the heating rate (β) by the follow equations:

$$k = A \times e^{\frac{-E_a}{RT}} \quad (\text{Eq. II})$$

$$\frac{d\alpha}{dt} = A \times e^{\frac{-E_a}{RT}} \times f[\alpha] \quad (\text{Eq. III})$$

$$\frac{d\alpha}{dT} = \frac{d\alpha}{dt} \times \frac{dt}{dT} \quad (\text{Eq. IV})$$

$$\frac{d\alpha}{dT} = \frac{d\alpha}{dt} \times \frac{1}{\beta} \quad (\text{Eq. V})$$

where $\beta = \frac{dT}{dt}$ (heating rate °C/min), and

$$\frac{d\alpha}{dT} = \frac{A}{\beta} \times e^{\frac{-E_a}{RT}} \times f[\alpha] \quad (\text{Eq. VI})$$

Rearranging (Eq. VI) makes possible the plot of $\log \beta$ vs. $1/T$, which slope is $0.457 E_a/R$, providing the E_a values.

Differential scanning calorimetry (DSC). Analyses were carried with a TA DSC Q100 equipment, where the sample (weight of 14 ± 2 mg) was sealed in aluminum pan and analyzed at a heating rate of $10^\circ\text{C} \cdot \text{min}^{-1}$. The studied temperature range was between 90 and 250°C .

Mechanical analysis. Mechanical characterization of the extruded films was realized by dynamic mechanical analysis (DMA) using a RSA3 equipment (TA Instruments, USA) working in tensile mode. The measurements were performed in the temperature range $100\text{-}200^\circ\text{C}$, with a heating rate of $2^\circ\text{C} \cdot \text{min}^{-1}$, frequency of 1 Hz, and a distance between jaws of 10 mm. To avoid some possible interference of residual solvents, all samples were kept at a temperature of 190°C for 10 min and quickly cooled to the initial analysis temperature before the test starts. All samples had dimensions of 5.5 ± 0.5 mm for width and 0.6 ± 0.1 mm for thickness.

X-ray diffraction. X-ray diffraction measurements for the nanocomposite films were recorded on a Philips PW 1720 X-ray generator operated at 45 kV and 40 mA in a Bragg-Brentano geometry. The 2θ range was from 5 to 65° using a fixed time mode with a step interval of 0.066° and Cu K α radiation ($\lambda = 1.5418 \text{ \AA}$).

Infrared spectroscopy. The infrared (IR) measurements were performed on a FTIR Perkin-Elmer Spectrum One equipment between 600 and 4000 cm^{-1} in 2 cm^{-1} intervals. All the analyses were carried out in the ATR mode with films deposited and dried at room temperature.

Viscosimetric measurements. For the viscosimetric experiments the PC pellets and films were dissolved in tetrahydrofuran (THF) and four solutions with different concentrations (2, 3, 4 and 5 $\text{mg}\cdot\text{mL}^{-1}$) were prepared. In a capillary viscometer, the measurement of the flow time was realized and the obtained data were used to calculate the relative and specific viscosities. The plot of the specific viscosity (divided by the solution concentration) vs. *the solution concentration provided the intrinsic viscosity*, that was used to obtain the molecular weight (M_v) of the sample using (Eq. VII).

$$[\eta] = K \times M_v^a \text{ (Eq. VII)}$$

where $[\eta]$ is the intrinsic viscosity of the polymer, M_v is the viscosimetric molecular weight, and for this system and at 25°C, $a = 0.67$ and $K = 0.049 \text{ mL}\cdot\text{g}^{-1}$ [20].

Visible light transmittance. The light transmittance test was performed with the same samples used for the DMA tests. The films were evaluated using an UV-Vis Shimadzu UV 2401-(PC) UV-vis spectrophotometer with a wavelength ranging between 300 and 800 nm.

Contact angle measurements. Contact Angle measurements were performed at room temperature with Attension Theta contact angle meter equipment. A drop of water was deposited on the film surface and the angle variation was registered during 30 seconds. The equipment software was used to calculate the angle variation with time. For PC and composites the films used for the experiments were the extruded films used for other analyses (like DMA). For CNC analysis a thin film was obtained from the CNC/pyridine suspension by casting evaporation (at room temperature).

3 RESULTS AND DISCUSSION

3.1 CNC/PC masterbatch

Microscopic observation. Atomic force microscopy (AFM) images in Figure 1a show the classical rod-like morphology of CNC sample. The average length and diameter were 179 ± 40 nm for the length, and 8.3 ± 1.8 nm respectively. The presence of some bigger particles in the AFM images was also reported. These particles were not considered in the size calculation due their micrometric nature. The presence of these particles can be detrimental for the properties of the final composite, since they can have very different crystallinity and surface area/charge compared to the nanoparticles present in the sample. Besides, these larger rods can be more easily mechanically disrupted by the screw during the extrusion process. Despite the size dispersion, the average nanoparticle aspect ratio (L/D) was around 11. The diluted water CNC suspension (Figure 1b) shows the presence of birefringent domains under polarized light, which are characteristic of a well dispersed CNC suspension due its alignment under low shear rate [1,21,22].

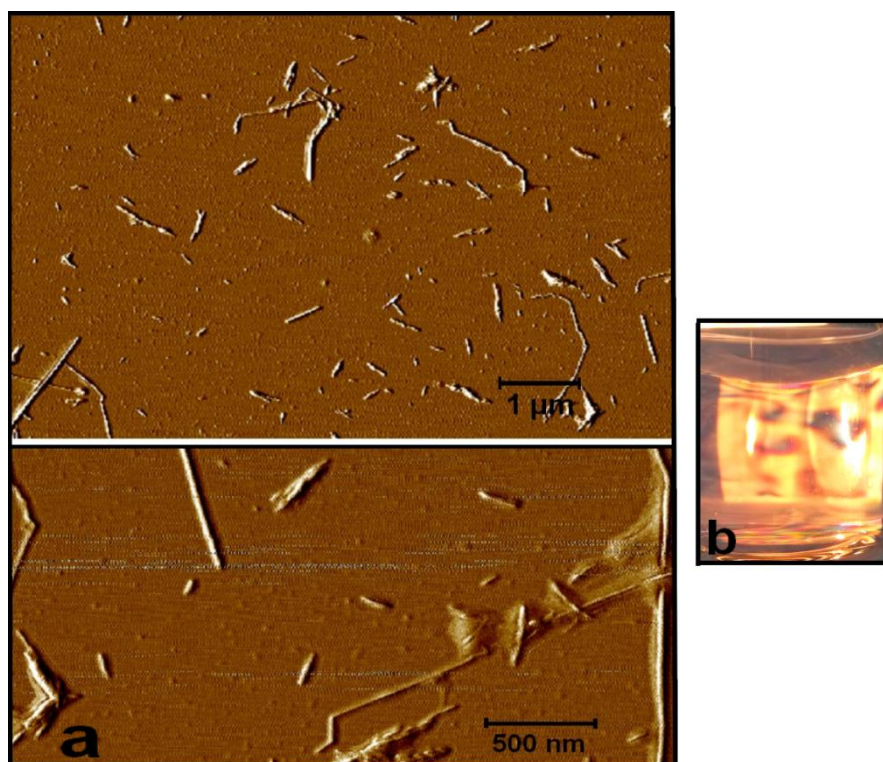


Figure 1. (a) AFM images of CNC, and (b) birefringent domains of the aqueous CNC suspension.

After the solvent exchange procedure from water to pyridine, and coating of CNC with PC chains, the ensuing masterbatch capsule material occurred as a white porous

material. Figure 2 shows the images obtained by scanning electronic microscopy (SEM) of the surface and inner structure of the capsules. Since pyridine and water are highly miscible, the immersion of the PC solution in water causes the diffusion of pyridine outside the drops, while the opposite happens for water. Because of the insolubility of the polymer in the new solvent mixture, the contact of some PC chains with water induces the progressive formation of a network of entangled chains that can trap the nanocrystals and create a solid capsule. The image of the surface of the capsules shows that when adding the nanocrystals (Figure 2e) to the system a rougher aspect is observed in comparison to the neat PC capsules (Figure 2d).

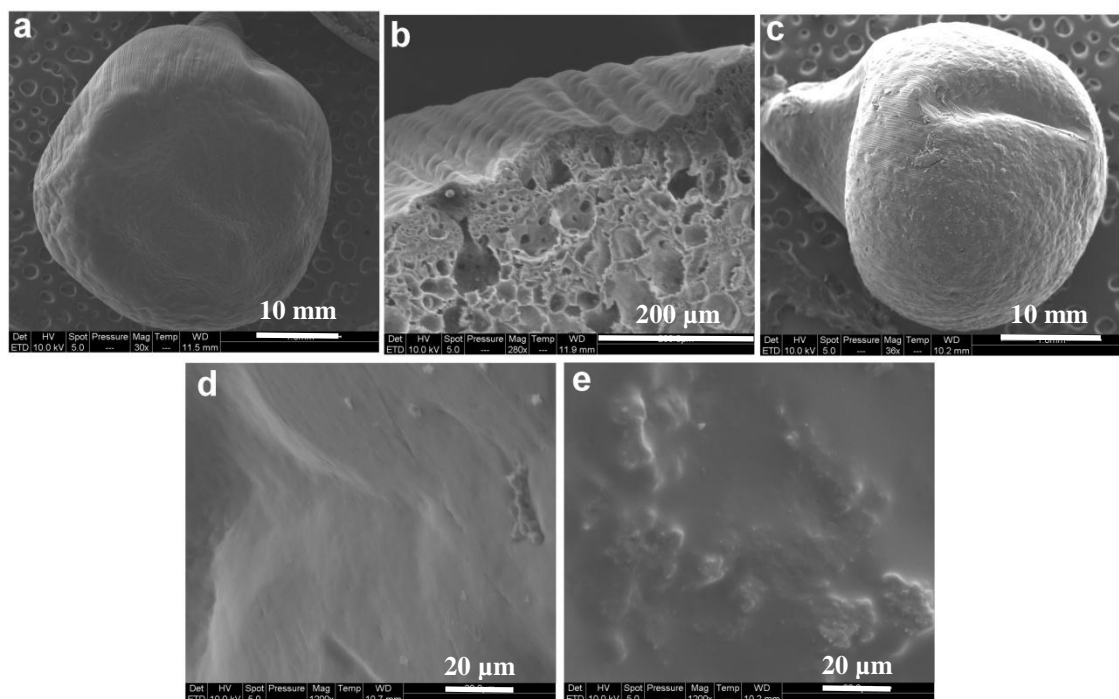


Figure 2. SEM observation of the masterbatch capsules: (a) neat PC capsule, (b) typical inner structure of the capsule, (c) CNC filled PC capsule; and surface of the capsules: (d) neat PC, and (e) CNC filled PC capsule.

Infrared spectroscopy. Figure 3 shows the FTIR spectra for PC, CNC and masterbatch CNC filled PC capsules. This technique can provide information on potential interactions in the multi-material capsule after the precipitation and drying process.

PC shows signals which are mainly located in the low wavenumber range of the spectrum (below 2000 cm^{-1}) due the presence of aromatic rings in its structure. The spectrum presents a characteristic signal attributed to $\text{C}=\text{O}$ at 1760 cm^{-1} . This signal normally appears at higher wavelengths for PC than for regular esters ($1750\text{--}1735\text{ cm}^{-1}$). The band at 1505 cm^{-1} is associated to stretching $\text{-C}=\text{C-}$ vibrations in the aromatic ring and is a strong reference band for PC because no change in the ring conformation is described for this polymer in literature. The signals between 1160

and 1250 cm^{-1} correspond to the different C-O-C links founded in the PC structure, in which the antisymmetric vibration can be associated with a doublet at 1235 cm^{-1} and consists of trans-trans and trans-cis conformational contributions at 1252 and 1223 cm^{-1} , respectively. The aromatic C=C double bonds show a weak triplet close to 1450 cm^{-1} region and the C-H bending characteristic vibrations of para-disubstituted rings are strong in the 830 cm^{-1} region.

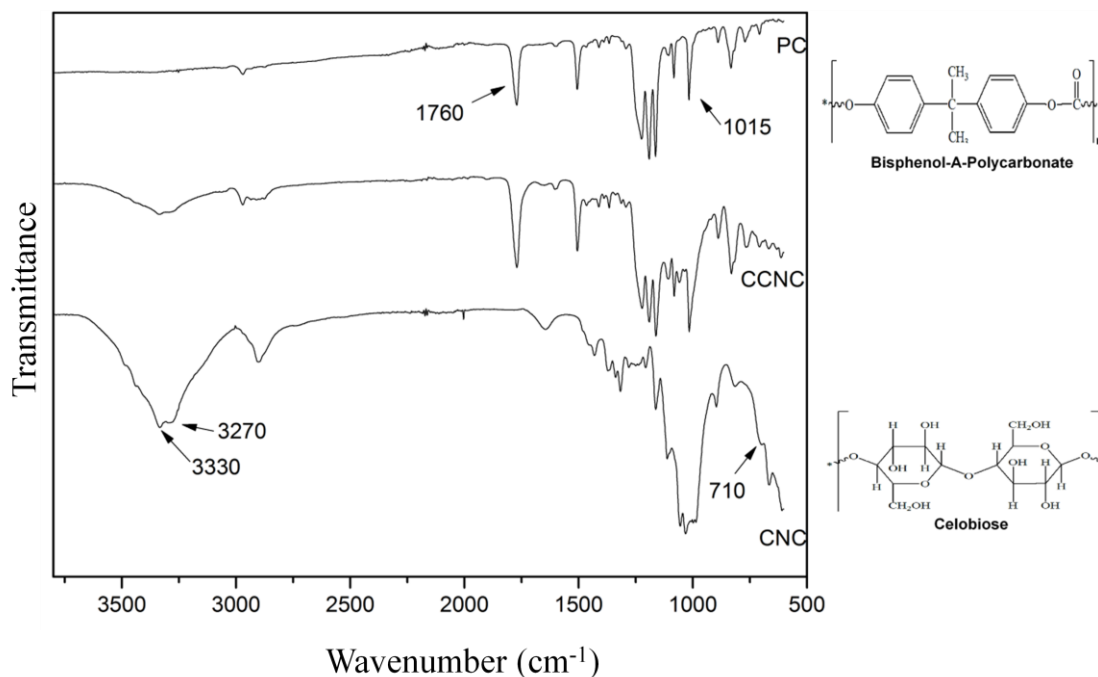


Figure 3. FTIR spectra for polycarbonate (PC), cellulose nanocrystals (CNC), and CNC/PC masterbatch capsules (CCNC).

The spectrum for the cellulosic material is typical of pure cellulose material (without signals corresponding to lignin, for example) with some characteristics vibrations of -CH groups at 2900 cm^{-1} and -C-O- stretching around the 1100 cm^{-1} region. An interesting observation in this spectrum is the O-H stretching band at 3270 cm^{-1} . It is a characteristic band of the I β polymorph of cellulose (confirmed by another weak band at 710 cm^{-1}). This signal is present in the CNC/PC masterbatch capsules as well, suggesting that no change in the cellulose structure occurred during the coating process that used a strong base as solvent for PC.

The FTIR spectrum for CCNC shows the contribution from both pristine materials. There is no formation of new bonds or disappearance of characteristic signals, indicating no degradation or formation of covalent links between the materials. In fact, the spectrum for the CNC/PC masterbatch capsules seems to be only the superimposition of the spectra corresponding to pristine materials. Signals at 1015 , 1760 and 3330 cm^{-1} are good examples of strong bands that overlap in the spectrum. The expected large number of intermolecular -OH interactions in PC and cellulose,

as well as the small shifts in signal positions, make difficult the observation of any interaction by FTIR.

Differential scanning calorimetry (DSC). The presence of nanocrystals embedded within the polymer structure can bring to the CCNC material new thermal properties in comparison to pristine CNC and PC. Figure 4 shows the DSC traces for the pristine materials and CNC/PC masterbatch capsules. The presence of residual water in all materials is observed through the presence of a slight endothermic peak starting around 100°C (indicated by a vertical dotted line) with a maximum around 105°C. It is obviously ascribed to the hydrophilic nature of the materials. Moreover, a stronger endothermic peak is observed for CNC around 120°C which is most probably ascribed to bonded water.

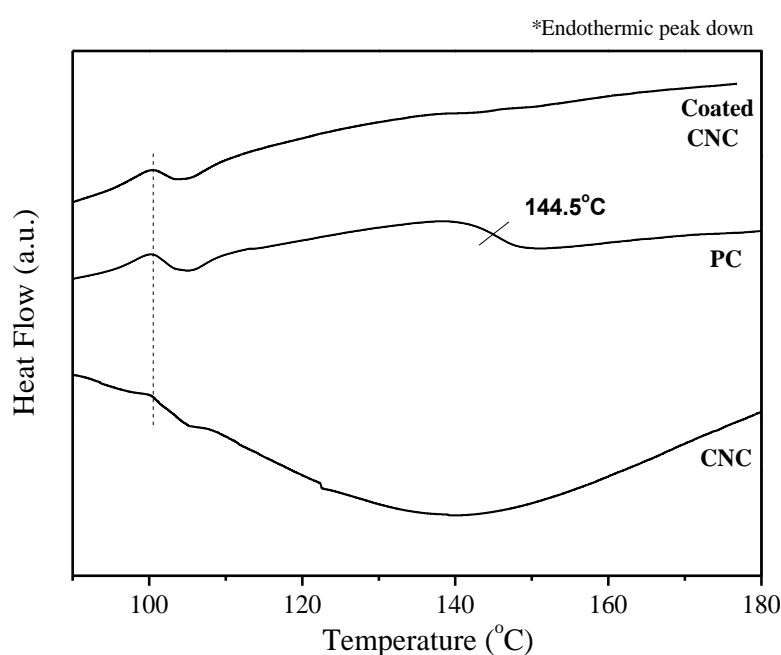


Figure 4. DSC traces for polycarbonate (PC), cellulose nanocrystals (CNC), and masterbatch CNC/PC capsules (CCNC).

PC displays a well-defined glass transition temperature (T_g) around 145°C. However, this thermal event is strongly reduced for the CNC/PC masterbatch capsules. It is obviously ascribed to the reduction of PC material since the capsules contain a 4/1 PC/CNC ratio, but possible reduction in the mobility of PC chains induced by the high specific surface area of the cellulose rod-like nanoparticle cannot be excluded. Moreover, the temperature range corresponding to the glass transition seems to be broader. This observation could be an indication of the efficient coating of the cellulosic nanomaterial with the polymeric chains. Some studies show that alterations (like weakening, broadening and shift to higher temperatures) can be

caused in thermal transitions of amorphous polymers by the presence of nanoentities [23].

Thermogravimetric Analysis (TGA). The thermal stability is one of the main issues in the processing of polymer nanocomposites reinforced with CNC. The rather low thermal stability of cellulose (around 200°C) may be further decreased for CNC [24]. This lower thermal stability for CNC is related to the acid hydrolysis procedure, generally carried out using H₂SO₄, since during the reaction the cellulose chains from the surface of the nanoparticles have some sulfate groups inserted in replacement of hydroxyl groups. These groups seem to catalyze the thermal degradation of the cellulosic nanoparticles [24,25].

Usually this material shows secondary's degradation peaks above 300°C, suggesting that the internal region of the nanocrystal, whose hydroxyl groups remain intact, keeps a thermal stability similar to native cellulose, since this value is close to the main degradation temperature of this material [26]. Figure 5 shows the TGA thermograms obtained for CNC, PC and CNC/PC masterbatch capsules. The main data from these thermograms are reported in Table 2.

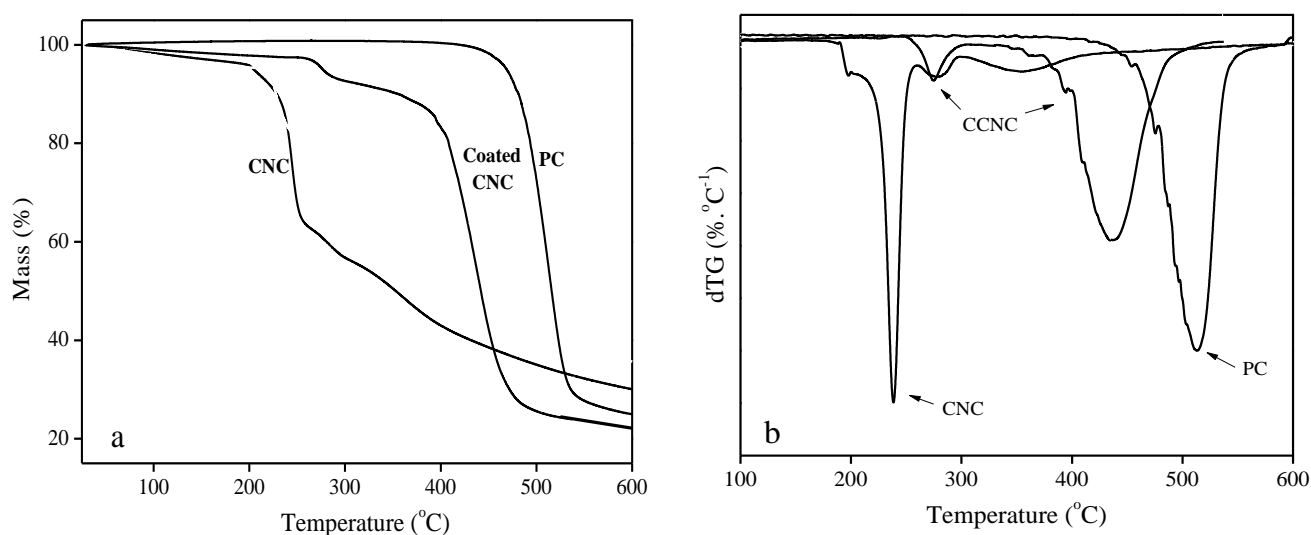


Figure 5. (a) TGA and (b) dTG curves for polycarbonate (PC), cellulose nanocrystals (CNC), and masterbatch CNC/PC capsules (CCNC).

The thermal degradation of CNC starts below 200°C as expected and the maximum degradation is around 230°C (Figure 5b). This value is relatively high for a sulfated nanocrystal, suggesting that sulfate groups at the surface were probably neutralized with some base (as NaOH), increasing its thermal stability [27,28].

Coating CNC with PC (CCNC) seems to impart a physical protection to the nanocrystals since the degradation onset is shifted to 250°C with a maximum degradation temperature around 275°C. This increase in the thermal degradation temperature shows that the polymeric coverage of the nanocrystals can increase their

thermal stability by almost 50°C. This effect can be attributed to two basic effects: (i) the lower thermal conductivity of the polymer layer can successfully protect the nanocrystals over a certain temperature range; (ii) the physical protection around the nanocrystal decreases the oxygen permeation up to the cellulose surface and avoid some earlier oxidation. Another interesting possible explanation is that the use of pyridine (a strong base) as solvent for PC can also remove/neutralize any residual acid coming from the hydrolysis process.

Table 2. Experimental data obtained from TGA experiments.

Sample	Stage of degradation	Onset temperature (°C)	Maximum degradation (°C)	Char fraction at 600°C (%)	Ea (kJ.mol ⁻¹)
CNC	I*	200	250	30.4	86.9
	II	230	275		
	III	300	350		
PC	I*	360	515	25.1	216.9
CCNC	I	250	275	21.9	178.1
	II*	350	475		

* stage of degradation related to the activation energy.

As a consequence of the presence of the nanocrystals, the maximum degradation temperature of PC in the capsules decreases from 515 to 475°C and the char fraction decreases slightly from 25.1 to 21.9%. This decrease in the thermal stability of the polymer in the CCNC sample can be also verified through the reduction of the activation energy (Ea). Figures 6a, 6b and 6c show the Ozawa plots for CNC, PC and CCNC materials, respectively, from which the Ea values can be determined. The corresponding Ea values are plotted in Figure 6d and reported in Table 2. A clear decrease of the Ea value for PC due the presence of CNC from 217 kJ.mol⁻¹ for the pristine polymer to 178 kJ.mol⁻¹ for the polymer in the masterbatch capsules was observed. CNC displays an Ea value of 87 kJ.mol⁻¹, being the most sensible material to thermal degradation, and causing the change in the PC degradation mechanism when embedded within the polymer entangled network. Cellulose is the main component responsible of the production of flammable volatiles during the thermal degradation of wood, producing rapidly these products when the temperature is above 200°C [1]. The production of degradation gases increases in the free space inside the polymer matrix (causing a change in the heat diffusion mechanism) and early radical reactions are common inducing accelerated polymer degradation [29].

Despite the difficulty in finding suitable techniques and signals corresponding to the nanocrystals in the polymer matrix using microscopic techniques, DSC and TGA results corroborate the idealized vision of coated nanocrystals where the stirring stage during the preparation of the masterbatch capsules enables the PC chains to coat the surface of the nanoparticles and provides stabilization against self-agglomeration during the precipitation stage and thermal degradation resistance

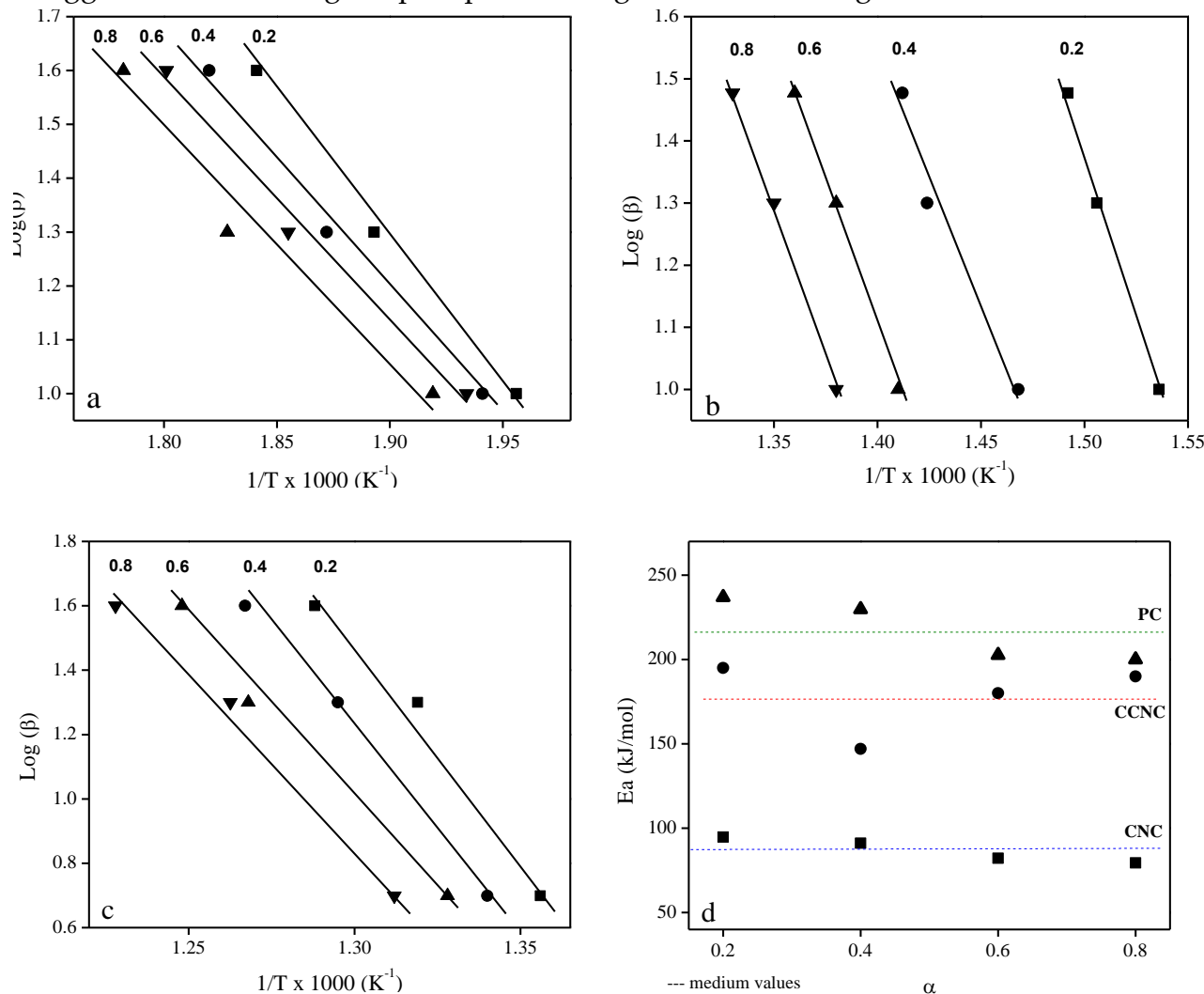


Figure 6. Ozawa plots for (a) CNC, (b) CCNC, (c) PC, and (d) average values of E_a .

3.2 CNC reinforced PC nanocomposites

PC nanocomposites reinforced with 1, 3 and 5 wt% CNC were prepared by extrusion. However, samples prepared with 5 wt% CNC were very brittle, making difficult an adequate characterization. In another work [30], CNC reinforced PC nanocomposites were prepared by casting/evaporation and poor mechanical properties for the material reinforced with 5 wt% were reported compared to those observed for lower CNC contents. Then, in the present study, the characterization was only focused on materials reinforced with 1 and 3 wt% CNC.

Transmittance analysis (UV-VIS). The light transmittance of the neat PC and nanocomposite films are shown in Figures 7a and 7b, for dissolved-extruded and milled-extruded materials, respectively. All materials exhibit similar behavior with a high light transmittance in the visible part of the spectrum (decreasing with the introduction of CNC) and a sharp reduction in the short wavelength region.

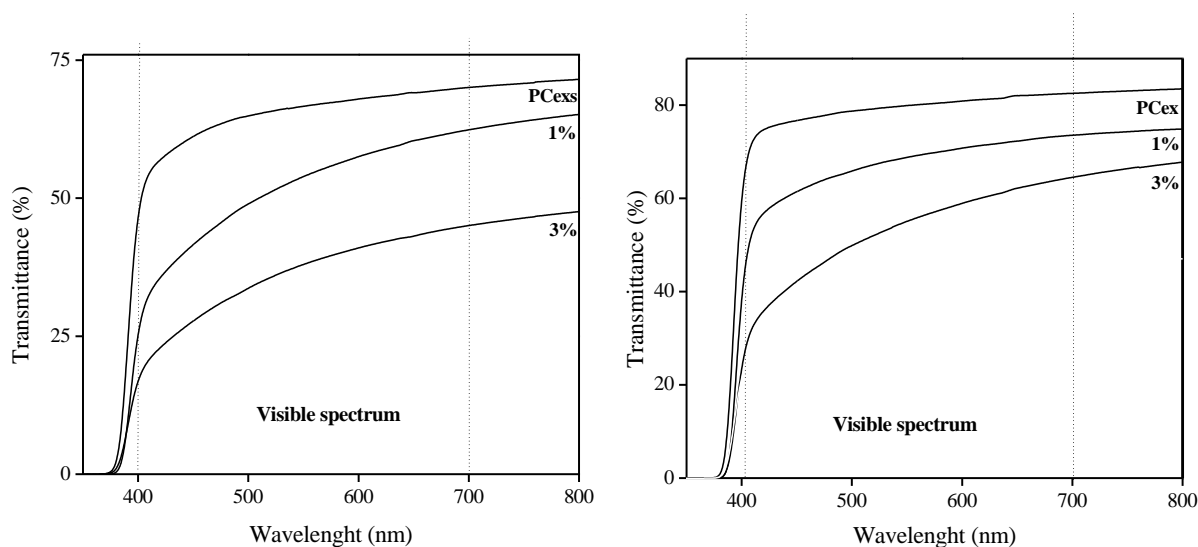


Figure 7. Transmittance for extruded (a) PCexs and (b) PCex films and nanocomposites.

It seems that the dissolution step of PC in pyridine during nanocomposite processing (PCexs samples, Figure 7a) affects negatively the optical properties of the material. Indeed, even for the CNC-free film the transmittance was only 70%. The presence of 1 and 3 wt% nanocrystals decreased this value to 65 and 45%, respectively. Figure 7b(milled-extruded materials) shows a transmittance level higher than 80% for the neat PCex film. However, the same effect of reduction in the light transmittance occurs due to the presence of CNC. The composite films reinforced with 1 and 3 wt% CNC have transmittances of 70 and 60%, respectively.

Moreover, for all samples a specific behavior is observed in the short wavelength range, between 360 and 410 nm. In this wavelength range, the nanocomposite films absorb much more light than neat PC samples. It is an indication that the nanocomposites absorb more violet than the PC films, and as a consequence absorb less yellow (the complementary color of violet) making the material more yellowish to human eye. Light absorption by polymers depends on their molecular weight, and in the case of PC the reduction of the molecular weight causes an increase in the UV absorption, probably due to the increase in the number of end-groups [31].

Viscosimetry. The viscosimetric molecular weight (M_v) values were determined for as-received PC pellets, dissolved-extruded (PCexs) and milled-extruded PC (PCex). These measurements were not possible for nanocomposites due to possible influences of CNC presence in the measurements. Results are reported in Figure 8. Compared to as-received PC pellets ($M_v = 25,000 \text{ g}\cdot\text{mol}^{-1}$), a significant decrease of the molecular weight to $20,000 \text{ g}\cdot\text{mol}^{-1}$ was observed after extrusion, and an even more significant decrease was reported when PC was first dissolved in pyridine and precipitated in water before extrusion, in this case the molecular weight was also decreased during the solubilization/precipitation stage.

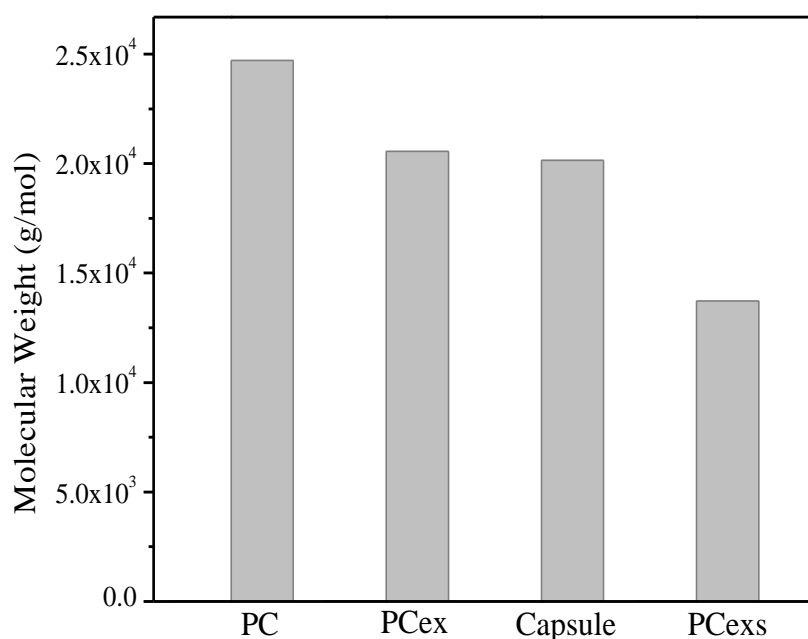


Figure 8. Viscosimetric molecular weight for PC pellets, milled-extruded PC (PCex), dissolved-precipitate (Capsule) and dissolved-extruded PC (PCexs).

The molecular weight reduction of PC upon processing was already reported by Ronkay, [31] Yoon et al. [32] also reported a reduction of the PC molecular weight induced by extrusion, when increasing the nanoparticle (organoclay) dispersion. This work also suggested a more severe degradation when using a surfactant containing hydroxy-ethyl groups.

Differential scanning calorimetry (DSC). Figure 9 shows the DSC traces for PC and nanocomposites reinforced with 1 wt% CNC. A clear glass transition was observed for all samples in the temperature range 140-150°C. For neat PC, the T_g value was around 144.5°C, and it decreased slightly to 143.7°C and more significantly to 141.2°C after extrusion of milled and dissolved/precipitated PC, respectively. This evolution is in line with the variation of the molecular weight. The stronger decrease observed for the T_g value of PCexs induced by the dissolution step could also suggest the presence of residual pyridine that could act as a plasticizer for the polymer.

A further decrease of T_g around 6-8°C was reported when adding only 1 wt% CNC. A similar effect was observed when adding nanosilica to PC. [33] The authors list some probable causes of T_g reduction in composites, and in particular the decrease of the overall physical crosslinking density per unit volume and addition of free volume due a disruption in the packing of the PC segments, induced by the nanofiller. Moreover, the presence of CNC can accelerate the depolymerization of PC. Indeed, TGA experiments for CCNC capsules already showed that the presence of CNC decreased the values of E_a for PC, leaving the polymer more susceptible to thermal degradation during the extrusion process.

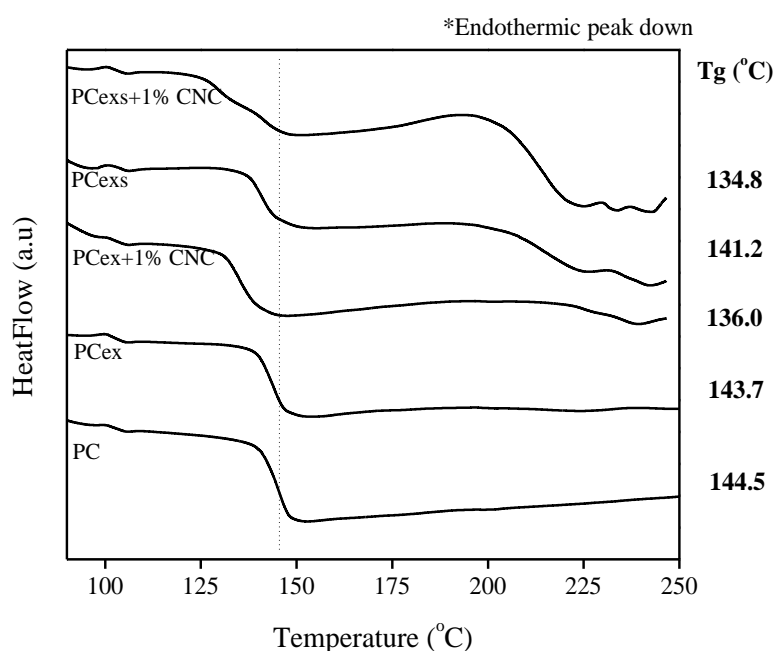


Figure 9. DSC thermograms for neat PC and nanocomposites reinforced with 1 wt% CNC.

The DSC thermograms (Fig. 9) show that PC pellets and milled-extruded PC (PCex) are fully amorphous polymers since no thermal transition was observed above T_g . For dissolved-extruded PC (PCexs) endothermic signals are observed above 200°C. These endothermic signals could be ascribed to the melting of PC crystalline domains that could be formed because of the decrease of the molecular weight [34]. This possible effect agrees with the decrease in light transmittance observed for this material. The presence of residual pyridine suggested by the decrease of T_g could also act as catalyst for the thermal degradation of the polymer as suggested by TGA experiments. Adding 1 wt% CNC seems to promote the occurrence of endothermal signals above 200°C. To further investigate the possible crystallization of PC chains upon dissolution/precipitation and addition of CNC, X-ray diffraction measurements were performed.

X-ray diffraction (XRD). Figure 10 shows XRD patterns obtained for extruded PC and nanocomposites reinforced with 1 wt% CNC. Due its non-destructive nature,

XRD can provide more reliable information about the material crystallinity in comparison to DSC. As an amorphous material PC presents a halo around 17° and no crystalline peak can be observed [35], but its crystalline form presents a strong peak around 25° and a shoulder around 21° , corresponding to an orthorhombic unit cell [36,37]. From XRD patterns shown in Figure 10, it appears that PCex and PCex+CNC materials are fully amorphous. The lack of crystallinity in these two samples suggests that the endothermal peak observed around 245°C in the DSC trace was related only to the CNC degradation. For PCexs and PCexs+CNC materials a sharp peak around 17° and two smaller peaks at 21° and 25° are observed, indicative of structural order [34]. These crystalline domains seem therefore to be induced by the dissolution/precipitation step performed prior to extrusion. From DSC experiments we can suggest that the melting of these crystalline domains corresponds to the endothermal peak around 225°C . Because of the low cellulose content in the nanocomposite samples, the typical diffraction peaks at 8° , 15° and 23° [38] for cellulose I (native cellulose) are not observed in the XRD patterns.

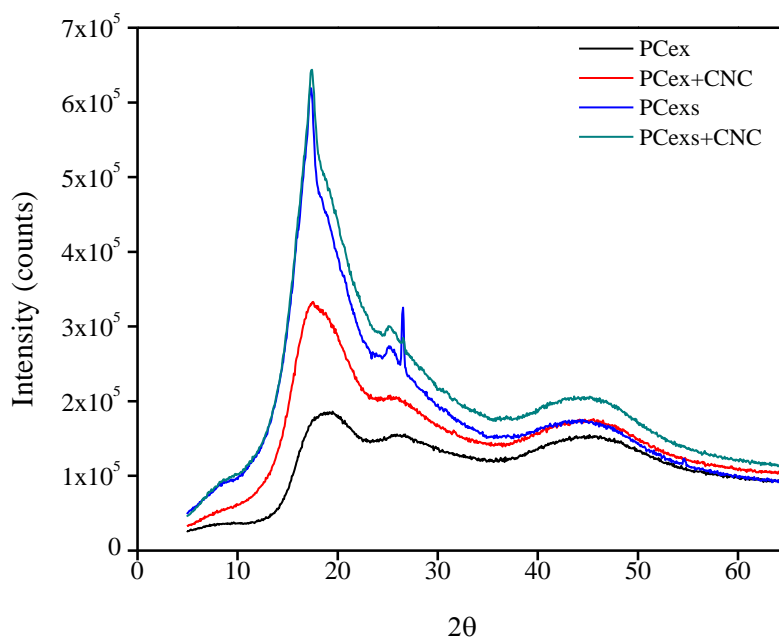


Figure 10. XRD patterns for neat PC and nanocomposites reinforced with 1 wt% CNC.

It was reported that PC seems to prefer the amorphous to the crystalline state when cooled from the melt state under normal circumstances, explaining why PC is almost exclusively amorphous after extrusion of injection-molding [39]. In the present study, extrusion of PC was performed below its melting point and this could play an important role in the capacity of reorganization presented by the polymeric chains in PCexs films, since these materials kept the crystallinity even after the rapid cooling to room temperature.

Scanning electron microscopy (SEM). The prepared films were homogeneous in appearance and no sign of CNC aggregation was observed. Figure 11 shows the SEM

images of the fractured surface for the films. The surface of PCex material (Fig. 11a) is smooth as expected for an amorphous material. Contrarily, the surface of PCexs (Fig. 11b) is rougher most probably because of the occurrence of crystallization induced by the solubilization/precipitation process, similar structures in PC were already reported and attributed to spherulites grown [40,41]. For both nanocomposites (panels c and d in Fig. 11) no CNC aggregation was observed and then the filler seems to be homogeneously dispersed within the polymeric matrix.

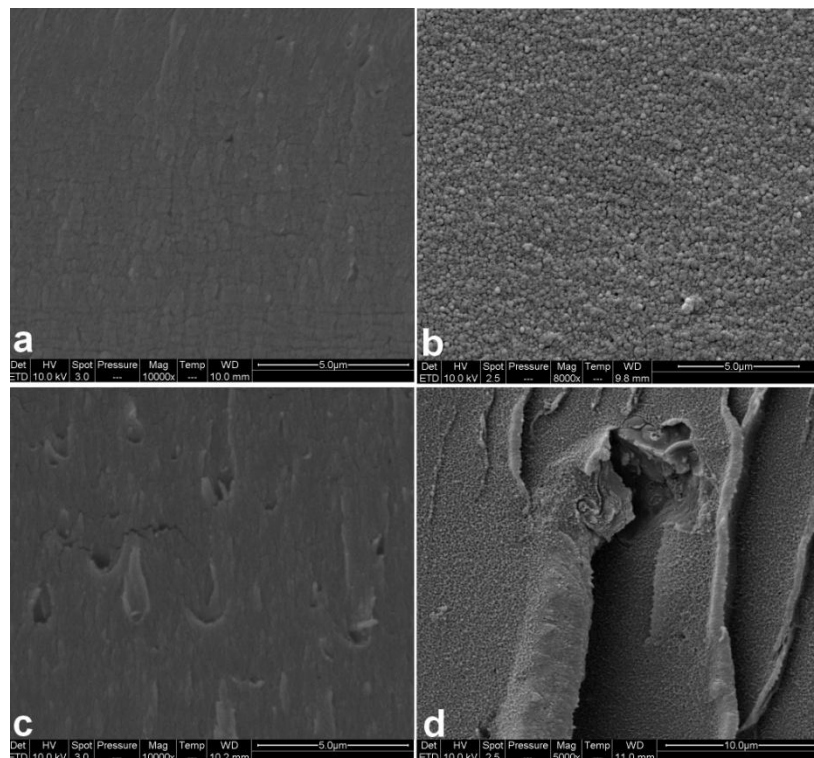


Figure 11. Scanning electron micrographs of the fractured surface for (a)PCex, (b)PCexs, (c) PCex+1% CNC and (d) PCexs+1% CNC.

Dynamic mechanical analysis (DMA). Figure 12 shows the evolution of the logarithm of the storage modulus (E') measured at a frequency of 1 Hz as a function of temperature for the pure polycarbonate films and nanocomposites reinforced with 1 and 3 wt% CNC. The curves show the classical pattern observed for thermoplastic materials with the glassy-viscoelastic-rubbery regions and two well-defined plateaus. Until the end of the glassy region (around 120°C) no significant change can be observed between the pristine material and the nanocomposites. This first plateau has a modulus value around 10^9 Pa, which is characteristic of any glassy polymer. Then a sharp modulus drop is observed corresponding to the main relaxation process associated with T_g of the polymer. It is worth noting that this modulus drop is shifted towards lower temperatures for nanocomposites in agreement with the decrease of T_g value observed from DSC measurements.

In the rubbery state of the PC matrix an increase of the modulus is observed when it is filled with CNC. Only a modest increase is reported for PCex based materials, but it is found to be much more significant for PCexs materials. Moreover, a progressive modulus increase is induced when adding increasing amounts of CNC for PCex materials, showing that this reinforcing effect can be undoubtedly ascribed to cellulosic nanoparticles. For PCexs, a sharp increase in modulus is reported when adding only 1 wt% CNC whereas higher filler level induces only a marginal increment, showing that the mechanical behavior of the nanocomposite is most probably governed by the crystallinity of the matrix. The use of CNC as possible driver in polymer crystallinity was recently described [42].

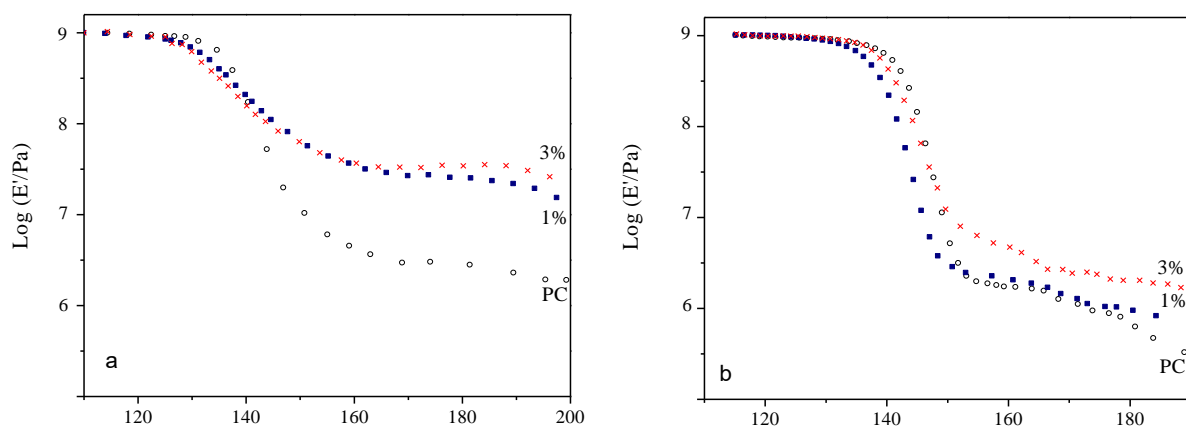


Figure 12. Evolution of the logarithm of the storage modulus as a function of temperature at 1 Hz for (a) PCexs and (b) PCex materials: neat matrix (\circ), and nanocomposites filled with 1 (\blacksquare) and 3 wt% (\times) CNC.

For CNC reinforced nanocomposites it is often referred to the formation of a CNC percolating network within the polymeric matrix to explain the high reinforcing effect of the cellulosic nanofiller. However, it is worth noting that this mechanical percolation phenomenon only occurs for CNC contents higher than the percolation threshold, which is around 6.5 vol%, i.e. around 8.0 wt%, for nano-rods with an aspect ratio of 11 as in this study. Therefore, the only reinforcing capability of CNC arises from the intrinsic mechanical properties of single nanoparticle, which modulus value has been estimated between 56 and 220 GPa depending to the cellulose source and method of measurement [43], with an average value around 130 GPa. The experimental values obtained at 175°C for both series of CNC/PC nanocomposites were compared to the prediction from the Halpin-Kardos model for the same temperature (Table 3). This mean field approach, which equations can be found in literature [1], is classically used to predict the mechanical reinforcement of CNC below the percolation threshold since it assumes no interactions between

nanocrystals (details in the Supporting Information). For CNC the assumed longitudinal and transverse modulus values were 130 GPa and 10 GPa, respectively.

Table 3. Experimental data (E_e) and predicted values from the Halpin-Kardos model (E_p) for the storage modulus of CNC/PC nanocomposites at 175°C.

Material	PCex		PCexs	
	E_e (MPa)	E_p (MPa)	E_e (MPa)	E_p (MPa)
PC	1.90	2.02	7.08	7.53
PC + 1% CNC	2.29	2.09	58.9	7.64
PC + 3% CNC	4.07	2.26	72.4	7.90

For PCex nanocomposites, the experimental data are slightly higher but of the same order of magnitude as the predicted data. However, for PCexs nanocomposites, the experimental values are much higher than the predicted modulus. This is ascribed to the fact that the extrusion-induced crystallization of the polymeric matrix for nanocomposites is not accounted for in the prediction. It shows the strong impact of PC crystallization upon mechanical properties for PCexs based nanocomposites.

Contact angle measurements. The surface characteristics have great importance for polycarbonate based materials due their intimate link with the material applications. After the extrusion process the hydrophilicity of the film material was studied by contact angle measurements. Figure 13 shows the variation of the contact angle of a water droplet with time for the pristine materials and for the nanocomposites (in the Figure, an extruded film containing 3 wt% CNC). Both polycarbonate film shows the highest contact angle value (between 85 and 90°), which remained almost constant with time. This material is therefore quite hydrophobic. The CNC film displays a hydrophilic nature as expected, with a much lower contact angle and a sharp variation of almost 20° over the analyses time, stabilizing around 25° after 40 s.

When adding only 3 wt% CNC to PC, it is observed that the hydrophobicity of the surface decreases, suggesting the presence of cellulosic nanoparticles at the surface of the film. Therefore, even with the coating of the nanocrystals by the polymer, it seems that CNC can influence the surface of the final material, increasing its hydrophilicity.

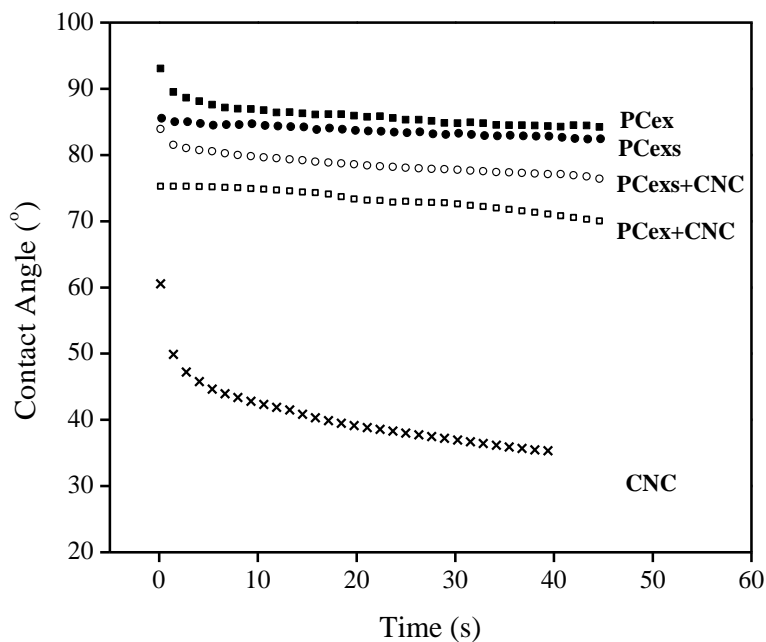


Figure 13. Evolution of the contact angle versus time for PCex (■), PCex+CNC (□), PCexs (●), PCexs+CNC (○) and CNC (x).

Scratch Tests

Some studies already showed that the addition of different nanomaterials such as carbon, metals and clays can modify the abrasion and scratch resistance of nanocomposite surface [43]. However, there is a lack of tribological investigations in nanocomposites that use polysaccharides, e.g. starch or nanometric cellulose, as fillers in polymer matrix. The influence of crystallinity and matrix-fillers interactions in the tests are also not very clear.

Here, this test was performed with the aim of verifying not only the surface behavior of the material under scratch, but also how the whole structure of the film is affected. The surface and bulk properties are not always identical and tests that can cause more than $1\mu\text{m}$ distortion in the materials are not appropriated to study their surface. Scratch tests seem to cause plastic deformation in polycarbonate materials. This deformation leads to the emergence of some ridges at the surface, causing an increase in the surface volume despite no detection of wear particles [44].

The samples prepared by extrusion show already a rough surface due to imperfections in the extruder die. Figure 1 shows the AFM images for the surface of the PCex films (with and without cellulose nanocrystals). In the center of the image the scratch performed by the equipment described in Figure 14 can be observed. The average values of depth and width founded for the scratches for each material are collected in Table 1.

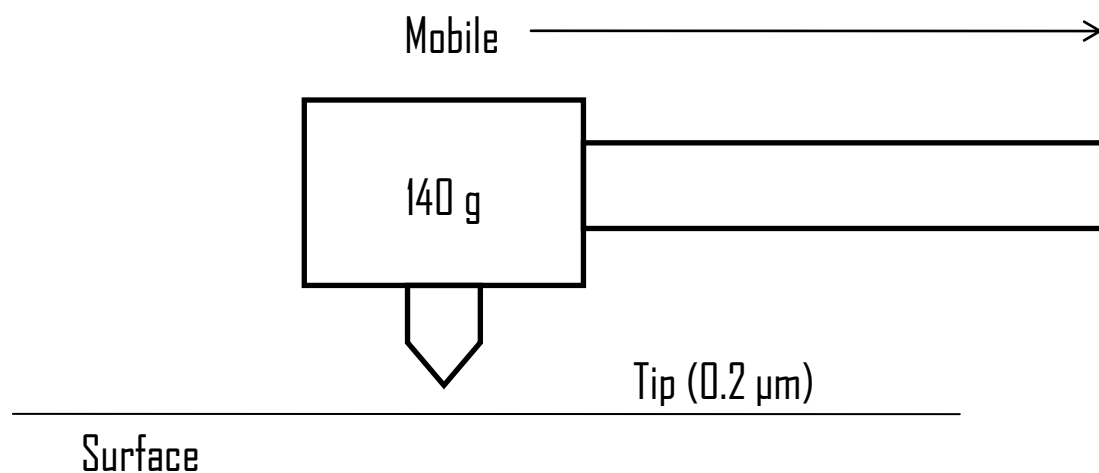


Figure 14. Scheme of scratch tests equipment.

The results are opposed to what was originally expected, Figure 15, with an increase of the scratch dimensions for the samples containing CNC. In the PCex samples the scratches seem to be as described by *Kaneko et al [44]*, with ridges covering all the lateral part of the scratch, indicating a plastic deformation. In the other samples, containing CNC, the scratch marks seem to be different. There are no clear ridges along all the scratches and for the 3% samples the deepest part of the scratch are more diagonal and less rounded.

Table 1. Values of depth and width of the scratches.

Sample	Depth (nm)	Width (μm)
PCex	52.7 ± 7.4	1.12 ± 0.25
PCex + 1% CNC	203.3 ± 61.5	3.61 ± 0.56
PCex + 3% CNC	237.5 ± 20.0	5.36 ± 0.63

At this point, the mechanical properties of the materials should be considered. The films with CNC are more brittle, being more susceptible to crack formation and deeper defects can be caused during the test due its propagation. At the same time, the relatively high scratch speed (around $0.5 \text{ cm}\cdot\text{s}^{-1}$) can cause some local temperature elevation during the frictional contact and lead the material to deform in different ways. This temperature increase and the friction also can induce covering of the metal needle after each test and consequently change its dimensions, modifying the metal – polymer interaction. This is important considering the order in which the tests were performed (PCex - PCex1 - Pcx3).

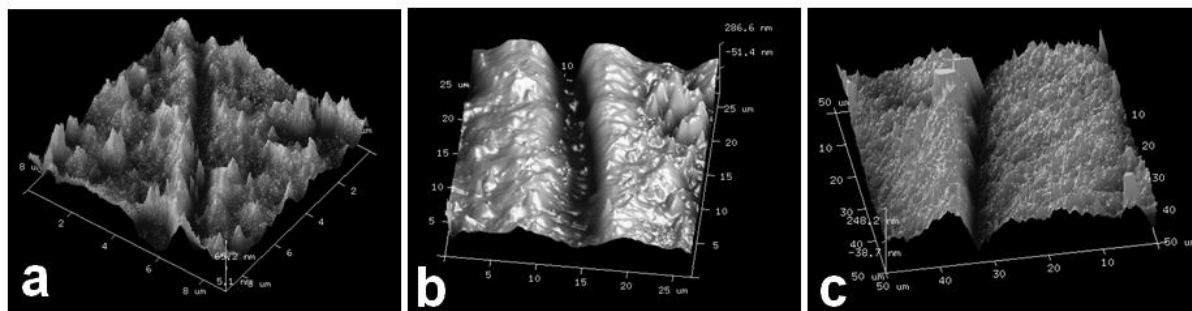


Figure 15. AFM surface images of PCex (a), PCex + 1wt% (b) and PCex + 3wt% (c) nanocomposites.

4 CONCLUSIONS

The first part of this study aimed in preparing a masterbatch consisting of cellulose nanocrystals (CNC) and polycarbonate (PC). The CNC/PC masterbatch capsules were prepared using a dissolution/precipitation process in which water from the CNC aqueous dispersion was exchanged to pyridine serving as solvent for PC. The mixture was subsequently precipitated in water allowing the recovery of the masterbatch capsules. Improved thermal stability for PC-coated CNC masterbatch compared to pristine CNC was reported which should have a positive impact for the ensuing extrusion of CNC reinforced PC nanocomposites at high temperature. Unfortunately, the presence of nanocrystals seemed to decrease at the same time the thermal stability of PC in the masterbatch, which can accelerate its depolymerization during the extrusion process, decreasing therefore its molecular weight. For the dilution process by extrusion with PC, two different methodologies were adopted. In the first one, PC was submitted to the same dissolution/precipitation process than masterbatch (PCexs), whereas in the second approach, the PC pellets were directly mixed with the solid master-batch capsules (PCex). It was founded that extrusion induced a decrease of the molecular weight of PC chains, which was amplified for PCexs. This degradation resulted in the crystallization of PCexs as shown from DSC and XRD measurements, inducing a lost in light transmittance. Improved mechanical properties were reported for nanocomposites which were assigned to the intrinsic stiffness of CNC, but crystallization of PCexs affected more significantly the mechanical behavior.

5 REFERENCES

- [1] A. Dufresne, *Nanocellulose: From Nature to High Performance Tailored Materials*, Walter de Gruyter GmbH, Berlin/Boston, 2012.
- [2] M.A.S. Azizi Samir, F. Alloin, A. Dufresne, A review of recent research into cellulosic whiskers, Their properties and their application in nanocomposite field, *Biomacromolecules* 6 (2005) 612–626.
- [3] S.J. Eichhorn, A. Dufresne, M. Aranguren, N.E. Marcovich, J.R. Capadona, S.R. Rowan, C. Weder, W. Thielemans, M. Roman, S. Renneckar, W. Gindl, S. Veigel, J. Keckes, H. Yano, K. Abe, N. Nogi, A.N. Nakagaito, A. Mangalam, J. Simonsen, A.S. Benight, A. Bismarck, L.A. Berglund, T. Peijs, Review: current international research into cellulose nanofibres and nanocomposites, *J. Mater. Sci.* 45 (2010) 1–33.
- [4] R.J. Moon, A. Martini, J. Nairn, J. Simonsen, J. Youngblood, Cellulose nanomaterials review: structure, properties and nanocomposites, *Chem. Soc.Rev.* 40 (2011) 3941–3994.
- [5] A. Dufresne, Nanocellulose – a new ageless bionanomaterial, *Mater. Today* 16 (2013) 220–227.
- [6] N. Lin, J. Huang, A. Dufresne, Preparations, properties and applications of polysaccharide nanocrystals in advanced functional nanomaterials: a review, *Nanoscale* 4 (2012) 3274–3294.
- [7] A.-L. Goffin, J.-M. Raquez, E. Duquesne, G. Siqueira, Y. Habibi, A. Dufresne, P. Dubois, From interfacial ring opening polymerization to melt processing of cellulose nanowhisker-filled polylactide-based nanocomposites, *Biomacromolecules* 12 (2011) 2456–2465.
- [8] A.-L. Goffin, J.-M. Raquez, E. Duquesne, G. Siqueira, Y. Habibi, A. Dufresne, P. Dubois, Poly(ϵ -caprolactone) based nanocomposites reinforced by surface grafted cellulose nanowhiskers via extrusion processing: morphology, rheology, and thermo-mechanical properties, *Polymer* 52 (2011) 1532–1538.
- [9] K. Ben Azouz, E.C. Ramires, W. Van den Fonteyne, N. El Kissi, A. Dufresne, Simple method for the melt extrusion of a cellulose nanocrystal reinforced hydrophobic polymer, *ACS Macro Lett.* 1 (2012) 236–240.
- [10] M. Pereda, N. El Kissi, A. Dufresne, Extrusion of polysaccharide nanocrystal reinforced polymer nanocomposites through compatibilization with poly(ethylene oxide), *ACS Appl. Mater. Interfaces* 6 (2014) 9365–9375.
- [11] A. Arias, M.C. Heuzey, M.A. Huneault, G. Ausias, A. Bendahou, Enhanced dispersion of cellulose nanocrystals in melt-processed polylactic-based nanocomposites, *Cellulose* 22 (2015) 483–498.
- [12] V. Khoshkava, M.R. Kamal, Effect of drying conditions on cellulose nanocrystal (CNC) agglomerate porosity and dispersibility in polymer nanocomposites, *Powder Technol.* 261 (2014) 288–298.

- [13] V. Khoshkava, M.R. Kamal, Effect of cellulose nanocrystals (CNC) particle morphology on dispersion and rheological and mechanical properties of polypropylene/CNC nanocomposites, *ACS Appl. Mater. Interfaces* 6 (2014) 8146–8157.
- [14] J. Sapkota, M. Jorfi, C. Weder, E.J. Foster, Reinforcing poly(ethylene) with cellulose nanocrystals, *Macromol. Rapid Comm.* 35 (2014) 1747–1753.
- [15] J. Sapkota, S. Kumar, C. Weder, E.J. Foster, Influence of processing conditions on properties of poly(vinyl acetate)/cellulose nanocrystal nanocomposites, *Macromol. Mater. Eng.* (2015), <http://dx.doi.org/10.1002/mame.201400313>.
- [16] A.C. Corrêa, E.M. Teixeira, V.B. Carmona, K.B.R. Teodoro, C. Ribeiro, L.H.C. Mattoso, J.M. Marconcini, Obtaining nanocomposites of polyamide 6 and cellulose whiskers via extrusion and injection molding, *Cellulose* 21 (2014) 311–322.
- [17] T. Ozawa, A new method of analyzing thermogravimetric data, *Bull. Chem. Soc. Jpn.* 38 (1965) 1881–1886.
- [18] A. Khawam, D.R. Flanagan, Solid-state kinetic models: basics and mathematical fundamentals, *J. Phys. Chem. B* 110 (2006) 17315–17328.
- [19] N. Koga, Ozawa's kinetic method for analyzing thermoanalytical curves, *J. Therm. Anal. Calorim.* 113 (2013) 1527–1541.
- [20] W.R. Moore, M. Uddin, Dilute solution properties of bisphenol A polycarbonate, *Eur. Polym. J.* 5 (1969) 185–193.
- [21] D.D.J. Silva, M.L.O. d'Almeida, Nanocrystals de cellulose: cellulose whiskers, *O Papel* 7 (2009) 34–52.
- [22] B.G. Zanetti-Ramos, M.B. Fritzen-Garcia, C.S. de Oliveira, A.A. Pasa, V. Soldi, R. Borsali, T.B. Creczynski-Pasa, Dynamic light scattering and atomic force microscopy techniques for size determination of polyurethane nanoparticles, *Mater. Sci. Eng. C* 29 (2009) 638–640.
- [23] R.A. Vaia, B.B. Sauer, O.K. Tse, E.P. Giannelis, Relaxations of confined chains in polymer nanocomposites – Glass transition properties of poly(ethylene oxide) intercalated in montmorillonite, *J. Polym. Sci. Part B* 35 (1997) 59–67.
- [24] N. Lin, A. Dufresne, Surface chemistry, morphological analysis and properties of cellulose nanocrystals with gradiented sulfation degrees, *Nanoscale* 6 (2014) 5384–5393.
- [25] M. Roman, W.T. Winter, Effect of sulfate groups from sulfuric acid hydrolysis on the thermal degradation behavior of bacterial cellulose, *Biomacromolecules* 5 (2004) 1671–1677.
- [26] V.A. Alvarez, A. Vázquez, Thermal degradation of cellulose derivatives/starch blends and sisal fibre biocomposites, *Polym. Degrad. Stab.* 84 (2004) 13–21.
- [27] Y. Habibi, A.L. Goffin, N. Schiltz, E. Duquesne, P. Dubois, A. Dufresne, Bionanocomposites based on poly (ε-caprolactone)-grafted cellulose nanocrystals by ring-opening polymerization, *J. Mater. Chem.* 18 (2008) 5002–5010.
- [28] N. Wang, E. Ding, R. Cheng, Thermal degradation behaviors of spherical cellulose nanocrystals with sulfate groups, *Polymer* 48 (2007) 3486–3493.

- [29] H.W. Moeller, *Progress in Polymer Degradation and Stability Research*, Nova Science Pub. Inc., 2008.
- [30] W. Xu, Z. Qin, H. Yu, Y. Liu, N. Liu, Z. Zhou, L. Chen, Cellulose nanocrystals as organic nanofillers for transparent polycarbonate films, *J. Nanoparticle Res.* 15 (2013) 1562.
- [31] F. Ronkay, Effect of recycling on the rheological, mechanical and optical properties of polycarbonate, *Acta Polytech. Hung.* 10 (2013) 209–220.
- [32] P.J. Yoon, D.L. Hunter, D.R. Paul, Polycarbonate Nanocomposites: Part 2. Degradation and Color Formation, *Polymer* 44 (2003) 5341–5354.
- [33] M. Biswal, S. Mohanty, S.K. Nayak, P.S. Kumar, Effect of functionalized nanosilica on the mechanical, dynamic-mechanical, and morphological performance of polycarbonate/nanosilica nanocomposites, *Polym. Eng. Sci.* 53 (2013) 1287–1296.
- [34] H. Münstedt, Influence of crystallinity on rheological properties of unfilled and particle-filled polycarbonates, *Polymer* 52 (2011) 3677–3680.
- [35] Y. Xu, Z. Sun, X. Chen, M. Chen, S. Hu, Z. Zhang, Mechanical properties and crystallization behavior of polycarbonate/polypropylene blends, *J. Macromol. Sci. Part B* 52 (2013) 716–725.
- [36] P.R. Sundararajan, S. Singh, M. Moniruzzaman, Surfactant-induced crystallization of polycarbonate, *Macromolecules* 37 (2004) 10208–10211.
- [37] S. Radhakrishnan, V.S. Iyer, S. Sivaram, Structure and morphology of polycarbonate synthesized by solid state polycondensation, *Polymer* 35 (1994) 3789–3791.
- [38] C. Driemeier, M.T.B. Pimenta, G.J.M. Rocha, M.M. Oliveira, D.B. Mello, P. Maziero, A.R. Gonçalves, Evolution of cellulose crystals during prehydrolysis and soda delignification of sugarcane lignocellulose, *Cellulose* 18 (2011) 1509–1519.
- [39] M.F. Garbaskas, Polycarbonate crystallinity, in: D.G. LeGrand, J.T. Bendler (Eds.), *Handbook of Polycarbonate Science and Technology*. Marcel Dekker Inc.: New York, 2000, pp. 293–302 (Chapter 13).
- [40] J. Lu, D. Xi, R. Huang, L. Li, Crystal morphology of high-pressure crystallized bisphenol-A polycarbonate, *J. Macromol. Sci. Part B* 50 (2011) 1018–1030.
- [41] S. Camarero-Espinosa, D.J. Boday, C. Weder, E.J. Foster, Cellulose nanocrystal driven crystallization of poly(D, L-lactide) and improvement of the thermomechanical properties, *J. Appl. Polym. Sci.* 132 (2015) 41607.
- [42] M. Mariano, N. El Kissi, A. Dufresne, Cellulose nanocrystals and related nanocomposites: review of some properties and challenges, *J. Polym. Sci. Part B Polym. Phys.* 52 (2014) 791–80.
- [43] S.S. Pesetskii, S.P. Bogdanovich, N.K. Myshkin, Polymer Nanocomposites with Thermoplastic Matrices—Processing and Tribology, *J. Macromol. Sci. Part B.* 52 (2013) 1784–1810. doi:10.1080/00222348.2013.808560.
- [44] R. Kaneko, E. Hamada, Microwear processes of polymer surfaces.pdf, *Wear.* 162 (1993) 370 – 377. doi:0043-1648/93.

Chapter IV.

Part I. *Impact of cellulose nanocrystal aspect ratio on crystallization and reinforcement of poly(butylene adipate-co-terephthalate)*

This chapter is based on **Impact of cellulose nanocrystal aspect ratio on crystallization and reinforcement of poly(butylene adipate-co-terephthalate)**. Published by **Journal of Polym. Science. Part B, Polym. Physics.** 54 (2016), 2284–2297.

CONTENTS

ABSTRACT.....	172
1 INTRODUCTION.....	173
2 EXPERIMENTAL	175
2.1 Materials.....	175
2.2 Preparation of cellulose nanocrystals.	175
2.3 Preparation of nanocomposites.	176
2.4 Characterizations.....	176
3 RESULTS AND DISCUSSION.....	178
3.1 Characterization of raw materials	178
3.2 Dispersion of CNC within PBAT.....	182
3.3 Non-isothermal crystallization of extruded materials.	183
3.4 Isothermal crystallization of extruded materials.	187
3.5 Mechanical properties at room temperature.	191
3.6 Viscoelastic properties in the molten state.	193
4 CONCLUSIONS	195
5 REFERENCES	196

ABSTRACT

Cellulose nanocrystals (CNCs) are appealing nanomaterials for the reinforcement of polymeric materials. It is now well established that high mechanical properties can be obtained when preparing the nanocomposite by slow casting/evaporation methods and using CNC contents above the percolation threshold. This phenomenon results from the formation of a stiff CNC network within the polymeric matrix meaning that the properties of the matrix play only a limited role on the mechanical properties of the material when the matrix is in the rubbery state. In subpercolation concentration or when using a different processing technique, the level of understanding is less clear, mainly when the CNC-induced crystallization of the matrix interfere with the reinforcing mechanism. In this study we used CNCs with different aspect ratios to prepare nanocomposites by extrusion with Poly(butylene adipate-co-terephthalate) (PBAT) as matrix. The impact of CNC on the crystallinity of the matrix and mechanical properties of the nanocomposite has been investigated.

1 INTRODUCTION

Improved thermal and mechanical performance can be obtained for macromolecular organic materials by adding inorganic or organic high strength and modulus particles. The use of biofillers to create renewable and functional biocomposites is a trend that now goes toward nanotechnology. Cellulose nanocrystals (CNC) are rod-like nanoparticles that can be extracted from native cellulose by the application of different methodologies [1-3]. Lightness, toughness, high mechanical properties and abundance make these nanoparticles a relevant material in nanotechnology. The potentially high reinforcing effect induced by CNC is well described in literature. Cellulosic sources that can provide nano-rods with high aspect ratio (length/diameter ratio), such as tunicate [4,5], capim dourado[6], and *Posidonia oceanica* leaves[7] are suitable materials to achieve very high mechanical properties of the ensuing nanocomposites.

These properties are driven by the capability of CNC to form a continuous rigid 3D network when its content is above the percolation threshold [4]. The materials prepared by casting/evaporation using these nanoparticles can show optimized properties in this ideal composition that is directly dependent of the CNC aspect ratio. The formation of this 3D network is only possible in casting/evaporation conditions due to the long time for solvent evaporation that provides to the particles enough time to interact and self-organize. However, for economic reasons, casting/evaporation is a less efficient way to prepare composites compared to extrusion or other solvent-free processing techniques. Nevertheless, extrusion does not seem to provide the ideal conditions to form the particle network. As a consequence, a higher amount of nanoparticles is needed to significantly improve the mechanical properties.

Nowadays, a trend to shift from the casting/evaporation method to melt processing is observed. Issues, such as early thermal degradation, difficulties in achieving a homogeneous dispersion and poor mechanical properties when compared to cast/evaporated materials are being extensively investigated by many research groups. Methodologies to improve the high temperature processing of CNC reinforced polymer are basically based on surface chemical modification of CNC [239,240] or physical interactions [10,11]. It was shown that similar nanocomposites prepared by casting/evaporation or extrusion can present very different properties[12]. Besides the non-formation of the CNC network, extrusion can also cause CNC breakage, modifying the size of the particle. Moreover, it seems to bring alterations in the crystallinity of the matrix, altering its macroscopic properties. However, in this study the competition between the particle content and the particle

size was not well defined and the different processing techniques make difficult the comparison of the samples.

Many works have reported the capability of CNC to act as nucleating agent for a semicrystalline matrix [13-15]. The crystallinity or kinetics of crystallization of the matrix can be affected which in turn can strongly impact the rheological and mechanical behavior of the material, mainly in subpercolation concentration. In our previous work [16], we have also noticed crystallization of the polycarbonate matrix after processing by extrusion. However, this phenomenon was predominantly ruled by a reduction of the molecular weight of the polymer during the preparation of a masterbatch. Nevertheless, the presence of CNC was able to slightly increase the crystallinity of the polymer, even for a normally amorphous matrix. For these materials it is always difficult to separate the effect of the CNC-induced crystallization and real reinforcing effect of the nanofiller.

Biodegradable semicrystalline polymers, such as aliphatic polyesters, are interesting candidates for the preparation of CNC reinforced nanocomposites due to their promising applications in compostable films, sheets, bottles and injection-molded products. To the best of our knowledge, no attempt was made to investigate the effect of CNC addition in poly(butylene adipate-co-terephthalate) (PBAT) matrix. PBAT is a rare case of biodegradable petroleum-based polymer [17]. Its chains that are formed as aliphatic-aromatic polyester by butylene glycol and adipic/terephthalic acids. Nanocomposites based on this material can be quite interesting due to the potential applications in areas such as medicine [18,19].

PBAT is an highly soft and ductile polymer that is extensively used for the preparation PBAT/PLA blends, aiming to combine the properties of elongation and toughness of both polymers [18,20,21]. Due to its high elongation capability, PBAT can be considered as a good candidate for packing applications, being a totally biodegradable film [22]. Some of its properties, as tensile strength (32-36 MPa) and elongation at break (close to 700%) makes this biopolymer comparable to low-density polyethylene (LDPE) [23]. However, its mechanical properties and price can be limiting factors for some applications. The use of organic fillers, such as CNC, could provide at the same time an increase in the mechanical properties and a cost reduction. Besides that, CNC are biosourced and can keep the total biodegradability of the composite material. Usually, PBAT presents low crystallization rates (and crystallinity). Some attempts were performed to increase its crystallinity using graphite nanosheets or nanoclays[24]. However, these trials were not completely successful.

In the present paper, we report the preparation of CNC reinforced PBAT nanocomposites by extrusion using rod-like nanoparticles with different aspect ratio. The composition of the nanocomposite was chosen to fit with the percolation

threshold of CNC. The thermal and mechanical properties of ensuing materials were investigated and discussed based on the dimensions of CNC.

2 EXPERIMENTAL

2.1 Materials

Commercial cellulose nanocrystals (CNCs) were purchased from the University of Maine as an 11% aqueous suspension and used without further purification. In addition, two different natural fibers were used as starting material for the preparation of CNCs, *viz* capim dourado and sisal. Capim dourado (*Syngonanthus nitens*) fiber was brought from Jalapão region (Tocantins, Brazil) and native sisal fibers (*Agave sisalana*) were purchased in Mariana (Minas Gerais, Brazil). Sulfuric acid, sodium hydroxide, acetate and chlorite were obtained from Sigma-Aldrich. Commercial biodegradable polyester, polybutyrate adipate terephthalate (PBAT)-ecoflex, was provided as pellets by BASF.

2.2 Preparation of cellulose nanocrystals

CNCs were prepared as previously reported in literature for capim dourado[6] and sisal [25,26]. Before hydrolysis, capim dourado and sisal fibers were submitted to a bleaching step to purify cellulose by removing secondary components, such as lignin and hemicelluloses, normally present in natural fibers. This step was firstly performed by soaking the cut fibers into a NaOH solution (4 wt%) at 80°C for 2 hours, assisted by mechanical stirring. This process was performed twice, with subsequent washing with hot water to eliminate the alkali and residual constituents. In sequence, equal parts of acetate buffer, aqueous chlorite (1.7 wt% in water) and distilled water were used to complete the bleaching stage. The fibers were kept under mechanical stirring for 3 hours at 80°C. Then, the fibers were filtered and washed until reaching neutral pH.

Once the fibers were bleached they were defibrillated in a knife mill to limit particle agglomeration. The hydrolysis step was performed by using apre-heated sulfuric acid solution (64 wt%) at 50°C under strong mechanical stirring. Capim dourado fiber was hydrolyzed during 60 min and sisal fiber for 40 min. The resultant acid suspensions were washed by successive centrifugation cycles at 10,000 rpm and 10°C for 10 min before dialysis against distilled water until reaching neutral pH. The aqueous suspensions were homogenized by using an Ultra Turax T25 homogenizer and ultrasonically dispersed prior to their utilization. CNC extracted from the different sources will be labeled CNC_x, where x correspond to the aspect ratio of CNC.

2.3 Preparation of nanocomposites

Before preparing the nanocomposites the acid sulfate groups of CNC were neutralized by adjusting the pH of the suspension to 10 using NaOH. The CNC suspension was kept at this pH condition under agitation for 24h and then neutralized again by dialysis against distilled water. This process was conducted to limit the thermal degradation of cellulose during melt processing. Nanocomposite materials were prepared by extrusion following two different methods. The first method consisted in freeze-drying the CNC dispersion and directly extruding the ensuing powder with PBAT pellets. For the second method, the CNC aqueous suspension was mixed with PBAT pellets and the resulting suspension was cast and dried overnight in a glass plate before extrusion.

In both cases, extrusion was performed with a twin-screw extruder DSM 15 Microcompounder from Xplore. Three heating zones (120, 125 and 130°C) and a screw speed of 40 rpm were set-up for a 10 min extrusion. Samples were sequentially prepared by injection-molding for rheological measurements. The extruded material was cut in small pieces and melted in a HAAKE Minijet II at 175-45°C (heater-mold temperatures) to be injected under a pressure of 270 bar. Discs with dimensions of 25 mm × 1.5 mm were obtained. Materials used for mechanical analysis (before and after annealing at 150°C) were prepared by hot-pressing the extruded samples at 130°C and 15 atm for 2 min. The CNC content of the nanocomposites was adjusted for each set of CNC to correspond to the critical percolation threshold. The different nanocomposites will be labeled PBATC_x, where x correspond to the aspect ratio of CNC.

2.4 Characterizations

Atomic force microscopy (AFM). AFM images were obtained on a Nanoscope IIIa microscope from Veeco Instruments. A drop of a diluted aqueous CNC suspension with 0.01 wt% concentration was deposited on a mica substrate and dried. It was imaged in tapping mode with a silicon cantilever. The nanocrystal dimensions were estimated from 100 measurements using the associated software.

Thermogravimetric analysis (TGA). TGA was carried out under air atmosphere (50 mL/min) using a Perkin-Elmer TGA-6 equipment by heating the samples from room temperature to 600°C with a heating rate of 10°C.min⁻¹.

Differential scanning calorimetry (DSC). DSC analyses were carried with TA DSC Q100 equipment, where the sample (weight of 8 ± 2 mg) was sealed in aluminum pan and analyzed at different heating rates under N₂ atmosphere.

Fourier transform infrared (FTIR). FTIR analysis was performed on FTIR Perkin-Elmer Spectrum One equipment between 600 and 4000 cm^{-1} with a 4 cm^{-1} resolution. All the analyses were carried out in the ATR mode with films obtained by hot-pressing (PBAT) or dried at room temperature from aqueous suspension (CNC).

Elemental analysis (EA). EA was performed mainly to determine the total sulfur content of the cellulose nanocrystals. The technique was carried out in an EA1110-CHNS/O elemental analyzer, CE Instruments.

Zeta Potential (ξ) measurement. It was performed with DTS0230 equipment from Malvern Instruments using diluted CNC suspensions (0.01 wt%). To avoid influence of ionic strength or pH, all the sample dilutions were prepared from a buffer solution with pH 10 and 5 mmol ionic strength, with a conductivity of 180 $\mu\text{S}/\text{cm}$.

X-ray diffraction (XRD). XRD measurements for neat PBAT and nanocomposites prepared by extrusion and hot-pressing were performed on Philips PW 1720 X-ray generator operated at 45 kV and 40mA in a Bragg-Brentano geometry. The 2θ range was from 5° to 65° using a fixed time mode with a step interval of 0.066° and Cu $K\alpha$ radiation ($\lambda = 1.5418 \text{ \AA}$). The crystallinity index (I_c) was determined by the peak height (h) method:

$$I_c = \frac{I_2 - I_1}{I_2} \quad \text{Eq I}$$

where I_1 is the intensity at the minimum ($2\theta = 22^\circ$) and I_2 is the intensity associated with the crystalline region of PBAT ($2\theta = 23.5^\circ$).

Mechanical properties. Mechanical characterization of the hot-pressed films was performed at room temperature by dynamic mechanical analysis (DMA) and tensile tests using a RSA3 equipment (TA Instruments, USA) working in tensile mode. Dynamical time sweep tests were performed with a frequency of 1 Hz and a force of 1 N. In these tests a dynamic stress is applied to the sample and the value of the storage modulus is followed as a function of time in isochronal conditions. For tensile tests a cross-head speed of $10 \text{ mm}\cdot\text{min}^{-1}$ and a distance between jaws of 10 mm were used. All samples had dimensions around $5.0 \pm 0.5 \text{ mm}$ for width and $0.5 \pm 0.1 \text{ mm}$ for thickness.

Rheological behavior. The rheological behavior of injection-molded materials was characterized in an ARG2 equipment from TA Instruments. A plate-plate (25 mm) geometry was used to study the polymer and composites in oscillatory modes at 150°C .

3 RESULTS AND DISCUSSION

3.1 Characterization of raw materials

The preparation of CNCs with different aspect ratios was based on previous results founded in literature. Three different cellulosic sources were chosen to provide expected distinct reinforcement effects due to variation in their percolation threshold. Figure 1 shows the AFM images of these nanomaterials used here in the present study, including examples of some individual particles length and height (Z axis) for each sample.

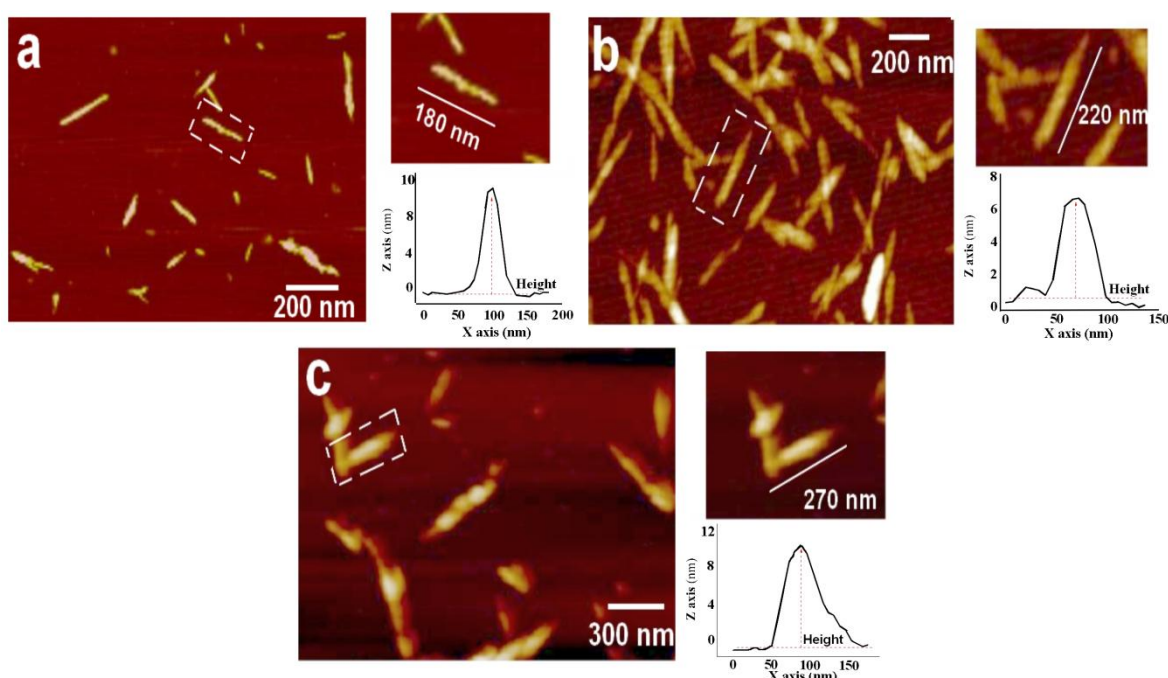


Figure 1. AFM images of the different CNCs, with CNC₂₂ (a), CNC₃₉ (b) and CNC₅₀ (c).

For all samples, as expected, elongated rod-like particles can be observed. The analysis of CNC particles by AFM images generally presents good agreements with particles dimensions obtained by TEM. However, the diameter of the particles obtained by TEM seems to be similar to the height of the particle obtained by AFM. It happens because the particle diameter directly measured by AFM could hide lateral aggregations that will not be detected. Here, the length (L) and height (d) of the particles were used to estimate their aspect ratio (L/d). These data, as well as some additional properties, are collected in Table 1.

The dimensions and aspect ratio for CNC purchased from University of Maine (CNC₂₂) or prepared from sisal fiber (CNC₃₉) were similar to data reported in

literature [27]. For CNC extracted from capim dourado fibers (CNC₅₀) the aspect ratio was lower than the value (67) reported in literature. [6]

It is well known that an increase in the filler aspect ratio results in a decrease of the particle content needed to form a percolating network in the composite. The percolation theory applied for CNCs, and developed by Favier et al.[4] is based on Equation II.

$$\phi_c = \frac{0.7}{L/d} \quad \text{Eq II}$$

Where ϕ_c is the critical CNC volume fraction at the percolation threshold and L/d the CNC aspect ratio. The specific surface area A_{sp} can be calculated from:

$$A_{sp} = \frac{4}{\rho \times d} \quad \text{Eq III}$$

With ρ and d are the density and diameter of CNC, respectively.

Table 1. Characteristics of the cellulose nanocrystals: length (L), diameter (d), aspect ratio (L/d), weight fraction at percolation threshold (w_c), specific surface area (A_{sp}) and zeta potential (ξ).

Nanoparticle	L (nm)	d (nm)	L/d	w_c^* (wt%)	A_{sp}^* (m ² .g ⁻¹)	ξ (mV.cm ⁻¹)
CNC ₂₂	180	8.3	22	4.0	309	-37
CNC ₃₉	215	5.5	39	2.2	466	-18
CNC ₅₀	268	5.4	50	1.8	475	-31

* w_c and A_{sp} values were calculated assuming 1.25g.cm⁻³ and 1.56 g.cm⁻³ for the density of PBAT and CNC, respectively.

As expected from Eq. (2) and Eq. (3), increasing the L/d value results in a reduction of the w_c value, and increasing the d value (and also decreasing the L/d value in this case) results in a decrease of the A_{sp} value. Both parameters can impact other properties than mechanical reinforcement. For example, the crystallization of PBAT can be affected by the specific surface area of CNC. Such properties will be discussed later.

One of the major concerns for biopolymer processing is the thermal degradation of the material in harsh conditions. Oxygen present in atmosphere, water content and mechanical stress can contribute to carbonization or depolymerization of the macromolecules, leading to irreparable damage of the material and affecting its final properties. For composites reinforced with H₂SO₄-prepared CNC, the polymer matrix usually displays higher thermal stability compared to the cellulosic nanoparticles. This behavior was investigated by thermogravimetric analysis. The corresponding thermograms are plotted in Figure 2

and all the data reported in Table 2. According to TGA curves (Fig. 2) it is observed that PBAT degradation starts above 300°C and occurs in a single stage.

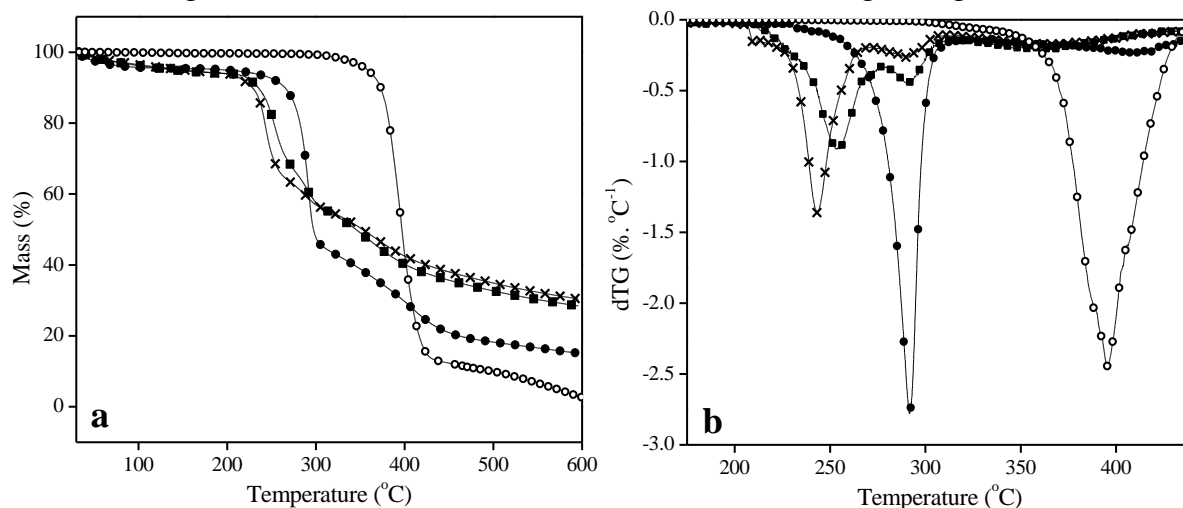


Figure 2. (a) TGA and (b) dTG curves for (o) PBAT, (x) CNC₂₂, (●) CNC₃₉, and (■) CNC₅₀.

The polymer maximum peak degradation is around 395°C (Fig. 2b) and at 600°C, almost all the polymer is already degraded leaving just less than 3% of residual mass, probably in the form of coal. It is important to know the thermal degradation range of the polymer to avoid its degradation during the melt processing. During extrusion, several degradation mechanisms have been proposed as route to the breakage of the ester-linkage in polyesters. For PBAT, a hydrolysis mechanism seems to be dominant at lower temperatures (from 180-215°C). Nevertheless, no significant chain modifications seem to occur until 200°C. [28]

Table 2. Thermogravimetric data for pristine materials: number of degradation stages (n), onset temperature (T_{onset}), maximum temperature (T_{max}) and char fraction at 600°C.

Sample	n	T_{onset} (°C)	T_{max} (°C)	Charfraction (%)
PBAT	1	300	395	2.7
CNC ₂₂	2	208	254	28.4
CNC ₃₉	1	210	290	15.0
CNC ₅₀	2	208	243	30.6

Much less thermally stable, CNC showed a different degradation pattern compared to PBAT. Its weight loss starts at much lower temperature and a higher char residue can be observed at 600°C. Among the different nanoparticles, a very similar onset degradation temperature around 210°C is reported (Table 2). However, it is observed that CNC₃₉ displays a higher maximum degradation temperature and lower char residue compared to CNC₂₂ and CNC₅₀. A broad range of thermal degradation temperatures has been reported for CNC [2].

It obviously depends on the acid hydrolysis conditions, but also on the specific surface area of the CNC that changes the density of sulfate groups [7]. The low thermal stability and high char residue of CNC is attributed to the presence of sulfate groups resulting from the H₂SO₄ hydrolysis step [29-32]. Surprisingly, CNC₃₉ shows the highest sulfur content (Table 3).

However, the CNC₃₉ sample stands out by its higher C and H contents and lower "Other elements" content (Table 3). The latter mainly consists of oxygen. This sample also displays the highest C/H ratio. This, along with a higher N content, indicates that this sample can present a higher number of unsaturation and residual molecules, such as hemicelluloses, waxes and even proteins, on its surface. These elements can cover the nanoparticle and cause a kind of physical barrier increasing the degradation temperature.

The CNC₃₉ sample also stands out by its much lower surface charge (zeta potential, Table 1). Samples with more negative charge are expected to be less thermally stable. It could result from a masking effect of the surface sulfate groups by coating elements. This indicates a direct relation between the surface charge and thermal stability (this charge is not necessarily related to the sulfur content). The reason why CNC prepared from sisal fiber presents this specific behavior remains unsolved and needs to be further investigated.

Table 3. Elemental analysis results for cellulose nanoparticles.

Nanoparticle	%C	%H	%S	%N	%Others	Elemental Ratio	C/H Ratio
CNC ₂₂	39.85	6.29	1.82	0.17	51.87	C ₂₃₄ H ₃₇ S ₁₁ N ₁	6.3
CNC ₃₉	46.47	6.98	1.96	0.37	44.22	C ₁₂₅ H ₁₉ S ₅ N ₁	6.7
CNC ₅₀	40.58	6.29	1.64	0.22	51.27	C ₁₈₄ H ₂₉ S ₇ N ₁	6.4

The raw materials were further characterized by FTIR. The chemical structure of PBAT and cellulose as well as FTIR spectra are presented in Figure 3. The basic structural differences can be easily observed between CNC and PBAT. PBAT shows vibrations around 3000 cm⁻¹ representing C–H stretching in aliphatic and aromatic segments. The bands located around 1710 and 1270 cm⁻¹ are characteristic of carbonyl groups (C=O) and C–O in the ester linkage. The sharp peak at 725 cm⁻¹ corresponds to four or more adjacent methylene (–CH₂–) groups.

The FTIR spectra for CNCs show the characteristic peaks of native cellulose. The absorbance peaks in the 3400-3300 cm⁻¹ and around 1640 cm⁻¹ regions are attributed to the stretching and bending vibrations, respectively, of the OH groups of cellulose. The signals around 2900-2800 cm⁻¹ correspond to C–H stretching. The bands observed in the range of 1420-1430 cm⁻¹ and 1330-1380 cm⁻¹ are attributed to

the symmetric bending of CH₂ and bending vibrations of the C–H and C–O groups of the aromatic rings in polysaccharides, respectively. The absorbance peaks observed in the 1000-1150 cm⁻¹ range are attributed to C–O stretching and C–H rocking vibrations of the pyranose ring skeleton. However, the peak observed around 1740 cm⁻¹ was not expected for native cellulose. It is generally attributed to the C=O stretching in ketones or esters (including carboxylic acids) [33,34] of hemicellulose or to the ester linkage of the carboxylic group in the ferulic and p-coumaric acids of lignin and/or hemicellulose. The occurrence of this peak, associated with the higher intensity of the 2850 cm⁻¹ peak (C–H peak in alkanes), for CNC₃₉ also suggest that this nanoparticle presents residual small molecules on its surface, which corroborates elemental analysis. Some comments can be found in Appendix C.3.

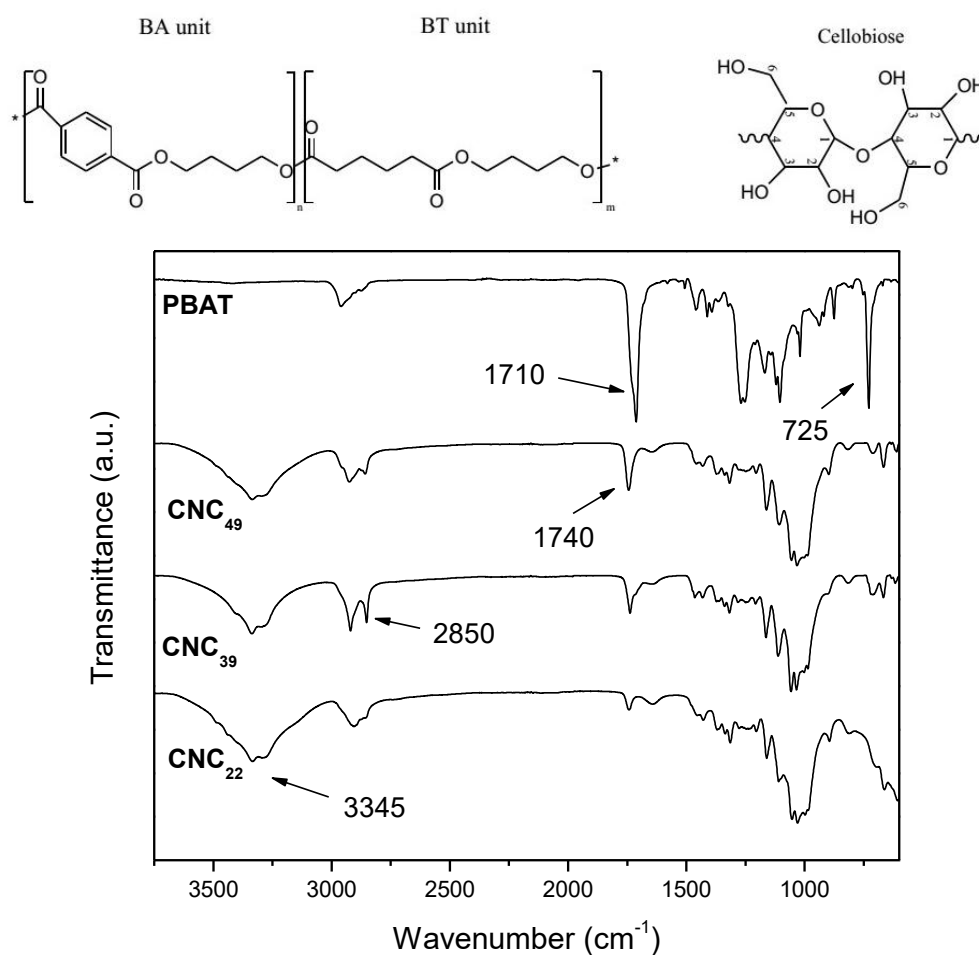


Figure 3. Chemical structure of PBAT and cellulose monomer units, and FTIR spectra for PBAT and the three sets of CNC.

3.2 Dispersion of CNC within PBAT

The processing step has a major importance for composite properties. The first processing attempt was performed by directly mixing the polymer pellets and freeze

dried CNC before extrusion. However, besides some chemical similarities between the filler and the matrix (i.e. the possible formation of hydrogen bonds), the dispersion of the nanoparticles was not satisfactory. This technique generated heterogeneous materials with poor dispersion and visible aggregates (white dots) as shown in Figure 4 for the nanocomposite film reinforced with CNC₂₂ (PBATC_{22d}). At least, no sign of thermal degradation (no browning) for CNC in these materials was observed despite the high processing temperature. Mixing the PBAT pellets with the aqueous dispersion of CNC before casting/evaporation and subsequent extrusion considerably improved the dispersion of the filler within the polymeric matrix and homogeneity of the film as shown in Figure 4. During the preparation of nanocellulose reinforced poly(β -hydroxybutyrate) (PHB) composites it was observed that the cellulosic nanoparticles stick to PHB powder in water suspensions[35]. A similar behavior was observed with PBAT. In the following all tested samples were prepared by this method.



Figure 4. Pictures of the extruded films: neat PBAT, PBAT reinforced with CNC₂₂ and prepared by direct extrusion of PBAT pellets and freeze-dried CNC (PBAT_{22d}), and nanocomposites prepared by casting/evaporation followed by extrusion reinforced with CNC₂₂ (PBATC₂₂), CNC₃₉ (PBATC₃₉), and CNC₅₀ (PBATC₅₀).

3.3 Non-isothermal crystallization of extruded materials

Besides particle dispersion, modification in polymer matrix crystallinity and possible reduction of molecular weight induced by melt processing are two of the most significant parameters that can impact the mechanical properties of the composites.

Characteristic thermal properties can be easily accessed by DSC. Parameters such as glass transition temperature (T_g), melting point (T_m) and heat of fusion (ΔH_m) are useful to understand and predict the material behavior after extrusion or injection-molding. The obtained data could be especially useful to provide information about how different nanoparticles can affect the nanocomposite micro structure. The effect of thermal history on polymer crystallinity can be deduced from its ΔH_m value. Obtained directly from DSC curves, ΔH_m was used to obtain the

degree of crystallinity (χ_c) of the sample by its relation with the theoretical 100% crystalline heat of fusion (ΔH_m°), using the following equation:

$$\chi_c = \frac{\Delta H_m}{\Delta H_m^\circ \times (1-w_f)} \times 100 \quad \text{Eq IV}$$

where ΔH_m is the heat of fusion of the sample, ΔH_m° is the heat of fusion of the 100% crystalline polymer matrix (114 J.g⁻¹ for PBAT)[36] and w_f is the weight fraction of the cellulosic filler, included to normalize the enthalpy according to the fraction of polymer present in the sample.

After extrusion, all composites were studied using acyclic heating-cooling-heating analysis as a way to obtain basic information about the sample. Some of the obtained curves are reported in Figure 5 and the results are collected in Table 4. This test can provide information about how the material prepared under stress (i.e. by extrusion) differs from the composite melted and cooled in controlled conditions.

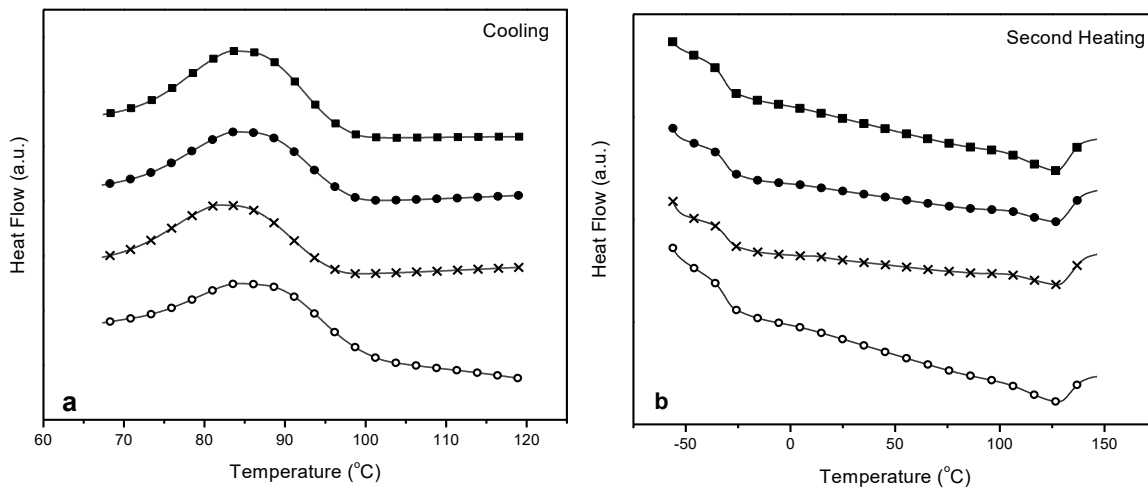


Figure 5. DSC curves recorded during (a) cooling and (b) second heating scan for PBAT and the three sets of CNC reinforced composites: (○)PBAT, (×) PBATC₂₂, (●) PBATC₃₉ and (■) PBATC₅₀.

The data shows that the degree of crystallinity of PBAT is relatively higher during the first sample heating cycle compared to the second one. This could be ascribed to the stress applied to the macromolecules during extrusion that can favor crystallization or to a lower cooling rate of the extruded material compared to the controlled cooling rate applied during DSC experiments. However, the size of crystalline domains reflected through the melting point is lower for extruded materials.

Regarding the influence of CNC, no significant effect was observed for T_c , T_g and T_m values of PBAT either during the first or the second heating scan for the latter. However, the degree of crystallinity tends to increase probably due to a nucleating effect of the nanoparticle [13,37] and this effect tends to become more

prominent when increasing the aspect ratio of CNC. This observation is in agreement with pictures in Figure 4 that show that increasing the aspect ratio of CNC results in less transparent films probably due to higher crystallinity. This may appear surprising considering the lower amount of high aspect ratio CNC used for the composites even if their specific surface area increases (Table 1). The interfacial area developed in 1g of material can be estimated for well dispersed nanorods by multiplying the weight fraction of CNC at the percolation threshold (ϕ_c) by the specific surface area (A_{sp}). It leads to 12.4, 10.3, and 8.55 m² for CNC₂₂, CNC₃₉ and CNC₅₀, respectively. It was expected that reduced interfacial area should impact to a lesser extent the nucleating effect of CNC. This apparent discrepancy suggests that the aspect ratio of CNC is probably more important than the interfacial area in driving the crystallization of the matrix.

Table 4. DSC data obtained for extruded materials in a cyclic analysis: melting point (T_m), temperature of crystallization (T_c), glass transition temperature (T_g), heat of fusion (ΔH_m), heat of crystallization (ΔH_c), and degree of crystallinity (χ_c).

Sample	1st Heating			Cooling			2nd Heating		
	T_m	ΔH_m	χ_c	T_c	ΔH_c	T_g	T_m	ΔH_m	χ_c
PBAT	121.1	16.7	14.6	86.7	8.9	-30.9	128.1	5.1	4.5
PBATC ₂₂	122.3	17.4	15.6	83.1	11.1	-30.4	128.4	5.7	5.0
PBATC ₃₉	122.2	17.5	15.6	84.8	11.4	-30.8	127.7	5.8	5.2
PBATC ₅₀	123.3	19.8	17.6	84.9	12.9	-31.7	127.4	8.5	7.1

Different behaviors have been reported for the effect of nanoparticles on the crystallization of PBAT including no influence as well as a decrease [18,21,38]. Considering the effect of the size of the cellulose nanofiber, Mukherjee et al. [22] used long cellulose nanofibrils (CNFs) to produce composites with PBAT, and a strong increase of the crystallinity of the matrix was reported with only 1 wt% CNF. The plot of the relative crystallinity (X_t), obtained from Equation V, can well illustrate how the non-isothermal crystallization kinetics of PBAT is impacted by the presence of CNC.

$$X_t = \frac{Q_t}{Q_\infty} \quad \text{Eq V}$$

Where Q_t is the heat involved in the crystallization at a specific time t and Q_∞ is the total heat involved in the crystallization for a specific cooling rate. The data are plotted in Figure 6.

The induction time for crystallization (arrows in Figure 6) is clearly modified when adding the nanofiller. It is observed that nanocomposite samples need more

time to initiate and to complete the crystallization. Quantitative data about this behavior can be obtained by determining the activation energy and half-crystallization time ($t_{1/2}$) of the process. To determine the activation energy, non-isothermal crystallization experiments have been accordingly performed for different cooling rates. The half-crystallization time ($t_{1/2}$) was estimated using Equation VI [39].

$$t_{1/2} = \frac{T_i - T_c}{\Phi} \quad \text{Eq VI}$$

where T_i and T_c are the onset and exothermic crystallization peak temperature, respectively, and Φ is the cooling rate. The values obtained for $\Phi = 10^\circ\text{C}\cdot\text{min}^{-1}$ are reported in Table 5. As suggested by the induction time curves profile, $t_{1/2}$ is higher for the composites than for the neat polymer.

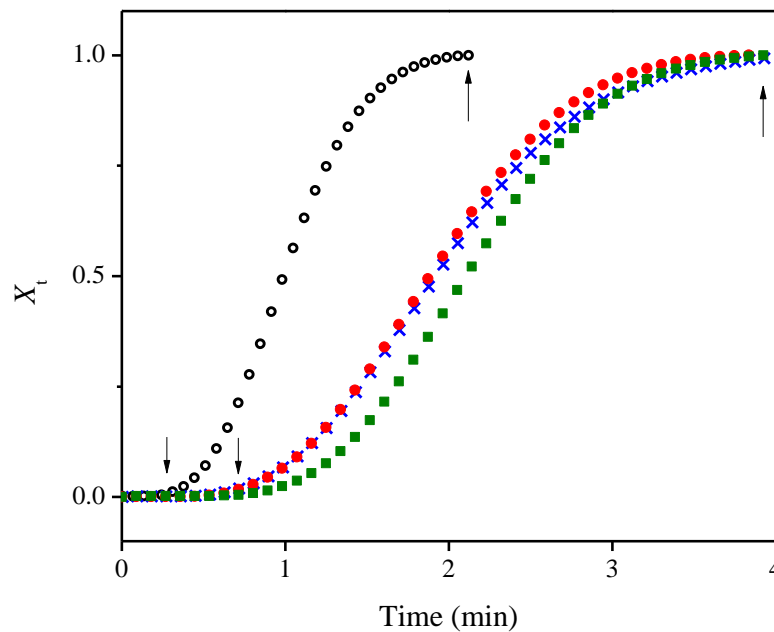


Figure 6. Non-isothermal crystallization data using a cooling rate of $-10^\circ\text{C}\cdot\text{min}^{-1}$ for (o)PBAT, (x) PBATC₂₂, (●) PBATC₃₉ and (■)PBATC₅₀.

The crystallization of a polymer, especially at short times, is strongly dependent on the ability of the chains to migrate from the melt state to the surface of a growing crystalline region. This migratory process involves energy, and the activation energy (E_a) of this transition can be calculated by the Kissinger Equation (Eq. VII), where the variation of the cooling rate ($^\circ\text{C}\cdot\text{min}^{-1}$) can be used to determine it during a non-isothermal crystallization process.

Table 5. Non-isothermal crystallization temperature, activation energy and half-crystallization time ($t_{1/2}$) determined for $10^{\circ}\text{C}\cdot\text{min}^{-1}$.

Cooling Rate ($^{\circ}\text{C}\cdot\text{min}^{-1}$)	Crystallization Temperature, T_c ($^{\circ}\text{C}$)			
	PBAT	PBATC ₂₂	PBATC ₃₉	PBATC ₅₀
10	86.7	83.1	84.8	84.9
20	78.9	74.2	77.2	78.2
30	69.8	70.3	71.7	73.4
40	66.1	67.2	67.7	66.1
Ea (kJ.mol⁻¹)	78.4	100.5	87.8	80.1
$t_{1/2}$(min)	1.38	1.70	1.67	1.51

$$\frac{d[\ln(\frac{\Phi}{T_c^2})]}{d(\frac{1}{T_c})} = \frac{Ea}{R} \quad \text{Eq VII}$$

where T_c is the crystallization temperature (in K), Φ is the cooling rate and R is the universal gas constant.

The results are reported in Table 5. In earlier works, Feng et al. [24] and Chivrac et al. [40] used this equation to estimate the Ea value for systems consisting of PBAT as the matrix and different nanoparticles as filler (graphite nanosheets and nanoclays, respectively). Conflicting results were reported, filler addition causing an increase of Ea for one system and a decrease for the other. In this present work, Ea values are higher for the composites than for neat PBAT. It could probably result from a decrease in polymeric chain mobility upon nanofiller addition. Indeed, increased viscosity can reduce the diffusion capacity of the polymeric chains from the bulk melt to the crystalline domains at short times. The reduction of mobility as principal motivation for the increase in Ea value can be confirmed by comparing the different sets of CNC. The Energy is systematically higher for highly filled nanocomposites.

This result seems to conflict with the values of the degree of crystallinity reported from cyclic analysis (Table 4) since a higher crystallinity was founded for composites. However, they are in agreement with the slight decrease observed for the crystallization temperature. The nanocomposites present reduced crystallization kinetics, while neat PBAT displays a faster crystallization, but the final crystallinity is higher for nanocomposites.

3.4 Isothermal crystallization of extruded materials

DSC analysis suggested that crystallization of PBAT can be impacted by the dimensions of CNC. Therefore, the crystallization process was investigated over a longer time period by annealing the sample for various durations at its crystallization temperature, around 85°C . DSC thermograms recorded after cooling

to room temperature the samples submitted to this isothermal crystallization treatment are shown for PBATC₅₀ as example in Figure 7. Thermal data determined from DSC experiments for PBAT and the three different sets of CNC can be found in Table 6.

When comparing the thermogram obtained for the extruded sample (I) with the one corresponding to the second heating (II) obtained after melting and controlled cooling at $-10^{\circ}\text{C}\cdot\text{min}^{-1}$, a clear decrease of the degree of crystallinity is observed as already discussed (Table 4). Moreover, a distinct broadening of the melting endotherm towards lower temperatures is observed for the extruded sample. It suggests a broader distribution in crystallite size and the presence of smaller crystalline domains. These trends (presence of smaller crystallites and increase in crystallinity) are amplified for annealed samples and even a double melting peak (with temperatures denoted T_{m1} and T_{m2} in Table 6) is reported. Also, it is noted that the magnitude of the first melting peak increases upon annealing. According to Fukushima et al.[18], the decrease of the melting point for PBAT is attributed to the formation of largely imperfect crystals, that can melt at lower temperatures. The slight increase of T_{m1} upon annealing at 85°C suggests that after their formation, these crystalline domains become more organized during annealing.

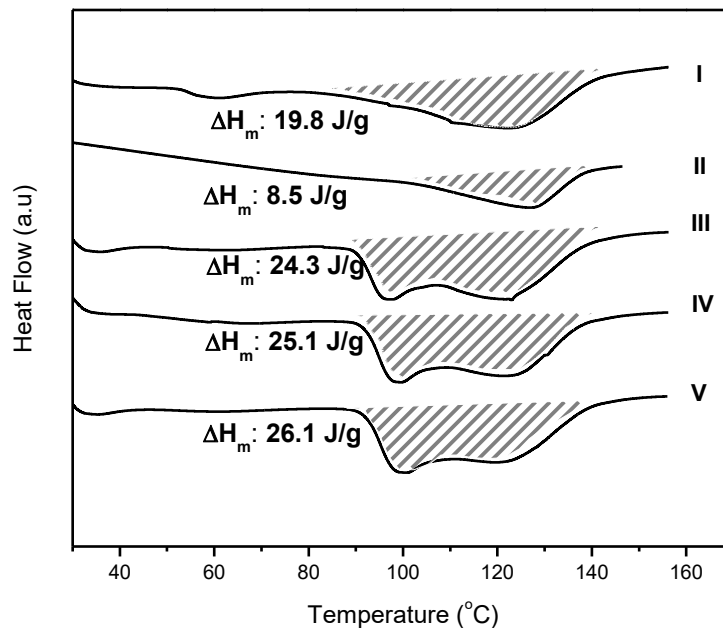


Figure 7. DSC curves recorded for PBATC₅₀: from top to bottom: (I) extruded material, (II) 2nd heating for extruded material, and (III) 2, (IV) 6 and (V) 18 hours annealed (85°C) sample.

Table 6. DSC data obtained after isothermal crystallization at 85°C for 2, 6 and 18 hours.

Sample	2 hours				6 hours				18 hours			
	T _{m1}	T _{m2}	ΔH _m	χ _c	T _{m1}	T _{m2}	ΔH _m	χ _c	T _{m1}	T _{m2}	ΔH _m	χ _c
PBAT	99.1	125.0	20.2	17.5	100.1	123.3	20.5	18.0	101.4	122.5	21.9	19.2
PBATC ₂₂	97.6	122.9	21.8	19.5	100.3	126.1	21.6	19.4	100.9	124.8	23.2	20.7
PBATC ₃₉	98.7	123.8	18.2	19.6	99.2	123.7	22.5	20.1	101.7	124.0	22.8	20.3
PBATC ₅₀	97.3	123.1	24.3	21.6	99.7	124.2	25.09	23.0	100.9	122.9	26.1	26.4

Since PBAT is a copolymer formed of BT and BA units, it has a direct implication on its solid structure. Kuwabara et al.[41] suggest that the crystalline domains of PBAT are basically composed of PBT chains, while PBA chains are in the amorphous state. However, theoretical calculations show that PBT can be responsible for up to 20% of PBAT crystallinity. This fact suggests that soft BA units can be introduced in BT crystal lattice [42]. Figure 7 shows that the extruded sample (I) displays a small endothermic peak around 60° C. This melting endotherm is usually attributed to the melting of PBA chains. This observation suggests that in as-received PBAT pellets some PBA chains are organized in crystalline domains. The disappearance of this peak upon melting and annealing suggests that these chains can be reorganized into the already existing crystalline domains to reach a more stable form.

There is clearly an increase in the organization of the composite after addition of CNC and upon annealing. However, no direct correlation is found between the size of the particle and the degree of crystallinity. The crystallinity for PBATC₂₂ and PBATC₃₉ are quite similar most samples but is higher for PBATC₅₀. In 1974, Gray published a study about the transcrystallization of polymers at the surface of fibers surface induced by mechanical stress [43]. This work was further extended to CNC [44]. In particular, the author discussed the effect of the amount of cellulose I at the particle surface on the polymer crystallization and it seems that increasing the amount of cellulose I favored the formation of the transcrystalline layer. This observation could explain why CNC₃₉ does not follow the same behavior as CNC₅₀ being largely more effective than CNC₂₂ to induce the formation of organized domains in the matrix. The presence of non-cellulosic components at the surface of the nanoparticle (as previously suggested) could cause an inhibition of the crystallization kinetics.

XRD experiments were carried out for the neat PBAT matrix and nanocomposite reinforced with CNC₅₀. The extruded nanocomposite was characterized and for all other samples, as for mechanical tests, the materials were

prepared by hot-pressing. The low crystallinity of PBAT samples generates XRD patterns with low intensity, as shown in Figure 8. Similar XRD patterns were found by Yeh et al. [45].

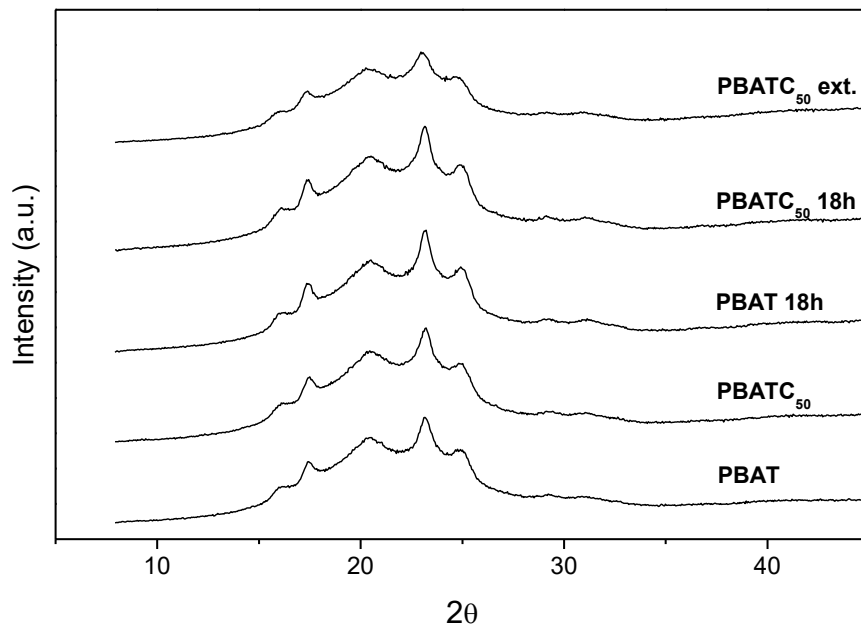


Figure 8. XRD patterns for neat PBAT and nanocomposite reinforced with CNC₅₀ prepared by extrusion (PBATC_{50ext}), and hot-pressing before (PBAT, PBATC₅₀) and after (PBAT18h, PBATC₅₀18h) annealing for 18 hours at 150°C.

All samples display weak peaks at 2θ values around 16, 18, 21, 23.5 and 25.5°. The position of these peaks is not influenced by the low CNC content. These diffraction patterns can be used to estimate the average dimension of the PBAT crystalline domains (τ) using the Scherrer equation (Equation VIII).

$$\tau = \frac{K \cdot \lambda}{\beta \cos \theta} \quad \text{Eq VIII}$$

where β is the peak width at half-height (in rad), λ is the diffraction wavelength, θ the diffraction angle and K is a constant, that was assumed to be 0.9 due to the possible spherulitic shape of the domains. The crystallinity index was also estimated by the peak height method. Beside its imprecision, the relation between $2\theta = 23.5^\circ$ and the amorphous phase was used as auxiliary technique. The results are collected in Table 7.

By comparing PBATC_{50ext} with PBATC₅₀, it is found that the hot-pressing stage increases the crystallinity of the material, but it is worth noting that cooling was not controlled after hot-pressing. However, annealing at 150°C for 18 h clearly increases the crystallinity of PBAT. Two important parameters can be obtained from the Scherrer equation. The first one is the average size of crystalline domains (τ), which

is found to systematically increase with crystallinity. The second parameter is the peak width at half-height (β), which is inversely proportional to the crystallinity. It indicates that the higher the crystallinity is, the thinner the peaks become. The broader peak observed for PBATC_{50ext} could be an indication of PBA crystalline domains since they show a diffraction peak around 23°. This observation agrees with DSC results and corroborates PBA crystallization during cooling after the stress imposed by the extrusion process.

Table 7. Peak width ($\beta_{23.5}$) at half-height for the most intense peak at $2\theta = 23.5^\circ$, corresponding average dimension of the PBAT crystalline domains (τ) determined from (Eq. VIII), and crystallinity index (I_c) determined from XRD experiments (Eq. I).

Sample	$\beta_{23.5}$ (rad)	τ (nm)	I_c (%)
PBAT	0.0121	11.7	29.4
PBATC ₅₀	0.0115	12.3	29.2
PBAT 18h	0.0108	13.1	32.9
PBATC ₅₀ 18h	0.0105	13.5	34.0
PBATC _{50ext}	0.0141	10.0	23.5

3.5 Mechanical properties at room temperature

Besides the impact of the size of CNC on the crystallinity of the PBAT matrix, the use of particles with higher aspect ratio is expected to significantly improve the mechanical properties. As described before, the outstanding mechanical properties that can be reached in cellulose nanocomposites are controlled by a percolation mechanism where a rigid 3D H-bonded CNC network is created, enhancing the material properties. This percolating network is usually assumed to be present in materials prepared by casting/evaporation. In this processing technique, the long evaporation time provides enough time to the nanocrystals to organize themselves and form the rigid structure.

During extrusion the duration of processing is normally much shorter and the nanocrystals cannot create the necessary interactions to build the percolating network. Moreover, a possible orientation of the rod-like nanoparticles can limit this organization. The impact of CNC with different aspect ratio on the properties of extruded nanocomposites seems to be unclear.

Two mechanical tests were performed to characterize the mechanical behavior of CNC reinforced PBAT nanocomposites. A Dynamic Time Sweep Test (DTST) was

accomplished for all samples and themodulus value was noted after 5 min experiment. Tensile tests were also performed. The obtained values are collected in Table 7.

Table 7. Tensile modulus determined from DTST tests (E_{DTST}) and tensile tests (E_T) for neat PBAT and CNC reinforced nanocomposites after extrusion and after annealing at 85°C for 18h. The relative increase (R.I.) in modulus upon annealing and CNC addition is also reported.

Sample	Extruded		18h annealing		R. I.	
	E_{DTST} (MPa)	E_T (MPa)	E_{DTST} (MPa)	E_T (MPa)	DTST (%)	Tensile (%)
PBAT	56	40.5 ± 1.1	67	46.6 ± 1.9	19.6	15.0
PBATC ₂₂	67	44.3 ± 1.3	70	49.7 ± 1.4	25.0	22.7
PBATC ₃₉	61	44.7 ± 1.1	64	45.5 ± 1.0	14.3	12.4
PBATC ₅₀	69	47.2 ± 3.1	76	51.6 ± 2.1	35.7	27.4

Both experiments show an increase in the modulus value when adding CNC and upon annealing at 85°C. This increase can be quantified by calculating the relative increase (R.I.) in modulus (Table 7) defined as:

$$\text{R.I. (\%)} = \frac{E_2 - E_1}{E_1} \times 100 \quad (\text{Eq. IX})$$

where E_1 corresponds to unfilled and unannealed PBAT and E_2 is the modulus of the annealed matrix or nanocomposite.

Therefore, for the unfilled PBAT matrix, this parameter only takes into account the effect of annealing (increase in crystallinity) while for nanocomposites it accounts for both the effect of annealing and CNC. Globally, the same trend is observed for DTST and tensile test experiment, but higher values are reported for the former. Indeed, it is worth noting that in DMA analysis the adhesion between the filler and the matrix is less involved than in tensile tests because of weaker stresses applied in the former technique.

The highest reinforcing effect is clearly observed for CNC₅₀ and CNC₂₂. These two samples also displayed the highest increase in crystallinity upon annealing (see Table 6). We can therefore conclude that the reinforcing effect is probably mainly due to the change in crystallinity since these two nanofillers have very distinct aspect ratio. It is also worth noting that low contents (1.8 wt%) of high aspect ratio CNC can be more effective and brings strong reinforcing effect even without formation of a percolating network, just by driving the crystallization of the matrix. This effect

obviously also depends on the surface chemistry of CNC since intermediate aspect ratio CNC extracted from sisal fibers show the lowest reinforcing effect because of the limited nucleating agent impact induced by possible non-cellulosic components on the surface.

3.6 Viscoelastic properties in the molten state

To investigate the reinforcing effect of CNC without the interference of crystallinity, oscillatory rheological tests were performed in the molten state (at 150°C). The results are reported in Figure 8. It is worth noting that during these experiments performed at high temperature (150°C) CNC and PBAT were thermally stable and no thermal degradation occurred. Indeed, it was shown that at this temperature PBAT was only slightly degraded after 75 min and the viscosity drop did not reach 5% [46]. For CNC, an isothermal TGA experiment was performed and no sign of mass loss was found for at least 90 min.

For these experiments, it is important to perform the tests in a linear region, where the structure of the material cannot be destroyed and could provide a response independent of the applied strain. Strain sweep tests were carried out (Fig. 8a) and it was shown that regardless the type of CNC used very similar linear viscoelasticity regions were observed. It suggests that CNC does not create a continuous structure that could be damaged by a strain increase. This is understandable, since the materials were prepared by extrusion and considering the low nanofiller content.

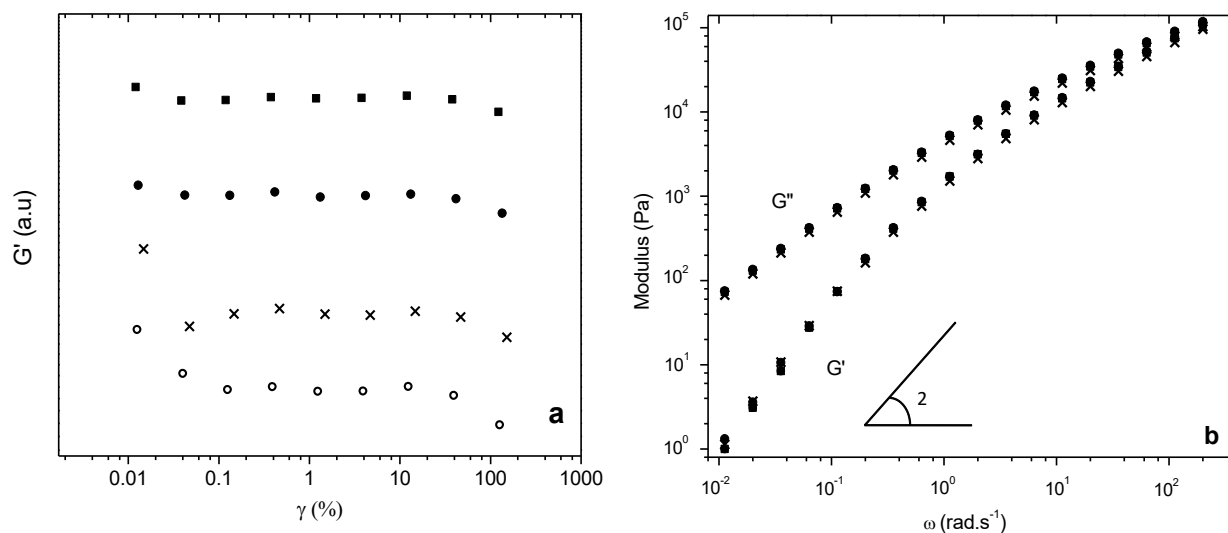


Figure 8.(a) Strain sweep tests and (b) frequency sweep measurements in linear conditions at 150°C for (○)PBAT, (×) PBATC₂₂, (●) PBATC₃₉ and (■) PBATC₅₀.

All the oscillatory tests were performed with a 1% strain and results are shown in Figure 8b. Similar G' and G'' values were reported for all samples, where the loss modulus was systematically higher than the storage modulus, a typical behavior of viscous-like systems. These curves are a clear representation of molten homogeneous polymers, with a slope equal to 2 and values similar to those reported in other works founded in literature for oscillatory tests performed on PBAT [47]. The persistence of this value for all samples in the logarithmic plot of the storage modulus versus the loss modulus (not shown) suggests the absence of micro-heterogeneities, since deviations in these curves seem to appear in a very characteristic way for a given temperature [14].

Therefore, the non-alteration of the rheological properties in the molten state highlights the quality of the CNC dispersion and also the good compatibility between the filler and the matrix. It is then reasonable to consider that the major factor causing the reinforcing effect in composites is the crystallization effect induced by the addition of CNC.

4 CONCLUSIONS

This chapter aimed in showing the impact of the aspect ratio of cellulose nanocrystals (CNCs) on the properties of nanocomposites prepared by extrusion using Poly(butylene adipate-co-terephthalate) (PBAT) as matrix. We showed that the dispersion of the nanoparticles in the matrix can be improved without any chemical modification by simply mixing the polymer pellets with the aqueous CNC dispersion prior to melt processing. It was observed that the dimensions of CNC have a stronger impact on the crystallinity of the matrix and mechanical stiffness of the nanocomposite than its volume fraction. The formation of crystalline PBAT domains also seems to depend of the thermal history of the material since both BA and BT units appear to be involved in the crystallization process for long annealing times. A comparison between rheological tests performed in the molten state of the matrix and mechanical test carried out at room temperature suggests that the observed mechanical reinforcing effect is mostly caused by the CNC-induced crystallinity of the PBAT matrix.

5 REFERENCES

- [1] M.A.S. Azizi Samir, F. Alloin, A. Dufresne, Review of recent research into cellulosic whiskers, their properties and their application in nanocomposite field., *Biomacromolecules*. 6 (2005) 612–26. doi:10.1021/bm0493685.
- [2] A. Dufresne, *Nanocellulose - From Nature to high performance tailored materials.*, De Gruyter, 2012.
- [3] M. Mariano, N. El Kissi, A. Dufresne, Cellulose nanocrystals and related nanocomposites: Review of some properties and challenges, *J. Polym. Sci. Part B Polym. Phys.* 52 (2014) 791–806. doi:10.1002/polb.23490.
- [4] V. Favier, G.R.. Canova, J.Y.. Cavallé, H..Chanzy, A.. Dufresne, C. Gauthier, Nanocomposite Materials from Latex and Cellulose Whiskers, *Polym. Adv. Technol.* 6 (1995) 351–355.
- [5] R. Rusli, K. Shanmuganathan, S.J. Rowan, C. Weder, S.J. Eichhorn, Stress transfer in cellulose nanowhisiker composites--influence of whisker aspect ratio and surface charge., *Biomacromolecules*. 12 (2011) 1363–9. doi:10.1021/bm200141x.
- [6] G. Siqueira, H. Abdillahi, J. Bras, A. Dufresne, High reinforcing capability cellulose nanocrystals extracted from syngonanthus nitens (Capim Dourado), *Cellulose*. 17 (2010) 289 – 298.
- [7] F. Bettaieb, R. Khiari, A. Dufresne, M.F. Mhenni, M.N. Belgacem, Mechanical and thermal properties of *Posidonia oceanica* cellulose nanocrystal reinforced polymer., *Carbohydr. Polym.* 123 (2015) 99–104. doi:10.1016/j.carbpol.2015.01.026.
- [8] A.L. Goffin, J.M. Raquez, E. Duquesne, G. Siqueira, Y. Habibi, A. Dufresne, et al., Poly(ϵ -caprolactone) based nanocomposites reinforced by surface-grafted cellulose nanowhiskers via extrusion processing: Morphology, rheology, and thermo-mechanical properties, *Polymer (Guildf)*. 52 (2011) 1532–1538. doi:10.1016/j.polymer.2011.02.004.
- [9] J.-M. Raquez, Y. Murena, a.-L. Goffin, Y. Habibi, B. Ruelle, F. DeBuyl, et al., Surface-modification of cellulose nanowhiskers and their use as nanoreinforcers into polylactide: A sustainably-integrated approach, *Compos. Sci. Technol.* 72 (2012) 544–549. doi:10.1016/j.compscitech.2011.11.017.
- [10] K. Ben Azouz, E.C. Ramires, W. Van den Fonteyne, N. El Kissi, A. Dufresne, Simple Method for the Melt Extrusion of a Cellulose Nanocrystal Reinforced Hydrophobic Polymer, *ACS Macro Lett.* 1 (2012) 236–240. doi:10.1021/mz2001737.
- [11] M. Pereda, N. El Kissi, A. Dufresne, Extrusion of polysaccharide nanocrystal reinforced polymer nanocomposites through compatibilization with poly(ethylene oxide)., *ACS Appl. Mater. Interfaces*. 6 (2014) 9365–75. doi:10.1021/am501755p.
- [12] F. Alloin, A. D'Apréa, A. Dufresne, N. El Kissi, F. Bossard, Poly(oxyethylene) and ramie whiskers based nanocomposites: influence of processing: extrusion and casting/evaporation, *Cellulose*. 18 (2011) 957–973. doi:10.1007/s10570-011-9543-x.

- [13] S. Camarero-Espinosa, D.J. Boday, C. Weder, E.J. Foster, Cellulose nanocrystal driven crystallization of poly(d, l-lactide) and improvement of the thermomechanical properties, *J. Appl. Polym. Sci.* 132 (2015) n/a–n/a. doi:10.1002/app.41607.
- [14] M.R. Kamal, V. Khoshkava, Effect of cellulose nanocrystals (CNC) on rheological and mechanical properties and crystallization behavior of PLA/CNC nanocomposites, *Carbohydr. Polym.* 123 (2015) 105–114. doi:10.1016/j.carbpol.2015.01.012.
- [15] G. Siqueira, C. Fraschini, J. Bras, A. Dufresne, R. Prud'homme, M.-P. Laborie, Impact of the nature and shape of cellulosic nanoparticles on the isothermal crystallization kinetics of poly(ϵ -caprolactone), *Eur. Polym. J.* 47 (2011) 2216–2227. doi:10.1016/j.eurpolymj.2011.09.014.
- [16] M. Mariano, N. El Kissi, A. Dufresne, Melt processing of cellulose nanocrystal reinforced polycarbonate from a masterbatch process, *Eur. Polym. J.* 69 (2015) 208–223. doi:10.1016/j.eurpolymj.2015.06.007.
- [17] P. Georgiopoulos, E. Kontou, M. Niaounakis, Thermomechanical Properties and Rheological Behavior of Biodegradable Composites, *Polym. Compos.* 35 (2014) 1140 – 1149. doi:10.1002/pc.
- [18] K. Fukushima, M.-H. Wu, S. Bocchini, A. Rasyida, M.-C. Yang, PBAT based nanocomposites for medical and industrial applications., *Mater. Sci. Eng. C. Mater. Biol. Appl.* 32 (2012) 1331–51. doi:10.1016/j.msec.2012.04.005.
- [19] N. Lin, A. Dufresne, Nanocellulose in biomedicine: Current status and future prospect, *Eur. Polym. J.* 59 (2014) 302–325. doi:10.1016/j.eurpolymj.2014.07.025.
- [20] L.C. Lins, S. Livi, J. Duchet-Rumeau, J.-F. Gérard, Phosphonium ionic liquids as new compatibilizing agents of biopolymer blends composed of poly(butylene-adipate-co-terephthalate)/poly(lactic acid) (PBAT/PLA), *RSC Adv.* 5 (2015) 59082–59092. doi:10.1039/C5RA10241C.
- [21] L. Liu, Y. Zhang, F. Lv, B. Yang, X. Meng, Effects of red mud on rheological, crystalline, and mechanical properties of red mud/PBAT composites, *Polym. Compos.* (2015) n/a–n/a. doi:10.1002/pc.23378.
- [22] T. Mukherjee, M. Czaka, N. Kao, R.K. Gupta, H.J. Choi, S. Bhattacharya, Dispersion study of nanofibrillated cellulose based poly(butylene adipate-co-terephthalate) composites., *Carbohydr. Polym.* 102 (2014) 537–42. doi:10.1016/j.carbpol.2013.11.047.
- [23] J.M. Raquez, Y. Nabar, R. Narayan, P. Dubois, Novel High-Performance Talc/Poly[(butylene adipate)-co-terephthalate] Hybrid Materials, *Macromol. Mater. Eng.* 293 (2008) 310–320. doi:10.1002/mame.200700352.
- [24] S. Feng, D. Wu, H. Liu, C. Chen, J. Liu, Z. Yao, et al., Crystallization and creep of the graphite nanosheets based poly(butylene adipate-co-terephthalate) biocomposites, *Thermochim. Acta.* 587 (2014) 72–80. doi:10.1016/j.tca.2014.04.020.
- [25] G. Siqueira, J. Bras, A. Dufresne, Cellulose whiskers versus microfibrils: influence of the nature of the nanoparticle and its surface functionalization on the thermal and mechanical properties of nanocomposites., *Biomacromolecules.* 10 (2009) 425–32. doi:10.1021/bm801193d.
- [26] K.B.R. Teodoro, E.M. Teixeira, A. Campos, J.M. Marconcini, L.H.C. Mattoso, Whiskers de Fibra de Sisal Obtidos sob Diferentes Condições de Hidrólise Ácida : Efeito do Tempo e da Temperatura de Extração, *Polímeros.* 21 (2011).

- [27] M. Mariano, N. El Kissi, A. Dufresne, Cellulose nanocrystal reinforced oxidized natural rubber nanocomposites, *Carbohydr. Polym.* 137 (2016) 174–183. doi:10.1016/j.carbpol.2015.10.027.
- [28] R. Al-Itry, K. Lamnawar, A. Maazouz, Improvement of thermal stability, rheological and mechanical properties of PLA, PBAT and their blends by reactive extrusion with functionalized epoxy, *Polym. Degrad. Stab.* 97 (2012) 1898–1914. doi:10.1016/j.polymdegradstab.2012.06.028.
- [29] M. Roman, W.T. Winter, Effect of sulfate groups from sulfuric acid hydrolysis on the thermal degradation behavior of bacterial cellulose., *Biomacromolecules.* 5 (2004) 1671–7. doi:10.1021/bm034519+.
- [30] N. Wang, E. Ding, R. Cheng, Thermal degradation behaviors of spherical cellulose nanocrystals with sulfate groups, *Polymer (Guildf).* 48 (2007) 3486–3493. doi:10.1016/j.polymer.2007.03.062.
- [31] F. Fahma, S. Iwamoto, N. Hori, T. Iwata, A. Takemura, Isolation, preparation, and characterization of nanofibers from oil palm empty-fruit-bunch (OPEFB), *Cellulose.* 17 (2010) 977–985. doi:10.1007/s10570-010-9436-4.
- [32] N. Lin, A. Dufresne, Surface chemistry, morphological analysis and properties of cellulose nanocrystals with gradiented sulfation degrees., *Nanoscale.* 6 (2014) 5384–93. doi:10.1039/c3nr06761k.
- [33] K. Benhamou, A. Dufresne, A. Magnin, G. Mortha, H. Kaddami, Control of size and viscoelastic properties of nanofibrillated cellulose from palm tree by varying the TEMPO-mediated oxidation time., *Carbohydr. Polym.* 99 (2014) 74–83. doi:10.1016/j.carbpol.2013.08.032.
- [34] E.I. Evier, A.E.J. De Nooy, A.C. Besemer, H. Van Bekkum, Highly selective nitroxyl radical-mediated oxidation of primary alcohol groups in water-soluble glucans, *Carbohydr. Res.* 269 (1995) 89–98.
- [35] U.J. Hänggi, Private Communication, (2015).
- [36] F. Chivrac, Z. Kadlecová, E. Pollet, L. Avérous, Aromatic Copolyester-based Nanobiocomposites: Elaboration, Structural Characterization and Properties, *J. Polym. Environ.* 14 (2006) 393–401. doi:10.1007/s10924-006-0033-4.
- [37] D.O. de; Castro, E. Frollini, A. Ruvolo-Filho, A. Dufresne, “Green Polyethylene” and Curaua Cellulose Nanocrystal Based Nanocomposites: Effect of Vegetable Oils as Coupling Agent and Processing Technique, *J. Polym. Sci. PART B Polym. Phys.* In press (2015). doi:10.1002/polb.23729.
- [38] P. Russo, B. Vetrano, D. Acierno, M. Mauro, Thermal and Structural Characterization of Biodegradable Blends Filled With Halloysite Nanotubes, *Polym. Compos.* 34 (2012) 1460 – 1470. doi:10.1002/pc.
- [39] J.-H. Chen, C.-C. Chen, M.-C. Yang, Characterization of Nanocomposites of Poly(butylene adipate-co-terephthalate) blending with Organoclay, *J. Polym. Res.* 18 (2011) 2151–2159. doi:10.1007/s10965-011-9625-3.

- [40] R.I.C. Chivrac, E. Pollet, L.U.C. Ave, Nonisothermal Crystallization Behavior of Poly (butylene adipate- co -terephthalate)/ Clay Nano-biocomposites, *J. Polym. Sci. Part B Polym. Phys.* 45 (2007) 1503–1510. doi:10.1002/polb.
- [41] K. Kuwabara, Z. Gan, T. Nakamura, H. Abe, Y. Doi, Crystalline/Amorphous Phase Structure and Molecular Mobility of Biodegradable Poly(butylene adipate-co-butylene terephthalate) and Related Polyesters, *Biomacromolecules*. 3 (2002) 390–396. doi:10.1021/bm0156476.
- [42] X.Q. Shi, H. Ito, T. Kikutani, Characterization on mixed-crystal structure and properties of poly(butylene adipate-co-terephthalate) biodegradable fibers, *Polymer (Guildf)*. 46 (2005) 11442–11450. doi:10.1016/j.polymer.2005.10.065.
- [43] D.G. GRAY, “Transcrystallization” induced by mechanical stress on a polypropylene melt, *Polym. Lett. Ed.* 12 (1974) 645–650.
- [44] D.G. Gray, Transcrystallization of polypropylene at cellulose nanocrystal surfaces, *Cellulose*. 15 (2007) 297–301. doi:10.1007/s10570-007-9176-2.
- [45] J. Yeh, C. Tsou, C. Huang, K. Chen, C. Wu, Compatible and Crystallization Properties of Poly (lactic acid)/ Poly (butylene adipate- co -terephthalate) Blends, *J. Appl. Polym. Sci.* 116 (2010) 680 – 687. doi:10.1002/app.
- [46] M.M. Reddy, M. Misra, A.K. Mohanty, Biodegradable Blends from Corn Gluten Meal and Poly(butylene adipate-co-terephthalate) (PBAT): Studies on the Influence of Plasticization and Destructurization on Rheology, Tensile Properties and Interfacial Interactions, *J. Polym. Environ.* 22 (2014) 167–175. doi:10.1007/s10924-014-0640-4.

Chapter IV.

Part II. *Structural reorganization of CNC in injection-moulded CNC/PBAT nanocomposites under thermal annealing*

This chapter is based on Structural reorganization of CNC in injection-moulded CNC/PBAT materials under thermal annealing. Published by **Langmuir**. (2016).

CONTENTS

ABSTRACT.....	204
1 INTRODUCTION.....	205
2 EXPERIMENTAL	207
2.1 Materials.....	207
2.2 Preparation of cellulose nanocrystals.	207
2.3 Preparation of nanocomposites.	207
2.4 Characterizations	208
3 RESULTS AND DISCUSSION.....	209
3.1 Cellulose nanocrystals.....	209
3.2 Thermal stability	210
3.3 Small amplitude oscillatory shear (SAOS) experiments	211
3.4 Brownian motion	214
3.5 SAOS experiments for conditioned samples	216
3.6 Samples Morphology	218
3.7 2D-SAOS experiments.....	219
3.8 Creep behaviour.....	223
4 CONCLUSIONS	225
5 REFERENCES	226

ABSTRACT

Nanocomposites were prepared by extrusion and injection-moulding from polybutyrate adipate terephthalate (PBAT) and high aspect ratio cellulose nanocrystals (CNCs) extracted from capim dourado fibres. Three CNC contents were used corresponding to 0.5, 1 and 2 times the theoretical percolation threshold. Small amplitude oscillary shear (SAOS) experiments show that as the CNC content increases, a more elastic behaviour is observed but no percolating network can form within the polymeric matrix due to the high shear rates involved during the injection-moulding process. Annealing of the samples at 170°C was performed and the possible reorganization of the nanofiller was investigated. This reorganization was further elucidated using 2D-SAOS and creep experiments.

1 INTRODUCTION

The progressive substitution of petroleum-based polymers as engineering materials by more environmentally-friendly biodegradable polymers and composites is a short term desire in our society. However, these "green" materials still present many unsolved drawbacks. Regarding the production of biocomposites, the use of cellulose nanocrystals (CNCs) appears as a good option to provide outstanding mechanical performance, permeability control and support to antimicrobial products, increasing the range of applications of many biodegradable polymers. [1-4]

Isolated from different cellulosic sources, CNCs are elongated rod-like crystalline domains that can present high aspect ratio and stiffness, and low density, in addition of being fully renewable.⁵⁻⁸ Their application in aliphatic polyesters, such as poly(butylene adipate-co-terephthalate) (PBAT), can improve the mechanical properties of the polymer, that is usually filled with nanoclays or blended with stiffer polymers such as polylactic acid (PLA) due to its potential application in biomedicine.[9-12] Besides, the use of CNCs can also be a good alternative as rheological modifier in inks, paints and greases to replace or partly substitute layered silicates in composite materials.[13]

The preparation of CNC based composites is normally performed by techniques such as melt-processing or casting/evaporation. With the latter technique, the impressive mechanical properties that can be reached are usually attributed to the formation of a 3D particle network that is based on hydrogen bonding between the nanoparticles, when the CNC content exceed the percolation threshold.[14,15] However, this process is time-consuming and not really adapted with industrial needs. Processing methods such as extrusion, hot-pressing and injection-moulding do not seem to provide the required conditions for network formation due to the imposed shear and relative short time of processing, besides the high temperature conditions.[16] As a consequence, composite materials prepared by this technique need a higher nanoparticle content to present similar properties than those produced by casting/evaporation.[17]

It was already demonstrated that for nanocomposites reinforced with anisotropic particles, such as rod-like CNC, and prepared by melt-processing, the applied shear induced orientation of the particles. As a consequence, the nanofibers tend to align in the flow direction assuming a roughly parallel alignment.[18,19] The properties of CNC reinforced nanocomposites prepared by extrusion have been reported. [20-22]

Sapkota et al. [23] studied the influence of processing conditions on the properties of poly(vinyl acetate) reinforced with CNC and observed lower mechanical properties for materials produced by extrusion compared to others techniques such as roller blade mixer or casting/evaporation. Also, other parameters such as crystallinity,[24,25] fillers dispersion,[26,27] chemical compatibility[28] and possible decrease of the CNC dimensions after processing[17] are especially important for these systems. However, there is a lack of information concerning the organization of CNC within the matrix as well as its role on the material properties in the absence of percolated network.

During the last 20 years a series of experiments based on rheology and light scattering have been used to investigate the influence of shear on the structure of particles in suspensions.[29] For many systems, it was found that the initial organization cannot be restored after applying a stress that leads the system to a nonlinear region. Recently, a broad range of conditioning times has been applied for polymeric systems reinforced with exfoliated silica.[30] In this study, several properties of the material seem to be impacted by conditioning, suggesting higher dispersion of the particles with time. The authors concluded that the solid-like behaviour of the nanocomposite strongly depends on the thermomechanical history of the material. This reorganization of the particles is based on their capability to move without outside interference by Brownian motions. This phenomenon can strongly influence the final dispersion of the particles in systems that present low viscosity (i.e. aqueous suspensions).

In the present study, we tried to go further on the traditional approach aiming to modify the mechanical properties of CNC reinforced nanocomposites, based on the control of filler content. The dispersion of the non-percolated CNC microstructure was studied by traditional small amplitude oscillatory shear (SAOS) experiments, and also more innovative 2D-SAOS experiments. As briefly suggested in the literature, 2D rheological tests can provide information about the impact of particle dispersion on the isotropy of the material.[31] More than an attempt to characterize a percolating network, which seems to be improbable to form when using high shear rate processing techniques, this paper aims to investigate a possible modification of the dispersion of the nanoparticles under thermal annealing. A good dispersion obtained by the auto-reorganization of the particles could be a first step to create an isotropic material, the initial condition to induce 3D-network formation under mild conditions.

2 EXPERIMENTAL

2.1 Materials

Capimdourado (*Syngonanthusnitens*) fibre was brought from Jalapão region (Tocantins, Brazil). Sulfuric acid, sodium hydroxide, acetate and chlorite were obtained from Sigma-Aldrich. Commercial biodegradable polyester, polybutyrateadipate terephthalate (PBAT)-ecoflex, with a melting point around 120°C, was provided as pellets by BASF.

2.2 Preparation of cellulose nanocrystals

CNCs were prepared from capimdouradofibres as described elsewhere.[32] Briefly, capimdouradofibres were submitted to a bleaching step to purify cellulose by removing secondary components normally present in natural fibres. It was performed by soaking the cut fibres into a NaOH solution (4 wt%) at 80°C for 2 hours under mechanical stirring, and washing with hot water until neutral pH. This process was performed twice. Then, equal parts of acetate buffer, aqueous chlorite (1.7 wt% in water) and distilled water were used to complete the bleaching stage by keeping the fibres under mechanical stirring for 3 hours at 80°C. Again, the fibres were filtered and washed until neutral pH. The hydrolysis of bleached fibres was performed by using a pre-heated sulfuric acid solution (64 wt%) at 50°C under strong mechanical stirring during 60 min. The acid suspension was washed by successive centrifugation cycles at 10,000 rpm and 10°C for 10 min and dialyzed against distilled water until reaching neutral pH. The aqueous suspension was homogenized by using an Ultra Turax T25 homogenizer and ultrasonically dispersed before use.

2.3 Preparation of nanocomposites

The surface sulphate groups of CNC were first neutralized by adjusting the pH of the suspension to 10 using a diluted NaOH solution. The suspension was kept under agitation for 24h and dialyzed against distilled water until reaching again a neutral pH. This CNC aqueous suspension was mixed and magnetically stirred for 10 min with PBAT pellets, and finally ultrasonicated for few minutes. The resulting suspension was cast in a glass plate and dried overnight under ambient conditions. The CNC content was controlled in order to obtain materials with 0.9, 1.8 and 3.6 wt% CNC, which correspond respectively to 0.5, 1 and 2 times the CNC content necessary to reach the theoretical percolation threshold. The samples were labelled PBATC_x, where x corresponds to the CNC weight content. The dry material was

mixed in a twin-screw extruder DSM 15 Microcompounder from Xplore. Three heating zones (125, 130 and 135°C) and a screw speed of 50 rpm during alimentation and 100 rpm during mixing was set-up for 10 min. The extruded material was cut in small pieces and melted in a HAAKE Minijet II at 175-45°C (heater-mould temperatures) to be injected under a pressure of 270 bar during 10 s. Discs with dimensions of 25 mm x 1.5 mm were obtained. These disks were analysed before (PBATC_x) and after conditioning for 30 min at 170°C (PBATC_{xc}).

Mixing the PBAT pellets with the aqueous dispersion of CNC before casting/evaporation and subsequent extrusion was expected to considerably improve the dispersion of the filler within the polymeric matrix and homogeneity of the film. During the preparation of CNC reinforced poly(β -hydroxybutyrate) (PHB) composites it was observed that the cellulosic nanoparticles stick to PHB powder in water suspensions.[32] We observed a similar behavior with PBAT. We expected therefore that after drying, the nanoparticles can form a thin layer around the pellets. This distribution of the nanoparticles should make easier their dispersion when compared to the simple freeze-drying of CNC.

2.4 Characterizations

Atomic force microscopy (AFM). AFM images were obtained on a Nanoscope III microscope from Veeco Instruments. A drop of a diluted aqueous CNC suspension with 0.01 wt% concentration was deposited on a mica substrate and dried overnight under ambient conditions. It was imaged in tapping mode with a silicon cantilever (OTESPA®, Bruker, tip diameter 5-10 nm). The nanocrystal dimensions were estimated from 100 measurements using the associated software.

Scanning electron microscopy (SEM). SEM was used to observe the nanocomposite cross section in order to check the possible filler aggregation. Prior to this, the samples were frozen using liquid nitrogen and broken to obtain a clear fracture. It was glued to the sample holder for cross section images. The samples were coated with gold to prevent charging of the sample due to the electron bombardment. The SEM images were captured by using FEI (MED) Quanta200.

Thermogravimetric analysis (TGA). The thermal stability of the materials was investigated by TGA. Samples around 10 mg were heated from room temperature to 170°C with a heating rate of 30°C.min⁻¹ and kept at this temperature for 180 min. The measurements were carried out under air atmosphere with thermal analyzer Perkin-Elmer TGA.

Rheometry. The rheometrical measurements for injection-moulded materials were performed with a plate-plate (25 mm) geometry to study the neat polymer and nanocomposites.

Small amplitude oscillatory shear (SAOS) experiments. First, oscillation strain sweep tests were carried out from 0.1 to 100% at the angular frequency of 1 rad.s⁻¹ to define the linear viscoelastic regime of the samples. Once the linear regime was defined (all the samples showed a linear regime until at least 5%) the oscillation frequency sweep tests (in the range 0.03-100 rad.s⁻¹) at 1% strain were performed for all the samples at 170°C. Time Sweep experiments were also performed at 170°C and 0.1 rad.s⁻¹ for PBAT and PBAT_{3.6}. Both experiments were performed with ARG2 equipment from TA Instruments under air atmosphere. Both experiments were performed with ARG2 equipment from TA Instruments under air atmosphere.

2D Small amplitude oscillatory shear (2D-SAOS) experiments. Two dimensional small angle amplitude oscillatory shear (2D-SAOS) experiments were performed using the same geometry and temperature conditions than for SAOS experiments. Both pristine injection-moulded and conditioned samples were tested. These experiments were performed with strain controlled ARES-G2 equipment from TA. The angle between the two dimensions was zero, meaning that the two frequencies were in phase and the device oscillation was applied without phase lag. The maximum elongation (i.e. 0.7%) was chosen so as to be in the linear regime of the material. During data analysis it was important to pay attention to possible pump effects caused by the compression of the polymer (since its high viscosity do not allow flowing properly), although this material is not incompressible like aqueous suspensions. To avoid possible distortion, experiments were performed with the nanocomposite disk positioned always in the same position to an arbitrary reference point of the equipment.

Creep experiments. The creep measurements were also performed with ARG2 equipment from TA Instruments at 170°C and under air atmosphere. For all samples, the same stress corresponding to a torque value of 0.25 μN.m was used.

3 RESULTS AND DISCUSSION

3.1 Cellulose nanocrystals

Figure 1 shows the AFM image of CNC prepared from capimindourado. As expected, elongated rod-like particles can be observed. The length and

diameter of the nanoparticles were estimated as 271 ± 47 nm and 5.5 ± 1.3 nm, respectively. These values provide an average aspect ratio (L/d) around 50. This high aspect ratio should warrant high reinforcing effect to the polymeric matrix compared to lower aspect ratio CNCs, e.g. those extracted from cotton. It is well known that the aspect ratio of rod-like nanoparticles can be used to estimate the CNC volume fraction (and weight fraction) necessary to reach the percolation threshold ϕ_c , using Equation (1).

$$\phi_c = \frac{0.7}{L/d} \quad (1)$$

Considering the average dimensions and aspect ratio obtained from AFM observations, it comes $\phi_c = 1.4$ vol%, i.e. around $w_c = 1.8$ wt% assuming 1.25 g.cm^{-3} and 1.56 g.cm^{-3} for the density of PBAT and CNC, respectively. Nanocomposite materials were prepared with CNC contents corresponding to this percolation threshold (PBATC_{1.8}), and half and double of this critical CNC content, being labelled as PBATC_{0.9} and PBATC_{3.6}, respectively.

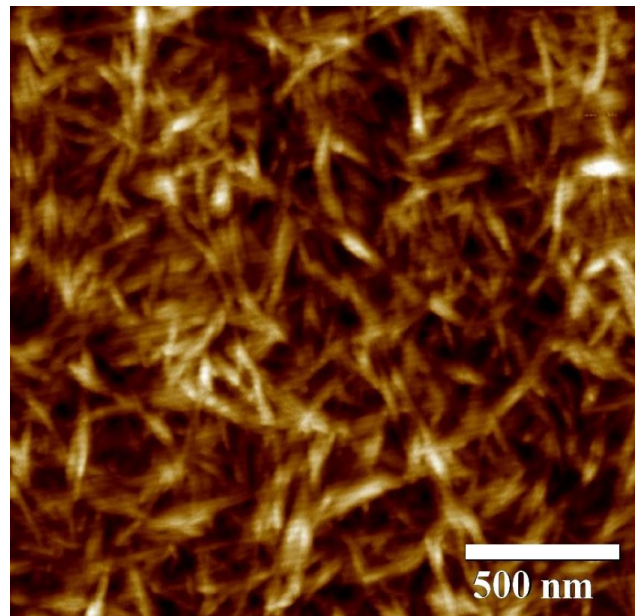


Figure 1. AFM image of CNC extracted from capim dourado.

3.2 Thermal stability

Inspired by the works reported by Treece and Oberhauser [18] and Domenech et al. [30] for clay reinforced polypropylene nanocomposites, the underlying strategy of our study was to condition the CNC reinforced PBAT nanocomposites at high temperatures, above the melting point of the matrix (i.e. 120°C), to promote the reorganization of the nanoparticles. To prevent any possible chemical modification of the samples due to thermal degradation, TGA experiments were first performed using the same conditions as for

rheological tests and annealing (170°C). The obtained curves are reported in Figure 2.

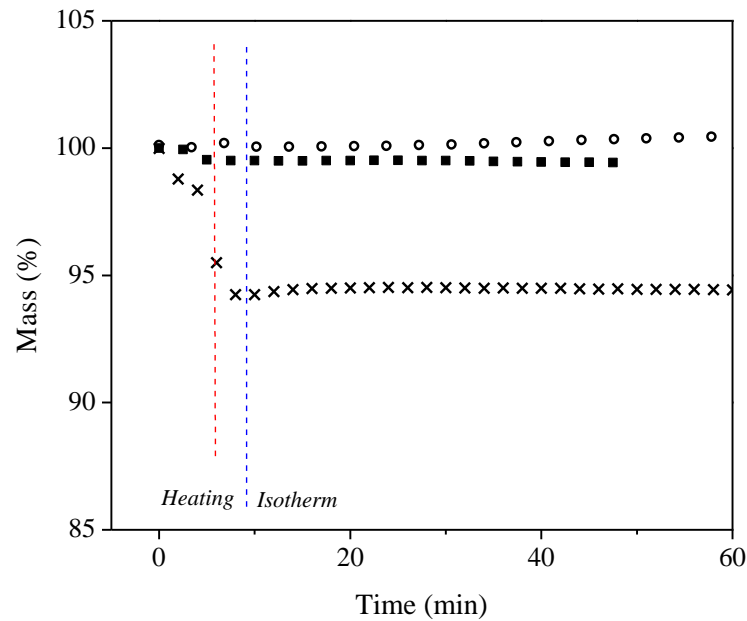


Figure 2. TGA curves obtained under air atmosphere for CNC extracted from capim dourado(x), neat PBAT (o) and PBATC_{3.6} (■). The vertical red line corresponds to the end of the stabilization step at 30°C before heating at 30°C.min⁻¹ and the vertical blue line corresponds to the end of the heating step before isothermal treatment at 170°C.

A 5% initial weight loss was observed for CNC upon heating. Cellulose being a hydrophilic material, it is obviously ascribed to the loss of water (possibly including both free and bonded water molecules). Then the weight loss stabilizes and tends to slightly decrease after about 50 min. No weight loss was observed for PBAT over the whole time range. A similar behavior was observed for the composite PBATC_{3.6} that showed only a small mass loss of 0.5% during the heating stage of the isotherm, probably due to some residual water coming from the cellulose nanoparticles. Based on these observations, we decided to fix the duration of the thermal annealing treatment to 30 min to avoid any thermal degradation of the material.

3.3 Small amplitude oscillatory shear (SAOS) experiments

The neat polymer and nanocomposites were first characterized at 170°C using SAOS experiments. The corresponding data are reported in Figures 3 and 4. Figure 3 shows the evolution of the complex viscosity (η^*) as a function of oscillation frequency (ω). A slight variation of η^* is observed but all materials display almost the same behaviour regardless the CNC content.

The addition of nanoparticles to a polymeric matrix can induce modifications of its viscosity. Both, increase [33] and decrease[34] were already reported. The first evolution can be explained by Einstein theory, according to which the addition of particles always increases the viscosity of the system. The second observation is less clear. However, for some polymer composites, it was observed that the use of nanoparticles with diameter close to the random coil radius of the polymer matrix chain can cause a remarkable decrease of the viscosity. [35] In the present study, the inclusion of CNC seems to slightly increase the Newtonian viscosity. However, the zero shear viscosity is quite similar for all samples. For example, the value of the complex viscosity at $\omega = 0.1 \text{ rad.s}^{-1}$ varies from 2450 to 2500 Pa.s for PBAT and PBATC_{3.6}, respectively.

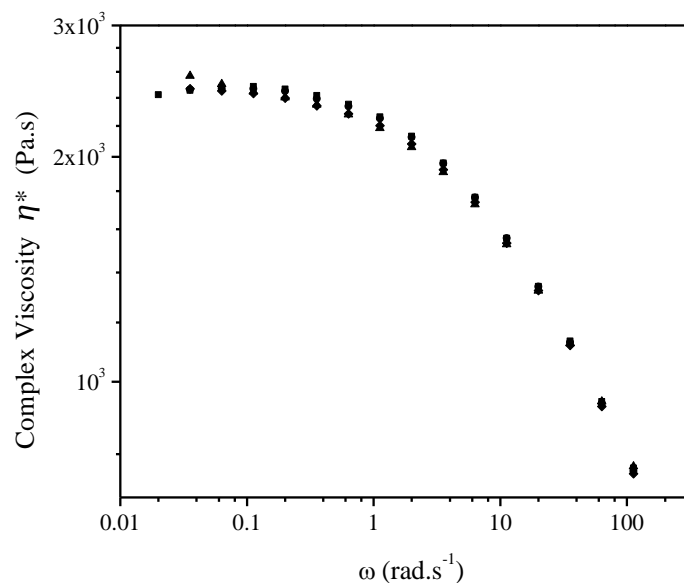


Figure 3. Evolution of the complex viscosity (η^*) as a function of the angular frequency (ω) for PBAT (■), PBATC_{0.9} (●), PBATC_{1.8} (◆), and PBATC_{3.6} (▲) at 170°C.

Independently of the CNC content, all samples showed a clear decrease of the viscosity when increasing the angular frequency, which is characteristic of a pronounced shear thinning behaviour founded for polymer melts. Indeed, it is well known that applying a stress to a polymer induces an organization of the chains that start to disentangle and to align in the flow direction. For composites, this decrease of the viscosity can also result from the organization of the asymmetric filler, which also starts to gradually align by an individual rotation movement in the flow direction. In this case, the imposed flow has a stronger influence than the particle Brownian motion, that tends to keep the particles disorganized. This effect is well reported for aqueous CNC systems [36] and polymer nanocomposites containing rod-like particles.[37]

The alignment of the particle depends on the particle size, since particles with different aspect ratios present distinct rotational periods.[38] It was suggested that for systems with sufficiently low viscosity the effect of rotational diffusion is clearly manifested through the modification of anisotropy factor and orientation angle of the particles.[19] In this earlier study, a montmorillonite suspension with a zero shear viscosity around 3000 Pa.s underwent considerable modification of these values. An observation should be made about particle concentration since the rotational periods of particles are hindered by the presence of other particles in non-dilute systems. This is frequently the case for nanocomposites.

For nanocomposites and colloidal systems possible fractal-like organization of the filler network can be observed. Together with the alignment of the particles, induced by the flow, the disruption of a possible 3D particle network can occur. This can be better understood by considering the evolution of the storage modulus (G') and loss modulus (G'') of the sample with the angular frequency as reported in Figure 4a.

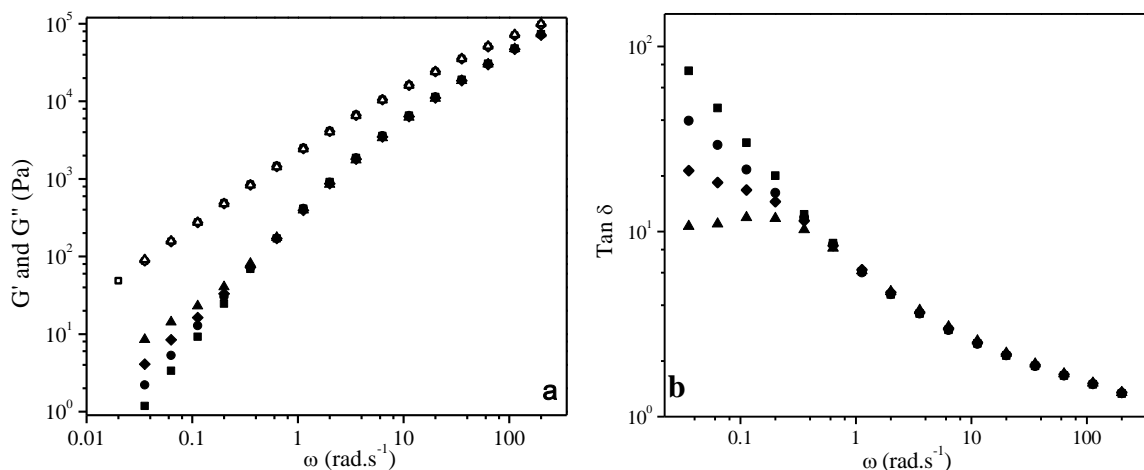


Figure 4. Evolution of (a) the storage modulus G' (filled symbols) and loss modulus G'' (open symbols), and (b) $\tan \delta = G''/G'$ as a function of the oscillation frequency for PBAT (■,□), PBATC_{0.9} (●,○), PBATC_{1.8} (◆,◇), and PBATC_{3.6} (▲,△) at 170°C.

The typical behaviour of a liquid-like system, with $G'' > G'$, was observed as expected for a polymer melt. The curves can be easily divided into two regions: a low frequency region (up to 1-10 rad.s^{-1}) and a higher frequencies region. For higher frequencies, the marked increase of G' results from the entanglement of the chains. In this region, the molecules are already completely stretched due to the high deformation rates and no relaxation of the chains is possible. In such conditions the molecules behave as a cross-linked material. This dominant effect hides some structural properties of the

material such as molecular weight or presence of the filler, and it is therefore not surprising to observe almost superimposed curves with a slope (n) close to 0.5. A similar behaviour was described elsewhere where the presence of nanotubes clearly had a substantial influence on polymer chain relaxations (i.e. for lower shear rates) and almost no effect for length scales comparable to the length of an entanglement.[39]

For lower frequencies, the PBAT chains are completely relaxed and exhibit typical melt polymer scaling properties close to $G' \sim \omega^2$ and $G'' \sim \omega^1$. In this lower frequencies the elastic or storage modulus varies according to the CNC content. The G' value increases from 1 Pa for the neat polymer (PBAT) at $\omega = 0.03 \text{ rad.s}^{-1}$ to 8.5 Pa for the nanocomposite reinforced with 3.6 wt% CNC (PBATC_{3.6}), whereas G'' keeps a constant value for a given frequency regardless the CNC content (e.g. around 90 Pa for $\omega = 0.03 \text{ rad.s}^{-1}$). It means that the behaviour of the material is predominantly viscous and, as expected, the incorporation of nanoparticles gradually transforms the terminal behaviour ($\omega \rightarrow 0$) from a liquid-like to a solid-like behaviour.

Figure 4b shows the evolution of $\tan \delta = G''/G'$ as a function of the oscillation frequency for all samples. Since G'' values are almost constant for all materials, $\tan \delta$ varies directly with G' values. The clear modification of the slope of the curves for $\tan \delta$ and G' in the low angular frequencies region is a classical behaviour of solid-like materials, differing from the viscoelastic behaviour of the neat melt polymer. While the viscoelastic behaviour of the material is governed by the properties of the polymer matrix for higher angular frequencies, the lower frequencies region is particularly sensitive to the presence of the nanoparticles. In this latter region, $\tan \delta$ values around 90 and 10 were observed for PBAT and PBATC_{3.6}, respectively. The higher values reported for G'' compared to G' for all samples are indicative of a non-solid behaviour, showing that no percolating CNC network was formed in the filled samples, even if the CNC content for PBATC_{3.6} was higher than the percolation threshold. This was expected since as reported elsewhere [17] no percolating CNC network is able to form for nanocomposites prepared by extrusion or injection-moulding under high shear rates.

3.4 Brownian motion

The strategy of sample conditioning as a way to promote the dispersion of the nanoparticles within the polymeric matrix is supported by their Brownian motion. Since the arrangement of CNCs in the polymer melt is a consequence of the stress applied to the material, their internal organization should correspond to a state with lower energy and, therefore thermodynamically favourable. However, under

suitable temperature conditions the Brownian motion can be used to lead the particles to a more disoriented and entropically favourable state. During thermal conditioning, the force that opposes to the particle dispersion is the physical limitation caused by the long relaxation time of the particle that makes the thermal motion of the chains insufficient and keeps the material trapped in a high energy state. [18] The tendency of the particle to diffuse within the matrix can be described by the translational diffusion coefficient D ($\text{m}^2.\text{s}^{-1}$), that can be derived from the Stokes-Einstein equation:

$$D = \frac{k_B \times T}{f} \quad (2)$$

where k_B is the Boltzmann constant (J.K^{-1}), T is the temperature (K) and f is the friction coefficient acting on the particle, defined as $f = 6 \times \pi \times \eta \times a_h$, where a_h is the hydrodynamic radius of the particle and η (Pa.s) the viscosity of the suspending medium.

The diffusion coefficient of the particle is inversely proportional to the viscosity of the suspending medium and directly proportional to temperature. For non-spherical particles, a translational diffusion mechanism is predominant and it is possible to associate the diffusion with the particle length.[40] (Eq. 2) was adapted for cellulose rod-like nanoparticles and the translational diffusion coefficient was defined as: [41]

$$D = \frac{k_B \times T}{3\pi\eta L} \times [\delta - (1/2) \times (\gamma_{\parallel} + \gamma_{\perp})] \quad (3)$$

where

$$\delta = \ln\left(2 \frac{L}{d}\right) \quad (4)$$

and

$$\gamma_{\parallel} = 0.807 + \frac{0.15}{\delta} + \frac{13.5}{\delta^2} - \frac{37}{\delta^3} + \frac{22}{\delta^4} \quad (5)$$

$$\gamma_{\perp} = -0.193 + \frac{0.15}{\delta} + \frac{8.1}{\delta^2} - \frac{1.8}{\delta^3} + \frac{9}{\delta^4} \quad (6)$$

The application of these equations using AFM observation for CNC length allows the calculation of the diffusion coefficient for the nanorods in the polymer melt at 170°C . A D value of $3.25 \times 10^{-18} \text{m}^2.\text{s}^{-1}$ was determined for a viscosity value of 2500 Pa.s . For a suspension of the same CNC particles in water at 20°C , the diffusion coefficient would be around $6.3 \times 10^{-12} \text{m}^2.\text{s}^{-1}$. Similar value was found for long rod-like particles. [42]

It shows that, as expected, the mobility of the nanoparticles is strongly impacted by the viscosity of the surrounding medium. Applying Equation (7), the Brownian particle displacement $\langle X^2(t) \rangle$ can be calculated and a value of 165 nm.hour^{-1} was found for CNC in the polymer melt at 170°C . For comparison,

this value is $2 \text{ mm}\cdot\text{hour}^{-1}$ in water considering the same particle dimensions. Assuming that CNCs are present as individual particles, it means that during a 30 min conditioning the particle could displace around half of that (or 82.5 nm).

$$\langle X^2(t) \rangle = 2Dt \quad (7)$$

However, it is worth noting that this value only expresses the movement of an isolated particle moving on an erratic pattern. Part of the nanocrystals is most probably organized in the form of aggregates as suggested by rheological measurements. The creation of new bonds, that could make the particle displacement even more difficult, is unlikely during the conditioning at this temperature. Moreover, besides the hydrodynamic radius, the interactions between the filler and the matrix strongly influence the displacement of the particle.[43]

The influence of the medium viscosity on the displacement of the particle was studied by Romeo et al. [44] and no clear difference in the nanoparticle position was observed after 3 hours conditioning at 200°C . [44] However, the viscosity of this system (around $100 \times 10^3 \text{ Pa}\cdot\text{s}$) was quite higher than for PBAT at 170°C (around $2.4 \times 10^3 \text{ Pa}\cdot\text{s}$).

3.5 SAOS experiments for conditioned samples

After conditioning at 170°C , the rheological behaviour of the samples was analysed again using SAOS measurements. The main parameters obtained for both injection-moulded and conditioned samples are collected in Table 1. This table reports the G' , G'' , η^* and $\tan \delta$ values estimated at $\omega = 0.1 \text{ rad}\cdot\text{s}^{-1}$, and the slopes $n(G')$ and $n(G'')$ of the curves G' vs. ω and G'' vs. ω , respectively, determined between 0.03 and $0.3 \text{ rad}\cdot\text{s}^{-1}$.

As previously described, the slope $n(G')$ of the G' vs. ω curve for low ω values should be around 2 according to the reptation theory. For neat PBAT a slightly lower value (1.74) is reported. This can be considered as a sign of heterogeneities in the polymer or even a consequence of the chains organization since the sample was prepared by injection-moulding. Adding increasing amounts of CNC induces a gradual decrease of the n value. However, no sample displayed independence of the variation of G' with respect to ω (i.e. the appearance of a horizontal plateau for lower ω values). The formation of a percolating network is reported to be associated with this plateau in rheological experiments.[33] The formation of such a network induces a scaling law of $n = 0.5$ (i.e. $G' \sim \omega^{0.5}$).

Table 1. Rheological data obtained from SAOS curves for injection-moulded samples and samples conditioned for 30 min at 170°C.

	Sample	G' (Pa) ^a	$n(G')$ ^b	G'' (Pa) ^a	$n(G'')$ ^b	η^* (Pa.s) ^a	\tan δ^a
Injection- moulded	PBAT	9.25	1.74	279	1	2477	30.2
	PBATC _{0.9}	12.8	1.50	277	0.99	2469	21.6
	PBATC _{1.8}	16.0	1.23	273	0.97	2450	16.7
	PBATC _{3.6}	23.0	0.90	274	0.96	2502	11.9
Conditioned	PBATC _{0.9C}	8.1	1.50	244	0.98	2419	27.2
	PBATC _{1.8C}	11.7	1.47	226	0.98	1930	29.4
	PBATC _{3.6C}	14.1	1.03	223	0.95	1730	15.8

^aValues estimated at $\omega = 0.1 \text{ rad.s}^{-1}$.

^bThe slope n was determined between 0.03 and 0.3 rad.s^{-1} and presented a R^2 value of 0.99.

For CNC/PBAT systems (Table 1), n values were never lower than 0.9 (in fact, $0.9 < n < 1.74$). By considering a simple linear relationship between our experimental data and the theoretical G' value necessary to reach 0.5 scaling law, we can estimate a possible percolation for a CNC content around 5 wt%.

It means that, due to the sample processing method, the percolation threshold should be almost 3 times higher than the theoretical value calculated from Equation 1 (i.e. 1.8 wt%), and only local structure organization of the particles can occur. In fact, it is most probably even much higher, depending on the organization of the particles. Investigation of highly filled PBAT would be most probably difficult because of much higher viscosity values of the mixture.

After conditioning the nanocomposite samples for 30 min at 170°C, the n value of the material with the lowest CNC content (PBATC_{0.9C}) remained unchanged, whereas it increased for other samples (PBATC_{1.8C} and PBATC_{3.6C}). This evolution suggests that the structure of these materials became more similar to the one of the unfilled PBAT and deviates accordingly even more from the percolating structure. It is an indication that during high temperature conditioning, the partially organized CNC structures tend to destroy. Subtle microstructural changes occur into the nanocomposite during the annealing process.[45] However, it was suggested that during nanocomposite annealing, the full restructuring of the nanoparticles cannot take place.[18] The non-occurrence of such a phenomenon for PBATC_{0.9C} most probably results from the too low CNC content that cannot induce any significant partial organized structure. As a consequence, thermal conditioning does not affect the general organization of the particles within the composite.

Since the behaviour of the material is mainly dominated by the elastic component, the G'' values are only slightly affected by conditioning and no significant evolution can be observed (Table 1). It shows that the presence of CNC does not impact the viscous component of the nanocomposites. The $\tan \delta$ values are found to increase upon annealing (Table 1), as a result of the decrease of G' and non-alteration of G'' . It is also observed that the complex viscosity of the nanocomposites globally decreases during conditioning, which could in turn promote the dispersion of the nanoparticles. However, it is much more significant for PBATC_{1.8C} and PBATC_{3.9C} than for PBATC_{0.9C}.

To investigate the possible effect of CNC on the decrease of the viscosity for nanocomposites, time sweeps tests were performed and results are reported in Figure 5. The Figure shows that for this experiment where the frequency was kept constant over time, both PBAT and PBAT_{3.6} (the sample with the highest CNC content) show a very similar behavior. It suggests that CNC does not impact the decrease of the viscosity during conditioning.

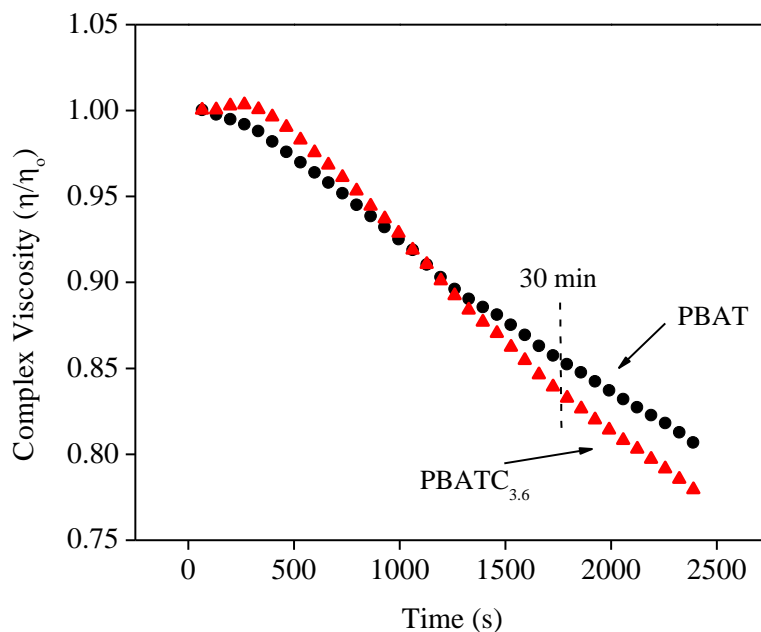


Figure 5. Time Sweeps of PBAT (●) and PBATC_{3.6} (▲) samples at 170°C and 0.1 rad.s⁻¹.

3.6 Samples Morphology

The characterization of the dispersion state of CNC in a polymeric matrix is a difficult issue. Generally, SEM observation is performed to check if CNC aggregates are present. The dispersion state of CNC within the PBAT matrix was investigated using SEM observations, as shown in Figure 6. These images show the fractured surface micrographs for injection-molded materials composed of neat PBAT (Fig. 6a) and its nanocomposites containing 1.8 wt% CNC before (Fig. 6b) and after thermal

conditioning (Fig. 6c). Cellulosic nanoparticles are hardly distinguishable as expected, but by comparing the micrographs showing the surface of fracture for unfilled PBAT and for composites, CNC can be identified. In fact, they appear like shiny dots indicated by arrows corresponding to the transversal section of the nanorods. Their diameter is higher than CNC's diameter as a result of the charge concentration effect due to the emergence of CNCs from the observed surface. However, no strong CNC aggregation was observed and the samples show a reasonable level of dispersion considering the simplicity of their preparation. No significant difference and possible restructuration of the nanoparticles can be evidenced after conditioning (Figure 6c).

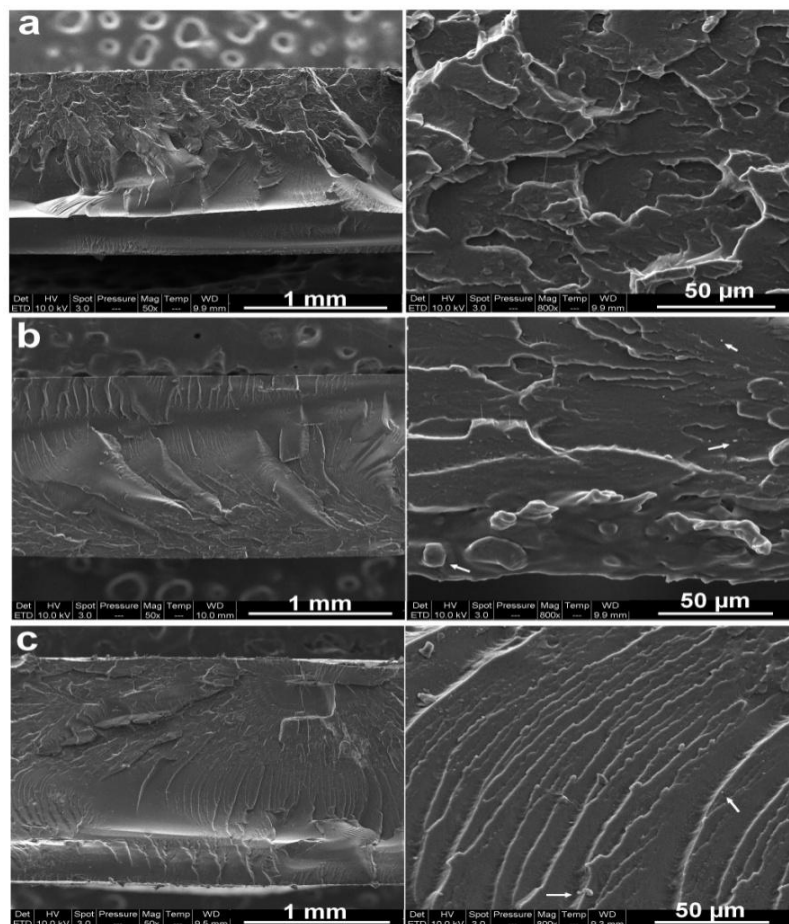


Figure 6. SEM images of PBAT (a), PBAT_{1.8} (b) and PBAT_{1.8C} (c) injected disks fracture. Additional images (PBAT_{0.9} and PBAT_{3.6} samples) can be found in Appendice C.

3.7 2D-SAOS experiments

Two dimensional small amplitude oscillatory shear (2D-SAOS) experiment is an extension of the traditional SAOS test performed to analyse the properties of systems such as suspensions or polymer melts. In traditional experiments, a frequency is imposed to the sample in one dimension, i.e. usually the z axes in dynamical mechanical analysis and an angular θ variation for oscillatory rheological tests. In

orthogonal rheology these two dimensions are evaluated at the same time, providing 2D data. It makes possible to observe anisotropic properties. The objective was not to go deep into the equations or experimental setups that were developed elsewhere by Vermant and collaborators during the last years.[13,46,47] Our aim was to explore this technique at a user-level and propose to apply this type of measurement for a polymer melt with conscience of the limitations that it brings. The results are reported in Figure 7.

In these experiments, the expected result for a completely isotropic sample is a symmetry and superposition of the normal and angular stress. Since the investigated samples present different viscosities, that could influence the measurement of the z-axis stress (σ_{\perp}), the data were normalized by dividing it by the higher stress value for each curve. It limits the stress range from -1 to 1 but provides a simple vision about how the parameter varies with sample elongation for all materials. PBAT shows almost symmetric results with a circle-like curve (Figure 5a). However, besides the good superposition between the stress in the axial and angular positions, the sample does not present a perfectly circular shape as described elsewhere for an isotropic latex suspension.[13] However, the authors also suggest that a slight deformation of the representation of an isotropic system due to equipment limitations can occur. Since PBAT was also prepared by injection-moulding, as the other samples, the chains can present a previous organization that can result in some anisotropy. The same basic profile was found for the other samples, with the emergence of a progressively more elliptic pattern. It is observed that adding CNC causes a gradual distortion of the properties of the material by creating increasingly anisotropic samples, as shown by the distortion of angular (σ_{θ}) and perpendicular (σ_{\perp}) stress for PBATC_{1.8} and PBATC_{3.6} in comparison with neat PBAT.

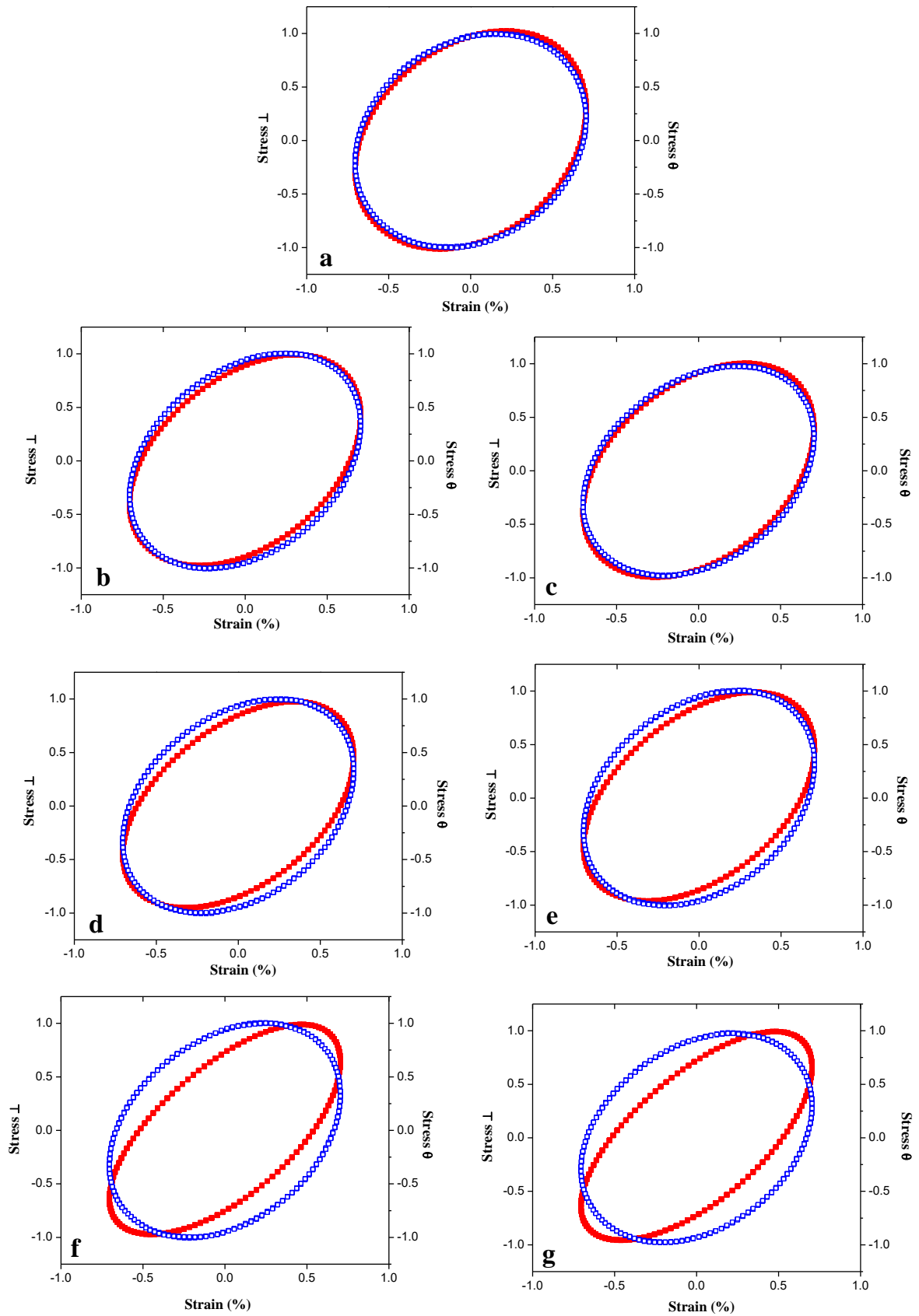


Figure 7. Projection of the normal (o) and angular (●) stress as a function of the imposed strain obtained by 2D-SAOS for injection-moulded materials: PBAT, PBATC_{0.9}, PBATC_{1.8}, and PBATC_{3.6}; and CNC/PBAT nanocomposites conditioned for 30 min at 170°C: PBATC_{0.9C}, PBATC_{1.8C}, and PBATC_{3.6C}. Data were obtained at $\omega = 1 \text{ rad}\cdot\text{s}^{-1}$.

Similar results were obtained for both injection-moulded and thermally conditioned samples suggesting that the forces that could be responsible for the reorganization of the material after imposing shear (and trapping the chains entanglements) are not sufficient, even at 170°C. In order to quantify the possible structural changes occurring after conditioning, we determined the value of the phase shift (δ) between the elongation (ϵ) and the stress (σ) on the oscillatory curves, for the same frequency, as shown in Figure 8. Results are reported in Table 2.

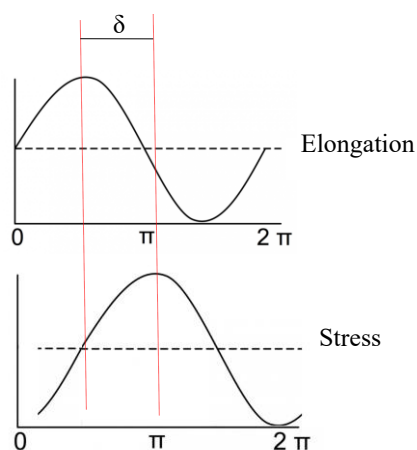


Figure 8. Schematic representation of the phase shift (δ) between the elongation (ϵ) and the stress (σ).

For viscoelastic materials, the value of δ varies from 0 (ideally elastic material) to 90° (ideally viscous material). It means that a material with higher δ value is more viscous. Neat PBAT displays similar δ values for σ_{\perp} and σ_{θ} . This is characteristic of an isotropic material. When increasing the CNC content, the δ value gradually decreases, mainly δ_{\perp} . It corroborates the oscillatory measurements indicating a more elastic behaviour for nanocomposites.

As expected, the difference between the δ value in the normal and angular direction started to differ when adding the nanoparticles. The δ_{\perp} value decreases much faster than δ_{θ} a clear sign of anisotropy. However, thermal annealing of the samples seems to slightly restore their viscous behaviour. It probably results from the Brownian motion of the nanoparticles. However, under these temperature conditions, the nanoparticles seem to be more inclined to break the existing hydrogen bonds and disperse energy rather than moving together and organize in a 3D network by the creation of new H-bonds

Table 2. Rheological data obtained from SAOS curves for extruded samples and samples conditioned for 30 min at 170°C.

Sample	δ_{\perp}	$\Delta\delta_{\perp}^*$	δ_{θ}	$\Delta\delta_{\theta}^*$
PBAT	39.6	-	39.9	-
PBATC _{0.9}	36.7	0.7	36.9	1.1
PBATC _{0.9C}	37.4		38.0	
PBATC _{1.8}	35.3	1.4	38.1	1.6
PBATC _{1.8C}	36.7		39.7	
PBATC _{3.6}	28.1	1.4	36.7	2.5
PBATC _{3.6C}	29.5		39.2	

* $\Delta\delta$ corresponds to the variation of the damping factor between two samples with the same CNC content after and before conditioning.

3.8 Creep behaviour

The alteration of the viscoelastic behavior and structural organization for a nanocomposite can change the response of the material under controlled stress. Figure 9 shows the evolution of the strain as a function of time when applying a constant stress to PBAT and PBATC_{1.8} before and after annealing at 170°C for 30 min. As expected, the neat polymer displays a linear behaviour, with a strain increasing regularly with the duration of stress application. However, the nanocomposite shows very distinct characteristics under the same testing conditions. First, the presence of CNC clearly modifies the way the material can withstand the stress. For a given experimental time, the experienced strain is clearly lower for the nanocomposite. However, as reported elsewhere,[17] the melt-processed nanocomposite still presented an almost linear behavior during the experiment, and besides its lower compliance value compared to the neat matrix, it corroborates that no percolating CNC network is present in the material.

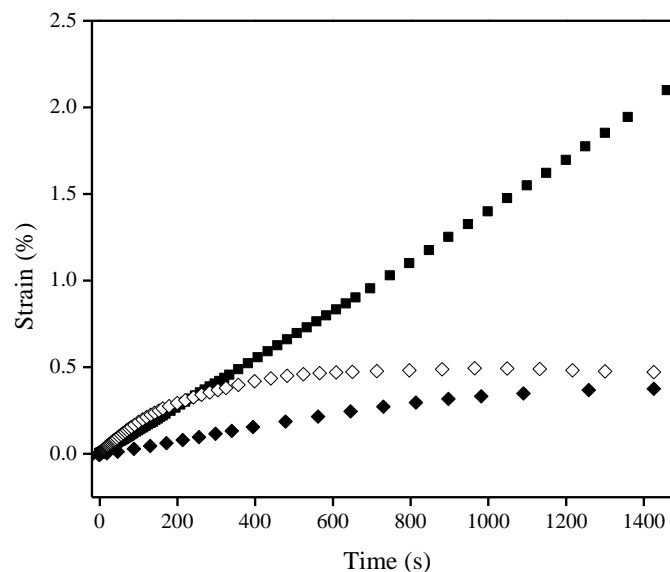


Figure 9. Short-time creep measurements ($\tau = 0.25 \mu\text{N.m}$, $T = 170^\circ\text{C}$) for PBAT (■), PBATC_{1.8} (◆) and PBATC_{1.8C} (◇).

The effect of annealing of the nanocomposite at 170°C for 30 min is also presented in Figure 7. For the conditioned sample, the experimental response of the material to the applied stress can be divided in two regions. For lower times (below 200 s), and in comparison with the non-annealed nanocomposite, a clear higher compliance value is observed. Its value is comparable to the one of the neat PBAT matrix. It agrees with SAOS results, where conditioning increased the slope of the G' vs. ω curve. After transition behaviour, the second region (starting around 500 s) is characterized by a plateau. It means that after a critical elongation, the material is able to support the imposed stress without deforming. Since no CNC network (that could be responsible for a solid-like behaviour) was formed for this sample, as discussed before, the predominant effect should be the higher dispersion level of the particles. Once the initial organization of CNC in clusters is broken, the nanoparticles seem to be more efficient to induce new entanglements after the material has experienced initial stretching. Apparently, it can support enough stress to keep the sample chains at the same position for this specific imposed torque.

4 CONCLUSIONS

Nanocomposites based on polybutyrateadipate terephthalate (PBAT) and cellulose nanocrystals (CNCs) were prepared by extrusion followed by injection-moulding. Capim dourado fibres were used as the cellulosic source for the preparation of CNC which led to high aspect ratio rod-like nanoparticles. The CNC content was adjusted to correspond to the theoretical percolation threshold, and two other nanocomposites with half and twice this critical fraction were also prepared. The rheological behaviour of these materials was characterized in the molten state at 170°C, i.e. about 50°C above the melting point of PBAT. As expected given the high shear rate melt processing technique used, no percolating CNC network formed even for CNC content higher than the percolation threshold. However, small amplitude oscillary shear (SAOS) experiments revealed a reinforcing effect of the nanoparticles and as the CNC content increased a more elastic behaviour was observed. Due to the shear stresses involved during processing, the nanocomposites presented a stronger anisotropic character than the neat PBAT matrix. The effect of a thermal annealing treatment at 170°C for 30 min on the rheological behavior of the materials was investigated. Even if the high viscosity of the polymer melt limits the movement of the nanoparticles and hinders the formation of a desired percolating network, a spatial reorganization of the nanorods was observed after this short conditioning time. It suggests that it is possible to partially alter the organization of the particle within the polymeric matrix imposed by the injection-moulding process.

5 REFERENCES

- [1] F. Bettaieb, R. Khiari, A. Dufresne, M.F. Mhenni, M.N. Belgacem, Mechanical and thermal properties of *Posidonia oceanica* cellulose nanocrystal reinforced polymer., *Carbohydr. Polym.* 123 (2015) 99–104. doi:10.1016/j.carbpol.2015.01.026.
- [2] K. Benhamou, H. Kaddami, A. Magnin, A. Dufresne, A. Ahmad, Bio-based polyurethane reinforced with cellulose nanofibers: a comprehensive investigation on the effect of interface., *Carbohydr. Polym.* 122 (2015) 202–11. doi:10.1016/j.carbpol.2014.12.081.
- [3] D.O. de Castro, J. Bras, A. Gandini, N. Belgacem, Surface grafting of cellulose nanocrystals with natural antimicrobial rosin mixture using a green process., *Carbohydr. Polym.* 137 (2016) 1–8. doi:10.1016/j.carbpol.2015.09.101.
- [4] R. Bardet, C. Reverdy, N. Belgacem, I. Leirset, K. Syverud, M. Bardet, et al., Substitution of nanoclay in high gas barrier films of cellulose nanofibrils with cellulose nanocrystals and thermal treatment, *Cellulose.* 22 (2015) 1227–1241. doi:10.1007/s10570-015-0547-9.
- [5] D. Bondeson, A. Mathew, K. Oksman, Optimization of the isolation of nanocrystals from microcrystalline cellulose by acid hydrolysis, *Cellulose.* 13 (2006) 171–180. doi:10.1007/s10570-006-9061-4.
- [6] S. Camarero Espinosa, T. Kuhnt, E.J. Foster, C. Weder, Isolation of thermally stable cellulose nanocrystals by phosphoric acid hydrolysis., *Biomacromolecules.* 14 (2013) 1223–30. doi:10.1021/bm400219u.
- [7] E.D.M. Teixeira, T.J. Bondancia, K.B.R. Teodoro, A.C. Corrêa, J.M. Marconcini, L.H.C. Mattoso, Sugarcane bagasse whiskers: Extraction and characterizations, *Ind. Crops Prod.* 33 (2011) 63–66. doi:10.1016/j.indcrop.2010.08.009.
- [8] Y. Habibi, L. a Lucia, O.J. Rojas, Cellulose nanocrystals: chemistry, self-assembly, and applications., *Chem. Rev.* 110 (2010) 3479–500. doi:10.1021/cr900339w.
- [9] L. Liu, Y. Zhang, F. Lv, B. Yang, X. Meng, Effects of red mud on rheological, crystalline, and mechanical properties of red mud/PBAT composites, *Polym. Compos.* (2015) n/a–n/a. doi:10.1002/pc.23378.
- [10] M. Nofar, a. Maani, H. Sojoudi, M.C. Heuzey, P.J. Carreau, Interfacial and rheological properties of PLA/PBAT and PLA/PBSA blends and their

- morphological stability under shear flow, *J. Rheol.* (N. Y. N. Y). 59 (2015) 317–333. doi:10.1122/1.4905714.
- [11] L.C. Lins, S. Livi, J. Duchet-Rumeau, J.-F. Gérard, Phosphonium ionic liquids as new compatibilizing agents of biopolymer blends composed of poly(butylene-adipate-co-terephthalate)/poly(lactic acid) (PBAT/PLA), *RSC Adv.* 5 (2015) 59082–59092. doi:10.1039/C5RA10241C.
- [12] K. Fukushima, M.-H. Wu, S. Bocchini, A. Rasyida, M.-C. Yang, PBAT based nanocomposites for medical and industrial applications., *Mater. Sci. Eng. C. Mater. Biol. Appl.* 32 (2012) 1331–51. doi:10.1016/j.msec.2012.04.005.
- [13] C. Mobuchon, P.J. Carreau, M.-C. Heuzey, N.K. Reddy, J. Vermant, Anisotropy of nonaqueous layered silicate suspensions subjected to shear flow, *J. Rheol.* (N. Y. N. Y). 53 (2009) 517. doi:10.1122/1.3094911.
- [14] L. Tang, C. Weder, Cellulose whisker/epoxy resin nanocomposites., *ACS Appl. Mater. Interfaces.* 2 (2010) 1073–80. doi:10.1021/am900830h.
- [15] S.J. Eichhorn, Cellulose nanowhiskers: promising materials for advanced applications, *Soft Matter.* 7 (2011) 303. doi:10.1039/c0sm00142b.
- [16] M. Pereda, N. El Kissi, A. Dufresne, Extrusion of polysaccharide nanocrystal reinforced polymer nanocomposites through compatibilization with poly(ethylene oxide)., *ACS Appl. Mater. Interfaces.* 6 (2014) 9365–75. doi:10.1021/am501755p.
- [17] F. Alloin, A. D’Apréa, A. Dufresne, N. El Kissi, F. Bossard, Poly(oxyethylene) and ramie whiskers based nanocomposites: influence of processing: extrusion and casting/evaporation, *Cellulose.* 18 (2011) 957–973. doi:10.1007/s10570-011-9543-x.
- [18] M.A. Treece, J.P. Oberhauser, Soft Glassy Dynamics in Polypropylene - Clay Nanocomposites, *Macromolecules.* (2007) 571–582. doi:10.1021/ma0612374.
- [19] L.M.C. Dykes, J.M. Torkelson, W.R. Burghardt, R. Krishnamoorti, Shear-induced orientation in polymer/clay dispersions via in situ X-ray scattering, *Polymer (Guildf).* 51 (2010) 4916–4927. doi:10.1016/j.polymer.2010.08.013.
- [20] N. Lin, A. Dufresne, Physical and/or Chemical Compatibilization of Extruded Cellulose Nanocrystal Reinforced Polystyrene Nanocomposites, *Macromolecules.* 46 (2013) 5570–5583. doi:10.1021/ma4010154.
- [21] L. Ma, Y. Zhang, Y. Meng, P. Anusonti-Inthra, S. Wang, Preparing cellulose nanocrystal/acrylonitrile-butadiene-styrene nanocomposites using the master-

- batch method., *Carbohydr. Polym.* 125 (2015) 352–9. doi:10.1016/j.carbpol.2015.02.062.
- [22] D. Oliveira de Castro, E. Frollini, A. Ruvolo-Filho, A. Dufresne, “Green polyethylene” and curauá cellulose nanocrystal based nanocomposites: Effect of vegetable oils as coupling agent and processing technique, *J. Polym. Sci. Part B Polym. Phys.* 53 (2015) 1010–1019. doi:10.1002/polb.23729.
- [23] J. Sapkota, S. Kumar, C. Weder, E.J. Foster, Influence of Processing Conditions on Properties of Poly (Vinyl acetate)/Cellulose Nanocrystal Nanocomposites, *Macromol. Mater. Eng.* 300 (2015) 562–571. doi:10.1002/mame.201400313.
- [24] M. Vestena, I.P. Gross, A.T.N. Pires, Nanocomposite of Poly(lactic acid)/Cellulose Nanocrystals: Effect of CNC Content on the Polymer Crystallization Kinetics, *J. Braz. Chem. Soc.* (2016) 1–7.
- [25] S. Camarero-Espinosa, D.J. Boday, C. Weder, E.J. Foster, Cellulose nanocrystal driven crystallization of poly(d,l-lactide) and improvement of the thermomechanical properties, *J. Appl. Polym. Sci.* 132 (2015) n/a–n/a. doi:10.1002/app.41607.
- [26] L. Lemahieu, J. Bras, P. Tiquet, S. Augier, A. Dufresne, Extrusion of Nanocellulose-Reinforced Nanocomposites Using the Dispersed Nano-Objects Protective Encapsulation (DOPE) Process, *Macromol. Mater. Eng.* 296 (2011) 984–991. doi:10.1002/mame.201100015.
- [27] A.C. Corrêa, E. Morais Teixeira, V.B. Carmona, K.B.R. Teodoro, C. Ribeiro, L.H.C. Mattoso, et al., Obtaining nanocomposites of polyamide 6 and cellulose whiskers via extrusion and injection molding, *Cellulose*. 21 (2013) 311–322. doi:10.1007/s10570-013-0132-z.
- [28] A. Junior de Menezes, G. Siqueira, A. a. S. Curvelo, A. Dufresne, Extrusion and characterization of functionalized cellulose whiskers reinforced polyethylene nanocomposites, *Polymer (Guildf)*. 50 (2009) 4552–4563. doi:10.1016/j.polymer.2009.07.038.
- [29] F. Pignon, A. Magnin, J.-M. Piau, Butterfly Light Scattering Pattern and Rheology of a Sheared Thixotropic Clay Gel, *Phys. Rev. Lett.* 79 (1997) 4689–4692. doi:10.1103/PhysRevLett.79.4689.
- [30] T. Domenech, R. Zouari, B. Vergnes, E. Peuvrel-disdier, Formation of Fractal-like Structure in Organoclay-Based Polypropylene Nanocomposites, *Macromolecules*. 42 (2014) 3417 – 3427. doi:dx.doi.org/10.1021/ma5001354.

- [31] M. Coletti, R. Pepi, Superposition of an orthogonal oscillation to study anisotropy in polymers, *AIP Conf. Proc.* 286 (2014) 286–289. doi:10.1063/1.4876834.
- [32] H.M. Hassanabadi, M. Wilhelm, D. Rodrigue, A rheological criterion to determine the percolation threshold in polymer nano-composites, *Rheol. Acta.* 53 (2014) 869–882. doi:10.1007/s00397-014-0804-0.
- [33] R.G. Schmidt, G. V. Gordon, C. a. Dreiss, T. Cosgrove, V.J. Krukonis, K. Williams, et al., A Critical Size Ratio for Viscosity Reduction in Poly(dimethylsiloxane)–Polysilicate Nanocomposites, *Macromolecules.* 43 (2010) 10143–10151. doi:10.1021/ma1004919.
- [34] R. Mangal, S. Srivastava, L. a Archer, Phase stability and dynamics of entangled polymer-nanoparticle composites., *Nat. Commun.* 6 (2015) 7198. doi:10.1038/ncomms8198.
- [35] M.-C. Li, Q. Wu, K. Song, Y. Qing, Y. Wu, Cellulose Nanoparticles as Modifiers for Rheology and Fluid Loss in Bentonite Water-based Fluids., *ACS Appl. Mater. Interfaces.* 7 (2015) 5006–16. doi:10.1021/acsami.5b00498.
- [36] R. Niu, J. Gong, D. Xu, T. Tang, Z.-Y. Sun, Flow-induced structure and rheological properties of multiwall carbon nanotube/polydimethylsiloxane composites, *RSC Adv.* 4 (2014) 62759–62768. doi:10.1039/C4RA10091C.
- [37] R. Pal, *Rheology of particulate dispersions and composites*, Taylor & Francis, London, 2007.
- [38] F. Du, R.C. Scogna, W. Zhou, S. Brand, J.E. Fischer, K.I. Winey, Nanotube Networks in Polymer Nanocomposites: Rheology and Electrical Conductivity, *Macromolecules.* 37 (2004) 9048–9055. doi:10.1021/ma049164g.
- [39] D.M. Kuntz, *Dilute and Concentrated Phase Behavior of Water-Soluble Rodlike Polyelectrolyte-Surfactant Aggregates*, BiblioBazaar, 2011.
- [40] M.M.D.S. Lima, J.T. Wong, M. Paillet, R. Borsali, R. Pecora, Translational and Rotational Dynamics of Rodlike, *Langmuir.* (2003) 24–29. doi:10.1021/la020475z.
- [41] J.K. Phalakornkul, a. P. Gast, R. Pecora, Rotational and Translational Dynamics of Rodlike Polymers: A Combined Transient Electric Birefringence and Dynamic Light Scattering Study, *Macromolecules.* 32 (1999) 3122–3135. doi:10.1021/ma981640d.

- [42] A.N. Morozov, A. V. Skripkin, Spherical particle Brownian motion in viscous medium as non-Markovian random process, *Phys. Lett. A.* 375 (2011) 4113–4115. doi:10.1016/j.physleta.2011.10.001.
- [43] H.-Y. Yu, D.M. Eckmann, P.S. Ayyaswamy, R. Radhakrishnan, Composite generalized Langevin equation for Brownian motion in different hydrodynamic and adhesion regimes., *Phys. Rev. E. Stat. Nonlin. Soft Matter Phys.* 91 (2015) 052303. doi:10.1103/PhysRevE.91.052303.
- [44] G. Romeo, G. Filippone, P. Russo, D. Acierno, Effects of particle dimension and matrix viscosity on the colloidal aggregation in weakly interacting polymer-nanoparticle composites: a linear viscoelastic analysis, *Polym. Bull.* 63 (2009) 883–895. doi:10.1007/s00289-009-0176-2.
- [45] G. Galgali, C. Ramesh, A. Lele, A Rheological Study on the Kinetics of Hybrid Formation in Polypropylene Nanocomposites, *Macromolecules.* 34 (2001) 852–858. doi:10.1021/ma000565f.
- [46] J. Vermant, P. Moldenaers, J. Mewis, M. Ellis, R. Garritano, Orthogonal superposition measurements using a rheometer equipped with a force rebalanced transducer, *Rev. Sci. Instrum.* 68 (1997) 4090. doi:10.1063/1.1148351.
- [47] S. Kim, J. Mewis, C. Clasen, J. Vermant, Superposition rheometry of a wormlike micellar fluid, *Rheol. Acta.* 52 (2013) 727–740. doi:10.1007/s00397-013-0718-2.

GENERAL CONCLUSIONS

This document focused on some aspects of the preparation of polymer nanocomposites based on cellulose nanocrystals. Different approaches were explored, including casting/evaporation and melt processing. Always aiming to use accessible and inexpensive preparation techniques, the priority was to use simple methodologies according to the particularities of different polymers. Thermal, rheological and mechanical properties of these new materials were studied. The obtained results were compared to available data and supported by a broad literature review.

This literature review is presented in **Chapter I**. A relevant literature research was presented and tried to expose the main topics involving nanocellulose such as basic characterizations, extraction, intrinsic properties and its applications in new materials. This section aimed to provide most of the information necessary to understand the context of the following chapters.

Chapter II showed some results about the preparation of nanocomposites based on natural rubber (NR) and cellulose nanocrystals. This is a classic system for the study of nanocellulose based materials. In this document, NR was used as model to understand the influence of polymer modification in filler-matrix interactions. For many systems, dispersion of CNC is a relevant issue due to the incompatibility of surface properties. As a general rule, chemical modifications are performed on nanoparticle surface aiming to improve the affinity between the materials. This chapter showed that a simple polymer oxidation, performed under mild conditions, can be used to increase the compatibility between a hydrophobic polymer and hydrophilic cellulose. The results showed that rheological and mechanical properties are strongly dependent of the degree of oxidation of the polymer.

In **Chapter III** we introduce the processing of materials at higher temperatures using melt extrusion. Besides the dispersion issue, extruded materials tend to show degradation at moderate temperatures (i.e. higher than 200°C). The preparation of a masterbatch was suggested as solution due to the use of never-dried nanoparticles and the physical-coating of the particles by the polymer, improving dispersion and thermal resistance. The use of an amorphous polymer was not successful in avoiding effects of crystallization since the masterbatch preparation led to a molecular weight reduction that impacted the mechanical properties of the nanocomposites.

Chapter IV aimed to further investigate the effects of crystallization on the properties of the new materials produced by extrusion and injection-molding. The first part presented results related to the use of cellulose nanocrystals with different aspect ratios (L/d ratio) on the crystallinity of the polymer. A semi-crystalline

thermoplastic (PBAT) was used in this study. Despite the competition between volume fraction and aspect ratio when used at the percolation threshold of the nanoparticle, it was clear that the nanoparticles can act as nucleating agents for the polymer. Short and long time crystallizations showed that longest nanoparticles were able to create a higher crystallinity, despite their lower volume fraction. Mechanical properties (i.e. Young modulus) proved to be strongly dependent on the degree of crystallinity of the samples. Since the longest filler was able to provide better reinforcement effect, it was chosen to be studied in the second part of this chapter. Inspired by the long thermal conditioning times imposed to the samples during annealing, this section investigated the possibility of Brownian motion to be used as driving force to promote particle reorganization. The samples were conditioned at temperatures above the polymer melting point and the possibility of particle reorganization was studied through rheological experiments. The particular interest in this topic came from the fact that extrusion and injection-molding are based on the imposition of shear to the samples that ultimately forced an orientation of polymer chains and filler. We were able to show that inclusion of increasing amounts of cellulose nanocrystals led to more anisotropic particle, but not to cause a relevant reorganization of the particles by increasing the mobility of the particles.

For many purposes, nanocellulose research shows now a general trend to avoid complex processes and chemical reactions as a target issue for many applications. The adaptation of nanocomposites processing to industrial level is still a challenge but presented clear progress over the last 5 years. The ongoing progress on preparation and characterization of these materials is essential since now nanocellulose can be produced in tons/day. In this context, the methods and results presented along this document are aligned with the path taken by nanocellulose research during the last years. We have explored different alternative methods for nanocomposite preparation always trying to get competitive results through alternative preparation. In that sense I believe that we were successful.

Appendix A.

Cellulose Nanomaterials: Size and Surface influence on the thermal and rheological behavior

Marcos Mariano^{1,2,3,4*}, Nadia El Kissi^{3,4} and Alain Dufresne^{1,2}

¹ *Univ. Grenoble Alpes, LGP2, F-38000 Grenoble, France*

² *CNRS, LGP2, F-38000 Grenoble, France*

³ *Univ. Grenoble Alpes, LRP, F-38000 Grenoble, France*

⁴ *CNRS, LRP, F-38000 Grenoble, France*

* Corresponding author: marcos.mariano@lgp2.grenoble-inp.fr

Abstract

Cellulose nanocrystals (CNC) and nanofibrils (CNF) were obtained by acid hydrolysis and mechanical treatment, respectively, of cellulosic fibers from paper. Additionally, surface modification was performed for CNC by neutralization (NaOH) and oxidation (TEMPO). The thermal stability, surface properties and rheological behavior of these nanomaterials were compared. A clear difference in CNC surface was found upon neutralization and oxidation treatments, leading to distinct thermal behaviors. Optical and rheological properties were found to be predominantly by the particles size, being strongly affected by inertial effects.

Keywords: Cellulose Nanocrystals; Cellulose Nanofibrils; Thermal Stability; Rheology.

*Accepted for publication in **Revista Polímeros** journal, 2016.*

1 Introduction

The use of natural fibers as raw materials to produce biocomposites is a tendency that fits perfectly the actual society needs. A combination of extensive research and recent technological advances allows the use of nanomaterials in new renewable material development. As the most abundant polymer on earth, cellulose studies goes toward the described scenario. Its fibers are now used to produce new composites with different matrix by different processing techniques [1–4]. The use of its natural structure to produce nanomaterials was developed during the last two decades and shows promising results. Many initial difficulties are now overcome and advances have been made concerning their obtention, surface modification and processing.[5].

Derivated from natural fibers, bacteria or algae, cellulose nanomaterials are versatile materials that are now applied in nanopapers[6], hydrogels[7], composites[8], electronic[9], biomedicine[10], etc. Being a versatile material, cellulose processing can be adjusted to provide different materials as, for example, cellulose nanofibril (CNF) or cellulose nanocrystal (CNC). The first one can be obtained by mechanical defibrillation or enzymatic treatment of cellulose fibers [11], which leads to individualization of cellulose nanofibers that compose the intrinsic structure of the polymer. The second one is obtained by the isolation of crystalline domains present in the structure by hydrolysis of amorphous part using acid or enzymatic steps[12,13].

Concerning its actual applications, CNF is used in hydrogels and high technology papers. During its production by mechanical defibrillation, it is common to use TEMPO (2,2,6,6-tetramethyl-1-piperidinyloxy radical) oxidation as pretreatment. This step facilitates the fiber individualization, being a way to save energy and make greener process. CNC is normally used in nanocomposite production to provide better barrier or mechanical properties [14,15]. To ensure the quality and explore the complete potential of this nanoparticle, its surface can be modified to improve the filler-matrix compatibility or increase the thermal stability. In the case of molecule grafting to nanocrystal surface, also a TEMPO modification has become a common process used as first stage to allow chemical modification [16]. Aiming in the production of nanocomposites at high temperatures, the CNC surface also can be modified. The presence of sulfate groups attached to its surface after hydrolysis can decrease its thermal stability. A desulfation process can be performed by the addition of a diluted NaOH solution into the suspension. In this case, the thermal degradation seems to be postponed [17].

In this study, these different materials were obtained from paper using different methodologies. Cellulose nanocrystals were obtained by acid hydrolysis

and neutralized (CNC-n) or oxidized (CNC-t) using TEMPO reagent. The nanocrystal properties were compared to cellulose nanofibrils (CNF) obtained by mechanical treatment. Aiming to compare the properties of these different materials, obtained from the same source, the nanoparticles were characterized by different techniques.

2 Materials and Methods

Materials

The paper used in this study was purchased from Whatman®. NaOH and sulfuric acid were obtained from Sigma-Aldrich.

Methods

In this section, the experimental process used during the preparation of the nanomaterials will be described. An illustrative scheme of the obtained materials is reported in Figure 1.

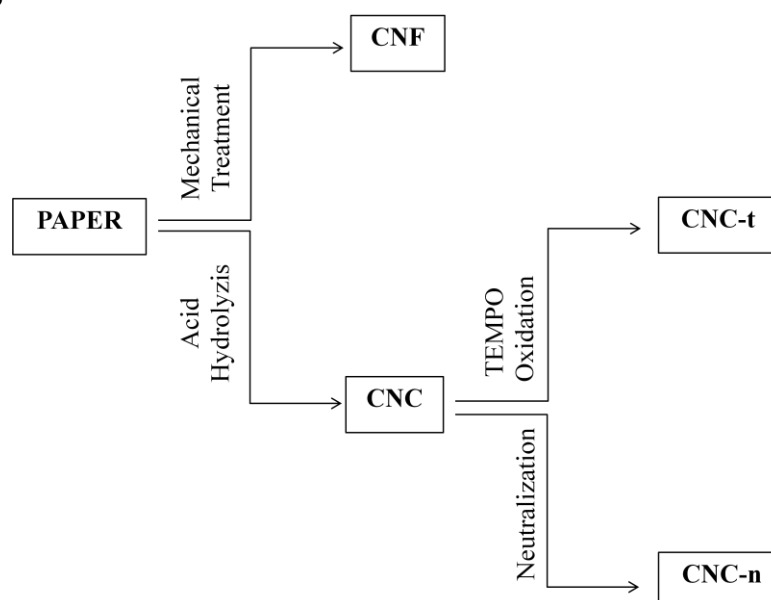


Figure 1. Illustrative scheme of the preparation methods and obtained materials

Nanomaterial obtention

Nanocrystal preparation. Firstly, the cellulose fibers obtained from paper were maintained under agitation in a 2% NaOH solution for 6 hours at 25°C and after that it was washed until neutral pH and dried in ambient conditions. For hydrolysis of bleached fibers, 400 mL of a sulfuric acid solution (65wt%) was heated up to 45°C and 20g of fibers was suspended in the solution under a strong mechanical stirring for 45 min. After the desired time, the reaction was stopped with the addition of some ice cubes and the suspension was centrifuged in cycles of 10 minutes under a centrifuge force of 1373.6 G. After each cycle the acid supernatant was discarded and replaced by distilled water, this process was repeated a few times to increase the pH of the suspension. The resultant water suspension was dialyzed with a cellulose

membrane against distilled water until its pH was around 5. Some drops of chloroform were added to avoid any bacterial proliferation and the suspension was stored under refrigeration.

Particle neutralization. After its preparation and dialysis, the pH of part of the cellulose nanocrystalsuspensionwas adjusted to 9 using a diluted NaOH solution. This suspension was kept under agitation for 24h and again dialysed until neutral pH.

Tempo oxidation. The oxidation of hydroxyl groups by TEMPO reagent was develop by Nooy [18] and is broadly used in the oxidation of cellulosic materials. Here, the generic procedure used for the modification of cellulose nanocrystals and cellulose fibers (pretreatment) is described. In an ice bath, a weight of 4 g of cellulose material was suspended in 400 mL of water to obtain a 1wt% suspension. The suspension was homogenized with a strong mechanical agitation and 0.4g of NaBr and 0.1g of 2,2,6,6-tetramethylpiperidine (TEMPO) were added to the suspension. This agitation was maintained for almost 20 min, to ensure a complete dissolution of the reagents, and slowly 10 mL of a 12% aqueous NaOCl⁻ solution was added to the reaction medium. The pH should be kept between 10 and11 with an eventual addition of diluted NaOH solution. After 2 hours, 10 mL of ethanol was added to the medium and the pH adjusted to 7 with a diluted acid solution. For the cellulose fibers, filtration and washing with distilled water was performed. CNC was dialysed against distilled water for several days.

Nanofibril preparation. The previous oxidized fibers were resuspended in water and the concentration was adjusted to 1wt%. This suspension was treated with a Masuko Supermass colloider grinder for 60 passes.

Materials Characterization

Atomic Force Microscopy (AFM). The images were obtained on a NanoscopeIIIa microscope from Veeco Instruments. A drop of a diluted aqueous CNC suspension with 0.01 wt% concentrationwas deposited on a mica substrate and dried. It was imaged in tapping mode with a Silicon cantilever. The nanoparticle dimensions were estimated from 50 measurements analyzed using the associated Nanoscope software.

Zeta Potential (ξ). Nano particle suspensions with concentration around 0.01 wt% were analyzed on an equipment model DTS0230 from Malvern Instruments. To avoid the effects of ionic strength and pH during measurements, all the concentrated solutions were diluted in an aqueous standard solution with pH 10 and 180 $\mu\text{S}/\text{cm}$ conductivity. This solution was prepared by the addition of diluted NaOH solution and solid NaCl into distilled water.

Contact Angle (CA). Films 0.1 ± 0.01 mm thick were prepared by casting/evaporation and analyzed with an Attension Theta contact angle meter equipment by using water as liquid. The samples were cast in a Teflon mold to ensure a smooth surface and the contact angle was measured during 120 s. The final angle value before surface deformation was used as reference.

Fourier Transform Infrared Spectroscopy (FTIR). ATR mode measurements were performed on a FTIR Perkin-Elmer Spectrum One equipment between 600 and 4000 cm^{-1} in 4 cm^{-1} intervals. All the analyses were carried out using films cast and dried at room temperature.

Thermogravimetric Analysis (TGA). The analysis was carried out under Air atmosphere using Perkin-Elmer TGA-6 equipment. The sample heating was performed from room temperature up to 600°C with a heating of 10°C.min⁻¹.

Rheological Measurements. The rheological behavior of the dispersions was characterized with a DHR-3 equipment from TA Instruments. A cone (2°, 50 mm) - plate (50 mm) geometry was used to study the dilute suspensions in flow and oscillatory modes at 20°C.

Degree of polymerization. The samples viscosity were measured by the TAPPI methodology T 230m 08 and the D.P. estimated by the Equation I.

$$\text{D.P.} = -449.6 + 598.4 \ln[\eta] + 118.02(\ln[\eta])^2 \quad \text{Equation I}$$

X-ray diffraction. XRD measurements for the samples were recorded on a Philips PW 1720 X-ray generator operated at 45 kV and 40mA in a Bragg–Brentano geometry. The 2θ range was from 5° to 65° using a fixed time mode with a step interval of 0.066° and Cu Ka radiation ($k = 1.5418 \text{ \AA}$). The crystallinity index (C.I.) was obtained by the relation between crystalline phase $2\theta = 22^\circ$ and amorphous phase on $2\theta = 18.5^\circ$ following the Equation II.

$$\text{C.I. (\%)} = \frac{I_{200} - I_{am}}{I_{200}} \times 100 \quad \text{Equation II}$$

Samples nomenclature and other obtained properties are on Table 1.

Table 1. Samples nomenclature and general properties

Sample	Nomenclature	D.P.	L (nm)	D (nm)	L/D	ξ (mV)	Contact Angle (°)	C.I.
Paper	CP	2598	-	-	-	-	-	-
NaOH-neutralized Cellulose Nanocrystals	CNC-n	462	147 ± 20	8.5 ± 2.5	17.3	-26.9	17	87
TEMPO-oxidized Cellulose Nanocrystals	CNC-t	375	145 ± 41	8.3 ± 2.7	17.4	-32.7	33	88
Cellulose Nanofibrils	CNF	485	~ 1000	6.0 ± 3.7	>100	-33.7	21	80

3 Results and Discussion

Atomic force microscopy and surface properties. Different procedures were applied to obtain cellulose nanomaterials with distinct characteristics. The morphology of the nanoparticles resulting from the acid and mechanical treatments is shown in Figure 2.

For the acid hydrolyzed material (CNC) rod-like structure can be observed (Figures 2a and 2b). These nanometric rods are the non-hydrolyzed crystalline domains present in the hierarchical structure of cellulose. After post-treatment performed on the pristine CNC, the dimensions (Table 1) of CNC-t and CNC-n seem to be basically the same, no visible sign of degradation caused by the basic or oxidative treatment at the surface could be found. In both cases, the particle dimensions are in agreement with dimensions reported in literature, being similar to the estimated size of nanocrystals obtained from hardwood [19]. Figure 2c shows CNF particles. These particles have very different characteristics when compared to the previous one. Longer and more flexible than CNC nanorods, CNF occurs as particles with higher aspect ratio (L/d). This characteristic is in agreement with the expected structure of particles obtained after mechanical or enzymatic treatment. In this process, hydrolysis of the amorphous part of cellulose does not occur, with the isolation of individual fibrils being the principal objective. From the AFM image it is possible to observe some microscale fibers. Probably, the mechanical treatment was not able to provide particles with a narrow size distribution, where individual nanofibers are completely isolated. However, the presence of fibers with a nanometric diameter (around 6 nm) is predominant compared to bigger agglomerates.

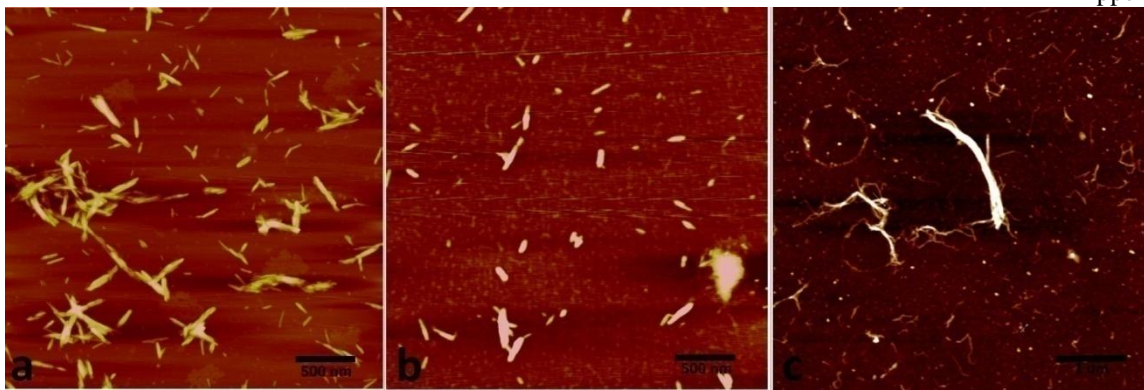


Figure 2. AFM images of (a) CNC-n, (b) CNC-t and (c) CNF.

Besides its dimensions, the particle surface also are quite different. The ξ measurements shows that the CNC-n present a less negative surface charge. This is probably a consequence of the neutralization stage, where the NaOH solution can neutralize acid residues and the negative sulfate groups presents at the nanoparticle surface. As a consequence, it means that this suspension is less stable against coalescence than the others. CNC-t and CNF have similar ξ values. It can suggest that the number of oxidized $-OH$ groups during the TEMPO reaction was not so different although the different surface areas available during the reaction.

Infrared Spectroscopy. Figure 3a shows the FTIR spectra for the different nanoparticles. The figure also shows the spectrum of pristine cellulose fibers (CP) to be used as reference. Firstly, all the curves show typical peaks of cellulose, i.e. C-H ($2900, 1300\text{ cm}^{-1}$), C-C (1600 cm^{-1}), C-O ($3330, 1000\text{ cm}^{-1}$), C-O-C (1150 cm^{-1}) and O-H (3330 cm^{-1}) bands. However, besides the homogeneous distribution of size and no sign of particle degradation, the FTIR analysis shows some modifications in CNC structure. Probably, these modifications occur at the surface of the nanorods during the post-treatment of oxidation or neutralization. Surprisingly, the spectra for CNC-n and CNC-t are quite similar. The presence of a C=O peak at 1740 cm^{-1} for CNC-t is a consequence of the TEMPO-oxidation, that can oxidize the C-O bonds naturally present in the cellulose structure. On CNC-t also is possible to observe a 2840 cm^{-1} peak, that is normally attributed to C-H bonds in alkanes. This peak can corroborate the higher value of contact angle if we assume some surface degradation during the reaction. It seems possible once the C.I. for this sample had a slight decrease when compared to the CNC-n sample.

The presence of the same C=O signal for CNC-n was not expected. In this sample, the neutralization process was supposed to cause just a desulfation of the nanocrystal surface [17]. However, this step seems to also cause an oxidation of the O-H groups to form carbonyl groups, probably resulting in carboxylic acids or aldehydes formation. CNF also presents the C=O peak, a consequence of the TEMPO pre-treatment. In this sample it is worth to notice a prominent band at 1600 cm^{-1} , that

can be related to a slightly offset O-H bending peak of absorbed water ($\sim 1620\text{ cm}^{-1}$) band or a C=C aromatic band. In the last case, it can be attributed to some residual hemicelluloses. Once in this sample no acid hydrolysis was performed, the presence of residual oligomers is possible.

Concerning the samples polymorphism, all the samples had shown cellulose I patterns with intense peaks on 2θ equals to 15° (110), 17° (110) and 23° (200). However, CNC-n shows a small peak on 2θ equals to 12° (101), that is characteristic of cellulose II. It suggests a cellulose conversion (of a small number of chains) from type I \rightarrow II during the neutralization step. Figure 3b shows the XRD curves for the CNC-t sample in comparison to CNC-n.

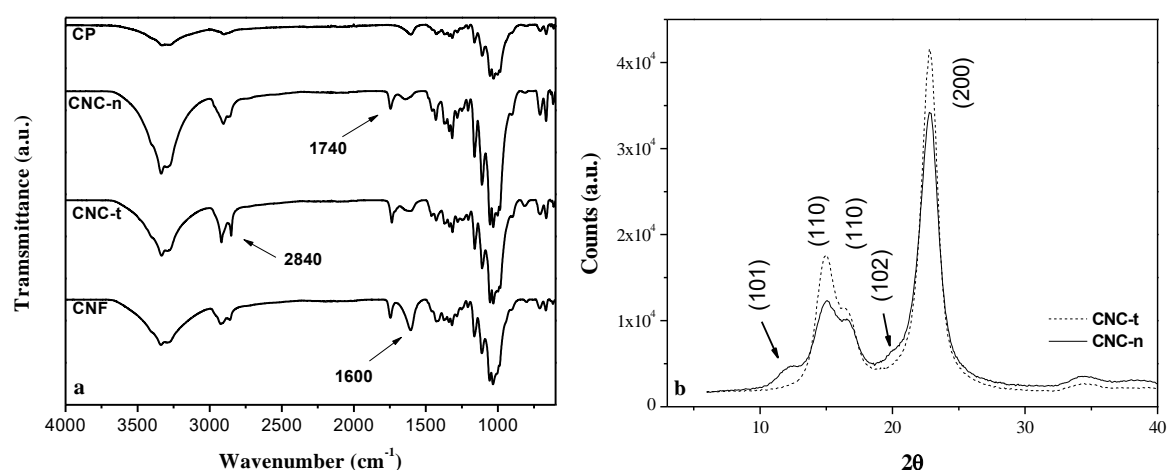


Figure 3. FTIR (a) spectra for paper and nanocellulosic materials and XRD (b) patterns for CNC-t and CNC-n.

Thermal behavior. As a consequence of the surface modification suggested by FTIR, C.I. and zeta potential (Table 1) values, the particles could show very different properties, once these parameters are critically important to define particle behavior in suspension and its thermal behavior. The thermal stability of the samples was investigated by thermogravimetric analysis. The obtained thermograms are shown in Figure 4 and the related data reported in Table 2.

Table 2. Thermogravimetric analysis data.

Sample	Water % (at 150 °C)	Degradation Stages	Onset degradation	dTg peak	Char residue % at 600 °C
CP	4.5	2	214	350	11.7
CNC-n	5.8	2	235	350	20.3
CNC-t	5.0	2	190	315	25.2
CNF	5.8	2	220	315	28.8

Firstly, a higher amount of water present in the nanometric samples is observed. This can be explained by the higher surface area of this particles, providing more available $-\text{OH}$ groups with which water molecules can interact. As suggested

by contact angle measurements (Table 1) and FTIR, CNC-t is more hydrophobic than other nanocellulosic samples, showing a lower water content. The thermal behavior and degradation stages of cellulose materials are very well described in literature. While cellulosic fibers tend to degrade in multiple stages due to their heterogeneous composition with presence of macromolecules such as lignin and hemicelluloses, acid hydrolyzed nanocrystals tend to degrade at lower temperatures due to the presence of sulfate groups [20] [21]. Here, the use of a bleached commercial paper seems to minimize the first phenomena for the CP sample. Nevertheless, it is possible to observe the degradation of cellulose over a very broad temperature range (Figure 4b), being the cellulose maximum degradation peak normally described around 360°C [22].

Concerning the nanomaterials (CNC and CNF) the thermal degradation can be distinguish in two groups. In the first one, CNC-n seems to have a similar degradation mechanism as CP. These nanoparticles presents a good thermal stability, with a dTG (Figure 4b) in the same temperature range as pristine cellulose (CP), but its degradation occurs within a narrower temperature range. This higher thermal stability is a direct consequence of the neutralization step, that avoids early degradation of the material by removing residual acids and causing desulfatation of the particle surface [23]. As expected, the molecular weight (expressed in terms of DP, Table 1) of the pristine cellulose was almost six times higher than for other samples. The nanomaterials had present similar values of DP on a range similar to the described by Matsuoka, Kawamoto, and Saka (2014) [24] as the length of cellulose crystalline region. However, it seems to not be the major influence on this property since the CP and CNC-n shows similar dTG values besides its different values of DP.

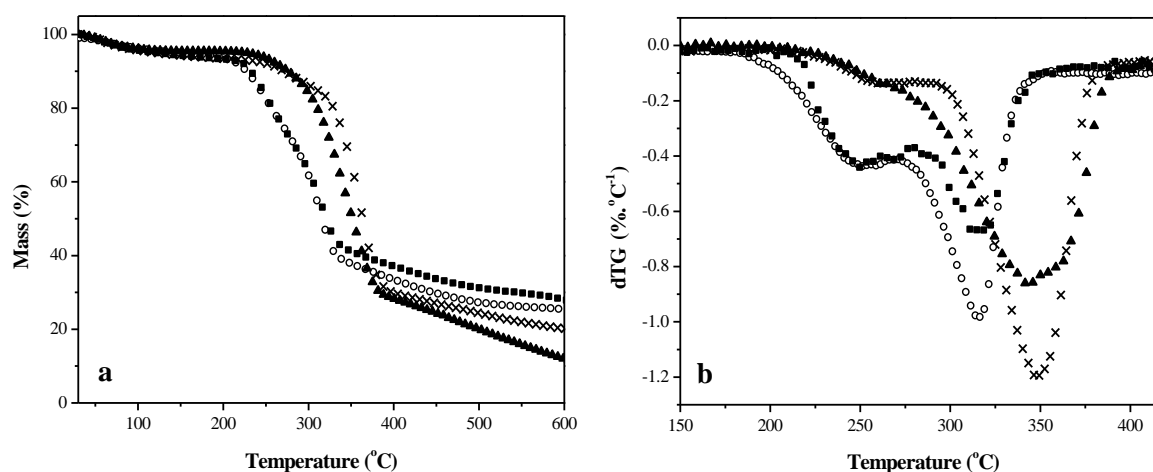


Figure 4. (a) TGA and (b) dTG curves for: CP (▲), CNC-n (X), CNC-t (o) and CNF (■).

In the second group, CNC-t and CNF also show similar thermal behavior. In these samples, the presence of two degradation stages is more pronounced than in the first group. These two stages are normally visible on acid hydrolyzed nanocrystals. In fact, it seems to be a consequence of the early degradation of external

chains of the particle that accelerates the formation of oligomers that can cause a kind of caramelisation effect in the sample surface that can coat the material core, retarding its degradation. The similar degradation temperatures and dTG for CNC-t and CNF suggests that carboxylic groups can also produce this kind of effect.

For all samples, there is a remarkable increase in char residue when comparing nanomaterials to pristine paper. It is known that the pathway of thermal degradation of the samples seems to be responsible to change the residual content and that parameters such as activation energy, heating rate, temperature of dehydration and levoglucosan formation can strongly affect the residues content and appearance [25]. Besides the normally cited presence of sulfate groups, other surface characteristics also can lead to modify the degradation pathway. For example, an increase on the surface area or presence of grafted groups on cellulose surface also can cause variation on the thermal degradation.

Here, the higher residues content were present on TEMPO-oxidized samples. It occurs due to the easy surface oxidation of the material and is clearly observable by comparison with the other samples (presenting C=O or -OH groups, for example). This oxidation seems to accelerate the process of coating the internal cellulose chains. Due to its lower C.I. (Table 1), the core chains of CNF and CNC-t are not so protected from external heat transfer as CNC-n and these samples presents lower dTG values. However, on these two samples the final mechanism seems to occur by a pathway of smaller E_a that leads to the formation of char [24].

Optical properties and suspension behavior. In water suspension, these particles also show different behaviors. The observation of nanoparticles under a polarized light is a way to observe oriented and crystalline structures. Figure 5 shows the presence of birefringence in the nanocrystal samples.

The birefringence of CNC suspensions can result from two factors: (i) the structural form anisotropy of cellulose nano-domains (anisotropic refractive index, Δn of 0.05) and (ii) a flow anisotropy resulting from alignment of the nanorods (if long enough) under flow. In this study, this alignment was induced by the creation of a shear in the suspension using magnetic stirring. Some studies demonstrated that an imposed shear can produce planar domains of randomly oriented nanoparticles that are aligned or broken with the shear rate variation [26]. The level of organization in the nanoparticle suspension is a key factor to its rheological properties and will be discussed in sequence.

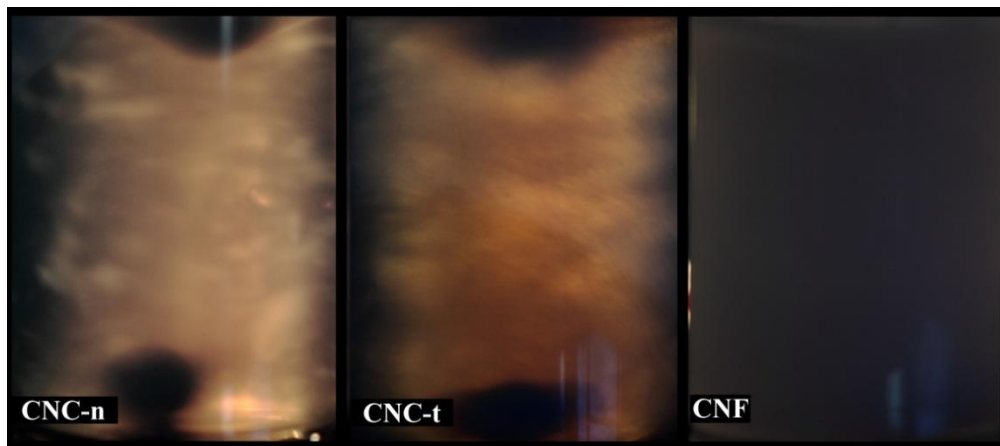


Figure 5. Birrefringencedomaines of nanoparticle suspensions with concentration of 0.6wt% .

This birefringence phenomenon cannot be observed in the CNF system. In addition to its big dimensions (at least in one axis), it was demonstrated by Karppinen [26] that CNF have a tendency to entangle (in a reversible way) when submitted to shear, making difficult their alignment with the flow.

Flow curves. According to Bercea and Navard [24], the critical concentrations for a regime transition between diluted-semidiluted (ϕ^*) and semidiluted-concentrated (ϕ^{**}) CNC particles suspended in water can be calculated using the rigid rod approximation:

$$\phi^* = \frac{d^2}{L^2} \quad \text{Equation III}$$

$$\phi^{**} = \frac{d}{L} \quad \text{Equation IV}$$

Equations III and IV can show the transitions limits calculated from the particle dimensions, where L is the length and d the diameter of the particle. In our system, the particle dimensions lead to a diluted to semi-diluted regime transition around 0.0033vol% (or 0.05 wt%) and a semi-diluted to concentrated transition around 0.057vol% (or 0.91 wt%) . In this study, we choose to perform all the rheological measurements in the semidiluted regime where the samples are in an isotropic-at-rest regime and no anisotropy can be found. For CNF suspensions, the concentration was chosen to be the same as for the CNC suspensions in order to facilitate the discussion and data comparison. Figure 6 presents the evolution of the viscosity as a function of the shear rate. For all samples it is possible to observe a decrease in the viscosity value with shear rate increase (shear thinning behavior). For the CNC samples, the viscosity value at lower shear rates is around 1 Pa.s, similar to values reported in the literature [27], [28]. For CNC suspensions, the shear thinning behavior is normally explained by the progressive organization of the particles in

suspension. At lower shear rates the nanocrystals are assumed to randomly organize. However the scenario starts to change with the shear rate increase and the rods are progressively align in the flow direction. This organization causes a decrease in the drag force, decreasing the viscosity value until a plateau. In this region, it is possible to observe an almost Newtonian flow behavior due to the maximum organization of the nanocrystals.

Besides the similar size and shape, CNC-n and CNC-t viscosity curves shows some slight differences. The viscosity for the CNC-n suspension is higher at lower shear rates and this sample reaches the Newtonian *plateau* before CNC-t. Probably this behavior is caused by the differences in the nanocrystal surface chemistry. Despite similar size and shape, CNC-n and CNC-t viscosity curves shows some slight differences. The viscosity for the CNC-n suspension is higher at lower shear rates and this sample reaches the Newtonian *plateau* before CNC-t. Probably, this behavior is caused by the differences in the nanocrystal surface chemistry.

For the CNF suspension, the viscosity values are significantly higher than for CNC at lower shear rate values, being around 30 Pa.s. This value is also similar to previous data reported in literature [11], [26]. The shear thinning behavior is even more accentuated in this system. As a diluted sample, it is not possible to observe an intermediary *plateau* that is described by some authors with the concentration increase. Concerning the flow kinetics and the microstructure of this system under shear, it seems to be much more complicated than for the CNF system. Inhomogeneous flow is caused by erratic mesostructural changes. Flocculation, fiber entanglement and wall slippage are phenomena present in this system due to the particles characteristics, i.e. size polydispersity, flexibility and surface charge [26], [29].

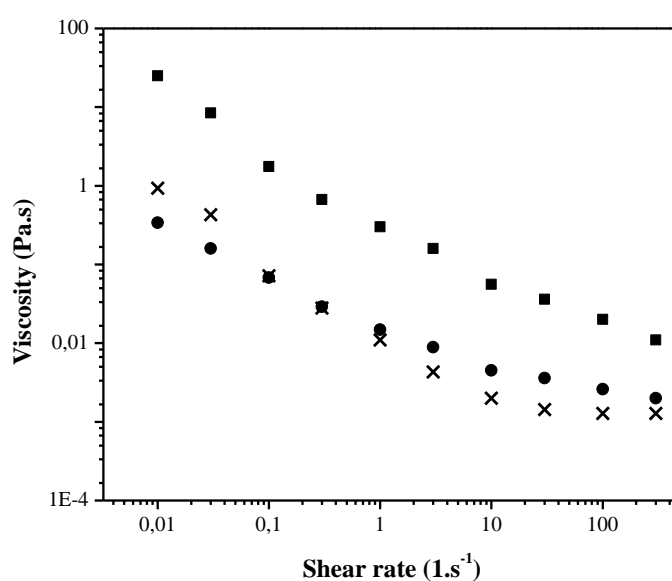


Figure 6. Steady-state viscosity versus shear rate for CNF (■), CNC-n (X) and CNC-t (●) suspensions with concentration of 0.6 wt%.

Oscillation measurements. The rheological behavior of the particle dispersions was also characterized by dynamic oscillatory measurements. The intrinsic difference between the nanorods and the nanofibers was very clear even during the oscillation strain sweeps were the CNC samples showed a critical strain around 0.5%, a much higher value than for CNF, which showed a critical strain around 0.025%. The evolution of the values of G' and G'' as a function of angular frequency is plotted in Figure 7. Cellulose nanomaterials are known for the possibility for form gels. These structures can be applied in different areas due to their great capacity to retain water and, still, behave as a solid. The “gel” state is defined by rheology as a suspension state where it presents a storage modulus (G') much higher than its loss modulus (G''), i.e. $G' \gg G''$.

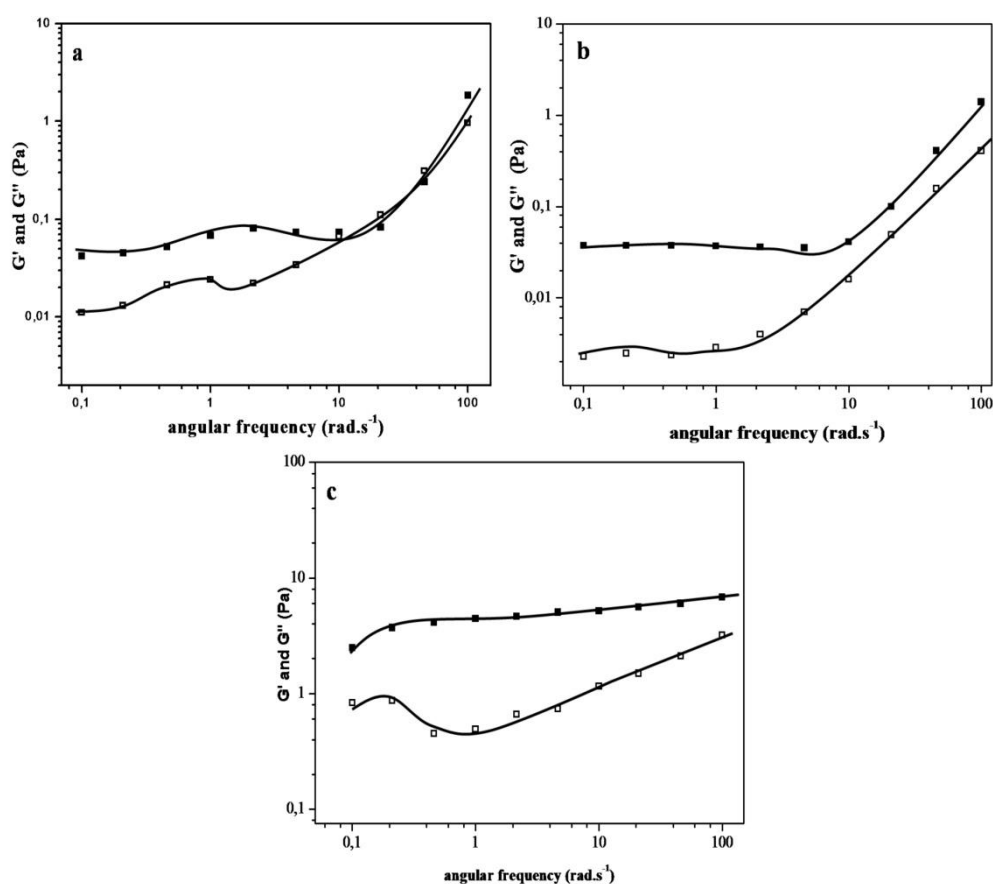


Figure 7. Storage, G' (solid symbols) and loss, G'' (empty symbols) moduli as a function of oscillation frequency for (a) CNC-t, (b) CNC-n and (c) CNF - The lines are just guide to the eyes.

The storage modulus values can be regarded as the suspension ability to restore energy, and therefore, as the gel strength of the suspensions. In this study, all the samples presents gel-like behavior with G' values higher than G'' . However, the ratio between G'' and G' (called $\tan \delta$) is greater than 0.1 for all studied samples until

intermediary angular frequencies (F_q). This means that the samples are not true gels, but can be considered as weak gels [30], what is reasonable considering their low concentrations. This denomination is corroborated by the dependence of G' with F_q , since very stiff CNC gels (arising from more concentrated CNCs suspensions) do not present this dependence, presenting an almost constant G' value [31], [32].

For the nanorod samples, the weak gel behavior is very clear until F_q values closer to $1 \text{ rad}\cdot\text{s}^{-1}$. After this F_q the values of loss and storage moduli start to be very similar (i.e. $\tan \delta$ is close to 1) and increase. This behavior is also described by Karppinen (2014) and Wu (2014) for diluted nanocellulose (fibers and rods) suspensions. The first one considers it as a consequence of the concentration proximity with the threshold concentration for gel-like behavior [33], [34]. However, this phenomenon seems to be more complex. Here, the G' and G'' values for diluted suspensions start to increase and became similar at intermediary F_q . This behavior is described by Etwold (2015) [35] as a consequence of inertial forces that can cause interferences in the measurements. It seems to be explained by the Reynolds number, Equation V.

$$Re = \frac{\rho \cdot v \cdot e}{\eta} \sim \frac{\text{Inertial Forces}}{\text{Viscous Forces}} \quad \text{Equation V}$$

Where: ρ is the fluid density, v is the fluid medium speed and e is the characteristic length of the flow process being considered (i.e. the rheometer plates gap in our case) and η the fluid viscosity.

This equation illustrates the relationship between inertial and viscous forces. When the fluid presents low viscosity or flow values, the inertial effect can be negligible due to compensation between both forces. However, in the case of systems with very low viscosity and/or high flow values, these effects begin to be representative and can influence the measurements, leading to false data. It is possible to observe in Figures 7a and 7b an increase in G' and G'' at higher frequency values. Probably it occurs because inertial effects are causing a stress that is measured by the equipment. After a critical frequency it begins to distort and the obtained modulus values and G' and G'' seems to grow. This critical frequency (F_{qc}) is a limit after which it is not possible to neglect inertial distortions in the obtained data. Equations VI and VII were suggested by Baravian (2013) and can provide quantitative information about this frequency due to inertial effects of fluid and equipment respectively. [36]

$$F_{qc} < \frac{\eta}{\rho \cdot e^2} \quad \text{Equation VI}$$

$$F_{qc} < \frac{\sqrt{G'/\alpha}}{2\pi} \quad \text{Equation VII}$$

Where: (Equation VI) F_{qc} is the critical frequency (in Hz), η is the viscosity values at 1 Hz frequency, ρ is the suspension density, e is the plates gap distance; (Equation VII) α is a 0.05 coefficient for standard geometries and G' is the modulus values at low frequencies. The respective obtained values for the studied suspensions are collected in Table 3.

Table 3. Samples viscosity and inertial critical frequencies.

Sample	Fluid Inertia		Equipment Inertia	
	Viscosity (mPa.s)	F_{qc} (rad.s ⁻¹)	G' (mPa)	F_{qc} (rad.s ⁻¹)
MNC-t	2.1	3.6	47	0.96
MNC-n	1.7	2.96	35	0.83
CNF	53.0	92.4	3800	8.71

For CNC samples, F_{qc} is quite similar, considering the fluid and equipment inertial effects. It means that most of the frequency range for the CNC suspension at this concentration is under influence of inertial effects. The inertial effect from the rheometer seems to arise at lower frequencies if compared to the fluid effects for all the samples. According to Baravian, above F_{qc} the rheometer error can be higher than 20% [36]. Since these effects are viscosity-dependent, they are much less observable for CNF in the studied F_q range. This sample presents higher viscosity values, the fluid inertial effects only become significant after 92.4 rad.s⁻¹ and probably shows most visibly distorted data at higher frequencies. For lower F_q , where no inertial effects are affecting the data, the magnitude of the modulus values are clearly different between CNC and CNF samples, being much superior for the nanofibril suspension. It suggests that nanofibrils could create a stronger fibrous network at this concentration. In this suspension G' value is higher than G'' over the whole studied frequency range and a relative weak influence of the frequency was found, a typical behavior of weak gels [32].

4 Conclusions

The aim of this study was to show how different properties can be obtained from the same cellulose source due to the versatility of this material. By controlling the size/shape of the particle and its surface charge and composition it was possible to modify its thermal and rheological characteristics. The presence of charged groups for CNCs seems to be a key parameter that induces their earlier degradation during heating, an important drawback for composite processing by extrusion or injection. The particle dimensions seem to be responsible for significant modifications in the

rheological parameters, such as viscosity and modulus of the nanoparticle suspensions in water. Also, we propose that diluted nanocellulose suspensions measurements can be highly influenced by inertial effects after a critical frequency, leading to false data obtainment. These effects also seem to be dependent of the sample dimensions, being more pronounced for CNC in the studied concentration and frequency range.

References

- [1] D. O. Castro, E. Frollini, J. Marini, and A. Ruvolo-Filho. (2013). Preparação e Caracterização de Biocompósitos Baseados em Fibra de Curauá, Biopolietileno de Alta Densidade (BPEAD) e Polibutadieno Líquido Hidroxilado (PBHL). *Polímeros: Ciência e Tecnologia*, 23, 65–73. doi: <http://dx.doi.org/10.1590/S0104-14282013005000002>
- [2] M. A. Martins and L. H. C. Mattoso (2003). Short Sisal Fiber-Reinforced Tire Rubber Composites : Dynamic and Mechanical Properties. *Journal Applied Polymer. Science.*, 91, 670 – 677
- [3] C. M. O. Müller, J. B. Laurindo, and F. Yamashita. (2009). Effect of cellulose fibers addition on the mechanical properties and water vapor barrier of starch-based films. *Food Hydrocolloids*, 23(5), 1328–1333. doi:10.1016/j.foodhyd.2008.09.002
- [4] S. Kalia, B. S. Kaith, and I. Kaur (2009). Pretreatments of Natural Fibers and their Application as Reinforcing Material in Polymer Composites — A Review. *Polymer Engineering Science*. doi: 10.1002/pen.21328
- [5] A. Dufresne and M. N. Belgacem (2013). Cellulose-reinforced Composites : From Micro-to Nanoscale. *Polímeros: Ciência e Tecnologia*, 23 (3), 277–286. doi: <http://dx.doi.org/10.4322/polimeros.2010.01.001>
- [6] H. Sehaqui, Q. Zhou, O. Ikkala, and L. a Berglund. (2011). Strong and tough cellulose nanopaper with high specific surface area and porosity. *Biomacromolecules*, 12(10), 3638–44. doi: dx.doi.org/10.1021/bm2008907
- [7] K. Abe and H. Yano. (2011). Formation of hydrogels from cellulose nanofibers. *Carbohydrate Polymers*, 85(4), 733–737. doi:10.1016/j.carbpol.2011.03.028
- [8] D. O. de; Castro, E. Frollini, A. Ruvolo-Filho, and A. Dufresne (2014). ‘Green Polyethylene’ and Curaua Cellulose Nanocrystal Based Nanocomposites: Effect of Vegetable Oils as Coupling Agent and Processing Technique. *Journal Polymer Science: PART B Polymer Physics*, 53, 1010–101. doi: 10.1002/polb.23729
- [9] F. Hoeng, A. Denneulin, C. Neuman, and J. Bras. (2015). Charge density modification of carboxylated cellulose nanocrystals for stable silver nanoparticles suspension preparation. *J. Nanoparticle Research*, 17(6), 244. doi: 10.1007/s11051-015-3044-z
- [10] N. Lin and A. Dufresne (2014). Nanocellulose in biomedicine: Current status and future prospect. *European Polymer Journal*, 59, 302–325. doi: <http://dx.doi.org/10.1016/j.eurpolymj.2014.07.025>

- [11] O. Nechyporchuk, M. N. Belgacem, and F. Pignon (2014). Rheological properties of micro-/nanofibrillated cellulose suspensions: wall-slip and shear banding phenomena. *Carbohydrate Polymers*, 112, 432–439. <http://dx.doi.org/10.1016/j.carbpol.2014.05.092>
- [12] W.L. Sun, W.F. Ye, and W.Y. Tao (2013). Improving Enzymatic Hydrolysis of Cellulose from Rice Straw Using an Ionic Liquid [EMIM]Ac Pretreatment. *Energy Sources, Part A: Recovery, Utilization, and Environmental Effects*, 35(21), 2042–2050. doi: 10.1080/15567036.2010.532192
- [13] K. B. R. Teodoro, E. de M. Teixeira, A. C. Corrêa, A. Campos, J. . Marconcini, and L. H. . Mattoso (2011). Whiskers de Fibra de Sisal Obtidos sob Diferentes Condições de Hidrólise Ácida : Efeito do Tempo e da Temperatura de Extração. *Polímeros: Ciência e Tecnologia*, 21(4), 280–285. doi: <http://dx.doi.org/10.1590/S0104-14282011005000048>
- [14] G. Siqueira, H. Abdillahi, J. Bras, and A. Dufresne. (2010). High reinforcing capability cellulose nanocrystals extracted from *syngonanthus nitens* (Capim Dourado). *Cellulose*, vol. 17, pp. 289 – 298, 2010. doi: 10.1007/s10570-009-9384-z
- [15] H. A. Silvério, W. P. Flauzino Neto, I. S. V. Da Silva, J. R. Rosa, D. Pasquini, R. M. N. De Assunção, H. D. S. Barud, and S. J. L. Ribeiro (2014). Mechanical, thermal, and barrier properties of methylcellulose/cellulose nanocrystals nanocomposites. *Polímeros: Ciência e Tecnologia*, 24(6), 683–688. doi: 10.1590/0104-1428.1691
- [16] N. Lin and A. Dufresne (2013) Physical and/or Chemical Compatibilization of Extruded Cellulose Nanocrystal Reinforced Polystyrene Nanocomposites. *Macromolecules*, 46(14), 5570–5583. doi: <dx.doi.org/10.1021/ma4010154>
- [17] N. Wang, E. Ding, and R. Cheng (2007). Thermal degradation behaviors of spherical cellulose nanocrystals with sulfate groups. *Polymer (Guildf)*, 48(12), 3486–3493. doi:10.1016/j.polymer.2007.03.062
- [18] E. I. Evier, A. E. J. De Nooy, A. C. Besemer, and H. Van Bekkum. (1995). Highly selective nitroxyl radical-mediated oxidation of primary alcohol groups in water-soluble glucans. *Carbohydrate Research*. 269 (1),89–98.
- [19] S. Beck-Candanedo, M. Roman, and D. G. Gray. (2015). Effect of reaction conditions on the properties and behavior of wood cellulose nanocrystal suspensions. *Biomacromolecules*, 6(2), 1048–54. doi: 10.1021/bm049300p
- [20] M. Roman and W. T. Winter. (2004). Effect of sulfate groups from sulfuric acid hydrolysis on the thermal degradation behavior of bacterial cellulose. *Biomacromolecules*, 5(5), 1671–1677. doi: 10.1021/bm034519+
- [21] V. A. Alvarez and A. Vázquez (2004). Thermal degradation of cellulose derivatives/starch blends and sisal fibre biocomposites. *Polymer Degradation Stability*, 84(1), 13–21. doi:10.1016/j.polymdegradstab.2003.09.003
- [22] M. A. S. Azizi Samir, F. Alloin, and A. Dufresne (2005). Review of recent research into cellulosic whiskers, their properties and their application in nanocomposite field. *Biomacromolecules*, 6(2), 612–2. doi: 10.1021/bm0493685
- [23] Lin, N., Dufresne, A. (2014). Surface chemistry, morphological analysis and properties of cellulose nanocrystals with gradiented sulfation degrees. *Nanoscale* 6, 5384–93. doi:10.1039/c3nr06761k

- [24] Matsuoka, S., Kawamoto, H., Saka, S. (2014). What is active cellulose in pyrolysis? An approach based on reactivity of cellulose reducing end. *J. Anal. Appl. Pyrolysis* 106, 138–146. doi:10.1016/j.jaap.2014.01.011
- [25] Shoji, T., Kawamoto, H., Saka, S. (2014). Boiling point of levoglucosan and devolatilization temperatures in cellulose pyrolysis measured at different heating area temperatures. *J. Anal. Appl. Pyrolysis* 109, 185–195. doi:10.1016/j.jaap.2014.06.014
- [26] A. Karppinen, T. Saarinen, J. Salmela, A. Laukkanen, M. Nuopponen, and J. Seppälä. (2012). Flocculation of microfibrillated cellulose in shear flow. *Cellulose*, 19(6), 1807–1819. doi: 10.1007/s10570-012-9766-5
- [27] M. Bercea and P. Navard (2000). Shear Dynamics of Aqueous Suspensions of Cellulose Whiskers. *Macromolecules*, 33(16), 6011–6016. doi: 10.1021/ma000417p
- [28] E. E. Ureña-Benavides, P. J. Brown, and C. L. Kitchens. (2010). Effect of jet stretch and particle load on cellulose nanocrystal-alginate nanocomposite fibers. *Langmuir*, 26(17), 14263–70. doi: 10.1021/la102216v.
- [29] F. Martoia, C. Perge, P. J. J. Dumont, L. Orgéas, M. a Fardin, S. Manneville, and M. N. Belgacem (2015). Heterogeneous flow kinematics of cellulose nanofibril suspensions under shear. *Soft Matter*, 11(24), 4742–55. doi: 10.1039/c5sm00530b
- [30] E. A. Pereira, E. M. Brandão, S. V Borges, and M. C. A. Maia (2008). Influence of concentration on the steady and oscillatory shear behavior of umbu pulp. *Revista Brasileira de Engenharia Agrícola e Ambiental*, 12(21), 87–90. doi: http://dx.doi.org/10.1590/S1415-43662008000100013
- [31] E. E. U. Benavides, G. Ao, V. A. .Davis, and C. L. Kitchens (2011). Rheology and Phase Behavior of Lyotropic Cellulose Nanocrystal Suspensions. *Macromolecules*, 44, 8990–8998. doi: 10.1021/ma201649f
- [32] M. V Tzoumaki, T. Moschakis, and C. G. Biliaderis (2013). Effect of soluble polysaccharides addition on rheological properties and microstructure of chitin nanocrystal aqueous dispersions. *Carbohydrate Polymers*, 95(1), 324–31. doi: 10.1016/j.carbpol.2013.02.066
- [33] A. Karppinen, (2014). Rheology and flocculation of polymer-modified microfibrillated cellulose suspensions. Aalto University.
- [34] Q. Wu, Y. Meng, S. Wang, Y. Li, S. Fu, L. Ma, and D. Harper. (2014). Rheological behavior of cellulose nanocrystal suspension: Influence of concentration and aspect ratio. *Journal Applied Polymer Science*, 131(15), 1 – 8. doi: 10.1002/app.40525
- [35] R. H. Ewoldt, M. T. Johnston & L. M. Caretta. (2015). Experimental challenges of shear rheology: how to avoid bad data. in *Complex Fluids in Biological Systems*, 1st ed., S. Spagnolie, Ed. Springer.
- [36] C. Baravian (2013). Effets inertiels en rhéométrie instationnaie. in *La mesure en rhéologie - des avancées récentes aux perspectives*, 1st ed., J. L. . Grossiord & A. Ponton, Eds. Edp sciences.

APPENDIX B – ADITONAL INFORMATIONS

B.1. Cellulose modulus values

Method	Material	E _L (GPa)
		77-121
		56
		172.9 ^a
	<i>Cellulose I</i>	70.8 ^b
		136 ± 6
		167.5
		134-135
		127.8
	<i>Cellulose Ia</i>	136-155 ^a
		114-117 ^b
		115.2
		124-155
Calculation		116-149 ^a
		124-127 ^b
	<i>Cellulose Iβ</i>	156
		85.2-126.0 ^a / 37.6-63.3 ^b
		139.5
		206
		89 ± 4
		162.1
		83
	<i>Cellulose II</i>	155
		109-166 ^a
		101-106 ^b
		134
	<i>Cellulose I</i>	122-135
X-ray diffraction		138
		70 - 90
	<i>Cellulose II</i>	106-112
		88
Raman	<i>Cellulose I</i>	57-105
	<i>Cellulose Iβ</i>	143
Inelastic X-ray scattering	<i>Cellulose I</i>	220
AFM	<i>Cellulose Iβ</i>	145-150

The complete data and references can be found on ref [37].

B.2. Additional data about cellulose thermal degradation

Atm.	Source	Hydrolysis Agent	Onset Degrad. Temperature	ξ (mv)	Ref
Nitrogen	Bamboo	Phosphoric Acid	200	-29	[38]
	Banana fibers	Sulfuric Acid	235	-20	[39]
	Lyocell Fibers	Ammonium Persulfate	220	-24	[40]
	Sisal	Sulfuric Acid	145	-41	[41]
	MCC	Microbial hydrolysis	230	-15	[42]
	Air	Cotton	Sulfuric Acid	128	-62
Sulfuric Acid			140	-48	
Sulfuric Acid			200	-33	
Sulfuric Acid			270	-07	
Hardwood		Sulfuric Acid /Tempo	190	-33	This work (Chapter 2)
Hardwood		Tempo/Mechanical	220	-34	This work (Chapter 2)
Capim dourado		Sulfuric Acid	208	-31	This Work (Chapter 5)
Sisal		Sulfuric Acid	220	-18	This work (Chapter 5)

B.3. Suggested references of different nanocellulose sources

Source	Ref.	Source	Ref.
Bacterial cellulose	[44]	Mulberry	[45]
Banana fibers	[46]	Palm tree	[47]
Bioethanol residues	[48]	Phormium tenax	[49]
Cassava Bagasse	[50]	Posidonia oceanica	[51]
Chili leftover	[52]	Ramie	[53]
Curauá	[54]	Rice	[55]
Coconut	[56]	Rice Husk	[55]
Eucalyptus	[57]	Rice straw	[58]
Flax	[59]	Sesame husk	[60]
Kenaf	[61]	Switgrass	[62]
Lemon	[63]	Softwood	[64]
Luffa cylindrica	[65]	Soy hulls	[66]
Maize	[63]	Wheat straw	[67]
Microcrystalline cellulose	[68]	Wood fibers	[69]
Mengkuang leaves	[70]		

Appendix C – supplementary data

C.1. Values of contact angle for pristine natural rubber and oxidized materials

Contact Angle measurements

Sample	Contact Angle
NRC	98°
ONR2C	80°
ONR3C	65°
ONR4C	60°
ONR5C	55°

C.3. Sugar analysis of CNC samples by HPLC

Experimental:

Samples preparation followed TAPPI T 249 cm-00 method. Briefly, freeze dried CNCs were submitted to acid hydrolysis using H₂SO₄ (72 wt%) for some minutes, until apparent dissolution of the solid content. The suspension was then diluted and the acid hydrolysis was complete in autoclave for 1 h at 120°C. The resultant suspensions were filtered to avoid presence of residual insolubles materials. Monosaccharides content were determined by using high-performance anion exchange chromatography with pulse amperometric detection (HPAEC PAD) in a Dionex ICS 5000 apparatus. Sugar separation takes place in a CarboPac PA column 10 (250 mm × 4 mm, Dionex) equipped with a pre-column.

Comments

Table 4 shows the results of sugar analysis performed by HPCL. The analysis had show only the presence of glucose for all samples, indicating no presence of hemicelluloses. However, we found a difference between the injected and detected amount of material. It was especially notable for CNC₃₉ sample. This sample presents almost 10% less cellulose and glucose content than other samples. Moreover, CNC₃₉ sample also presented material sedimentation during preparation, with formation of a brown insoluble material in acid pH.

Table 4. Glucose and cellulose content obtained by HPLC.

Sample	Glucose Content	Cellulose Content
CNC ₂₂	95.7	92.2
CNC ₃₉	85.1	81.3
CNC ₅₀	96.3	91.5

Similar descriptions about the characteristics of CNC covered by an oligosaccharide layer (OSL) were recently described by Bouchard and co-workers [73]. Apparently,

under certain conditions, an OSL can be deposited on the CNC surface during the dilution of the H_2SO_4 after hydrolysis causing different surface properties and precipitation in acid. This is a very interesting topic that is under investigation.”

C.4. Additional microscopies (SEM) of PBAT+ CNC nanocomposites

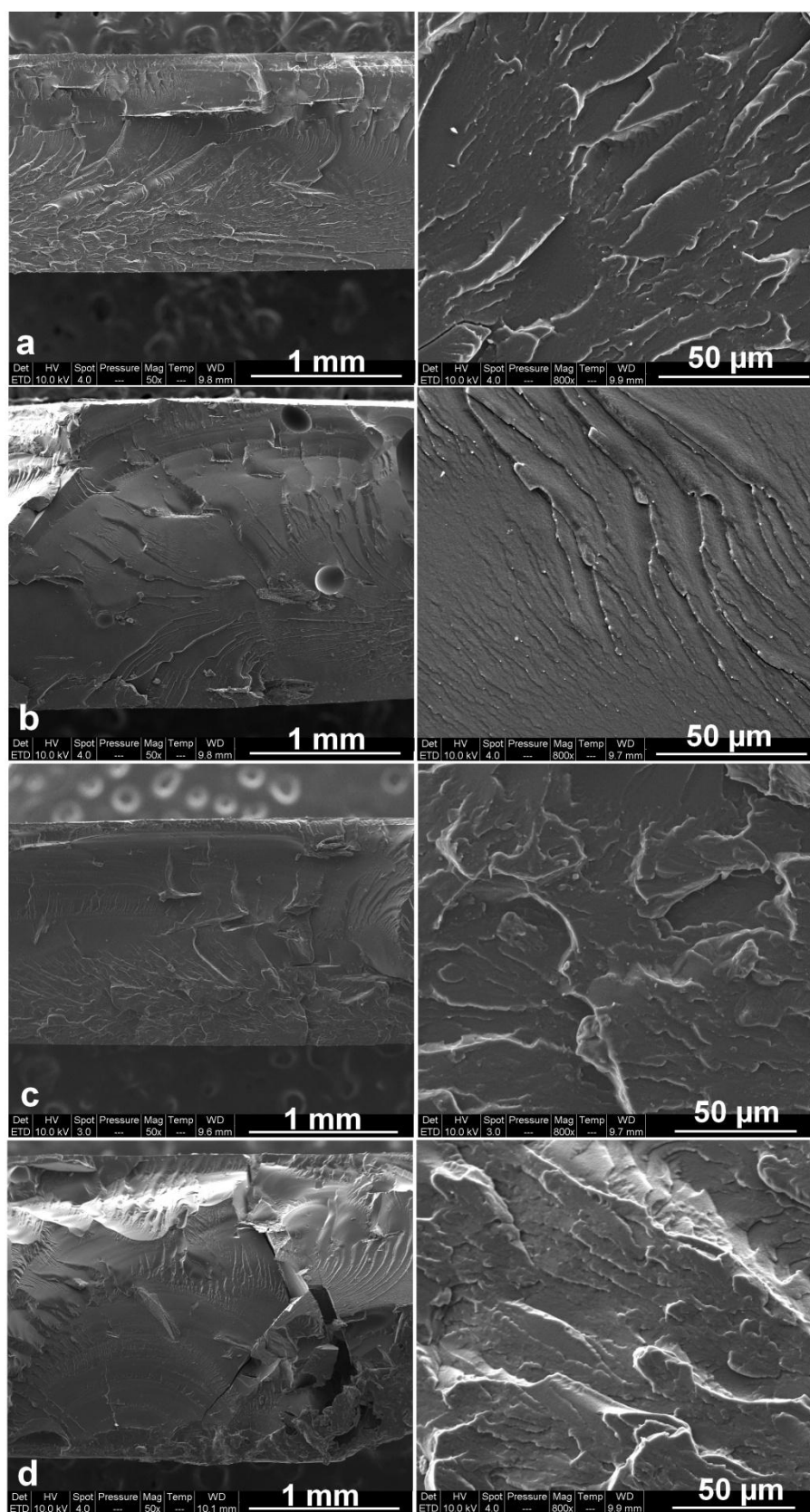


Figure 1. Fracture images of PBAT0.9 (a), PBAT 0.9C (b), PBAT3.6(c) and PBAT 3.6C (d).

APPENDIX D - LISTS

D.1. Symbols and Abbreviations

Symbols

ω ($\dot{\gamma}$)	Angular frequency / Shear (strain) rate
μ_n	Chemical potential
χ	Crystallinity index
$\tan \delta$	Damping factor
E	Elastic modulus (Young Modulus)
G'' (E'')	Loss modulus
H	Enthalpy
S	Entropy
ΔH_m	Melt Enthalpy
μ	Poisson's ratio
γ	Strain
σ	Stress
G' (E')	Storage modulus
η	Viscosity
φ	Volume fraction
Ψ	Volume fraction of the percolating rigid phase
ξ	Zeta potential
λ	Wavelength

Abbreviations

AFM	Atomic force microscopy
BA	Butylene adipate
DT	Dimethyl terephthalate
CD	Circular dichroism (chapter i)
CNC	Cellulose nanocrystals
CNF	Cellulose nanofibers
DP	Polymerization degree
DSC	Differential scanning calorimetry
FTIR	Fourier transform infrared spectroscopy
HDPE	High density poly ethylene
LBL	Layer – by – layer
NR	Natural rubber
PBAT	Poly(butylene adipate-co- terephthalate)
PC	Polycarbonate
PUR	Polyurethanes
PVA	Poly vinyl alcohol
SAOS	Small amplitude oscillatory shear
SAXS	Small Angle X-ray Scattering
SBR	Styrene butadiene resin
SIC	Strain induced crystallization
TAPPI	Technical Association of the Pulp and Paper Industry
T_c	Crystallization temperature
TEMPO	2,2,6,6-tetramethylpiperidine
TG	Thermogravimetry
T_g	Glass transition temperature
T_m	Melting temperature

APPENDIX E - ADDITIONAL REFERENCES

- [37] M. Mariano, N. El Kissi, A. Dufresne, Cellulose nanocrystals and related nanocomposites: Review of some properties and challenges, *J. Polym. Sci. Part B Polym. Phys.* (2014) n/a–n/a. doi:10.1002/polb.23490.
- [38] Q. Lu, W. Lin, L. Tang, S. Wang, X. Chen, B. Huang, A mechanochemical approach to manufacturing bamboo cellulose nanocrystals, *J. Mater. Sci.* 50 (2014) 611–619. doi:10.1007/s10853-014-8620-6.
- [39] S. Elanthikkal, U. Gopalakrishnapanicker, S. Varghese, J.T. Guthrie, Cellulose microfibrils produced from banana plant wastes: Isolation and characterization, *Carbohydr. Polym.* 80 (2010) 852–859. doi:10.1016/j.carbpol.2009.12.043.
- [40] M. Cheng, Z. Qin, Y. Liu, Y. Qin, T. Li, L. Chen, et al., Efficient extraction of carboxylated spherical cellulose nanocrystals with narrow distribution through hydrolysis of lyocell fibers by using ammonium persulfate as an oxidant, *J. Mater. Chem. A*. 2 (2014) 251–258. doi:10.1039/C3TA13653A.
- [41] M. Mariano, Obtenção, caracterização e aplicação de nanocristais de celulose obtidos a partir do sisal, UFSC, 2013.
- [42] H. Yu, C. Yan, X. Lei, Z. Qin, J. Yao, Novel approach to extract thermally stable cellulose nanospheres with high yield, *Mater. Lett.* 131 (2014) 12–15. doi:10.1016/j.matlet.2014.05.159.
- [43] N. Lin, A. Dufresne, Surface chemistry, morphological analysis and properties of cellulose nanocrystals with gradiented sulfation degrees., *Nanoscale*. 6 (2014) 5384–93. doi:10.1039/c3nr06761k.
- [44] I.A. Sacui, R.C. Nieuwendaal, D.J. Burnett, S.J. Stranick, M. Jor, C. Weder, et al., Comparison of the Properties of Cellulose Nanocrystals and Cellulose Nanofibrils Isolated from Bacteria, Tunicate, and Wood Processed Using Acid, Enzymatic, Mechanical, and Oxidative Methods, *Appl. Mater. Interfaces*. (2014) 6127 – 6138.

- [45] R. Li, J. Fei, Y. Cai, Y. Li, J. Feng, J. Yao, Cellulose whiskers extracted from mulberry: A novel biomass production, *Carbohydr. Polym.* 76 (2009) 94–99. doi:10.1016/j.carbpol.2008.09.034.
- [46] M.M. Ibrahim, A. Dufresne, W.K. El-Zawawy, F. a. Agblevor, Banana fibers and microfibrils as lignocellulosic reinforcements in polymer composites, *Carbohydr. Polym.* 81 (2010) 811–819. doi:10.1016/j.carbpol.2010.03.057.
- [47] K. Benhamou, H. Kaddami, A. Magnin, A. Dufresne, A. Ahmad, Bio-based polyurethane reinforced with cellulose nanofibers: a comprehensive investigation on the effect of interface., *Carbohydr. Polym.* 122 (2015) 202–11. doi:10.1016/j.carbpol.2014.12.081.
- [48] K. Oksman, J. a. Etang, A.P. Mathew, M. Jonoobi, Cellulose nanowhiskers separated from a bio-residue from wood bioethanol production, *Biomass and Bioenergy.* 35 (2011) 146–152. doi:10.1016/j.biombioe.2010.08.021.
- [49] E. Fortunati, D. Puglia, M. Monti, L. Peponi, C. Santulli, J.M. Kenny, et al., Extraction of Cellulose Nanocrystals from Phormium tenax Fibres, *J. Polym. Environ.* 21 (2012) 319–328. doi:10.1007/s10924-012-0543-1.
- [50] D. Pasquini, E. De Moraes, A. Aprígio, M. Naceur, A. Dufresne, Extraction of cellulose whiskers from cassava bagasse and their applications as reinforcing agent in natural rubber, *Ind. Crop. Prod.* 32 (2010) 486–490. doi:10.1016/j.indcrop.2010.06.022.
- [51] F. Bettaieb, R. Khiari, A. Dufresne, M.F. Mhenni, M.N. Belgacem, Mechanical and thermal properties of *Posidonia oceanica* cellulose nanocrystal reinforced polymer., *Carbohydr. Polym.* 123 (2015) 99–104. doi:10.1016/j.carbpol.2015.01.026.
- [52] M. Nagalakshmaiah, N. El Kissi, G. Mortha, A. Dufresne, Structural investigation of cellulose nanocrystals extracted from chili leftover and their reinforcement in cariflex-IR rubber latex, *Carbohydr. Polym.* 136 (2015) 945 – 954. doi:10.1016/j.carbpol.2015.09.096.
- [53] F. Alloin, A. D'Apréa, A. Dufresne, N. El Kissi, F. Bossard, Poly(oxyethylene) and ramie whiskers based nanocomposites: influence of processing: extrusion and casting/evaporation, *Cellulose.* 18 (2011) 957–973. doi:10.1007/s10570-011-9543-x.

- [54] D. Oliveira de Castro, E. Frollini, A. Ruvolo-Filho, A. Dufresne, "Green polyethylene" and curauá cellulose nanocrystal based nanocomposites: Effect of vegetable oils as coupling agent and processing technique, *J. Polym. Sci. Part B Polym. Phys.* 53 (2015) 1010–1019. doi:10.1002/polb.23729.
- [55] N. Johar, I. Ahmad, A. Dufresne, Extraction, preparation and characterization of cellulose fibres and nanocrystals from rice husk, *Ind. Crops Prod.* 37 (2012) 93–99. doi:10.1016/j.indcrop.2011.12.016.
- [56] M.F. Rosa, E.S. Medeiros, J. a. Malmonge, K.S. Gregorski, D.F. Wood, L.H.C. Mattoso, et al., Cellulose nanowhiskers from coconut husk fibers: Effect of preparation conditions on their thermal and morphological behavior, *Carbohydr. Polym.* 81 (2010) 83–92. doi:10.1016/j.carbpol.2010.01.059.
- [57] G.H.D. Tonoli, E.M. Teixeira, a. C. Corrêa, J.M. Marconcini, L. a. Caixeta, M. a. Pereira-da-Silva, et al., Cellulose micro/nanofibres from Eucalyptus kraft pulp: Preparation and properties, *Carbohydr. Polym.* 89 (2012) 80–88. doi:10.1016/j.carbpol.2012.02.052.
- [58] K. Abe, H. Yano, Comparison of the characteristics of cellulose microfibril aggregates of wood, rice straw and potato tuber, *Cellulose.* 16 (2009) 1017–1023. doi:10.1007/s10570-009-9334-9.
- [59] X. Cao, Starch-based nanocomposites reinforced with flax cellulose nanocrystals, *eXPRESS Polym. Lett.* 2 (2008) 502–510. doi:10.3144/expresspolymlett.2008.60.
- [60] B.S. Purkait, D. Ray, S. Sengupta, T. Kar, A. Mohanty, M. Misra, Isolation of Cellulose Nanoparticles from Sesame Husk, *Ind. Eng. Chem. Res.* 50 (2011) 871–876. doi:10.1021/ie101797d.
- [61] H. Kargarzadeh, I. Ahmad, I. Abdullah, A. Dufresne, S.Y. Zainudin, R.M. Sheltami, Effects of hydrolysis conditions on the morphology, crystallinity, and thermal stability of cellulose nanocrystals extracted from kenaf bast fibers, *Cellulose.* 19 (2012) 855–866. doi:10.1007/s10570-012-9684-6.
- [62] Q. Wu, Y. Meng, K. Concha, S. Wang, Y. Li, L. Ma, et al., Influence of temperature and humidity on nano-mechanical properties of cellulose nanocrystal

films made from switchgrass and cotton, *Ind. Crops Prod.* 48 (2013) 28–35.

doi:10.1016/j.indcrop.2013.03.032.

[63] C. Rondeau-Mouro, B. Bouchet, B. Pontoire, P. Robert, J. Mazoyer, a. Buléon, Structural features and potential texturising properties of lemon and maize cellulose microfibrils, *Carbohydr. Polym.* 53 (2003) 241–252. doi:10.1016/S0144-8617(03)00069-9.

[64] P. Krishnamachari, R. Hashaikeh, M. Tiner, Modified cellulose morphologies and its composites; SEM and TEM analysis., *Micron.* 42 (2011) 751–61.

doi:10.1016/j.micron.2011.05.001.

[65] N. Follain, S. Belbekhouche, J. Bras, G. Siqueira, S. Marais, A. Dufresne, Water transport properties of bio-nanocomposites reinforced by *Luffa cylindrica* cellulose nanocrystals, *J. Memb. Sci.* 427 (2013) 218–229. doi:10.1016/j.memsci.2012.09.048.

[66] W.P. Flauzino Neto, H.A. Silvério, N.O. Dantas, D. Pasquini, Extraction and characterization of cellulose nanocrystals from agro-industrial residue – Soy hulls, *Ind. Crops Prod.* 42 (2013) 480–488. doi:10.1016/j.indcrop.2012.06.041.

[67] A. Kaushik, M. Singh, Isolation and characterization of cellulose nanofibrils from wheat straw using steam explosion coupled with high shear homogenization., *Carbohydr. Res.* 346 (2011) 76–85. doi:10.1016/j.carres.2010.10.020.

[68] L.P. Novo, J. Bras, A. Garcia, M.N. Belgacem, A. a. S. Curvelo, Subcritical water: A method for green production of cellulose nanocrystals, *ACS Sustain. Chem. Eng.* 3 (2015) 2839 – 2846. doi:10.1021/acssuschemeng.5b00762.

[69] S. Panthapulakkal, M. Sain, Preparation and Characterization of Cellulose Nanofibril Films from Wood Fibre and Their Thermoplastic Polycarbonate Composites, *Int. J. Polym. Sci.* 2012 (2012) 1–6. doi:10.1155/2012/381342.

[70] R.M. Sheltami, I. Abdullah, I. Ahmad, A. Dufresne, H. Kargarzadeh, Extraction of cellulose nanocrystals from mengkuang leaves (*Pandanus tectorius*), *Carbohydr. Polym.* 88 (2012) 772–779. doi:10.1016/j.carbpol.2012.01.062.

[71] S.S. Pesetskii, S.P. Bogdanovich, N.K. Myshkin, Polymer Nanocomposites with Thermoplastic Matrices—Processing and Tribology, *J. Macromol. Sci. Part B.* 52 (2013) 1784–1810. doi:10.1080/00222348.2013.808560.

[72] R. Kaneko, E. Hamada, Microwear processes of polymer surfaces.pdf, *Wear*. 162 (1993) 370 – 377. doi:0043-1648/93.

[73] Bouchard, J., Méthot, M., Fraschini, C., Beck, S., Effect of oligosaccharide deposition on the surface of cellulose nanocrystals as a function of acid hydrolysis temperature. (2016). *Cellulose*. doi:10.1007/s10570-016-1036-5